



**HAL**  
open science

# Functionalized polymer implants for the trapping of glioblastoma cells

Muhammad Haji Mansor

► **To cite this version:**

Muhammad Haji Mansor. Functionalized polymer implants for the trapping of glioblastoma cells. Human health and pathology. Université d'Angers; Université de Liège, 2019. English. NNT : 2019ANGE0015 . tel-03270912

**HAL Id: tel-03270912**

**<https://theses.hal.science/tel-03270912>**

Submitted on 25 Jun 2021

**HAL** is a multi-disciplinary open access archive for the deposit and dissemination of scientific research documents, whether they are published or not. The documents may come from teaching and research institutions in France or abroad, or from public or private research centers.

L'archive ouverte pluridisciplinaire **HAL**, est destinée au dépôt et à la diffusion de documents scientifiques de niveau recherche, publiés ou non, émanant des établissements d'enseignement et de recherche français ou étrangers, des laboratoires publics ou privés.

# THESE DE DOCTORAT DE

L'UNIVERSITE D'ANGERS  
COMUE UNIVERSITE BRETAGNE LOIRE  
et  
L'UNIVERSITE DE LIEGE

ECOLE DOCTORALE N° 605  
*Biologie Santé*  
Spécialité : « *Sciences Pharmaceutiques* »

Par  
**« Muhammad Sallehuddin Bin HAJI MANSOR »**  
**« Functionalized polymer implants for the trapping of glioblastoma cells »**

**Thèse présentée et soutenue à** « Salle de conférence – Institut de Biologie en Santé-IRIS »,  
**le** « 25/09/2019 »

**Unité de recherche** : CRCINA Equipe 17 GLIAD (INSERM U1232), Université d'Angers &  
CERM, Université de Liège

**Thèse N°** : 181329

## Rapporteurs avant soutenance :

Dr. Avi SCHROEDER  
Associate Professor  
Technion – Israel Institute of Technology, Israel  
Prof. Giovanni TOSI  
Professor  
University of Modena and Reggio Emilia, Italy

## Composition du Jury :

Dr. Avi SCHROEDER, Rapporteur  
Associate Professor  
Technion – Israel Institute of Technology, Israel  
Prof. Giovanni TOSI, Rapporteur  
Professor  
University of Modena and Reggio Emilia, Italy  
Prof. Catherine LE VISAGE, Examineur  
Professeure  
Université de Nantes, France  
Dr. Antoine DEBUIGNE, Examineur  
Chercheur  
Université de Liège, Belgium  
Prof. Frank BOURY, Directeur de thèse  
Professeur  
Université d'Angers, France  
Prof. Christine JÉRÔME, Co-directeur de thèse  
Professeure  
Université de Liège, Belgium

**L'auteur du présent document vous autorise à le partager, reproduire, distribuer et communiquer selon les conditions suivantes :**



- Vous devez le citer en l'attribuant de la manière indiquée par l'auteur (mais pas d'une manière qui suggérerait qu'il approuve votre utilisation de l'œuvre).
- Vous n'avez pas le droit d'utiliser ce document à des fins commerciales.
- Vous n'avez pas le droit de le modifier, de le transformer ou de l'adapter.

**Consulter la licence creative commons complète en français :  
<http://creativecommons.org/licences/by-nc-nd/2.0/fr/>**

Ces conditions d'utilisation (attribution, pas d'utilisation commerciale, pas de modification) sont symbolisées par les icônes positionnées en pied de page.



## RÉSUMÉ

Le glioblastome (GBM) est la forme de cancer du cerveau la plus courante et la plus meurtrière. Sa nature diffuse entraîne une impossibilité d'élimination complète par chirurgie. Une récurrence de la tumeur chez  $\geq 90\%$  des patients peut être provoquée par des cellules GBM résiduelles se trouvant près du bord de la cavité de résection. Un implant pouvant libérer de manière durable la protéine SDF-1 $\alpha$ , qui se lie aux récepteur CXCR4 à la surface des cellules GBM, peut être utile pour induire le recrutement des cellules GBM résiduelles, permettre leur élimination sélective et finalement réduire la récurrence de la tumeur. Dans ce travail, le SDF-1 $\alpha$  a été initialement encapsulé dans des nanoparticules à base d'acide poly-lactique-co-glycolique (PLGA). Une efficacité d'encapsulation élevée (76%) a pu être obtenue en utilisant un processus simple de séparation de phase. Les nanoparticules chargées de SDF-1 $\alpha$  ont ensuite été incorporées dans un scaffold à base de chitosan par électrofilage pour obtenir des implants nanofibreux imitant la structure de la matrice extracellulaire du cerveau. Une étude de libération in vitro a révélé que l'implant pouvait fournir une libération prolongée de SDF-1 $\alpha$  jusqu'à 35 jours, utile pour établir un gradient de concentration de SDF-1 $\alpha$  dans le cerveau et induire une attraction des cellules GBM. Une étude de biocompatibilité in vivo à 7 jours a révélé des signes d'inflammation locale sans aucun signe visible de détérioration clinique chez les sujets animaux. Une étude à 100 jours visant à confirmer l'innocuité in vivo des implants avant de passer aux études d'efficacité dans un modèle de résection GBM approprié est actuellement en cours.

**mots-clés** : Glioblastome; Facteur-1 $\alpha$  dérivé des cellules stromales (SDF-1 $\alpha$ ); Nanoparticules; Scaffold nanofibreux; Libération contrôlée de protéines; Piège à cellules tumorales

# ABSTRACT

Glioblastoma (GBM) is the most common and lethal form of brain cancer. The diffusive nature of GBM means the neoplastic tissue cannot be removed completely by surgery. Often, residual GBM cells can be found close to the border of the resection cavity and these cells can multiply to cause tumor recurrence in  $\geq 90\%$  of GBM patients. An implant that can sustainably release chemoattractant molecules called stromal cell-derived factor-1 $\alpha$  (SDF-1 $\alpha$ ), which bind selectively to CXCR4 receptors on the surface of GBM cells, may be useful for inducing chemotaxis and recruitment of the residual GBM cells. This may then give access to selective killing of the cells and ultimately reduce tumor recurrence. In this work, SDF-1 $\alpha$  was initially encapsulated into poly-lactic-co-glycolic acid (PLGA)-based nanoparticles. A high encapsulation efficiency (76%) could be achieved using a simple phase separation process. The SDF-1 $\alpha$ -loaded nanoparticles were then incorporated into a chitosan-based scaffold by electrospinning to obtain nanofibrous implants that mimic the brain extracellular matrix structure. In vitro release study revealed that the implant could provide sustained SDF-1 $\alpha$  release for 5 weeks. The gradual SDF-1 $\alpha$  release will be useful for establishing SDF-1 $\alpha$  concentration gradients in the brain, which is critical for the chemotaxis of GBM cells. A 7-day in vivo biocompatibility study revealed evidence of inflammation at the implantation site without any visible signs of clinical deterioration in the animal subjects. A long-term study (100 days) aiming to confirm the in vivo safety of the implants before proceeding to efficacy studies in a suitable GBM resection model is currently underway.

**keywords** : Glioblastoma; Stromal cell-derived factor-1 $\alpha$  (SDF-1 $\alpha$ ); Nanoparticles; Nanofibrous scaffolds; Sustained protein release; Tumor cell trap

# ENGAGEMENT DE NON PLAGIAT

Je, soussigné(e) Muhammad Sallehuddin bin HAJI MANSOR  
déclare être pleinement conscient(e) que le plagiat de documents ou d'une  
partie d'un document publiée sur toutes formes de support, y compris l'internet,  
constitue une violation des droits d'auteur ainsi qu'une fraude caractérisée.  
En conséquence, je m'engage à citer toutes les sources que j'ai utilisées  
pour écrire ce rapport ou mémoire.

signé par l'étudiant(e) le **15 / 07 / 2019**



**Cet engagement de non plagiat doit être signé et joint  
à tous les rapports, dossiers, mémoires.**

Présidence de l'université  
40 rue de rennes – BP 73532  
49035 Angers cedex  
Tél. 02 41 96 23 23 | Fax 02 41 96 23 00



## **Acknowledgements**

First and foremost, I would like to thank Frank and Christine for your trust and confidence in my abilities to lead this thesis project. To Frank, it has been an absolute pleasure working under your supervision. I enjoyed every single friendly conversations that we had and I am highly grateful to have someone that I know I can always talk to as my advisor. You have always made great effort to remove any obstacles that could hinder my progress. You also gave me the autonomy to decide what is best for the project, a privilege that has really helped me thrive in the last three years. To Christine, I really admire the composure and insightfulness that you displayed every time I approached you for an advice. Your guidance has been really important in helping me to pull through the crucial stages of this project. Like Frank, you fully understood my personal and professional interests and always respected my decisions, and for that, I can never thank you enough.

Of course, this thesis project would not have progressed to the current stage without the help of Mathie Najberg. I could not have ever wished for, or even imagined of, a better colleague than you. Your sincerity and kindness have always left me deeply moved. If I have to point out one thing that I feel regretful about you, it would be the fact that I did not use all the available opportunities to express how grateful I am to have you as a companion during this amazing journey.

I would also like to thank Jean-Michel Thomassin for your unquestionable willingness to contribute to this project. I have to admit that I was feeling very nervous when I came to Liège to start working on electrospinning, a subject that was totally new to me, but your casual approach made the steep learning process feel very relaxed.

The experience that I have gained since the first day of this journey had undoubtedly helped me to become a better person. However, the period preceding this thesis project had been equally important as it had prepared me well for all the challenges that I faced in the last three years. As such, I feel indebted to my wonderful family who have instilled in me great personal and professional values. In particular, I would like to thank my late mother who taught me the importance of hard work and self-discipline. I am also very grateful to my late brother, who had been my source of inspiration during difficult times. Mizi, for your amazing courage and humility, you will always be the person I look up to.

It goes without saying that the journey to this day has been physically and mentally challenging. Therefore, it would be wrong for me to not thank Sue Wen Yong for being the person who has always been there for me during the happy and gloomy days alike. I am very grateful to be blessed by your presence in my life and to get to share so many memorable moments with you. Your undivided support and your random silliness have always filled my heart with warmth and joy. Thank you for always believing in me and pushing me to do one thing better at a time.

As the scope of work covered in this thesis is relatively broad, I am very grateful to have received assistance from a long list of kind-hearted people in Angers and Liège. I would like to thank Baya Gueza for her work on toxicity studies. It was very nice to have someone as helpful as you. I would also like to thank Romain Mallet for your assistance in microscopy. I am also very glad to have met Valérie Collard; when I first met you, you told me that I should always let you know if I ever have a problem at or outside work. I think that is the best way to welcome someone to a new place. I am also indebted to Martine Dejeneffe; like Valérie, you have always been approachable and heartwarming. Many thanks also to Clément Tetaud who has been an absolute wonder in helping with the animal studies.

I would also like to thank my thesis committee members, especially Prof Marc Sallé, for providing me with many constructive comments and recognizing my accomplishments during the annual committee meetings.

It has also been a privilege for me to have Dr Emmanuel Garcion and Prof Carmen Alvarez-Lorenzo as reliable advisors during the preparation of scientific articles and a review paper for publication.

From a broader perspective, during this wonderful PhD journey, I am very grateful to have met so many wholesome people that have really helped me grow as a person and perceive life from a different and dynamic perspective. Thanks a lot to Héléne Grégoire, Zeynep Ergul, Charlotte Dannemark, Nela Buchtova, Deborah Casas, Rahmet Parilti and Thao-Quyen Nguyen-Pham for your sweet companionship in the office. To Philip Scholten, Pierre Stiernet, Jérémie Caprasse and Grégory Cartigny, I cherished very much all the squash games that we played together. Being part of the awesome NanoFar family, I am very fortunate to have met inspiring figures in the form of Chiara Bastiancich, Reatul Karim, Saikrishna Kandalam, Shubaash Anthiya, Bathabile Ramalapa, among many others. I also feel blessed to have known Janske Nel, Bhanu Teja Surikutchi, Sohaib Mahri, Raneem Jatal, Paul Noel, Vincent Pautu, Natalija Tatic, Héléne Lajous and Maruthi Prasanna.

Certainly, this project would fail to materialize had it not receive the financial support from a number of funding bodies, including the Erasmus Mundus NanoFar Joint Doctorate program, the NanoFar+ network and the “Ministère de l'Enseignement supérieur” (MESR). I would also like to thank Marion Toucheteau for her help in countless administrative tasks. Your presence was such a blessing to me especially in my early days in France and during the crucial periods of mobility.

Finally:

Terima kasih Abah

Terima kasih sekali lagi Mak

Terima kasih sekali lagi Mizi

Terima kasih Mohd Noor dan Zul

Merci encore Frank and Christine

Merci encore Mathie

and

Many thanks again my dear Sue.



*Dedicated to my late mother,  
who raised me to become the person I am today*

# CONTENTS

---

1.	GENERAL INTRODUCTION.....	2
1.1.	Glioblastoma.....	2
1.1.1.	GBM tumor morphology and composition.....	2
1.1.2.	Current treatments and their shortcomings.....	4
1.2.	Tumor cell trapping: a novel strategy in cancer therapy.....	8
1.2.1.	Background and rationale of the tumor cell trapping concept.....	9
1.2.2.	Tumor cell trapping as a strategy for treating GBM.....	10
1.2.2.1.	Chemotaxis as a means of recruiting GBM cells.....	11
1.3.	Polymer-based protein delivery systems.....	13
1.3.1.	Common forms of polymer-based protein delivery systems.....	13
1.3.1.1.	Micro/nanoparticles.....	13
1.3.1.2.	Hydrogels.....	16
1.3.1.3.	Porous scaffolds.....	17
1.3.2.	Fibrous scaffolds as a polymer-based protein delivery system.....	19
1.3.2.1.	Fibrous scaffolds with embedded protein molecules.....	20
1.3.2.2.	Fibrous scaffolds with surface-bound protein molecules.....	21
1.3.3.	Electrospinning as a method to prepare protein-loaded fibrous scaffolds.....	23
1.3.3.1.	Overview of the electrospinning process.....	25
1.3.3.2.	Important processing parameters in electrospinning.....	27
1.3.3.3.	Important solution parameters in electrospinning.....	30
1.3.3.4.	Nozzle configuration options in electrospinning.....	33
1.3.3.5.	Polymers for electrospinning.....	35
1.4.	References.....	45
2.	THESIS AIM AND OBJECTIVES.....	64
3.	ENCAPSULATION OF SDF-1 $\alpha$ INTO POLYMER-BASED NANOPARTICLES.....	68
3.1.	Introduction.....	68
3.3.	Results.....	70
3.3.1.	Publication 1: EJPB 125 (2018) 38-50.....	70
3.3.2.	Unpublished results.....	98
3.3.2.1.	Materials and Methods.....	98
3.3.2.2.	Results and Discussion.....	99
3.4.	Conclusion of chapter 3.....	100
3.5.	References.....	104
4.	INCORPORATION OF SDF-1 $\alpha$ -LOADED PLGA/PEG-PLGA NANOPARTICLES INTO CHITOSAN NANOFIBERS.....	112

4.1.	Introduction.....	112
4.2.	Summary of the results .....	113
4.3.	Results.....	114
4.3.1.	Publication 2 (to be submitted to the Journal of Materials Chemistry B).....	114
4.3.2.	Unpublished results.....	140
4.3.2.1.	Materials and methods .....	141
4.3.2.2.	Results and Discussion.....	144
4.4.	Conclusion of chapter 4 .....	150
4.5.	References .....	152
5.	GENERAL DISCUSSION, CONCLUSION AND PERSPECTIVES .....	160
5.1.	General discussion .....	160
	Objective 1: To prepare SDF-1 $\alpha$ -loaded polymer-based nanoparticles .....	161
	Objective 2: To incorporate SDF-1 $\alpha$ -loaded nanoparticles into chitosan-based nanofibers.....	165
5.2.	Conclusion and Perspectives.....	167
5.3.	References.....	173
Annex 1	.....	178

## Abbreviations

<b><sup>1</sup>H-NMR</b>	<sup>1</sup> H nuclear magnetic resonance
<b>AFM</b>	Atomic force microscopy
<b>ATR-FTIR</b>	Attenuated total reflectance-Fourier transform infrared
<b>B2R</b>	Bradykinin B2 receptor
<b>BBB</b>	Blood-brain barrier
<b>BCALL</b>	B-cell acute lymphoblastic leukemia
<b>bFGF</b>	Basic fibroblast growth factor
<b>BMDC</b>	Bone marrow-derived cells
<b>BMP</b>	Bone morphogenetic protein
<b>BMSC</b>	Bone marrow stromal cells
<b>BP</b>	Boiling point
<b>BSA</b>	Bovine serum albumin
<b>CAF</b>	Cancer-associated fibroblast
<b>CAR</b>	Chimeric antigen receptor
<b>CCP</b>	Cell culture plate
<b>CMCS</b>	Carboxymethyl-chitosan
<b>CNS</b>	Central nervous system
<b>cP</b>	Centipoise
<b>CSF-1</b>	Colony-stimulating factor 1
<b>CT</b>	Computerized tomography
<b>CTC</b>	Circulating tumor cell
<b>CXCR4</b>	C-X-C chemokine receptor type 4
<b>DCM</b>	Dichloromethane
<b>Dex-GMA</b>	Glycidyl methacrylated dextran
<b>DL</b>	Drug loading
<b>DLS</b>	Dynamic light scattering
<b>DMAc</b>	N,N-dimethylacetamide
<b>DME</b>	Dulbecco's Modified Eagle's (medium)
<b>DMF</b>	Dimethylformamide
<b>DMI</b>	Isosorbide dimethyl ether/dimethyl isosorbide
<b>DMSO</b>	Dimethyl sulfoxide
<b>ECM</b>	Extracellular matrix

<b>EDC</b>	1-ethyl-3-(3-dimethylaminopropyl) carbodiimide
<b>EE</b>	Encapsulation efficiency
<b>EGF</b>	Epidermal growth factor
<b>ELISA</b>	Enzyme-linked immunosorbent assay
<b>EMT</b>	Epithelial-mesenchymal transition
<b>EpCAM</b>	Epithelial cell adhesion molecule
<b>FBS</b>	Fetal bovine serum
<b>FDA</b>	Food and Drug Administration
<b>F<sub>E</sub></b>	Electrostatic force
<b>F<sub>ST</sub></b>	Surface tension
<b>GASP-6</b>	Growth arrest-specific 6
<b>GBM</b>	Glioblastoma
<b>GP</b>	β-glycerol phosphate disodium salt
<b>GSC</b>	Glioblastoma stem-like cell
<b>HA</b>	Hyaluronic acid
<b>HCl</b>	Hydrochloric acid
<b>HFP</b>	1,1,1,3,3,3-hexafluoro-2-propanol
<b>HIF</b>	Hypoxia-inducible factor
<b>HPBCD</b>	Hydroxypropyl-β-cyclodextrin
<b>ICH</b>	International Conference on Harmonization
<b>IDH</b>	Isocitrate dehydrogenase
<b>LiCl</b>	Lithium chloride
<b>LMWH</b>	Low molecular weight heparin
<b>LNC</b>	Lipid nanocapsules
<b>MC</b>	Methyl cellulose
<b>MGMT</b>	O <sup>6</sup> -methylguanine–DNA methyltransferase
<b>MMP</b>	Matrix metalloproteinase
<b>M<sub>n</sub></b>	Number average molecular weight
<b>MRI</b>	Magnetic resonance imaging
<b>MSC</b>	Mesenchymal stem cell
<b>M<sub>w</sub></b>	Weight average molecular weight
<b>NaCl</b>	Sodium chloride
<b>NaOH</b>	Sodium hydroxide

<b>NF</b>	Nanofibrous scaffold
<b>NGF</b>	$\beta$ -nerve growth factor
<b>NHS</b>	N-hydroxysuccinimide
<b>NIR</b>	Near infrared
<b>NMMO</b>	N-methyl-morpholine N-oxide
<b>NP</b>	Nanoparticles
<b>NPC</b>	Neural progenitor cell
<b>O/W</b>	Oil-in-water
<b>P188</b>	Ploxamer 188
<b>PANCMMA</b>	Poly(acrylonitrile-co-maleic acid)
<b>PBS</b>	Phosphate-buffered saline
<b>PCLEEP</b>	Poly( $\epsilon$ -caprolactone-ethyl ethylene phosphate)
<b>PCU</b>	Poly(carbonate urethane)
<b>PD-1</b>	Programmed cell death protein 1
<b>PDB</b>	Protein Data Bank
<b>PDGF</b>	Platelet derived growth factor
<b>PDI</b>	Polydispersity index
<b>PDLA</b>	Poly(D,L-lactic acid)
<b>PDTEC</b>	Poly(desaminotyrosyl-tyrosine ethyl ester carbonate)
<b>PE</b>	Precipitation efficiency
<b>PEG</b>	Poly(ethylene glycol)
<b>PEI</b>	Poly(ethylene imine)
<b>PEO</b>	Poly(ethylene oxide)
<b>PGS</b>	Poly(glycerol sebacate)
<b>pI</b>	Isoelectric point
<b>PLCL</b>	Poly(L-lactide-co-caprolactone)
<b>PLGA</b>	Poly(lactic-co-glycolic acid)
<b>PLGA-COOH</b>	PLGA with uncapped carboxylic acid terminal
<b>PLGA-COOR</b>	PLGA with ester capped carboxylic acid terminal
<b>PLLA</b>	Poly(L-lactic acid)
<b>PMA</b>	Phorbol 12-myristate 13-acetate
<b>PMN</b>	Polymorphonuclear neutrophils
<b>PNIPAAm</b>	Poly(N-isopropylacrylamide)

<b>PPCN</b>	Poly(polyethylene glycol citrate-co-N-isopropylacrylamide)
<b>PPX</b>	Poly( <i>p</i> -xylylene)
<b>PS</b>	Polystyrene
<b>PTH</b>	Parathyroid hormone
<b>PU</b>	Polyurethane
<b>PVA</b>	Poly(vinyl alcohol)
<b>PVC</b>	Poly(vinyl chloride)
<b>PVDF</b>	Poly(vinylidene fluoride)
<b>PVF</b>	Poly(vinyl fluoride)
<b>PVP</b>	Poly(vinyl pyrrolidone)
<b>RPMI</b>	Roswell Park Memorial Institute (medium)
<b>SD</b>	Standard deviation
<b>SDF-1<math>\alpha</math></b>	Stromal cell-derived factor-1 $\alpha$
<b>SEC</b>	Size exclusion chromatography
<b>SEM</b>	Scanning electron microscopy
<b>SF</b>	Silk fibroin
<b>SRT</b>	Stereotactic radiotherapy
<b>SWNT</b>	Single-walled carbon nanotubes
<b>T<sub>c</sub></b>	Collapse temperature
<b>TEM</b>	Transmission electron microscopy
<b>TGF-<math>\beta</math></b>	Transforming growth factor- $\beta$
<b>THF</b>	Tetrahydrofuran
<b>TiO<sub>2</sub></b>	Titanium dioxide
<b>TMZ</b>	Temozolomide
<b>Tris</b>	Tris(hydroxymethyl)aminomethane
<b>TTF</b>	Tumor-treating field
<b>U87-MG</b>	Human malignant glioblastoma cell line U87-MG
<b>VEGF</b>	Vascular endothelial growth factor
<b>W/O</b>	Water-in-oil
<b>ZP</b>	Zeta-potential

# **Chapter 1:**

## **General Introduction**

---

## 1. GENERAL INTRODUCTION

---

### 1.1. GLIOBLASTOMA

Glioblastoma (GBM) is the most common form of brain cancer that affects between 0.59 and 3.69 per 100 000 persons [1,2]. It is a subset of gliomas, which are cancers that originate in the glial cells of the brain [3]. In fact, GBM arises mainly in the astrocytes and oligodendrocytes [4], the two most abundant members of the glial family that play important roles in regulating synaptic transmission between neurons [5,6]. Due to its malignant and invasive phenotype, GBM is classified as a grade IV central nervous system (CNS) tumor by the World Health Organization [7]. Indeed, the prognosis of this disease is very poor; less than 5% of GBM patients survive 5 years past diagnosis [2].

#### 1.1.1. GBM tumor morphology and composition

GBM tumors develop mainly in the right and left cerebral hemispheres [8], and rarely in the cerebellum [9] or brain stem [10] (Figure 1.1). The tumors arise *de novo* without a known precursor in 90% of the cases to form what is called as primary GBM, or develop progressively from lower grade gliomas into secondary GBM [11]. Despite their invasiveness, these tumors are usually confined to the brain and cases of metastasis outside the CNS are extremely rare. Anatomically, this could be due to the barrier created by the cerebral meninges and the absence of lymphatic vessels in the brain [12,13]. Another possible explanation is that the short survival time of GBM patients prevent the completion of the lengthy metastasis process before the death of the patients [13]. Macroscopically, GBM tumors are characterized by infiltrating growth into the surrounding normal brain tissues, making it an extremely difficult task to define their borders accurately [14,15]. Although the tumors are highly vascularized, the blood vessels tend to be leaky and disorganized [16]. The endothelium of the tumor vasculature is lined with frail basement membrane, which is covered by a discontinuous layer of pericytes (Figure 1.2A) [17]. As the neighboring tumor cells produce high concentrations of pro-coagulation factors [18], the narrow blood capillaries are prone to intravascular occlusion. Furthermore, the blood vessels also lack contact with the astrocyte processes, meaning that the integrity of the blood-brain barrier (BBB) is almost always compromised [19]. Due to the suboptimal vascular functions, GBM tumors receive inconsistent blood supply and oxygen delivery that result in hypoxia and subsequent formation of necrotic regions [20,21]. GBM cells align themselves neatly around these necrotic foci to form dense layers of cells known as ‘pseudopalisades’, which is a prominent morphological feature of GBM (Figure 1.2B) [22].

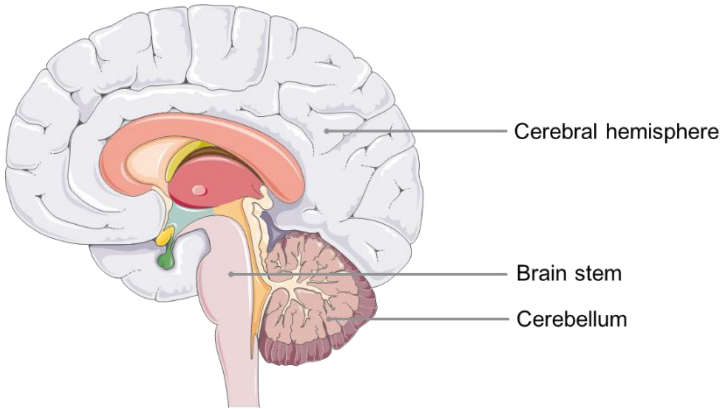


**Figure 1.1:** The compartments of the brain susceptible to GBM development. Image courtesy of Servier Medical Art.

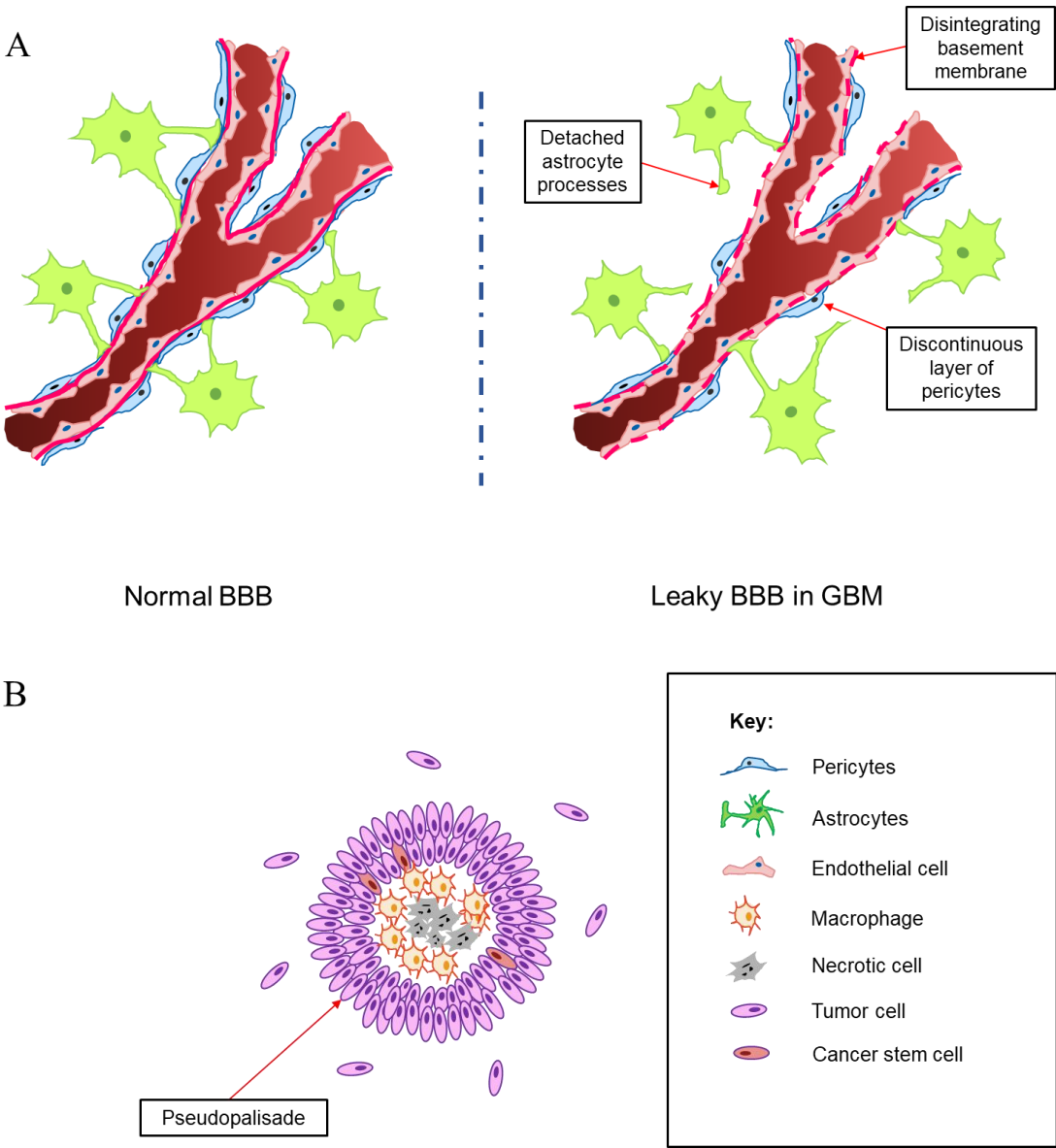


**Figure 1.2:** (A) The state of the blood-brain barrier in normal brain and that typically seen in GBM, and (B) the typical pseudopalisade formed around a necrotic region in GBM. Image adapted from [23].

GBM tumors have a highly heterogenous microenvironment [23]. Their propagation is a result of close interactions between GBM cells and the supportive non-neoplastic cells present in the tumor niche. Due to the compromised BBB, circulating immune cells including monocytes [24] and neutrophils [25] can be found abundantly in the tumor microenvironment. These infiltrating immune cells, together with the resident brain macrophages called microglial cells, can secrete pro-angiogenic and immunosuppressive factors to promote maintenance of the GBM cells and their escape from immune surveillance [24–27]. Furthermore, the paracrine interaction between GBM cells and astrocytes can promote tumor invasiveness. Indeed, these glial cells are known to activate multiple signaling pathways in a subset of GBM cells identified as GBM stem-like cells (GSCs) to promote infiltration into adjacent healthy tissues [28–30]. Being one of the most abundant cell families in the brain, neurons are also implicated in GBM progression. The synaptic protein neuroligin-3 secreted by these cells has been shown to promote GBM cell proliferation [31].

Due to the heterogenous and invasive nature of GBM tumors, the clinical management of patients with this disease involves the use of a multi-modal approach to immediately reduce tumor burden. The execution of an aggressive therapeutic repertoire is important to halt tumor progression and to alleviate the debilitating symptoms resulting from increased intracranial pressure that include seizures, headaches and changes in mental status [32].

### **1.1.2. Current treatments and their shortcomings**

Surgical resection of the tumor is the first-line therapy for newly-diagnosed GBM patients. The aim of this approach is to reduce as much of the tumor volume as possible [33]. Simultaneously, the excised tissue can be used for tumor characterization purposes. Although there is a proven association between gross total tumor resection and longer survival time, only 73% of GBM patients are fit for surgery at the time of diagnosis [34,35]. When surgical resection is deemed to be not feasible, such as when the anatomical location of the tumor impedes its resection without any significant damage to the surrounding healthy brain tissues, or when patients show impaired neurological functions, a biopsy should still be carried out to characterize the tumor [33]. Tumor characterization is very important as the presence of certain molecular markers can guide treatment planning and predict disease outcomes. For example, the methylation of the promoter sequence that leads to the silencing of the gene encoding for the DNA repair enzyme O<sup>6</sup>-methylguanine–DNA methyltransferase (MGMT) predicts a better response to alkylating agent chemotherapy [36,37]. In addition, the expression of the mutant form of the

enzyme isocitrate dehydrogenase (IDH) suggests that the tumor has a prior history of being a lower grade lesion, which is characteristic of secondary GBM and associated with a more positive prognosis [7]. To facilitate tumor resection, the intra-operative use of well-established imaging technologies that help to differentiate between normal brain and tumor tissues such as magnetic resonance imaging [38] is fundamental. More recent technologies such as fluorescent guides in the form of 5-aminolevulinic acid [39] and BLZ-100 [40,41] are gradually being adopted in the clinic. Despite this, achieving complete tumor resection continues to be a major challenge due to the extensive dissemination of GBM cells deep into the surrounding brain tissues.

To kill the residual tumor cells, patients will be initiated with concomitant chemoradiotherapy that forms the standard treatment after surgery. The combination treatment consists of 5 sessions per week of external beam radiation for a duration of 6 weeks to irradiate the resection area with a total dose of 60 Gy, and concurrent oral chemotherapeutic drug temozolomide (TMZ) at a daily dose of 75 mg/m<sup>2</sup> of body surface area. After the completion of the radiotherapy, the dose of TMZ is changed to 150-200 mg/m<sup>2</sup> of body surface area daily to be taken for 5 days every 4 weeks for six repeats [33]. Despite the intensive therapeutic regimen, the median survival of GBM patients is only 14.6 months [42]. The selective pressures from the chemoradiotherapy favor the survival of certain tumor subpopulations with more resistant phenotypes, leading to tumor recurrences and subsequent patient deaths. GBM cells can overcome the cytotoxic effect of TMZ by overexpressing the MGMT enzymes that reverse the alkylating action of this chemotherapy [43]. The hypoxic niche of a GBM tumor can also confer radioresistance to the GSC population via the action of the hypoxia-inducible factors (HIFs) [44].

As the standard treatments mentioned above yield poor clinical outcomes in GBM patients, other adjuvant therapies are being used by clinicians to improve patient survival time. Gliadel® are chemotherapy-impregnated wafers designed to be implanted intra-operatively into the resection cavity following the removal of the bulk tumor (Figure 1.3) [33]. They are approved by the Food and Drug Administration (FDA) as a bridging therapy between the tumor resection and the conventional chemoradiotherapy, as the latter can only be initiated several weeks after the surgery to permit wound healing [45]. The wafers are made up of the biodegradable co-polymer polifeprosan 20 impregnated with the chemotherapeutic drug carmustine [46]. The hydrophobic nature of the co-polymer protects carmustine from hydrolytic degradation and maintain its release into the local environment over time [47]. The recommended dose of

carmustine is 61.6 mg, and this amount can be delivered by implanting eight wafers that each contain 7.7 mg carmustine onto the border of the resection cavity [46]. Although Gliadel® helps to provide high local concentrations of carmustine [47], their use in combination with TMZ after surgery and radiotherapy only confer a 3.6-month median survival advantage over the treatment with TMZ alone (18.2 vs 14.6 months) [48]. Tumor relapse could still be observed in all Gliadel®-treated patients [49] as the residual GBM cells tend to develop resistance against the alkylating action of carmustine by overexpressing MGMT enzymes as mentioned above [50]. In addition, the cytotoxic effect of carmustine on the residual GBM cells is also limited by its poor diffusion into the brain tissues. Studies in rats and monkeys revealed that negligible carmustine concentrations could be detected at 3 mm and beyond from the wafer/tissue interface [47]. This prevents complete killing of the residual GBM cells, which may reside more than one centimeter away from the bulk tumor border [14,15].

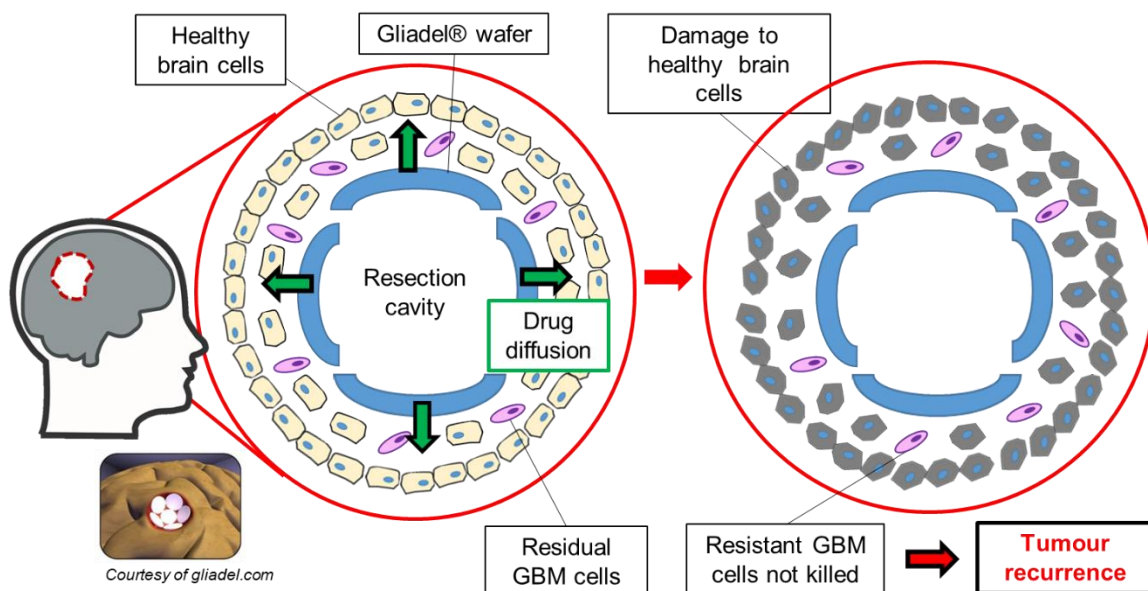


**Figure 1.3:** The implantation of Gliadel® wafers in the tumor resection cavity and the undesirable outcome of the treatment.

Optune® is another common adjuvant treatment for GBM. It consists of four adhesive patches to be placed on the scalp of the patient to deliver low-intensity, alternating electric fields called Tumor Treating Fields to the tumor [51]. These fields disrupt the cell division process in GBM cells by targeting the spindle microtubules, the protein-based structures responsible for the separation and equal distribution of chromosomes during mitosis. The cell cycle arrest can eventually lead to the apoptosis of the GBM cells as a result of an abnormal chromosome segregation [52]. The selectivity of this treatment is based on targeting only the cells that are

actively undergoing cell division such as the cancer cells [53]. Optune® is approved in the United States, European Union and Switzerland for the treatment of newly-diagnosed GBM alongside TMZ after surgery and radiotherapy, and recurrent GBM as a monotherapy [54,55]. For the first indication, Optune® improved the median survival of GBM patients by less than 5 months compared to the control group (20.9 vs 16.0 months). The marginal survival benefit is underwhelming considering that the long-term exposure to an electric field has been reported to cause side effects including convulsion and scalp irritation [56]. While these side effects may seem intuitively less troubling, they can certainly impair the quality of life of terminal GBM patients. In addition, the treatment procedure does not greatly promote patient convenience as patients are required to wear the patches and carry the associated device with them throughout the treatment duration.

Bevacizumab (Avastin®) is a human monoclonal antibody that targets the vascular endothelial growth factor (VEGF) [57]. GBM tumors are known to overexpress VEGF, especially within the hypoxic regions adjacent to the necrotic foci of the tumor to stimulate the formation of new blood vessels, a process known as angiogenesis that is crucial to tumor growth [58,59]. Avastin® is administered by intravenous infusion at a dose of 10 mg/kg of body weight every 2 weeks and currently holds FDA approval for the treatment of recurrent GBM [60]. Despite its large molecular size and the consequential inability to cross the blood-brain barrier, bevacizumab is claimed to exert its effect on the GBM tumors by neutralizing VEGF in the lumen of blood vessels in the brain [61]. However, the use of bevacizumab in combination with a cytotoxic agent such as TMZ or irinotecan prolonged the median survival of recurrent GBM patients by only 4 months compared to the use of the cytotoxic agent alone [62]. The limited benefit of bevacizumab could be explained by the downstream consequences of its suppressive action on angiogenesis. The deprivation of tumor blood supply may result in acute suppression of tumor growth but GBM lesions are known to respond to the resultant hypoxic condition by acquiring more malignant and resistant phenotypes via the action of HIFs as mentioned earlier [63].

In addition to the clinically-approved treatments mentioned so far, many experimental therapies have been tested in clinical trials to optimize the current standard of care for GBM patients [64]. These include immunotherapy (e.g. anti-tumor vaccines) [65,66], inhibitors of epidermal growth factor receptor (e.g. erlotinib and gefitinib) [67,68], radiation sensitizer (e.g. NVX-108) [69], protease inhibitor (e.g. nelfinavir) [70] and photodynamic therapy (e.g. Photofrin®) [71]. Nevertheless, all these modalities seem to be unable to yield significant

improvement in disease outcome. Due to these shortcomings, it is necessary to re-evaluate the clinical relevance of existing approaches and adopt appropriate novel measures to tackle this disease more successfully.

## **1.2. TUMOR CELL TRAPPING: A NOVEL STRATEGY IN CANCER THERAPY**

This section briefly discusses tumor cell trapping approach as a novel strategy for treating cancers, with links to the rationale of its use in the treatment of GBM presented later on. More detailed appraisal of this strategy can be found in a review paper included in Annex 1 at the end of the manuscript.

Over the last century, the development of treatments for cancers including GBM has been driven mainly by the “magic bullet” concept put forward by Paul Ehrlich in 1913. The concept idealizes the possibility of delivering chemotherapeutic agents exclusively to tumor cells by targeting specific oncoproteins to induce their death without harming healthy tissues [72]. Although targeted drug delivery has gained traction in the treatment of some cancers (e.g. Kadcyla® for the treatment of HER2-positive breast cancer [73], Adcetris® for CD30-positive lymphoma [74] and very recently, Polivy® for CD79b-positive lymphoma [75]), the same feat could not be achieved in the case of GBM due to their unique anatomical location and biological features. Although the areas closer to the center of a GBM tumor tend to have leaky BBB, this is not the case in the peripheries [76], presenting a huge challenge for targeting vectors such as monoclonal antibody to reach GBM cells after intravenous administration. In addition, as the GBM cells have high tendency to develop chemoresistance [43,50], the targeting vectors will have to deliver high concentration of chemotherapeutic drug to induce tumor cell death that may inevitably harm healthy brain cells.

An attractive novel approach to cancer treatment that is gaining increasing attention over the last few years is based on the reversal of the current “search-and-destroy” strategy. This refers to the trapping of tumor cells within a pre-defined location to enable their selective killing using conventional treatments [77]. This “attract-and-kill” idea was inspired by the “ecological trap” phenomenon, in which organisms in a certain ecosystem can be influenced by a misleading cue that leads to their migration into a low-quality habitat where they eventually die. For example, when sea turtle hatchlings leave their nests on the beach at night, they normally move towards the bright horizon, which naturally will lead them to the open sea. However, light sources from man-made constructions in the mainland may act as a

misinforming cue that causes the hatchlings to migrate away from the sea, ultimately resulting in their deaths (Figure 1.4A) [78]. The idea of trapping tumor cells has great appeal as it provides possibilities for limiting undesirable damages on normal brain tissues upon treatment. Once the tumor cells are recruited to a specific location, cytotoxic doses of existing therapies, such as chemotherapy or x-/ $\gamma$ -ray microbeams, can be applied to the trap (Figure 1.4B). The translation of an “ecological trap” into a tumor cell trap can possibly be realized by providing tumor cells with suitable structural and biological cues that direct their migration.

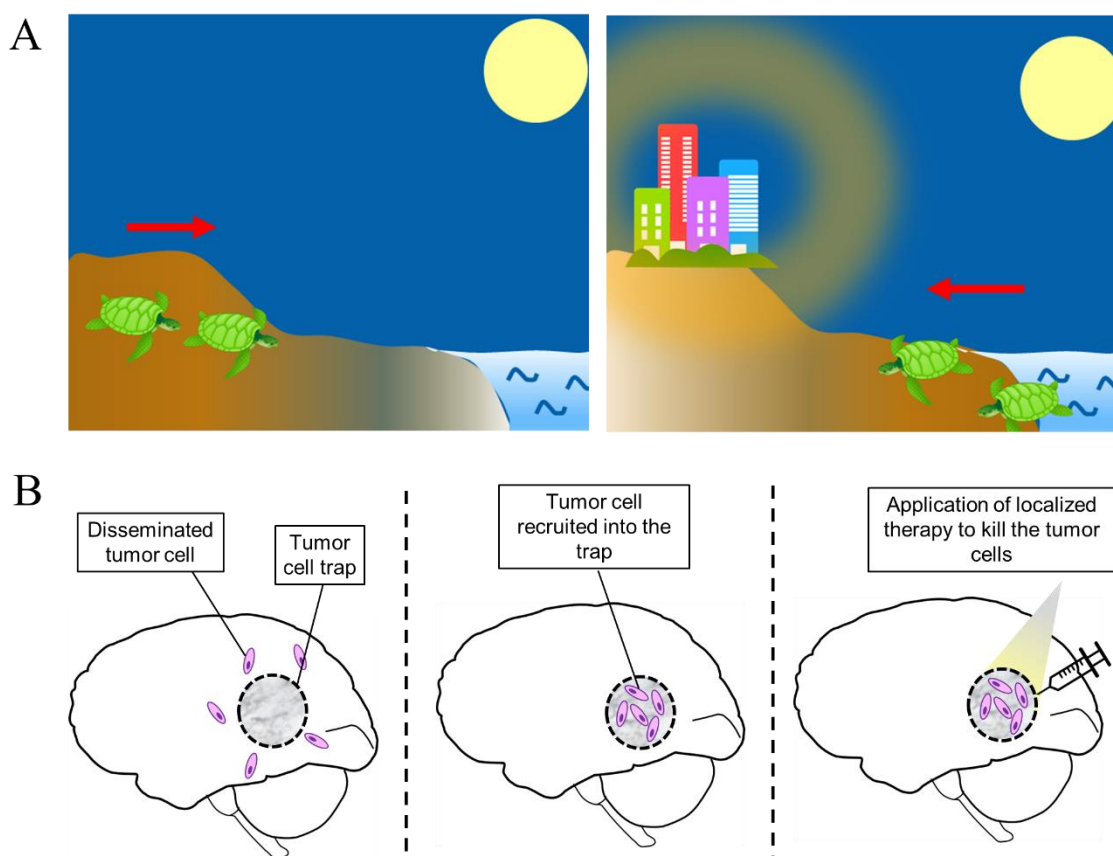


**Figure 1.4:** (A) An illustration of the “ecological trap” phenomenon: turtle hatchlings are misguided to migrate towards man-made lights on the mainland instead of towards the bright horizon of the open sea. (B) A representation of the potential use of a tumor cell trap in the treatment of GBM. Images adapted from [77].

### 1.2.1. Background and rationale of the tumor cell trapping concept

In addition to their aberrant proliferation and anti-apoptotic property, tumor cells are well-known for their high tendency to invade surrounding healthy tissues. Upon reaching a certain tumor size, tumor cells can escape from their primary location to colonize distant sites in a process called metastasis. Importantly, this process does not happen by random chance.

Stephen Paget first proposed his “seed and soil” hypothesis in 1889 upon observing breast cancer patients having frequent metastases only in certain organs such as the liver and bone [79]. His theory inspired the idea of using scaffolds that are carefully designed to mimic metastatic niches to lure tumor cells away from their conventional colonization sites. Several groups have engineered scaffolds that emulate bone microenvironments, and these tools were shown to be successful in attracting and trapping metastasizing breast cancer cells [80,81]. Other groups have attempted to replicate pathological events that are intrinsic to the sites of metastasis to recruit metastasizing tumor cells. For example, Ko *et al.* utilized scaffolds made of several types of material to induce different degrees of inflammatory response at the implantation site. Such an approach was taken on the basis that a localized inflammatory cascade usually precedes the colonization of a metastatic site. Indeed, they showed that a localized and controllable immune response induced by the implanted scaffolds was successful in recruiting metastasizing melanoma cells, and there was a strong correlation between the number of accumulated immune cells at the implantation site and the extent of tumor cell recruitment [82]. A more recent work by Azarin *et al.* also showed that immune cell infiltration into an implanted scaffold contributed to the recruitment of metastasizing breast cancer cells [83]. These findings suggest that there are multiple ways in which a scaffold can be engineered to manifest an environment conducive to tumor cell trapping.

### **1.2.2. Tumor cell trapping as a strategy for treating GBM**

In addition to luring metastasizing tumor cells, scaffolds functionalized with relevant structural and biological cues also have the potential to recruit locally disseminated tumor cells. This approach may be useful for addressing the recurrence issues arising from an incomplete tumor resection as seen in GBM. By implanting suitably designed scaffolds into the resection cavity, the residual tumor cells can be recruited and subsequently killed to prevent tumor reformation. It is worth recalling that GBM cells are well-known for their highly motile phenotype. By designing a relevant tumor cell-attracting field, their invasiveness can be exploited for therapeutic purposes. In line with this objective, Jain *et al.* designed a “tumor guide” in the form of aligned polymer-based nanofibers that mimic the topography of white matter tracts and blood vessels, the structures known to provide pathways for the local migration and dissemination of GBM cells in the brain [84]. They reported that the scaffold was successful in promoting the migration of GBM cells to an extracortical location, resulting in a reduction of tumor burden in the brain [85].

### 1.2.2.1. Chemotaxis as a means of recruiting GBM cells

Another way of recruiting tumor cells, apart from relying on structural cues, is to load scaffolds with biological molecules known to attract tumor cells. These molecules are called chemoattractants and may include many growth factors and cytokines. When released into the local environment, these molecules may recruit tumor cells to move into the scaffold by a process known as chemotaxis. Chemotaxis refers to the migration of cells in response to gradients of soluble chemoattractants. More specifically, the cells move towards regions with higher chemoattractant concentrations i.e. the source of the chemoattractant (Figure 1.5).

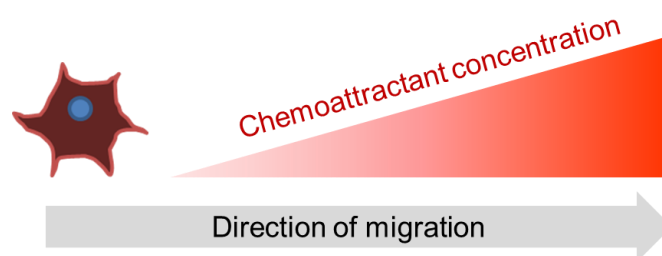


**Figure 1.5:** The principle of chemotaxis.

Metastatic breast and prostate cancer cells have been reported to migrate up the concentration gradient of epidermal growth factor (EGF), and the number of migrated cells as well as their migration speed correlate closely with the steepness of the concentration gradient [86,87]. Chemotaxis of GBM cells has also been well-documented. The cytokine stromal cell-derived factor-1 $\alpha$  (SDF-1 $\alpha$ ) could induce directed migration of several GBM cell lines, including LN827, LN308 and U87-MG. SDF-1 $\alpha$  is an example of chemokines; a cytokine subgroup known to have the capacity to induce chemotaxis. This 68-amino-acid protein binds strongly to the C-X-C chemokine receptor type 4 (CXCR4). GBM cells are frequently reported to over-express this receptor but they often lack the capacity to produce SDF-1 $\alpha$  [88,89]. As a result, CXCR4-positive GBM cells tend to migrate towards the structures in the brain that secrete SDF-1 $\alpha$  such as the blood vessels (Figure 1.6) [89,90]. In fact, the chemotactic migration of GBM cells towards the blood vessels is an important driver of their invasiveness. In general, GBM cell invasion can take place through two main compartments of the brain: the perivascular spaces and the brain parenchyma [91]. The former is a much more feasible route as they are typically fluid-filled and thus present fewer mechanical and physical barriers to GBM cell migration. On the other hand, the brain parenchyma is characterized by narrow and tortuous extracellular spaces that are less permeable to cell movement [91]. Therefore, by being

chemoattracted towards the blood vessels, GBM cells can subsequently disseminate into neighboring brain tissues with minimal hindrance.

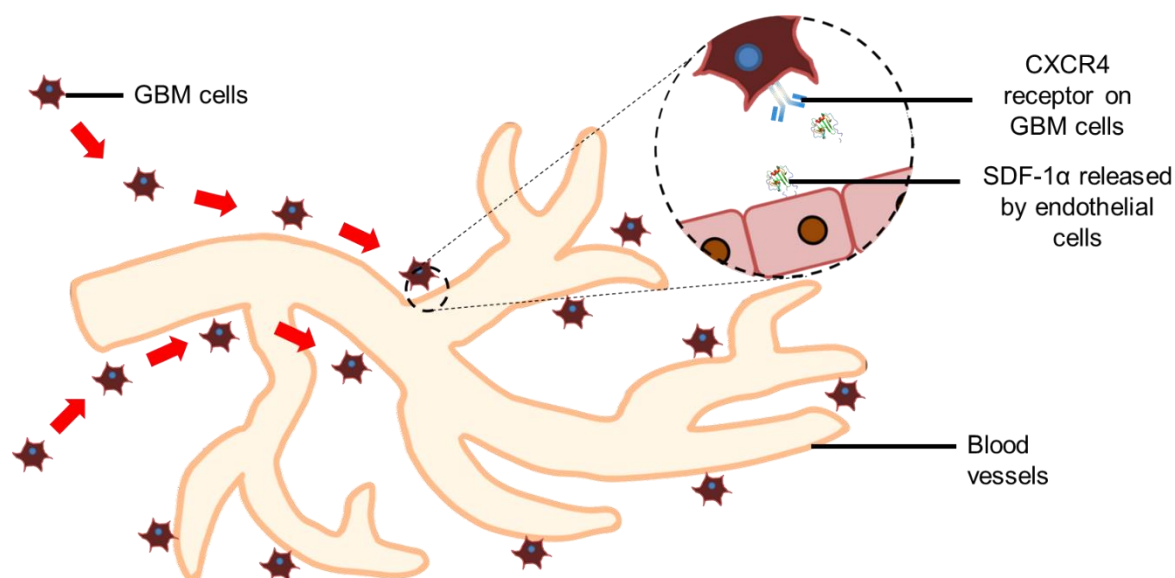


**Figure 1.6:** The migration of CXCR4-expressing GBM cells towards and along the blood vessels induced by the secretion of SDF-1 $\alpha$  from endothelial cells.

As the standard treatments in the form of surgery followed by chemoradiotherapy fail to remove tumors from the brain completely, the strategy of implanting SDF-1 $\alpha$ -releasing tumor traps into the resection cavity to attract residual GBM cells for their selective killing is of interest. However, to establish and maintain concentration gradients of SDF-1 $\alpha$  that is important for the chemotaxis of GBM cells, it is necessary to first develop scaffolds that can provide sustained release of this chemokine. As mentioned earlier, residual GBM cells can reside more than one centimeter away from the resection cavity border. Prolonged release of SDF-1 $\alpha$  will be crucial to expand the time window for the chemotaxis of GBM cells and thus increase the likelihood of trapping the entire residual GBM cell population. The scaffolds also need to be biocompatible to reduce the risk of an unfavorable immune or toxicological response during the implantation period. Like other protein molecules, SDF-1 $\alpha$  may possess inherent structural instabilities, making its incorporation into a delivery vehicle a challenging process. In the next section, relevant polymer-based protein delivery systems that may be employed to achieve sustained and controlled release of SDF-1 $\alpha$  will be discussed.

### 1.3. POLYMER-BASED PROTEIN DELIVERY SYSTEMS

The previous two decades have seen remarkable progress in biotechnology that enables production of many proteins for use in biomedical research. To improve their therapeutic values, much attention has been dedicated to prolonging the biological activity of these proteins after administration in patients. A common approach involves incorporating the protein molecules into an appropriate matrix that permits gradual release of the protein load. In doing so, the matrix limits the exposure of the protein molecules from proteases and neutralizing antibodies that may be present in the immediate physiological environment, thus preventing them from undergoing rapid degradation. SDF-1 $\alpha$ , for example, can be cleaved by matrix metalloproteinase-2 and 9 (MMP-2/9) released during a traumatic event such as tumor resection, resulting in loss of its chemotactic activity [92,93]. Furthermore, gradual release of SDF-1 $\alpha$  from the entrapping matrix may be useful to replenish the SDF-1 $\alpha$  supply in the surrounding brain tissues, maintaining a local concentration gradient necessary for GBM cell recruitment. Polymers have been widely-used to produce protein-loaded matrices due to the high versatility of this material group. By changing the type of monomers, controlling the polymerization conditions or functionalizing the polymer chains with chemical groups of interest, the physicochemical and biological properties of the polymer matrix, including surface charge, hydrophobicity, biodegradability and biocompatibility can be regulated.

#### 1.3.1. Common forms of polymer-based protein delivery systems

Common examples of polymer-based systems that have been utilized in recent years to deliver various drug molecules, including therapeutic proteins, include micro/nanoparticles, hydrogels and porous scaffolds (Figure 1.7).

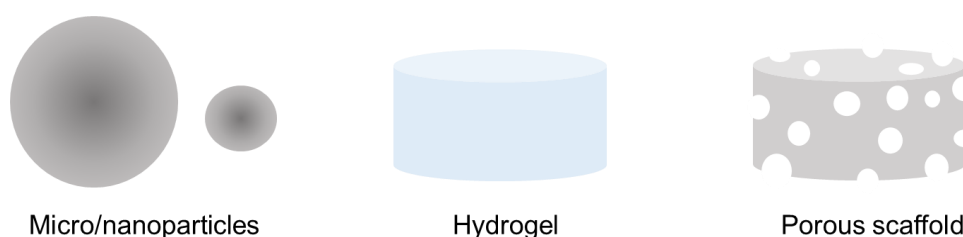


**Figure 1.7:** Common polymer-based systems for drug delivery applications.

##### 1.3.1.1. Micro/nanoparticles

Micro/nanoparticles are injectable drug carriers that are usually prepared from hydrophobic polymers using straightforward processes such as solvent evaporation, phase separation and

spray-drying [94]. In the solvent evaporation method, an organic phase is first formed by dissolving a hydrophobic polymer and the drug molecules to be encapsulated in a water-immiscible, volatile organic solvent. This phase is then dispersed in an aqueous phase containing stabilizers such as polyvinyl alcohol under continuous mechanical agitation to form an oil-in-water (O/W) emulsion. Drug-loaded particles are formed upon evaporation of the organic solvent from the inner phase at reduced or atmospheric pressure. The particles can then be collected by filtration or centrifugation, washed to remove the stabilizing molecules adsorbed to the particle surface and lyophilized to minimize hydrolytic degradation of the particles during long-term storage. However, the single emulsion technique may not be suitable for encapsulating hydrophilic drugs such as proteins as they tend to diffuse into the external aqueous phase during the emulsification step. Therefore, protein molecules are first solubilized in an aqueous solvent, and then dispersed in a polymer-containing organic phase to form a primary water-in-oil (W/O) emulsion, followed by dispersion in another aqueous solvent to form the secondary O/W emulsion [95]. The preparation of the primary W/O emulsion is also relevant to the phase separation method. Following this step, instead of adding an aqueous solvent, an organic solvent that is non-solvent to the dissolved polymer is gradually introduced to extract the polymer solvent and decrease the polymer solubility. The phase separation of the polymer from its solution contributes to the formation of polymer-rich liquid phase (coacervate) that surrounds the inner drug-containing aqueous phase. Upon completion of the phase separation process, the coacervate solidifies to produce drug-loaded particles [96]. An obvious drawback of this method is the requirement for a large volume of organic solvent. Recent work proposed the use of water-miscible organic solvents to dissolve the polymer. This replaces the need for organic solvents to induce phase separation as aqueous solvents such as water can be used to extract the polymer solvent [97]. Finally, in the spray-drying method, the W/O emulsion is sprayed into a heated chamber that leads to a spontaneous production of drug-loaded particles. This method is more rapid and convenient and has fewer processing parameters than the other two but is limited by the adhesion of the formed particles to the inner surfaces of the drying chamber [94].

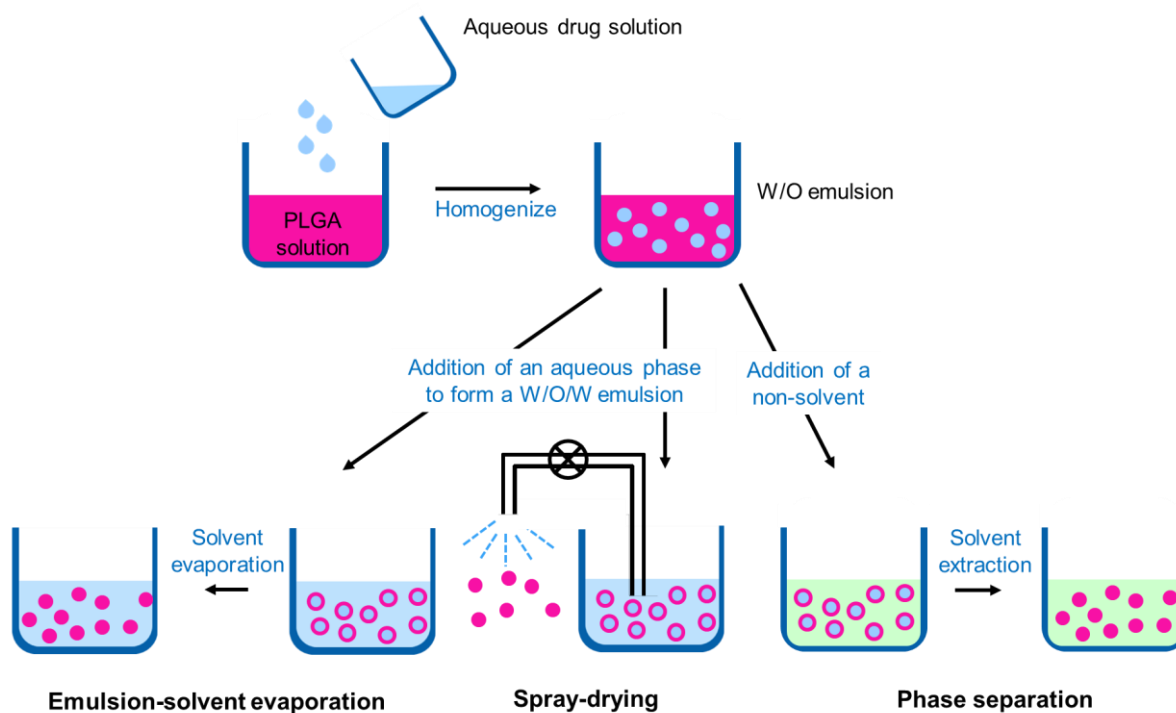


**Figure 1.7:** Examples of micro/nanoparticle preparation process.

Due to their small size, micro/nanoparticles can be administered either directly to the intended site of action or into the systemic circulation to reach a desired location by passive or active targeting mechanisms [98]. Several peptide-loaded polymer-based microparticle formulations have been approved by FDA for clinical use. The first one is Lupron Depot®, which received approval in 1989 to provide sustained release of leuprolide acetate for prostate cancer treatment [99]. A more recent example is Bydureon® that was approved in 2012, which releases exenatide to improve glycemic control in type 2 diabetes patients [100].

In general, the drug release from the particles is dependent upon the diffusion rate of the drug molecules and the degradation rate of the polymer-based matrix [94][99]. However, as significant proportion of the drug load can be weakly-adsorbed onto the large surface area of the micro/nanoparticles rather than incorporated in the polymer-based matrix, the drug release profile of this system is usually characterized by a huge initial burst that is followed by relatively short duration of release of the remaining drug load [101]. Another disadvantage of this system is that the particles can move away from the targeted drug release site. The gradual translocation of the particles can become more prominent as the size of the particle decreases [98]. This limits the potential of micro/nanoparticles as SDF-1 $\alpha$  delivery vehicles in tumor trapping application, due to the principle requirement for the vehicle to remain at the resection cavity border to maintain a uniform tumor-attracting field.

### 1.3.1.2. Hydrogels

Hydrogels are three-dimensional networks of cross-linked hydrophilic polymers. The cross-linking can be mediated by the physical interactions (e.g. hydrogen bonds, electrostatic interactions) between the polymer chains [102,103] or the covalent bonds resulting from the use of chemical crosslinkers (e.g. carbodiimide, glutaraldehyde) [104–107]. Most hydrogels are characterized by highly-porous structure. The pore size can range from 10 to 500  $\mu\text{m}$  and is dependent upon the degree of cross-linking in the hydrogel matrix [108,109]. The porous structure is responsible for the deformability of hydrogels, enabling them to conform to the shape of the site to which they are applied [110]. Due to their hydrophilicity, water-soluble drug molecules can be conveniently loaded into the porous structure of a pre-formed hydrogel. However, this is not always true for high molecular weight drug molecules such as proteins, which have diffusive limitations to their partitioning into the pores of the hydrogel [110]. The high dependency of the drug loading process on the pore size of the hydrogel also means that the loaded drug molecules are usually released rapidly at the site of application as the release process is governed mainly by the diffusion rate of the drug molecules through the pores [99]. In fact, the release of hydrophilic molecules from a hydrogel system typically lasts for only several hours or days, shorter than the release durations achieved with micro/nanoparticles made of hydrophobic polymers [99]. To counter this, several strategies to enhance drug-hydrogel interactions have been proposed, including the introduction of charged moieties into the hydrogel to boost ionic interactions [111] and the direct conjugation of the drug molecules to the hydrogel via covalent bond formation [112]. Another credible strategy to prolong drug release is to load the drug molecules directly into the hydrogel matrix during the hydrogel fabrication process instead of loading into the pores of a pre-formed hydrogel [113]. Finally, several groups proposed the strategy of pre-encapsulating drug molecules into suitable micro/nanoparticles and co-formulating the particulate system into the hydrogel matrix to achieve sustained drug release [114,115].

As virtually any water-soluble polymer can be manipulated to produce this system, it is possible to obtain hydrogels with physicochemical and biological properties that are useful for a wide range of applications. Despite this, the number of hydrogel-based drug delivery systems approved for clinical use is still limited. An example of these is Regranex®, which consists of a carboxymethylcellulose gel that releases recombinant human platelet-derived growth factor (becaplermin) for the treatment of diabetic foot ulcers [109].

In addition to the rapid drug release issue mentioned above, hydrogels possess several drawbacks that limit its use in tumor trapping application. Their poor mechanical strengths make them susceptible to premature dissolution [110], limiting the time window for tumor cell recruitment. In addition, in the absence of cell adhesive proteins, hydrogels tend to have low capacity for cell adhesion and attachment due to their low stiffness [116–118], suggesting that the system may not be able to retain the recruited tumor cells until the subsequent killing step.

### 1.3.1.3. Porous scaffolds

Porous scaffolds refer to three-dimensional solid polymer matrices characterized by interconnected pores. Generally, they are formed by removing the solvent from a polymer solution that leads to the precipitation of the polymer molecules. Methods that have been employed to produce porous scaffolds include freeze-drying [119], particulate leaching [120] and gas foaming [121]. In the first method, a polymer solution is initially frozen at a sub-zero temperature inside an airtight chamber. The pressure is then gradually decreased to vaporize the frozen liquid. As more and more solvent evaporates, the polymer molecules precipitate and solidify to form a porous scaffold [119]. In the particulate leaching method, a polymer solution is first mixed with salt particles of well-defined size. The polymer solvent is subsequently removed under vacuum, leaving behind a solid polymer matrix loaded with salt particles. The subsequent leaching of the salt particles in distilled water results in the formation of a porous scaffold [120]. Gas foaming is another common method used to make porous scaffolds. It relies on the nucleation and growth of gas bubbles in a polymer phase. Traditionally, the gas bubbles can be formed in situ by adding into the polymer phase a foaming agent such as ammonium bicarbonate, which generates inert gas such as CO<sub>2</sub> when the pH of the system is decreased. A porous scaffold is formed upon removal of the dispersed gas bubbles from the polymer phase [121]. Recently, supercritical fluids have been used as an alternative foaming agent. A supercritical fluid is any substance existing at a temperature and pressure above its critical point with an intermediate behavior between that of a liquid and a gas. The use of supercritical fluids is useful especially in making porous scaffolds from hydrophobic polymers as it circumvents the need for organic solvents during the preparation of the polymer phase. CO<sub>2</sub> is widely-used as a supercritical fluid due to its minimal toxicity and low cost. Initially, polymers can be dissolved or plasticized in supercritical CO<sub>2</sub>. Upon depressurization of the system, the rapid expansion of the polymer phase as a result of the escape of CO<sub>2</sub> gas leads to the formation of a porous scaffold [122,123].

Similar to hydrogels, the use of porous scaffolds as a drug delivery system can be achieved by loading drug molecules into the pores of a pre-formed scaffold or incorporating them directly into the polymer phase before the scaffold fabrication process. A notable example of clinically-used porous scaffold-based drug delivery systems is Infuse®, which consists of a porous collagen scaffold that can be conveniently loaded with recombinant human bone morphogenetic protein-2 (BMP-2) prior to administration in patients undergoing bone reconstruction procedure [124]. Interestingly, the osteoinductive effect of this treatment relies on the chemotactic effect of BMP-2 that induces the infiltration of mesenchymal stem cells (MSCs) into the pores of the collagen scaffold (Figure 1.8) [125]. The considerable mechanical strength of the scaffold means that it can withstand the traction forces generated during cell attachment and migration, thus sustaining the cell infiltration process. After initial proliferation, the MSCs are further stimulated by BMP-2 to undergo differentiation into bone-forming osteoblasts to enable new bone formation [126]. Considering its huge clinical success, Infuse® presents a working example to the idea of using a chemotactic agent and a suitable scaffold to recruit a certain cell population.

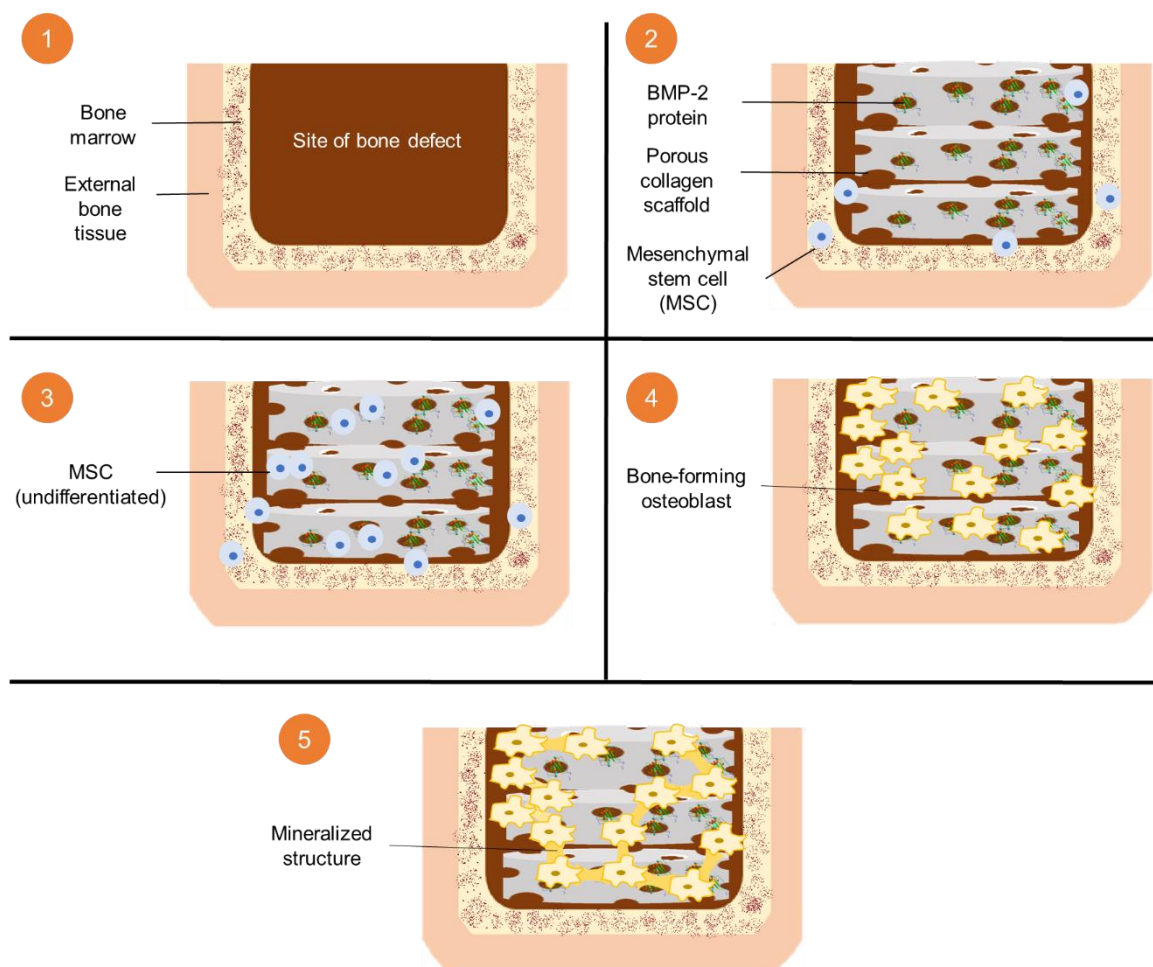


**Figure 1.8:** Schematic description of the bone healing action of Infuse®. During a bone reconstruction surgery, the site of bone defect can be accessed (1) and filled with the Infuse® bone graft consisting of BMP-2-loaded porous collagen scaffolds to recruit MSCs by chemotaxis (2). Upon infiltration into the injury site, the MSCs proliferate to increase their number (3) before undergoing differentiation into the bone-forming osteoblasts (4), which secrete collagen and calcium-binding proteins to support the formation of mineralized bone tissues.

### 1.3.2. Fibrous scaffolds as a polymer-based protein delivery system

Fibrous scaffolds refer to scaffolds made of fibers with diameters on the order of several micrometers down to the tens of nanometers that are stacked layer-by-layer to form a three-dimensional non-woven mesh (Figure 1.9). Compared to micro/nanoparticles, hydrogels and porous scaffolds, the use of fibrous scaffolds as a delivery vehicle for therapeutic proteins is less common despite many advantages offered by this system. This being said, the amount of research conducted to investigate the value of fibrous scaffolds in this field of application has increased steadily over the last two decades and multiple strategies for loading protein molecules into fibrous scaffolds have been proposed.

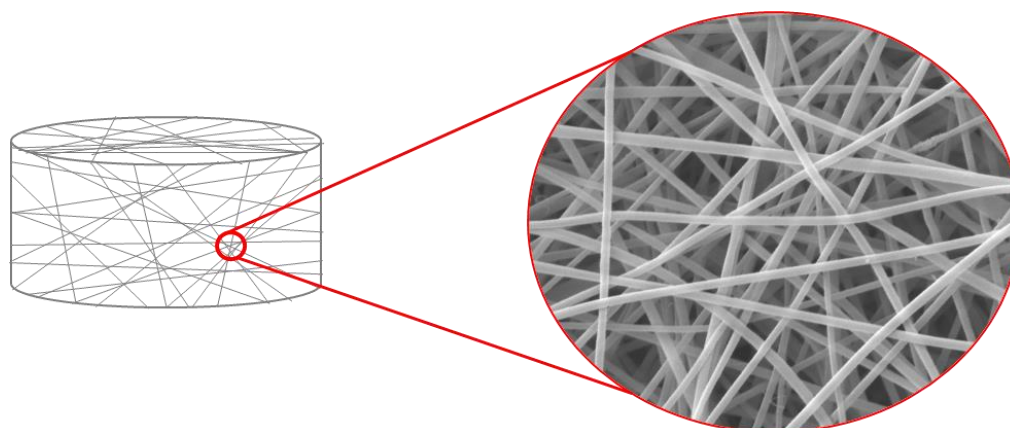


**Figure 1.9:** A simplified representation of a fibrous scaffold and its internal structure.

### 1.3.2.1. Fibrous scaffolds with embedded protein molecules

Depending on the scaffold preparation technique, protein molecules can be embedded randomly in the fibers or partitioned into a specific fiber compartment as in the case of core-shell fibers (Figure 1.10). Chew *et al.* incorporated  $\beta$ -nerve growth factor (NGF) into fibers made of poly( $\epsilon$ -caprolactone-ethyl ethylene phosphate) (PCLEEP) and examined the release profile. They observed that the fibrous scaffold was able to sustain NGF release over a period of 90 days. They claimed that the slow degradation of PCLEEP contributed to the sustained release profile as NGF molecules could only be released by diffusion through the hydrophobic matrix of the fiber [127]. On the other hand, Zhang *et al.* produced fibers with a core-shell structure as a vehicle to deliver bovine serum albumin (BSA). The outer shell was made of the hydrophobic PCL while the core compartment dispersed with the BSA molecules was made of the hydrophilic poly(ethylene glycol) (PEG). They reported that the core-shell system produced lower initial burst and longer duration of BSA release than fibers made of a single blend of PCL, PEG and BSA [128]. Jiang *et al.* further explored the possibility of tuning the kinetics of protein release from core-shell fibers. They showed that by varying the mass ratio of PCL and PEG in the outer shell, the time to achieve complete release of BSA from the inner dextran core could be varied from one week to approximately one month. BSA release was accelerated with increasing PEG mass in the outer shell as its water-solubility resulted in formation of pores through which BSA molecules could escape from the dextran core [129].

Protein molecules may also be encapsulated into micro/nanoparticles prior to incorporation into fibrous scaffolds. Liu *et al.* prepared dextran-based nanoparticles loaded with basic fibroblast growth factor (bFGF) that were subsequently embedded in poly(L-lactic acid) (PLLA) nanofibers. The duration of bFGF release provided by the nanoparticle-nanofiber

composite scaffold was 10 days longer compared to what was achieved with nanofibers with directly embedded bFGF (28 vs. 18 days). In addition, the encapsulation of bFGF into the dextran-based nanoparticles was also useful in reducing bFGF structural changes during the fiber-making process [130]. Qi *et al.* also adopted a similar approach. They incorporated BSA-loaded alginate microparticles into PLLA fibers and observed that the composite scaffold produced a longer duration of BSA release compared to the naked alginate microparticles [131].

### 1.3.2.2. Fibrous scaffolds with surface-bound protein molecules

Alternatively, protein molecules can be loaded onto the surface of a pre-fabricated fibrous scaffold. This is especially useful when preparing protein-loaded fibrous scaffold using a hydrophobic polymer and there is a need to reduce the exposure of the protein molecules to organic solvents that are needed to solubilize the polymer prior to the scaffold fabrication step. The nano/micro dimension of the fibers confer a large surface area for adsorption of protein molecules. In fact, the amount of protein that can be adsorbed by a fibrous scaffold is generally four times greater than that afforded by a porous scaffold of equal volume [132].

Immobilization of protein molecules to the surface of the fibers can be mediated by non-covalent interactions including hydrophobic interaction, van der Waals interaction, hydrogen bonding and electrostatic interaction. Heparin, a naturally-occurring polysaccharide, is known to have strong binding affinity for various growth factors (e.g. VEGF, transforming growth factor- $\beta$  (TGF- $\beta$ )), morphogens (e.g. BMP-2, BMP-7, BMP-14) [133] and extracellular matrix (ECM) proteins (e.g. laminin) [134] due to its ability to form non-covalent interactions with these proteins. Therefore, heparin-functionalized fibrous scaffolds can be conveniently loaded with these proteins for local delivery applications. Casper *et al.* prepared poly(ethylene oxide) (PEO) and poly(lactic-co-glycolic acid) (PLGA) nanofibers functionalized with low molecular weight heparin (LMWH) that were adsorbed with bFGF. To slow down the dissociation of LMWH from the fibrous scaffold and thus prolong the duration of bFGF release, LMWH was conjugated to PEG prior to its incorporation into the nanofibers. Although the bFGF release profile was not assessed in their study, they reported that LMWH was retained in the fibrous scaffolds for at least 14 days [135]. Furthermore, Patel *et al.* prepared heparin-functionalized PLLA nanofibers as a delivery vehicle for bFGF and laminin. The adsorption of bFGF and laminin to the surface of PLLA nanofibers was very stable, with less than 0.1% of the total amount of immobilized protein molecules released into the surrounding solution after 20 days.

The slow release of the adsorbed protein molecules could be useful in certain neuroregenerative applications as the immobilized bFGF was found to be as effective as its soluble counterpart in inducing neurite outgrowths from dorsal root ganglion tissues [136]. Fiber surfaces can also be adsorbed with protein-loaded nanoparticles. Wei *et al.* prepared BMP-7-loaded PLGA nanoparticles that were subsequently immobilized onto PLLA nanofibers. They reported that the release kinetics of BMP-7 could be controlled by varying the degradation rate of the PLGA nanoparticles. However, as the nanoparticle surfaces were exposed to the surrounding solutions, a characteristic burst release could be observed with each formulation of BMP-7-loaded PLGA nanoparticles prepared in their study [137].

Another widely-used method for functionalizing fiber surfaces with proteins is by chemical immobilization. This approach results in formation of covalent bonds between the fiber surfaces and the protein molecules. As the covalently-attached protein molecules cannot be easily desorbed from the fibers, this functionalization method is especially useful in many regenerative applications, where long-term immobilization of protein molecules in the fibrous scaffold is often necessary for the reparative actions to take place. Primary amine and carboxyl groups are the most common example of functional groups utilized in covalent conjugation of fibers and protein molecules. Many groups have prepared polymer-based nanofibers functionalized with carboxyl groups that can be activated by a combination of 1-ethyl-3-(3-dimethylaminopropyl) carbodiimide (EDC) and N-hydroxysuccinimide (NHS) for subsequent conjugation with primary amine groups present in protein molecules. Ye *et al.* prepared nanofibers from poly(acrylonitrile-co-maleic acid) (PANCMA) that were subsequently functionalized with lipase. However, the immobilized lipase molecules were found to have lower enzymatic activities than their soluble counterparts [138]. A similar loss in activity was also reported by a group that functionalized polystyrene (PS) nanofibers with  $\alpha$ -chymotrypsin [139]. There are two possible explanations for the partial inactivation of the immobilized enzymes. First, the immobilization process may introduce covalent alterations to the active sites of the enzyme. The other is that direct conjugation of protein molecules to the fiber surfaces may cause certain parts of the immobilized molecules to be sterically inaccessible to their corresponding ligands [140]. To address the latter issue, several polymer-based linkers have been utilized to introduce a physical gap between the immobilized molecules and the fiber surfaces. To obtain these linkers, primary amine-terminated hydrophilic polymers such as PEG-diamine can be chemically-conjugated to a hydrophobic polymer such as PCL and PLGA. The linker can then be mixed with an unconjugated hydrophobic polymer to prepare fibers

displaying primary amine groups on their surface that can be conjugated with protein molecules. Choi *et al.* immobilized EGF on the surface of fibers composed of PCL and PCL-PEG-NH<sub>2</sub> for wound healing applications. They showed that the EGF-functionalized fibers were able to induce differentiation of keratinocytes to a greater extent than fibers supplemented with EGF solution. The enhanced activity of the former could potentially be attributed to the fact that covalently-immobilized EGF could be better retained at the wound site and thus was able to induce more durable pro-differentiation signals in the locally-residing keratinocytes [141]. Kim *et al.* also utilized a polymer-based linker to conjugate lysozyme to the surface of PLGA nanofibers. The immobilized lysozyme displayed comparable activity to its soluble counterpart [142]. This is opposite to the significant loss of enzymatic activities observed with direct conjugation of enzyme molecules to the fiber surfaces as discussed above.

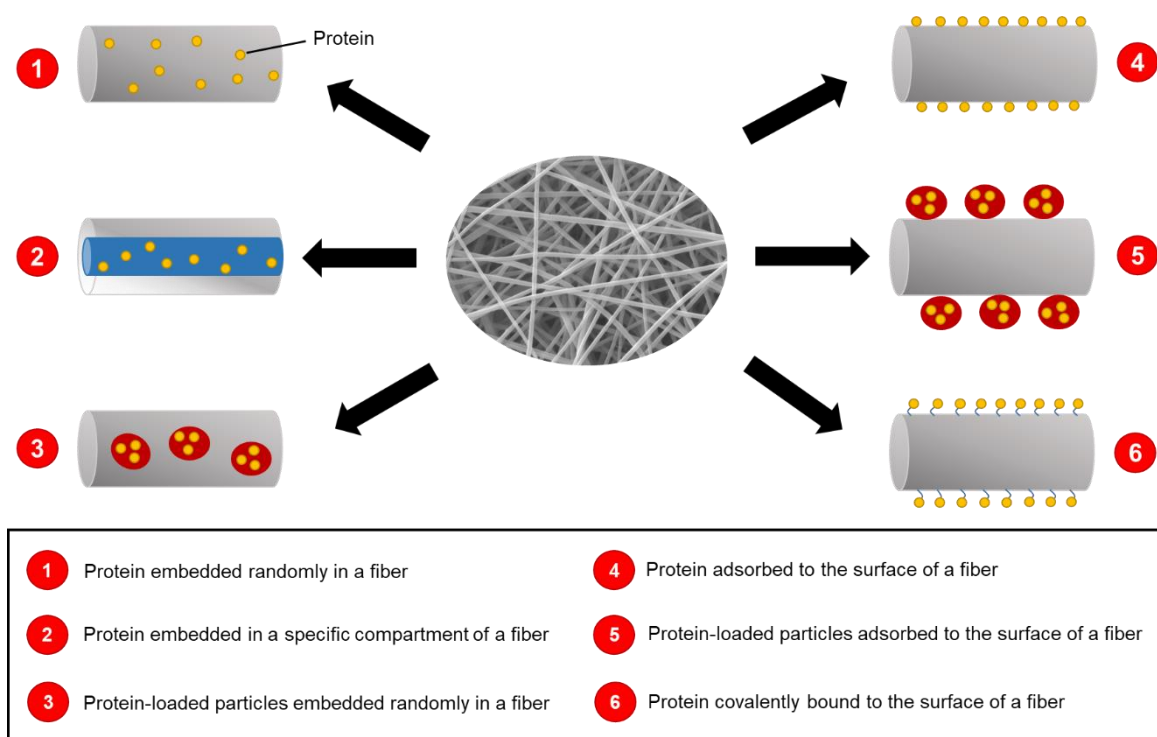


**Figure 1.10:** Different modes of protein loading into a fibrous scaffold. Adapted from [143,144].

### 1.3.3. Electrospinning as a method to prepare protein-loaded fibrous scaffolds

In addition to their great potential to function as a delivery system for proteins such as SDF-1 $\alpha$  as discussed in the previous section, fibrous scaffolds are known to provide excellent substrates for cell adhesion and migration [145–147]. Their large surface area enables extensive adsorption of adhesive proteins commonly found in the ECM such as fibronectin and vitronectin that mediate cell interactions with the scaffold [132]. Furthermore, the range of

fiber diameter in these scaffolds correlates to the size scale of the fibrous ECM network, providing suitable structural and potentially mechanical cues for cell migration [148,149]. Relevant modifications during their preparation process may also permit fabrication of fibrous scaffolds with a degree of porosity that is most conducive to cell infiltration to maximize tumor cell trapping capacity.

Electrospinning is arguably the most common method of producing fibrous scaffolds. Table 1 summarizes the work that utilized electrospinning to fabricate fibrous scaffolds loaded with therapeutic proteins. The widespread use of electrospinning is driven by its relative ease of use and versatility. By changing one or more of its processing parameters, this method can permit the fabrication of micro/nanofibers from a number of natural and synthetic materials. The possibility of varying the diameter, orientation and composition of the electrospun fibers means fibrous scaffolds with a wide range of mechanical and biological properties can be prepared. In addition, proteins such as SDF-1 $\alpha$  can be loaded conveniently into fibrous scaffolds during or after electrospinning to form protein delivery systems.

**Table 1:** Fibrous scaffolds loaded with therapeutic proteins prepared by electrospinning.

Polymer	Protein	Application	Mechanism of protein loading	References
PCLEEP	NGF	Nerve regeneration	Direct embedment	[127]
PLLA	bFGF	Tendon regeneration	Embedment as protein-loaded particles	[130]
PEO/PLGA	bFGF	Nerve regeneration	Heparin-mediated surface adsorption	[135]
PLLA	bFGF	Nerve regeneration	Heparin-mediated surface adsorption	[136]
PCL/PCL-PEG	EGF	Treatment of diabetic ulcers	Chemically-mediated surface adsorption	[141]
PLLACL/collagen	BMP-2	Bone tissue engineering	Direct embedment	[150]
PCL/PEO	bFGF	Connective tissue regeneration	Direct embedment	[151]
PCL	PDGF	Non-specific tissue engineering	Direct embedment	[151]
PLCL	VEGF	Cardiac tissue engineering	Direct embedment	[152]

### 1.3.3.1. Overview of the electrospinning process

Electrospinning involves the use of high voltage to draw fibers out of a solubilized or molten polymer. A typical electrospinning setup consists of a capillary (e.g. a metal needle) through which the polymer solution/melt to be electrospun can flow, a high voltage generator and a grounded collector (Figure 1.11A). A syringe pump is usually employed to maintain a constant flow of the polymer solution/melt towards the tip of the capillary. An electrode from the high voltage generator is then attached to the capillary to introduce charges of a certain polarity into the polymer phase. As the voltage is increased, there will be an increasing repulsion between the like charges in the liquid. Simultaneously, the attractive force between the liquid and the collector arising from their opposite polarity becomes stronger. These two forces combine to stretch the pendant drop at the tip of the capillary (Figure 1.11B). Eventually, these forces balance the surface tension of the liquid, causing the leading edge of the liquid to change from a rounded meniscus to what is known as the Taylor cone. Upon further increase in the electric field strength, a fiber jet is eventually ejected from the tip of the cone and subsequently accelerated towards the grounded collector [153,154].

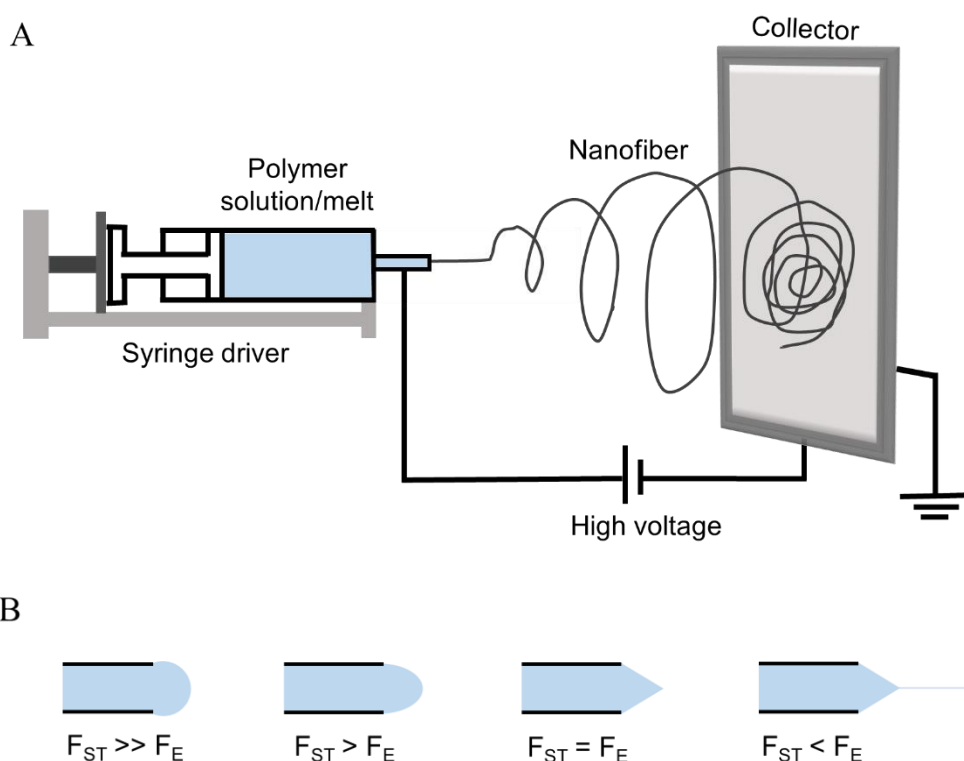


**Figure 1.11:** (A) A schematic representation of a typical electrospinning setup. (B) The interaction between surface tension ( $F_{ST}$ ) and electrostatic force ( $F_E$ ) at the tip of the capillary. The increasing electrostatic force initially stretches the pendant drop. When it matches the surface tension of the liquid, a Taylor cone is formed. Eventually, a fiber jet is formed when the electrostatic force exceeds the surface tension.

As the fiber jet travels through the atmosphere towards the collector, the interactions between the charges in the jet and the applied electric field induce a chaotic bending instability, which increasing the path length to the collector. The corresponding increase in the transit time of the jet allows for more complete solvent evaporation and further decrease in the jet diameter. In fact, as the jet gets thinner, the like charges in it are brought closer to one another, leading to an increase in the repulsion that further contributes to the chaotic whipping movement and reduction in the fiber diameter [155]. The jet whipping can be so rapid that it may appear as if it has split into multiple smaller fibers [156]. However, recent studies employing high speed photography confirmed that the jet reached the collector as a single, rapidly whipping fiber [157].

The fiber jet is eventually deposited onto the collector to gradually form a non-woven mat. Depending on the intended application, a range of collector configurations has been studied to manipulate the overall structure and shape of the fibrous scaffold. The use of a stationary collector can lead to the assembly of fibers with random orientation [158–160]. On the other hand, mats composed of aligned fibers can be formed using a rotating collector [161–163]. Regardless of the degree of anisotropy, fibrous mats generated by electrospinning tend to have high fiber packing density, which may be less desirable in applications requiring cell infiltration into the scaffold. However, the packing density may be reduced by using a collector made of a material with low conductivity. Liu and Hsieh found that the porosity of cellulose acetate fibrous scaffolds increases when the fibers were collected on a piece of paper instead of a copper mesh. Non-conducting collectors are less capable of dissipating the charges entrapped in the deposited fibers than collectors made of conductive materials, resulting in increased electrostatic repulsions and thus a looser packing of the fibers. The same authors also found that by using a more porous collector, the fiber packing density could be decreased. For example, fibers collected on a copper mesh were more loosely packed than those deposited onto a piece of aluminum foil. This could be due to the difference in the rate of diffusion and evaporation of solvents from fibers deposited on the different targets. The authors hypothesized that the slower removal of solvent molecules from fibers collected on solid targets may cause the fibers to be pulled together and pack more closely [164]. Finally, it is also possible to control the final shape of the generated fibrous scaffold by changing the geometry of the collector. For example, a flat piece of aluminum foil can be used to form a sheet [159,160], while a tubular structure can be obtained by using a rotating rod or drum [165,166].

### 1.3.3.2. Important processing parameters in electrospinning

Despite its relative ease of use, electrospinning can only generate uniform fibers if several processing parameters have been carefully optimized. These parameters include the applied voltage, the flow rate of the polymer solution/melt and the distance between the capillary tip and the collector.

- Applied voltage

As the applied voltage influences the strength of the stretching force on the pendant drop at the tip of the capillary, there is a threshold voltage for the Taylor cone formation and fiber jet generation for each polymer solution/melt. However, the effect of applied voltage on the morphology of the electrospun fibers has been rather controversial. Contradicting results have been reported by research groups who studied different types of polymer. Yuan *et al.* observed that increasing voltage does not significantly change the overall morphology of polysulfone nanofibers [167]. A similar result was obtained by Zhu *et al.* who studied poly(vinylidene fluoride) (PVDF) nanofibers [168]. However, Lee *et al.* reported a decrease in poly(vinyl alcohol) (PVA) fiber diameter with increasing applied voltage [169]. This finding was echoed by Beachley and Wen when the pair who produced nanofibers from different concentrations of PCL solution [170]. The decrease in fiber diameter could be explained by the greater stretching force exerted on the pendant drop at the capillary tip with higher applied voltage, leading to more pronounced jet elongation (Figure 1.12). Interestingly, Meechaisue *et al.* found that increasing the electric field strength actually increases the diameter of poly(desaminotyrosyl-tyrosine ethyl ester carbonate) (PDTEC) [171]. A potential explanation for this is that as the voltage reaches a certain value, the attractive force between the travelling fiber jet and the collector becomes so strong that it reduces the flight time and thus decreases the stretching time of the jet prior to its deposition on the collector (Figure 1.12). With this, it can be concluded that the influence of voltage over fiber diameter varies across different polymer solutions and may be dependent on other processing and solution parameters.

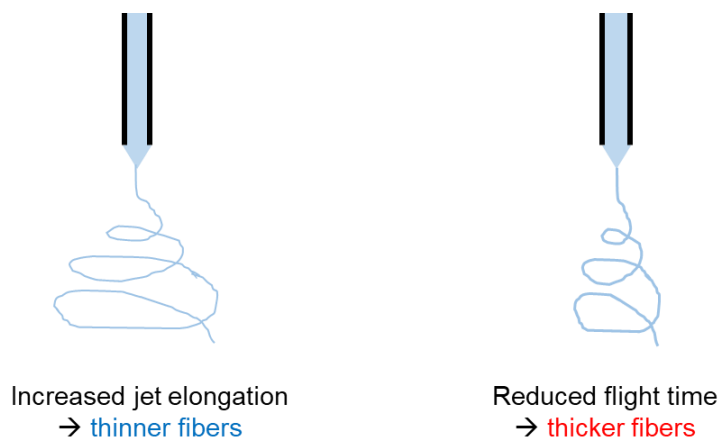


**Figure 1.12:** Two possible outcomes of increasing the applied voltage in electrospinning. Alternatively, the two effects may balance each other out to cause no change in the fiber diameter.

- Solution flow rate

To produce uniform fibers, it is important to maintain the balance between the flow rate of the polymer solution/melt through the capillary and the rate at which the liquid is ejected toward the collector. Zargham *et al.* showed that at this optimum flow rate, a stable and symmetric Taylor cone can be formed that permits production of fibers with a narrow diameter distribution (Figure 1.13) [172]. Beyond this point, beaded nanofibers of larger diameter may be produced [173,174]. The formation of beads at high flow rates could be a result of excess liquid that accumulated at the tip of the capillary being ejected as intermittent lumps of polymer instead of a smooth jet (Figure 1.13) [175]. High flow rates can also distort the shape of the Taylor cone and increase the initial radius of the ejected fiber jet that leads to deposition of large ribbon-like fibers on the collector [176]. Conversely, when the flow rate is below its optimum value, fiber diameter tends to decrease as the Taylor cone recedes and the fiber jet is ejected from the inside of the capillary (Figure 1.13) [172]. Someswararao *et al.* reported that the diameter of titanium dioxide-poly(vinyl pyrrolidone) (TiO<sub>2</sub>-PVP) nanofiber decreased from 247 to 111 nm as the flow rate of the liquid material was reduced from 1.2 to 0.6 mL/h. They also observed that the reduction in fiber diameter coincided with a decrease in the formation of beads [177].

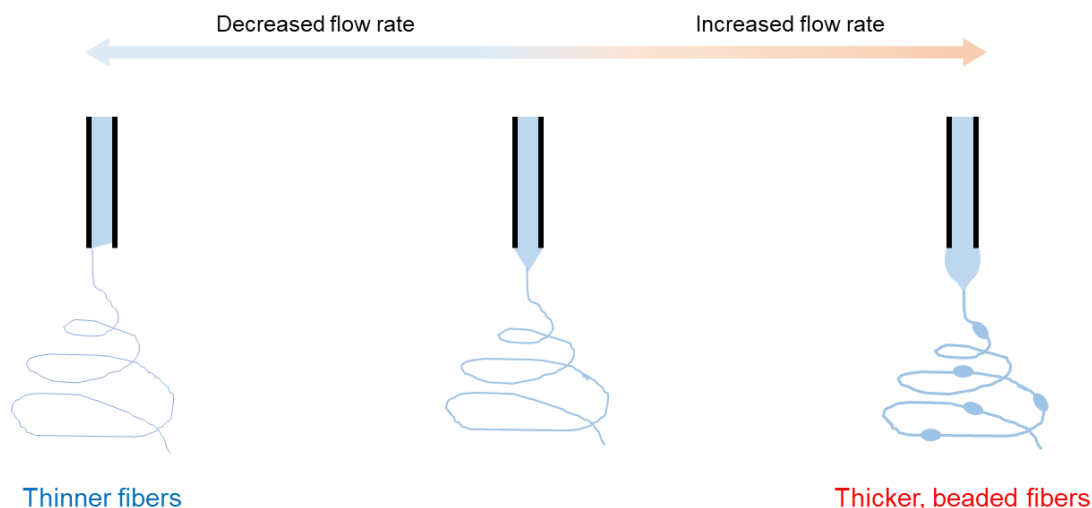


**Figure 1.13:** Effect of changing solution flow rate on the morphology of electrospun fibers.

- Tip-to-collector distance

The distance between the tip of the capillary and the collector is another key parameter that influences the morphology of the electrospun fibers. This parameter determines the travel time for the jet fiber to reach the collector. As mentioned earlier, the jet fiber undergoes chaotic bending instabilities that causes it to whip around during its travel through the atmosphere, which increases the path length to the collector, leaving more time for solvent evaporation and fiber thinning. If the distance between the capillary tip and the collector is too short, the path length of the jet is shortened and there is less time for fiber drying and thinning. The subsequent diffusion of the residual solvent out of the deposited fibers can contribute to the formation of fused fibers [178]. Typically, a distance of between 10 to 15 cm is needed to achieve a flight time that is sufficient for complete solvent evaporation [167,169,171,174–176]. As the distance is increased, dry fibers of thinner diameter can be produced [179,180]. However, beyond a certain limit, fiber diameter may start to increase again, and fusion of fibers deposited on the collector may reappear. As the bending instability that is responsible for the elongation of the fiber jet depends on the electrostatic interaction between the charged jet and the external electric field, too high of a capillary tip-collector distance will result in a weaker electric field strength that contributes to less whipping movement of the jet and a shorter path length to the collector. This consequently reduces the time available for fiber thinning and solvent removal [178].

### 1.3.3.3. Important solution parameters in electrospinning

Equally important as the processing conditions to the success of electrospinning are the properties of the polymer solution or melt itself. Electrospinning of polymer melt takes place at high temperature to maintain the fluidity of the material and thus is less useful in preparing fibrous scaffolds loaded with protein molecules that are often thermally labile. Therefore, solubilization of a polymer in a suitable solvent is a more popular way of preparing materials for electrospinning. Depending on several solution parameters, the same polymer and processing conditions can yield fibers of very different morphologies. These parameters include the solution viscosity, solvent volatility and solution conductivity.

- Solution viscosity

The viscosity of a polymer solution determines whether a fiber jet can be ejected towards the collector or not. This parameter is closely related to the concentration and molecular weight of the dissolved polymer. When the viscosity is too high, the electrostatic force induced by the applied voltage may not be sufficient to induce the formation of Taylor cone and subsequent jet ejection. Conversely, if the solution is too dilute, the fiber jet will break up into droplets during its travel through the atmosphere. Thus, there is an optimum range of viscosity in which a stable fiber jet can be ejected when all other processing and solution parameters are kept constant. For example, Doshi and Reneker prepared PEO solutions with different viscosities by dissolving different amount of the polymer in a given volume of water. They reported that only those solutions with viscosity ranging from 800 to 4,000 centipoises (cP) can be electrospun to generate nanofibers [181]. Within the optimal viscosity range, fibers of larger diameter can be obtained with increasing viscosity. Huan *et al.* observed that the diameter of PS nanofibers increased from 1 to 5  $\mu\text{m}$  as the concentration of PS solution in dimethylformamide (DMF) is increased from 23 to 40% (w/v), which corresponded to an increase in viscosity from 300 to 1210 cP [182]. On the other hand, Nezarati *et al.* varied the viscosity of poly(carbonate urethane) (PCU) solution by dissolving the same mass of different molecular weight variants of this polymer in N,N-dimethylacetamide (DMAc). They showed that a small decrease in PCU molecular weight (from 241 to 217 kDa) could significantly reduce the viscosity of the polymer solution (from 10,000 to 8,000 cP). They also reported that the solution with the lower viscosity yielded fibers with more beads. This could be due to the increasing effect of surface tension, which forces the travelling fiber jet to assume a more rounded shape to reduce the surface area [183].

- Solvent volatility

Solvent volatility influences the minimum flight time required for complete solvent evaporation and obtention of dry fibers on the collector. As less volatile solvents require a longer time to evaporate, polymer solutions prepared from these solvents are more likely to contribute to the generation of fused fibers if appropriate changes in the processing conditions such as increasing the capillary tip-collector distance and decreasing the relative humidity are not implemented. Yuya *et al.* prepared 10% (w/v) solutions of PVP in four solvents with different volatility; methanol (boiling point (BP) = 64.7 °C), ethanol (BP = 78.4 °C), water (BP = 100 °C) and DMF (BP = 153 °C). All solutions were eventually electrospun at a relative humidity of 30% and a capillary tip-collector distance of 15 cm. With the solutions prepared from the more volatile methanol and ethanol, dry fibers could be deposited on the collector. Conversely, blobs and films were obtained with the solutions prepared from water and DMF [184]. The use of volatile solvents does not only permit the production of dry and separate fibers, but also encourage the formation of pores on the fiber surfaces. Megelski *et al.* studied the surface structure of PS nanofibers electrospun from solutions containing DMF and tetrahydrofuran (THF) (BP = 66 °C) at different ratios. They observed that PS solutions containing THF produced fibers with porous surfaces, and the pores became smaller and more frequent as the proportion of THF in the total solvent volume was increased [185]. A similar result was also obtained by Celebioglu and Uyar. The pair reported that fibers with porous surfaces can be obtained from a solution of cellulose acetate in a mixture of dichloromethane (DCM) (BP = 39.6 °C) and acetone (BP = 56.1 °C). However, the microtexture disappeared and fibers with smooth surfaces were obtained when DCM was replaced with the less volatile DMAc (BP = 165 °C) [186]. The formation of porous fibers with the use of volatile solvents increases the surface area of the formed fibrous scaffolds, which may be beneficial in drug delivery applications as more drug molecules can be adsorbed onto the fiber surfaces. However, using solvents that are too volatile may hinder the formation of continuous fibers altogether. If a solvent evaporates too fast, solidification of polymer may take place at the capillary tip. The solids may grow and eventually block the flow of the polymer solution. As more solution is delivered toward the tip, the increasing pressure inside the capillary may dislodge the solidified plug, enabling the ejection of a new fiber jet. However, this intermittent fiber formation is likely to promote the introduction of artefacts onto the collector [154].

- Solution conductivity

Solution conductivity determines the magnitude of electrostatic force exerted on a fiber jet. Highly conductive solutions carry high number of charges per unit volume and thus will be subjected to a stronger electrostatic force in an electric field of a certain strength than will a solution of low conductivity. This property is also responsible for greater bending instabilities observed with fiber jets ejected from highly conductive polymer solutions that lengthen the jet path to the collector. Consequently, the diameter of electrospun fibers often decreases with an increase in the conductivity of the polymer solution [187]. Two most common ways of changing the solution conductivity is by varying the concentration or type of salt dissolved in the polymer solution. Zhang *et al.* dissolved different amount of NaCl in the same volume of PVA solutions and measured the diameter of fibers electrospun from these solutions. As the NaCl concentration was increased from 0.05 to 0.2 % (w/v), the solution conductivity increased from 1.53 to 10.5 mS/cm and the fiber diameter decreased from 214 to 159 nm. The authors claimed that an increase in NaCl concentration can increase the net charge density of the fiber jet, resulting in a greater electrostatic force exerted on the jet that favors its elongation and thinning [175]. On the other hand, Zong *et al.* prepared poly(D,L-lactic acid) (PDLA) solutions containing the same concentration of three different salts; NaCl, NaH<sub>2</sub>PO<sub>4</sub> and KH<sub>2</sub>PO<sub>4</sub>. They found that the diameter of fibers electrospun from the NaCl-containing solution was 210 nm, but this value increased to 330 and 1000 nm when NaCl was replaced with NaH<sub>2</sub>PO<sub>4</sub> and KH<sub>2</sub>PO<sub>4</sub> respectively. The authors proposed that ions with smaller atomic radius have a higher mobility in an electric field than larger-sized ions of the same net charge. The higher mobility leads to better conductivity and thus greater electrostatic force exerted on the jet [188]. Although the addition of salts into a polymer solution generally reduces the diameter of the electrospun fibers, in some cases, the opposite may happen. Mit-uppatham *et al.* prepared polyamide-6 solutions containing different concentrations of NaCl or LiCl. While the solution conductivity increased with increasing salt concentration, the solution viscosity also followed the same trend. The authors proposed that the increase in the viscosity outweighed the increase in the electrostatic force exerted on the fiber jet, resulting in fibers with larger diameter [189]. Based on these results, it is important to consider any potential interaction between the salt and polymer molecules when attempting to vary the solution conductivity to achieve control over the fiber diameter.

### 1.3.3.4. Nozzle configuration options in electrospinning

Depending on the modes of protein loading, different nozzle configurations can be employed to produce fibers with different internal structures. These include single, side-by-side and co-axial nozzle configurations.

- Single nozzle configuration

The most common and straightforward configuration involves the use of a single nozzle where a polymer solution is channeled through a single capillary during electrospinning. This configuration has been used to electrospin polymer-protein co-solutions and emulsions consisting of an inner protein phase and an external polymer phase. In the former case, Zeng *et al.* co-dissolved PVA and BSA or luciferase in water and electrospun the co-solution to produce protein-loaded nanofibers. Both proteins could be incorporated into the PVA nanofibers. The authors also coated the electrospun nanofibers with poly(*p*-xylylene) (PPX) using a technique called chemical vapor deposition polymerization. The PPX coating helped to minimize the burst release of proteins from the PVA nanofibers [190]. For the preparation of protein-loaded nanofibers from hydrophobic polymers, protein solutions can be emulsified in a polymer-containing organic phase prior to electrospinning. Maretschek *et al.* emulsified an aqueous solution of cytochrome *c* in PLLA-containing chloroform and electrospun the emulsion. To vary the cytochrome *c* release kinetics, they include different concentration of hydrophilic poly(ethylene imine) (PEI) into the aqueous phase. The authors observed that the rate of release is proportional to the PEI concentration in the emulsified cytochrome *c* solution [191].

- Side-by-side/co-axial nozzle configuration

In certain cases, generation of nanofibers with distinct compartments made of different polymers may be useful to achieve better control over the drug loading and release processes. Two types of nozzle configurations, namely side-by-side and co-axial (Figure 1.14), are commonly used to produce such nanofibers. In these configurations, component polymers are dissolved separately instead of blended into a single solution. The individual polymer solutions are then forced to flow through separate capillaries, never coming into contact with each other until they reach the very end of the capillaries. As such, these configurations are useful to produce fibers from a combination of polymers that are not mutually soluble (e.g. hydrophobic vs. hydrophilic polymer) or interact non-favorably (hydrophilic polymers with opposite charge) in a common solvent. In the side-by-side nozzle configuration, two separate polymer

solutions flow through two equally sized capillaries placed next to each other. This setup usually results in fibers composed of two distinct halves; each contributed by one of the two polymer solutions. However, to achieve this balanced fiber composition, it is important that the processing parameters (e.g. flow rate) and solution parameters (e.g. viscosity and conductivity) of the component polymer solutions are kept roughly the same. Gupta and Wilkes conducted side-by-side electrospinning of bicomponent polymer systems in the form of (1) poly(vinyl chloride) (PVC) and segmented polyurethane (PU) (PVC/PU) and (2) PVC and poly(vinyl fluoride) (PVF) (PVC/PVF). They found that for each of the two systems, two Taylor cones and subsequently two fiber jets were generated. They claim that this was due to the much higher conductivity of the PVC solution compared to the PU or PVF solution. Upon decreasing the electric field strength to minimize the difference in the electrostatic force exerted on the solutions, a single Taylor cone could be generated from each system to ensure production of fibers with a more balanced composition [192]. In the more widely used co-axial nozzle configuration, two separate polymer solutions are forced through two different-sized capillaries, where the larger capillary encases the smaller one. Consequently, this setup produces fibers with a distinct core-shell morphology. Core-shell fibers have been used as a vehicle for many therapeutic proteins including bFGF [151], BMP-2 [150], platelet derived growth factor (PDGF) [193] and EGF [194]. Similar to the side-to-side configuration, the success of coaxial electrospinning requires that the two polymer solutions to have similar conductivity and viscosity. However, due to the difference in the size of the two capillaries, it is important that the flow rate in the outer capillary is set to be higher than that in the inner one. The recommended relative flow rate of polymer solution in the two capillaries may depend on multiple factors such as polymer type, solution concentration and the actual size of the two capillaries, but a ratio of between 3:1 to 16:1 has been shown to produce uniform core-shell fibers [150,151,193–195]. Regardless of the slight differences in the processing requirement between the side-to-side and the coaxial configuration, both setups produce compartmentalized fibers composed of two or more polymers. By varying the type of the constituent polymers, the physicochemical properties of each fiber compartment can be tailored accordingly to achieve better control over the release kinetics of the protein load. For example, the incorporation of protein molecules into a hydrophobic compartment that is stable to hydrolytic degradation may help to slow down protein release. Furthermore, the spatial distribution of the protein molecules also dictates the kinetics of release. In core-shell fibers, proteins loaded into the outer shell may be released quicker than when they were loaded into the inner core.

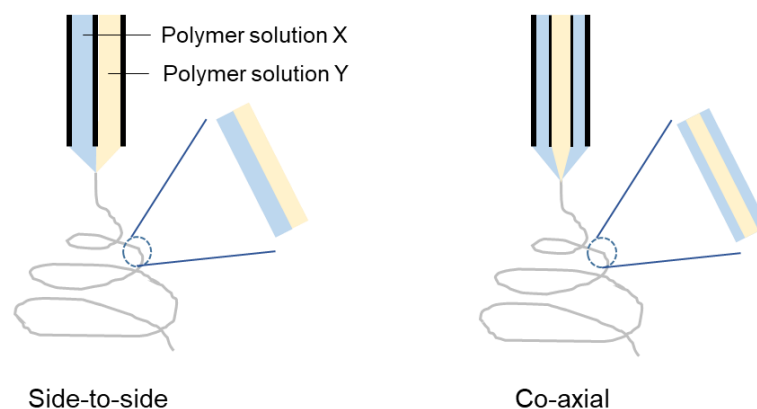


**Figure 1.14:** Schematic representation of the side-to-side and co-axial nozzle configurations and the typical structure of fibers produced from these setups.

### 1.3.3.5. Polymers for electrospinning

Various polymers have been successfully electrospun to produce micro/nanofibers for numerous biomedical applications. These polymers can be roughly categorized into natural and synthetic polymers. Of particular interest is the former group as these polymers generally offer excellent biocompatibility due to their biologically relevant structures. These polymers include polysaccharides (e.g. alginate, hyaluronic acid, cellulose, chitin and chitosan) (Figure 1.15) and protein-based polymers (e.g. collagen, silk) and they are extractable from numerous animal-based and plant-based sources. Some of these polymers are constituents of the human ECM, granting them desirable biological properties that include good cell adhesion and proliferation capacity. However, their natural origin may also introduce several drawbacks. These include batch-to-batch variations, complex purification procedures and the possible transmission of disease from the source organisms. In the context of electrospinning, many of these polymers are implicated with processing difficulties that stem from their innate physicochemical properties. In these cases, the use of synthetic polymers as an additive may improve the electrospinnability of these natural polymers.

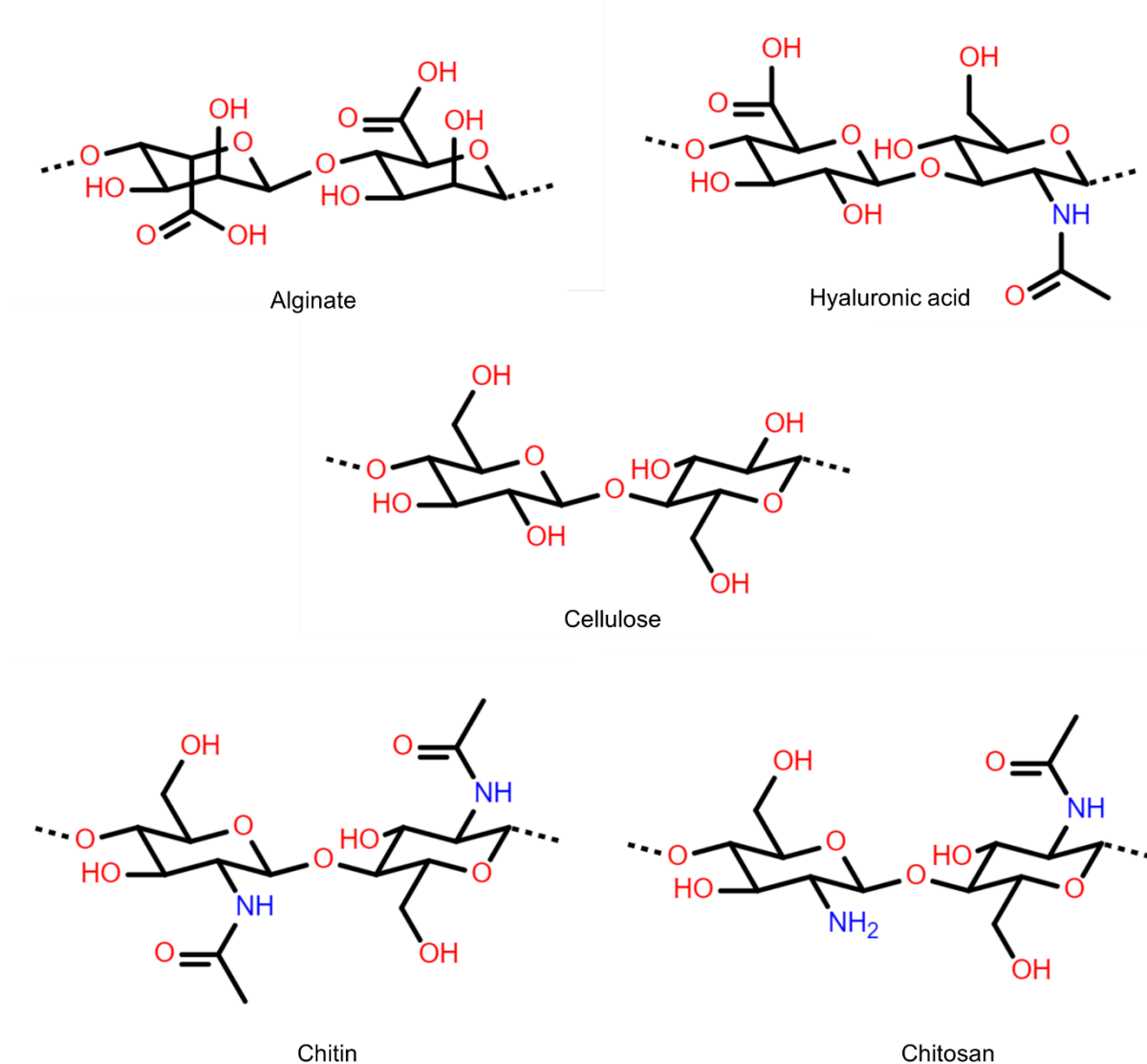


**Figure 1.15:** Chemical structures of polysaccharides that are commonly-used in electrospinning.

- Alginate

Alginate is an anionic polysaccharide composed of  $\beta$ -(1,4)-D-mannuronic acid and  $\alpha$ -(1,4)-L-guluronic acid residues (Figure 1.15) that is extractable from brown seaweed. Prior to electrospinning, it can be easily dissolved in water due to the presence of ionizable carboxylate groups along its molecular backbone. However, the same functional groups are responsible for intermolecular repulsion that prevent chain entanglement required for the production of continuous and uniform fibers. This problem is further exacerbated by the rigid and extended conformation of alginate molecules in aqueous solution. To improve the electrospinnability of alginate, water-soluble synthetic polymers such as PEO and PVA could be added to an alginate solution. These polymers increase chain entanglement by forming hydrogen bonds with the

hydroxyl groups of alginate [196]. Generally, the fiber morphology becomes smoother and more uniform as the mass ratio of the synthetic polymer to alginate exceeds 1:1 [196,197]. To prevent the dissolution of the electrospun fibers in aqueous physiological media, relevant crosslinking procedures must be carried out after electrospinning. Lu *et al.* combined physical and chemical crosslinking methods to obtain alginate/PEO fibers that remained stable in water for 3 days. The electrospun fibers were initially treated with hexamethylene diisocyanate that facilitated covalent crosslinking between the hydroxyl groups of alginate. This was followed by immersion into  $\text{CaCl}_2$  solution to achieve  $\text{Ca}^{2+}$ -mediated crosslinking of the carboxyl groups [197].

- Hyaluronic acid

Hyaluronic acid (HA), also known as hyaluronan or hyaluronate, is a linear polysaccharide consisting of repeating disaccharide units of  $\beta$ -(1,4)-D-glucuronic acid and  $\beta$ -(1,3)-N-acetyl-D-glucosamine (Figure 1.15). Like alginate, it is also an anionic polysaccharide. It is a member of the glycosaminoglycans, which can be found abundantly in the human body especially in the connective, epithelial and the neural tissues. However, unlike other glycosaminoglycans, its molecular weight can reach millions of Daltons. High molecular weight HA serves as a matrix, in which cells are embedded, in soft tissues such as the brain, dermis and umbilical cord. In addition, its ability to imbibe water to form a viscoelastic network makes HA useful as a shock absorber in synovial joints [198]. In the context of electrospinning, the high molecular weight of HA can pose significant processing difficulties. HA solutions have very high viscosity at concentrations well below the one required to achieve a degree of chain entanglement that is sufficient for generation of continuous fibers during electrospinning [199–201]. Several modifications have been tested to overcome this problem. Ji *et al.* used a low molecular weight HA derivative to reduce viscosity and added PEO to the HA solution at a 1:1 mass ratio to promote chain entanglement [202]. To obtain fibers made of pure HA without any synthetic polymer, Liu *et al.* utilized a combination solution of formic acid/DMF/water as a solvent for HA. They claimed that formic acid reduced the rigidity of HA chains to increase entanglement while DMF decreased the surface tension to facilitate the ejection of a stable fiber jet [203]. However, formic acid reduces the pH of the polymer solution, leading to protonation of the carboxyl groups of HA that reduces the conductivity of the polymer solution. Kim *et al.* dissolved HA in NaOH/DMF to achieve complete deprotonation of HA's carboxyl groups to increase the solution conductivity and thus the magnitude of electrostatic force exerted on the pendent drop at the tip of the capillary [200]. Despite the improvement in the

electrospinnability, the extremely high pH of the solution induces rapid degradation of the HA chains. Brenner *et al.* observed that HA solution prepared in a 4:1 NaOH/DMF solvent system lost its electrospinnability after 30 minutes. This coincided with a decrease in viscosity that highlighted significant degradation of HA chains. To counter this, the authors replaced the NaOH with the less basic NH<sub>4</sub>OH to reduce the solution pH and ensure no interruption to the electrospinning process [201]. In addition to the high viscosity issue, the high water retention capacity of HA can pose another challenge to the electrospinning of this polymer. Under atmospheric conditions, electrospinning of HA often generates fused fibers on the collector plate as a result of insufficient solvent evaporation from the travelling fiber jet. To facilitate fiber drying, Um *et al.* modified their electrospinning setup to introduce a continuous stream of hot air into the space between the capillary tip and the collector. The degree of fiber fusion decreased significantly with an increase in the temperature of the blown air from 25 to 57 °C [204]. Li *et al.* took a step further by raising both the solution and ambient temperature to 40 °C to break the hydrogen bonds that mediate the interaction between HA chains and water molecules [199]. As the temperature is comparable to the physiological condition, their setup may be useful for incorporating protein molecules into HA fibers. Finally, as in the case of alginate, electrospun HA fibers are water-soluble and must be crosslinked to prevent rapid dissolution in the aqueous physiological environment. Various chemicals have been used to crosslink HA molecules functionalized with relevant chemical groups [205,206]. For example, Ji *et al.* utilized PEG-diacrylate to cross link electrospun fibers composed of 3,3'-dithiobis-(propanoic dihydrazide)-modified HA. The crosslinked fibers were stable in the cell culture medium and able to support the attachment of mouse fibroblast cells [202].

- Collagen

Collagen is the most abundant protein in mammals. In humans, collagen makes up about one third of the total protein content [207]. It is commonly found as insoluble fibers in the extracellular matrix of connective tissues such as bones, tendons and skin. Each collagen fiber is an aggregate of collagen fibrils, each of which consists of a triple helical structure referred to as the collagen monomer (Figure 1.16) [208]. Each of the three polypeptide strands that make up a collagen monomer has a distinct amino acid composition in the sense that it is rich in glycine, proline and hydroxyproline [209]. Although there are more than 20 types of collagen identified to date, some of which are of non-fibrillar structures, 70 to 90% of the collagen found in humans are of the fibrillar type 1 [210]. Collagen is poorly soluble in water, unlike alginate and HA, as it has an isoelectric point that is close to the physiological pH [211]. The water

solubility of collagen can be improved by increasing the temperature or decreasing the pH of the solution. Huang *et al.* prepared collagen solution for electrospinning by dissolving lyophilized collagen in 10 mM HCl solution at room temperature. Uniform nanofibers could be obtained only when PEO was added to the collagen solution at a PEO/collagen mass ratio of 2:1 [212]. To obtain fibers made of pure collagen, other solvents have been utilized. For example, Matthews *et al.* used 1,1,1,3,3,3-hexafluoro-2-propanol (HFP) and managed to obtain pure collagen fibers at a minimum collagen concentration of 83 mg/mL [213]. Despite this, the use of HFP in collagen processing is limited by its toxic and volatile nature that poses significant health risks to humans. The corrosive property of HFP can also damage the natural triple helical configuration of collagen. Yang *et al.* reported that 45% of the collagen's triple helical structure was denatured after electrospinning in HFP. This structural alteration rendered the electrospun fibers more soluble in water and thus less stable in the aqueous physiological environment [214]. Several groups have utilized ethanol-based solvent systems to replace the toxic HFP [215,216]. Although these solvents enabled the production of collagen fibers without requiring any additive polymer, the electrospun fibers remained characteristically soluble in water, suggesting that the collagen's triple helical structure was not fully preserved during electrospinning. To improve water stability, Dong *et al.* employed the NHS/EDC reaction to crosslink collagen fibers without losing the nanofibrous morphology of the electrospun construct. The authors reported that the collagen fibers were stable in water after the crosslinking reaction [215]. However, Jiang *et al.* argued that such a crosslinking process can only provide short-term water stability. They instead used a citric acid/sodium hypophosphite crosslinking method that yielded fibers that were stable in phosphate-buffered saline (PBS) at 37 °C for at least 30 days [216].

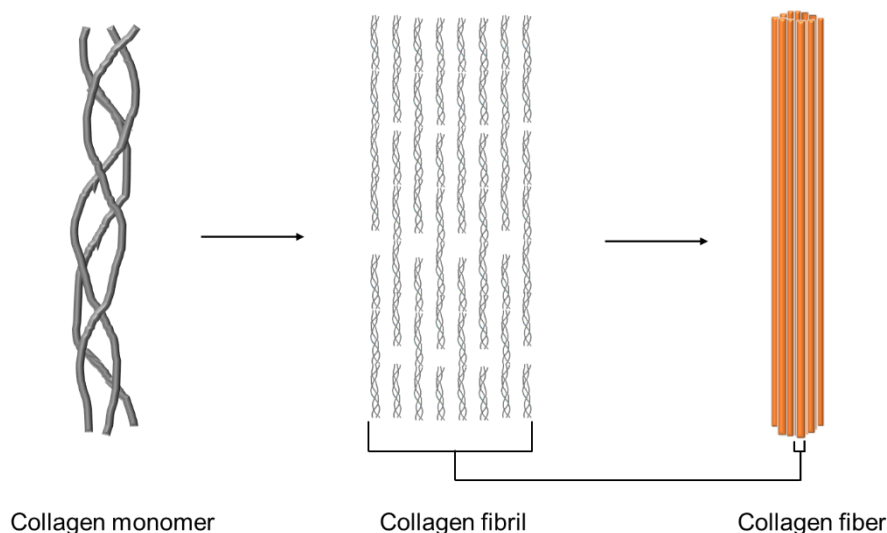


**Figure 1.16:** Three different levels of structure of fibrous collagen.

- Silk fibroin

Silk fibroin (SF) refers to insoluble proteins found in silk produced by spiders, silkworms (*Bombyx mori*), scorpions, bees and many types of insect [217]. Among these sources, silk from *Bombyx mori* is highly favored for research and industrial use due to the ease of its acquisition from the advanced sericulture industry [218]. SF is a fibrous protein that makes up approximately 70 – 75% of silk composition [219]. The rest of the silk is made up mostly of sericin, an amorphous protein with adhesive property that functions to bind SF fibers together [220]. As it is water-soluble, sericin can be removed from SF using a simple process known as degumming [221]. The amino acid composition of SF sourced from *Bombyx mori* is rich in glycine (43%), alanine (30%) and serine (12%). The high number of small-sized amino acids in the form of glycine and alanine allows for tight packing of the anti-parallel  $\beta$ -sheets in SF, contributing to the immense strength of this protein [218]. Traditionally, the electrospinning of silk fibroin is conducted in an organic solvent. Zarkoob *et al.* successfully prepared nanofibers by electrospinning SF solution in HFP [222]. Similarly, Ohgo *et al.* utilized hexafluoroacetone as an electrospinning solvent to produce beadless SF fibers [223]. However, concerns have been raised over the potential risks posed by the residual solvents in the fibers upon administration into patients. In response to this, several groups have attempted to remove the dependency on the toxic organic solvents by electrospinning from an aqueous SF solution. Wang *et al.* dissolved SF in a LiBr solution and removed the salt by dialysis prior to electrospinning. They reported that fibers of 400 – 800 nm in diameter could be electrospun from the SF solution. However, this was only true when the SF concentration in the solution

was 17% (w/v) or higher [224]. The requirement for such a high polymer concentration to achieve sufficient molecular entanglement presents an additional processing difficulty as the working solutions tend to be highly viscous and can transform into gel very easily to disrupt the electrospinning process. Kishimoto *et al.* utilized the same solvent system but managed to produce fibers at a much lower SF concentration (as low as 5% (w/v) for the highest molecular weight tested). This feat was achieved by increasing the pH of the SF solution before electrospinning. The authors claimed that under basic conditions, SF molecules have a higher number of charged residues [225]. The resultant increase in the repulsion between different segments along the polypeptide chain could possibly contribute to the relaxation of the packed structure of SF, leading to an increase in molecular entanglement that facilitated electrospinning. Regardless of the solvent used, electrospun SF fibers dissolve easily in water and require appropriate stabilizing treatment before they can be used in any biomedical application that demands slow biodegradation. For this, the electrospun fibers can be treated with methanol to increase SF's  $\beta$ -sheet content and achieve greater water stability [225].

- Cellulose and cellulose derivatives

Cellulose is a linear polysaccharide composed of a few hundreds to several thousands of  $\beta$ -(1,4)-D-glucose units (Figure 1.15) [226]. Unlike alginate and hyaluronic acid, cellulose is a neutral polysaccharide as it does not bear any ionizable chemical groups. It is the main structural component of the cell walls in plants and algae. It also makes up a large component of the biofilms produced by some species of bacteria [227]. As it is the most abundant natural polymer on earth, the research and industrial use of cellulose is widespread. However, the use of cellulose in electrospinning is very restricted due to the limited number of solvents that can be used to dissolve this polymer. Two common solvent systems used in the electrospinning of cellulose are N-methyl-morpholine N-oxide (NMMO)/water and lithium chloride (LiCl)/DMAc [228,229]. Each of these has its own drawback that complicates the fiber manufacturing process. In the case of NMMO/water, electrospinning is only possible at a temperature above the melting temperature of this solvent system (between 80 to 130 °C) [230], restricting the incorporation of any thermo-labile drugs such as proteins into the cellulose fibers. As for LiCl/DMAc, the preparation of this solvent system involves lengthy steps and the  $\text{Li}^+$  and  $\text{Cl}^-$  cannot be completely removed from the electrospun fibers [231]. Recently, electrospinning of cellulose in ionic liquids has been reported [232]. However, the low volatility of these solvents means appropriate modifications must be made to the electrospinning setup to obtain dry, unfused fibers.

To improve the solubility of cellulose, and thus increase the range of solvents that can be used for the electrospinning of this polymer, various cellulose derivatives have been synthesized. These include cellulose acetate [230,233,234], hydroxypropyl cellulose [235] and alkyl cellulose (e.g. methyl and ethyl cellulose) [236,237]. Han *et al.* produced cellulose acetate nanofibers by electrospinning the polymer in a simple acetic acid/water solvent system [230]. To increase the water stability of the electrospun fibers, cellulose derivatives can be converted to cellulose using a straightforward hydrolysis process. For example, Son *et al.* stabilized cellulose acetate nanofibers electrospun in a water/ethanol solvent system by treating them with KOH solution in ethanol. They reported that the fibers were completely deacetylated after 20 minutes [233].

- Chitin and chitosan

Chitin is the second most abundant natural polymer behind cellulose. It is a linear polysaccharide consists of  $\beta$ -(1,4)-N-acetyl-D-glucosamine units (Figure 1.15). This polymer forms a major structural component of fungal cell walls and the exoskeletons of arthropods (e.g. crustaceans and insects) [238]. Like cellulose, chitin is a neutral polymer that is soluble in a limited range of solvents. Published work on the electrospinning of chitin mostly utilized HFP as a solvent [239–241]. For example, Min *et al.* successfully obtained nanofibers of 40 – 600 nm diameter by electrospinning 5 % (w/v) chitin solution in HFP. However, the solubility of native chitin molecules in HFP is relatively poor (no more than 0.65 % (w/v)). To achieve a concentration that is feasible for electrospinning, the authors pre-treated the native chitin with gamma irradiation to reduce the polymer chain length prior to dissolving it in HFP [239].

To obtain a polymer with a better solubility profile, chitin can be partially deacetylated through a simple chemical or enzymatic process to form chitosan. Chitosan can be described as a copolymer of  $\beta$ -(1,4)-linked N-acetyl-D-glucosamine and D-glucosamine (Figure 1.15), with the latter comprising at least 50% of the total number of monomers [242]. The free amino groups generated by the deacetylation reaction make chitosan the only pseudo-natural cationic polymer on earth. These amino groups are, however, only weakly-basic ( $pK_a = 6.5$ ) [243]. Chitosan remains insoluble in water at neutral pH as only a small percentage of its amino groups are ionized under this condition. Consequently, the electrospinning of chitosan is usually conducted in dilute or concentrated solutions of organic acids such as acetic acid [158,244–247] and, to a lesser extent, formic acid [248,249]. However, the electrospinning of chitosan alone often fails to generate uniform fibers [158,250,251]. As in the case of alginate

and HA, the electrostatic repulsion between charged groups along the chitosan polymer backbone can inhibit molecular entanglement that is needed to sustain the generation of fiber jet from the capillary tip during electrospinning [239]. Therefore, the addition of high molecular weight synthetic polymers is often necessary to increase the electrospinnability of chitosan. It should be noted that the minimum mass percentage of the synthetic polymer needed to ensure good electrospinnability is generally much lower in the case of chitosan than in the case of alginate and HA. While the latter polymers often require the addition of a synthetic polymer at a 1:1 mass ratio [196,197,202], successful electrospinning of chitosan/PEO solutions mixed at a 9:1 mass ratio and above has been reported [252–254]. This confers an important advantage to chitosan as a polymer for making fibers to be used as a vehicle for protein delivery. As discussed in the earlier section of this chapter, proteins can be embedded into polymer-based fibers by mixing protein molecules or protein-loaded particles with a polymer solution prior to electrospinning. However, if a significant proportion of the fiber matrix is made of water-soluble synthetic polymers such as PEO and PVA, there is a strong probability for burst release to be seen upon the introduction of the fibrous scaffold into an aqueous environment, as the protein molecules/protein-loaded particles can escape rapidly from the soluble portions of the fibers. In fact, this fiber solubilization issue may become apparent during aqueous crosslinking or other stabilization treatments, contributing to loss of protein load even before the *in vivo* administration of the fibrous scaffold. Electrospun chitosan fibers are composed of the protonated version of this polymer that form ionic complexes with the conjugate base of the organic acid used to dissolve chitosan in the first place (e.g. acetate or formate ions). Not unexpectedly, these fibers are susceptible to dissolution in water. To improve their aqueous stability, the fibers can be treated with an alkaline solution (e.g. NaOH, Na<sub>2</sub>CO<sub>3</sub>, K<sub>2</sub>CO<sub>3</sub>) to deprotonate the amino groups [246,255,256]. Alkali-treated fibers have been shown to possess good aqueous stability. Sangsanoh *et al.* reported that chitosan fibers treated with an aqueous Na<sub>2</sub>CO<sub>3</sub> solution were stable in PBS for up to 3 months [256]. Furthermore, Lemma *et al.* utilized K<sub>2</sub>CO<sub>3</sub> solution in ethanol/water for the neutralization step and obtained chitosan fibers that were resistant to aqueous dissolution for half a year [246]. The simple alkaline stabilization procedure also eliminates the need for chemical crosslinkers, thus avoiding any potential toxicity associated with these agents [257,258].

As discussed above, chitosan is a polymer with unique physicochemical properties owing to its weakly-basic nature. The small number of positively-charged groups at neutral pH allow chitosan molecules to form electrostatic complexes with numerous negatively-charged natural

or synthetic polymers [259–263]. This special aspect of chitosan may contribute greatly to the development of highly biocompatible protein delivery vehicles. Protein molecules can be loaded into micro/nanoparticles composed of FDA-approved polymers such as PLA and PLGA to form primary protein carriers. The negatively-charged carboxyl groups in these polyesters can facilitate the incorporation of these particles into chitosan fibers to produce a composite vehicle that may provide sustained protein release. In addition, as chitosan is not naturally found in human tissues, it is reasonable to coat the surface of chitosan fibers with relevant human ECM components to obtain a more biologically relevant final construct. For example, for implantation into the brain, it may be useful to coat the fibers with HA, which is negatively-charged, as this polysaccharide forms a major component of the brain ECM [264]. Furthermore, the well-reported aqueous stability of neutralized chitosan fibers may present a twofold advantage to its use as a chemokine delivery vehicle in tumor trapping applications. First, chitosan fibers may act as a stable scaffold to hold the chemokine-loaded particles in place during the chemokine release process, helping to create and maintain a chemokine concentration gradient that is essential for the chemotaxis of tumor cells. Second, the slow degradation of the chitosan fibers can prolong the time window for the tumor cells to move up the chemokine concentration gradient and be trapped within a well-confined space, rendering these cells accessible to subsequent selective killing procedures. All of these potential benefits warrant the use of chitosan in the development of SDF-1 $\alpha$ -releasing electrospun fibrous scaffolds to be used in the glioblastoma cell trapping application.

## 1.4. REFERENCES

- [1] E. Ozdemir-Kaynak, A.A. Qutub, O. Yesil-Celiktas, Advances in glioblastoma multiforme treatment: New models for nanoparticle therapy, *Front. Physiol.* 9 (2018) 1–14. doi:10.3389/fphys.2018.00170.
- [2] Q.T. Ostrom, L. Bauchet, F.G. Davis, I. Deltour, J.L. Fisher, C.E. Langer, M. Pekmezci, J.A. Schwartzbaum, M.C. Turner, K.M. Walsh, M.R. Wrensch, J.S. Barnholtz-Sloan, The epidemiology of glioma in adults: A state of the science review, *Neuro. Oncol.* 16 (2014) 896–913. doi:10.1093/neuonc/nou087.
- [3] T.F. Cloughesy, W.K. Cavenee, P.S. Mischel, Glioblastoma: From Molecular Pathology to Targeted Treatment, *Annu. Rev. Pathol. Mech. Dis.* 9 (2014) 1–25. doi:10.1146/annurev-pathol-011110-130324.
- [4] M. Yao, S. Li, X. Wu, S. Diao, G. Zhang, H. He, L. Bian, Y. Lu, Cellular origin of glioblastoma and its implication in precision therapy, *Cell. Mol. Immunol.* (2018) 1–3. doi:10.1038/cmi.2017.159.
- [5] W.S. Chung, N.J. Allen, C. Eroglu, Astrocytes control synapse formation, function, and elimination, *Cold Spring Harb. Perspect. Biol.* (2015). doi:10.1101/cshperspect.a020370.
- [6] R.D. Fields, D.H. Woo, P.J. Bassar, Glial regulation of the neuronal connectome through local and long-distant communication, *Neuron.* 86 (2015) 374–386. doi:10.1016/j.neuron.2015.01.014.
- [7] D.N. Louis, A. Perry, G. Reifenberger, A. von Deimling, D. Figarella-Branger, W.K. Cavenee, H. Ohgaki, O.D. Wiestler, P. Kleihues, D.W. Ellison, The 2016 World Health Organization Classification of Tumors of the Central Nervous System: a summary, *Acta Neuropathol.* 131 (2016) 803–820. doi:10.1007/s00401-016-1545-1.
- [8] D. Krex, B. Klink, C. Hartmann, A. Von Deimling, T. Pietsch, M. Simon, M. Sabel, J.P. Steinbach, O. Heese, G. Reifenberger, M. Weller, G. Schackert, Long-term survival with glioblastoma multiforme, *Brain.* 130 (2007) 2596–2606. doi:10.1093/brain/awm204.
- [9] P. Sciacero, G.F. Girelli, D. Cante, P. Franco, V.C. Borca, P. Grosso, A. Marra, S. Bombaci, S. Tofani, M.R. La Porta, U. Ricardi, Cerebellar glioblastoma multiforme in an adult woman, *Tumori.* 100 (2014) 74–78. doi:10.1700/1578.17236.
- [10] S.E. Lakhani, L. Harle, Difficult diagnosis of brainstem glioblastoma multiforme in a woman: A case report and review of the literature, *J. Med. Case Rep.* 3 (2009) 1–3. doi:10.1186/1752-1947-3-87.
- [11] C. Bastiancich, P. Danhier, V. Pr at, F. Danhier, Anticancer drug-loaded hydrogels as drug delivery systems for the local treatment of glioblastoma, *J. Control. Release.* 243 (2016) 29–42. doi:10.1016/j.jconrel.2016.09.034.
- [12] B.B. Tysnes, R. Mahesparan, Biological mechanisms of glioma invasion and potential therapeutic targets, *J. Neurooncol.* 53 (2001) 129–147. doi:10.1023/A:1012249216117.
- [13] M.C. Robert, M.E. Wastie, Glioblastoma multiforme: A rare manifestation of extensive liver and bone metastases, *Biomed. Imaging Interv. J.* 4 (2008) 2–5. doi:10.2349/bij.4.1.e3.
- [14] M. Watanabe, R. Tanaka, N. Takeda, Magnetic resonance imaging and histopathology of cerebral gliomas, *Neuroradiology.* 34 (1992) 463–469. doi:10.1007/BF00598951.
- [15] T. Yamahara, Y. Numa, T. Oishi, T. Kawaguchi, T. Seno, A. Asai, K. Kawamoto, Morphological and flow cytometric analysis of cell infiltration in glioblastoma: A comparison of autopsy brain and neuroimaging, *Brain Tumor Pathol.* 27 (2010) 81–87. doi:10.1007/s10014-010-0275-7.

- [16] A. Radbruch, O. Eidel, B. Wiestler, D. Paech, S. Burth, P. Kickingereder, M. Nowosielski, P. Bäumer, W. Wick, H.P. Schlemmer, M. Bendszus, M. Ladd, A.M. Nagel, S. Heiland, Quantification of tumor vessels in glioblastoma patients using time-of-flight angiography at 7 Tesla: A feasibility study, *PLoS One*. 9 (2014) 1–13. doi:10.1371/journal.pone.0110727.
- [17] H.F. Dvorak, Tumors: Wounds That Do Not Heal--Redux, *Cancer Immunol. Res.* 3 (2015) 1–11. doi:10.1158/2326-6066.CIR-14-0209.
- [18] T. Ogiuchi, Y. Hirashima, S. Nakamura, S. Endo, M. Kurimoto, A. Takaku, Tissue factor and cancer procoagulant expressed by glioma cells participate in their thrombin-mediated proliferation, *J. Neurooncol.* 46 (2000) 1–9. doi:10.1023/A:1006323200001.
- [19] G. Bergers, The role of pericytes in blood-vessel formation and maintenance, *Neuro. Oncol.* 7 (2005) 452–464. doi:10.1215/S1152851705000232.
- [20] R. Rampling, G. Cruickshank, A.D. Lewis, S.A. Fitzsimmons, P. Workman, Direct measurement of pO<sub>2</sub> distribution and bioreductive enzymes in human malignant brain tumors, *Int. J. Radiat. Oncol. Biol. Phys.* 29 (1994) 427–431. doi:10.1016/0360-3016(94)90432-4.
- [21] D.R. Collingridge, J.M. Piepmeier, S. Rockwell, J.P.S. Knisely, Polarographic measurements of oxygen tension in human glioma and surrounding peritumoural brain tissue, *Radiother. Oncol.* 53 (1999) 127–131. doi:10.1016/S0167-8140(99)00121-8.
- [22] D.J. Brat, E.G. Van Meir, Vaso-occlusive and prothrombotic mechanisms associated with tumor hypoxia, necrosis, and accelerated growth in glioblastoma, *Lab. Investig.* 84 (2004) 397–405. doi:10.1038/labinvest.3700070.
- [23] D. Hambardzumyan, G. Bergers, Glioblastoma: Defining Tumor Niches, *Trends in Cancer.* 1 (2015) 252–265. doi:10.1016/j.trecan.2015.10.009.
- [24] X. Feng, F. Szulzewsky, A. Yerevanian, Z. Chen, D. Heinzmann, R.D. Rasmussen, V. Alvarez-Garcia, Y. Kim, B. Wang, I. Tamagno, H. Zhou, X. Li, H. Kettenmann, R.M. Ransohoff, D. Hambardzumyan, X. Feng, F. Szulzewsky, A. Yerevanian, Z. Chen, D. Heinzmann, R.D. Rasmussen, V. Alvarez-Garcia, Y. Kim, B. Wang, I. Tamagno, H. Zhou, X. Li, H. Kettenmann, R.M. Ransohoff, D. Hambardzumyan, Loss of CX3CR1 increases accumulation of inflammatory monocytes and promotes gliomagenesis, *Oncotarget.* 6 (2015) 15077–15094. doi:10.18632/oncotarget.3730.
- [25] J. Liang, Y. Piao, L. Holmes, G.N. Fuller, V. Henry, N. Tiao, J.F. De Groot, Neutrophils promote the malignant glioma phenotype through S100A4, *Clin. Cancer Res.* 20 (2014) 187–198. doi:10.1158/1078-0432.CCR-13-1279.
- [26] M.B. Nijaguna, V. Patil, S. Urbach, S.D. Shwetha, K. Sravani, A.S. Hegde, B.A. Chandramouli, A. Arivazhagan, P. Marin, V. Santosh, K. Somasundaram, Glioblastoma-derived macrophage colony-stimulating factor (MCSF) induces microglial release of insulin-like growth factor-binding protein 1 (IGFBP1) to promote angiogenesis, *J. Biol. Chem.* 290 (2015) 23401–23415. doi:10.1074/jbc.M115.664037.
- [27] B. Badie, J. Schartner, S. Prabakaran, J. Paul, J. Vorpahl, Expression of Fas ligand by microglia: Possible role in glioma immune evasion, *J. Neuroimmunol.* 120 (2001) 19–24. doi:10.1016/S0165-5728(01)00361-7.
- [28] O.J. Becher, D. Hambardzumyan, E.I. Fomchenko, H. Momota, L. Mainwaring, A.M. Bleau, A.M. Katz, M. Edgar, A.M. Kenney, C. Cordon-Cardo, R.G. Blasberg, E.C. Holland, Gli activity correlates with tumor grade in platelet-derived growth factor-induced gliomas, *Cancer Res.* 68 (2008) 2241–2249. doi:10.1158/0008-5472.CAN-07-6350.
- [29] V. Clement, P. Sanchez, N. de Tribolet, I. Radovanovic, A. Ruiz i Altaba, HEDGEHOG-GLI1 Signaling Regulates Human Glioma Growth, Cancer Stem Cell Self-Renewal, and Tumorigenicity, *Curr. Biol.* 17 (2007) 165–172.

- doi:10.1016/j.cub.2006.11.033.
- [30] L.A. Edwards, K. Woolard, M.J. Son, A. Li, J. Lee, C. Ene, S.A. Mantey, D. Maric, H. Song, G. Belova, R.T. Jensen, W. Zhang, H.A. Fine, Effect of brain- and tumor-derived connective tissue growth factor on glioma invasion, *J. Natl. Cancer Inst.* 103 (2011) 1162–1178. doi:10.1093/jnci/djr224.
- [31] H.S. Venkatesh, T.B. Johung, V. Caretti, A. Noll, Y. Tang, S. Nagaraja, E.M. Gibson, C.W. Mount, J. Polepalli, S.S. Mitra, P.J. Woo, R.C. Malenka, H. Vogel, M. Bredel, P. Mallick, M. Monje, Neuronal activity promotes glioma growth through neuroligin-3 secretion, *Cell.* 161 (2015) 803–816. doi:10.1016/j.cell.2015.04.012.
- [32] S.A. Grossman, J.F. Batara, Current management of glioblastoma multiforme, *Semin. Oncol.* 31 (2004) 635–644. doi:10.1053/j.seminoncol.2004.07.005.
- [33] R. Stupp, M. Brada, M.J. van den Bent, J.C. Tonn, G. Pentheroudakis, High-grade glioma: ESMO clinical practice guidelines for diagnosis, treatment and follow-up, *Ann. Oncol.* 25 (2014) 93–101. doi:10.1093/annonc/mdu050.
- [34] M. Lacroix, D. Abi-Said, D.R. Fourney, Z.L. Gokaslan, W. Shi, F. DeMonte, F.F. Lang, I.E. McCutcheon, S.J. Hassenbusch, E. Holland, K. Hess, C. Michael, D. Miller, R. Sawaya, A multivariate analysis of 416 patients with glioblastoma multiforme: prognosis, extent of resection, and survival, *J. Neurosurg.* 95 (2001) 190–198. doi:10.3171/jns.2001.95.2.0190.
- [35] K. Yabroff, L. Harlan, C. Zeruto, J. Abrams, B. Mann, Patterns of care and survival for patients with glioblastoma multiforme diagnosed during 2006, *Neuro. Oncol.* 14 (2012) 351–359.
- [36] M.E. Hegi, A.C. Diserens, S. Godard, P.Y. Dietrich, L. Regli, S. Ostermann, P. Otten, G. Van Melle, N. De Tribolet, R. Stupp, Clinical Trial Substantiates the Predictive Value of O-6-Methylguanine-DNA Methyltransferase Promoter Methylation in Glioblastoma Patients Treated with Temozolomide, *Clin. Cancer Res.* 10 (2004) 1871–1874. doi:10.1158/1078-0432.CCR-03-0384.
- [37] M.E. Hegi, A.-C. Diserens, T. Gorlia, M.-F. Hamou, N. de Tribolet, M. Weller, J.M. Kros, J.A. Hainfellner, W. Mason, L. Mariani, J.E.C. Bromberg, P. Hau, R.O. Mirimanoff, J.G. Cairncross, R.C. Janzer, R. Stupp, *MGMT* Gene Silencing and Benefit from Temozolomide in Glioblastoma, *N. Engl. J. Med.* 352 (2005) 997–1003. doi:10.1056/NEJMoa043331.
- [38] M. Napolitano, G. Vaz, T.M. Lawson, M.A. Docquier, A. van Maanen, T. Duprez, C. Raftopoulos, Glioblastoma surgery with and without intraoperative MRI at 3.0T, *Neurochirurgie.* 60 (2014) 143–150. doi:10.1016/j.neuchi.2014.03.010.
- [39] W. Stummer, U. Pichlmeier, T. Meinel, O.D. Wiestler, F. Zanella, H.J. Reulen, Fluorescence-guided surgery with 5-aminolevulinic acid for resection of malignant glioma: a randomised controlled multicentre phase III trial, *Lancet Oncol.* 7 (2006) 392–401. doi:10.1016/S1470-2045(06)70665-9.
- [40] P. V. Butte, A. Mamelak, J. Parrish-Novak, D. Drazin, F. Shweikeh, P.R. Gangalum, A. Chesnokova, J.Y. Ljubimova, K. Black, Near-infrared imaging of brain tumors using the Tumor Paint BLZ-100 to achieve near-complete resection of brain tumors, *Neurosurg. Focus.* (2014) E1. doi:10.3171/2013.11.FOCUS13497.
- [41] J. Parrish-Novak, K. Byrnes-Blake, N. Lalayeva, S. Burlison, J. Fidel, R. Gilmore, P. Gayheart-Walsten, G.A. Bricker, W.J. Crumb, K.S. Tarlo, S. Hansen, V. Wiss, E. Malta, W.S. Dernell, J.M. Olson, D.M. Miller, Nonclinical Profile of BLZ-100, a Tumor-Targeting Fluorescent Imaging Agent, *Int. J. Toxicol.* 36 (2017) 104–112. doi:10.1177/1091581817697685.
- [42] R. Stupp, W.P. Mason, M.J. van den Bent, M. Weller, B. Fisher, M.J.B. Taphoorn, K. Belanger, A.A. Brandes, C. Marosi, U. Bogdahn, J. Curschmann, R.C. Janzer, S.K.

- Ludwin, T. Gorlia, A. Allgeier, D. Lacombe, J.G. Cairncross, E. Eisenhauer, R.O. Mirimanoff, Radiotherapy plus Concomitant and Adjuvant Temozolomide for Glioblastoma, *N. Engl. J. Med.* 352 (2005) 987–996. doi:10.1056/NEJMoa043330.
- [43] S.Y. Lee, Temozolomide resistance in glioblastoma multiforme, *Genes Dis.* 3 (2016) 198–210. doi:10.1016/j.gendis.2016.04.007.
- [44] J.P. Sheehan, M.E. Shaffrey, B. Gupta, J. Larner, J.N. Rich, D.M. Park, Improving the radiosensitivity of radioresistant and hypoxic glioblastoma, *Futur. Oncol.* 6 (2010) 1591–1601. doi:10.2217/fon.10.123.
- [45] L.S. Ashby, K.A. Smith, B. Stea, Gliadel wafer implantation combined with standard radiotherapy and concurrent followed by adjuvant temozolomide for treatment of newly diagnosed high-grade glioma: A systematic literature review, *World J. Surg. Oncol.* 14 (2016) 1–15. doi:10.1186/s12957-016-0975-5.
- [46] T.A. Juratli, G. Schackert, D. Krex, Current status of local therapy in malignant gliomas - A clinical review of three selected approaches, *Pharmacol. Ther.* 139 (2013) 341–358. doi:10.1016/j.pharmthera.2013.05.003.
- [47] A.B. Fleming, W.M. Saltzman, Pharmacokinetics of the Carmustine Implant, *Clin. Pharmacokinet.* 41 (2002) 403–419. doi:10.2165/00003088-200241060-00002.
- [48] L.S. Ashby, K.A. Smith, B. Stea, Gliadel wafer implantation combined with standard radiotherapy and concurrent followed by adjuvant temozolomide for treatment of newly diagnosed high-grade glioma: A systematic literature review, *World J. Surg. Oncol.* 14 (2016) 1–15. doi:10.1186/s12957-016-0975-5.
- [49] D.A. Bota, A. Desjardins, J.A. Quinn, M.L. Affronti, H.S. Friedman, Interstitial chemotherapy with biodegradable BCNU (Gliadel®) wafers in the treatment of malignant gliomas, *Ther. Clin. Risk Manag.* 3 (2007) 707–715.
- [50] R.J. Hansen, R. Nagasubramanian, S.M. Delaney, M.M. Cherian, S. Lin, S.C. Kogan, M.E. Dolan, Role of O<sup>6</sup>-Alkylguanine-DNA Alkyltransferase in Protecting Long-Term Toxicities, *J. Pharmacol. Exp. Ther.* 315 (2005) 1247–1255. doi:10.1124/jpet.105.083501.ment.
- [51] A.F. Hottinger, P. Pacheco, R. Stupp, Tumor treating fields: A novel treatment modality and its use in brain tumors, *Neuro. Oncol.* 18 (2016) 1338–1349. doi:10.1093/neuonc/nov182.
- [52] M. Giladi, R.S. Schneiderman, T. Voloshin, Y. Porat, M. Munster, R. Blat, S. Sherbo, Z. Bomzon, N. Urman, A. Itzhaki, S. Cahal, A. Shteingauz, A. Chaudhry, E.D. Kirson, U. Weinberg, Y. Palti, Mitotic Spindle Disruption by Alternating Electric Fields Leads to Improper Chromosome Segregation and Mitotic Catastrophe in Cancer Cells, *Sci. Rep.* 5 (2015) 1–16. doi:10.1038/srep18046.
- [53] E.D. Kirson, Z. Gurvich, R. Schneiderman, E. Dekel, A. Itzhaki, Y. Wasserman, R. Schatzberger, Y. Palti, Disruption of Cancer Cell Replication by Alternating Electric Fields, *Cancer Res.* (2004). doi:10.1158/0008-5472.CAN-04-0083.
- [54] M. Mehta, P. Wen, R. Nishikawa, D. Reardon, K. Peters, Critical review of the addition of tumor treating fields (TTFields) to the existing standard of care for newly diagnosed glioblastoma patients, *Crit. Rev. Oncol. Hematol.* 111 (2017) 60–65. doi:10.1016/j.critrevonc.2017.01.005.
- [55] L. Benson, Tumor Treating Fields Technology: Alternating Electric Field Therapy for the Treatment of Solid Tumors, *Semin. Oncol. Nurs.* 34 (2018) 137–150. doi:10.1016/j.soncn.2018.03.005.
- [56] R. Stupp, S. Taillibert, A. Kanner, W. Read, D.M. Steinberg, B. Lhermitte, S. Toms, A. Idbaih, M.S. Ahluwalia, K. Fink, F. Di Meco, F. Lieberman, J.J. Zhu, G. Stragliotto, D.D. Tran, S. Brem, A.F. Hottinger, E.D. Kirson, G. Lavy-Shahaf, U. Weinberg, C.Y. Kim, S.H. Paek, G. Nicholas, J. Burna, H. Hirte, M. Weller, Y. Palti,

- M.E. Hegi, Z. Ram, Effect of tumor-treating fields plus maintenance temozolomide vs maintenance temozolomide alone on survival in patients with glioblastoma a randomized clinical trial, *JAMA - J. Am. Med. Assoc.* 318 (2017) 2306–2316. doi:10.1001/jama.2017.18718.
- [57] N. Ferrara, K.J. Hillan, W. Novotny, Bevacizumab (Avastin), a humanized anti-VEGF monoclonal antibody for cancer therapy, *Biochem. Biophys. Res. Commun.* 333 (2005) 328–335. doi:10.1016/j.bbrc.2005.05.132.
- [58] N. Ferrara, H.P. Gerber, J. LeCouter, The biology of VEGF and its receptors, *Nat. Med.* (2003). doi:10.1038/nm0603-669.
- [59] M. Johansson, T. Brännström, A. Tommy Bergenheim, R. Henriksson, Spatial expression of VEGF-A in human glioma, *J. Neurooncol.* 59 (2002) 1–6. doi:10.1023/A:1016317407043.
- [60] D.T. Blumenthal, L. Mendel, F. Bokstein, The optimal regimen of bevacizumab for recurrent glioblastoma: does dose matter?, *J. Neurooncol.* 127 (2016) 493–502. doi:10.1007/s11060-015-2025-5.
- [61] A.-M. Chacko, C. Li, D.A. Pryma, S. Brem, G. Coukos, V. Muzykantov, Targeted delivery of antibody-based therapeutic and imaging agents to CNS tumors: crossing the blood–brain barrier divide, *Expert Opin. Drug Deliv.* 10 (2013) 907–926. doi:10.1517/17425247.2013.808184.
- [62] R.J. Diaz, S. Ali, M.G. Qadir, M.I. De La Fuente, M.E. Ivan, R.J. Komotar, The role of bevacizumab in the treatment of glioblastoma, *J. Neurooncol.* 133 (2017) 455–467. doi:10.1007/s11060-017-2477-x.
- [63] V. Miranda-Gonçalves, D. Cardoso-Carneiro, I. Valbom, F.P. Cury, V.A. Silva, S. Granja, R.M. Reis, F. Baltazar, O. Martinho, Metabolic alterations underlying Bevacizumab therapy in glioblastoma cells, *Oncotarget.* 8 (2017) 103657–103670. doi:10.18632/oncotarget.21761.
- [64] J. Bianco, C. Bastiancich, A. Jankovski, A. des Rieux, V. Pr at, F. Danhier, On glioblastoma and the search for a cure: where do we stand?, *Cell. Mol. Life Sci.* 74 (2017) 2451–2466. doi:10.1007/s00018-017-2483-3.
- [65] H. Ardon, S.W. Van Gool, T. Verschuere, W. Maes, S. Fieuws, R. Sciot, G. Wilms, P. Demaerel, J. Goffin, F. Van Calenbergh, J. Menten, P. Clement, M. Debiec-Rychter, S. De Vleeschouwer, Integration of autologous dendritic cell-based immunotherapy in the standard of care treatment for patients with newly diagnosed glioblastoma: Results of the HGG-2006 phase I/II trial, *Cancer Immunol. Immunother.* 61 (2012) 2033–2044. doi:10.1007/s00262-012-1261-1.
- [66] V.E.J.C. Schijns, C. Preto, L. Devillers, D. Pierre, F.M. Hofman, T.C. Chen, P. Mespouille, P. Hantos, P. Glorieux, D.A. Bota, A. Stathopoulos, First clinical results of a personalized immunotherapeutic vaccine against recurrent, incompletely resected, treatment-resistant glioblastoma multiforme (GBM) tumors, based on combined allo- and auto-immune tumor reactivity, *Vaccine.* 33 (2015) 2690–2696. doi:10.1016/j.vaccine.2015.03.095.
- [67] J.J. Raizer, L.E. Abrey, A.B. Lassman, S.M. Chang, K.R. Lamborn, J.G. Kuhn, W.K.A. Yung, M.R. Gilbert, K.A. Aldape, P.Y. Wen, H.A. Fine, M. Mehta, L.M. DeAngelis, F. Lieberman, T.F. Cloughesy, H.I. Robins, J. Dancey, M.D. Prados, A phase II trial of erlotinib in patients with recurrent malignant gliomas and nonprogressive glioblastoma multiforme postradiation therapy, *Neuro. Oncol.* 12 (2010) 95–103. doi:10.1093/neuonc/nop015.
- [68] J.H. Uhm, K. V. Ballman, W. Wu, C. Giannini, J.C. Krauss, J.C. Buckner, C.D. James, B.W. Scheithauer, R.J. Behrens, P.J. Flynn, P.L. Schaefer, S.R. Dakhil, K.A. Jaeckle, Phase II evaluation of gefitinib in patients with newly diagnosed grade 4 astrocytoma:

- Mayo/north central cancer treatment group study n0074, *Int. J. Radiat. Oncol. Biol. Phys.* 80 (2011) 347–353. doi:10.1016/j.ijrobp.2010.01.070.
- [69] K. Graham, E. Unger, Overcoming tumor hypoxia as a barrier to radiotherapy, chemotherapy and immunotherapy in cancer treatment, *Int. J. Nanomedicine*. 13 (2018) 6049–6058. doi:10.2147/IJN.S140462.
- [70] M. Alonso-Basanta, P. Fang, A. Maity, S.M. Hahn, R.A. Lustig, J.F. Dorsey, A phase I study of nelfinavir concurrent with temozolomide and radiotherapy in patients with glioblastoma multiforme, *J. Neurooncol.* 116 (2014) 365–372. doi:10.1007/s11060-013-1303-3.
- [71] P.J. Muller, B.C. Wilson, Photodynamic therapy of brain tumors - A work in progress, *Lasers Surg. Med.* 38 (2006) 384–389. doi:10.1002/lsm.20338.
- [72] K. Strebhardt, A. Ullrich, Paul Ehrlich's magic bullet concept: 100 years of progress, *Nat. Rev. Cancer*. 8 (2008) 473–480. doi:10.1038/nrc2394.
- [73] D.R. Oostra, E.R. Macrae, Role of trastuzumab emtansine in the treatment of HER2-positive breast cancer, *Breast Cancer Targets Ther.* 6 (2014) 103–113. doi:10.2147/BCTT.S67297.
- [74] P.D. Senter, E.L. Sievers, The discovery and development of brentuximab vedotin for use in relapsed Hodgkin lymphoma and systemic anaplastic large cell lymphoma, *Nat. Biotechnol.* 30 (2012) 631–637. doi:10.1038/nbt.2289.
- [75] H. Tilly, F. Morschhauser, N.L. Bartlett, A. Mehta, G. Salles, C. Haioun, J. Munoz, A.I. Chen, K. Kolibaba, D. Lu, M. Yan, E. Penuel, J. Hirata, C. Lee, J.P. Sharman, Polatuzumab vedotin in combination with immunochemotherapy in patients with previously untreated diffuse large B-cell lymphoma: an open-label, non-randomised, phase 1b–2 study, *Lancet Oncol.* (2019) 1–13. doi:10.1016/S1470-2045(19)30091-9.
- [76] S. Agarwal, P. Manchanda, M.A. Vogelbaum, J.R. Ohlfest, W.F. Elmquist, Function of the blood-brain barrier and restriction of drug delivery to invasive glioma cells: Findings in an orthotopic rat xenograft model of glioma, *Drug Metab. Dispos.* 41 (2013) 33–39. doi:10.1124/dmd.112.048322.
- [77] B. van der Sanden, F. Appaix, F. Berger, L. Selek, J.-P. Issartel, D. Wion, Translation of the ecological trap concept to glioma therapy: the cancer cell trap concept., *Future Oncol.* 9 (2013) 817–24. doi:10.2217/fon.13.30.
- [78] T.N. Simões, A. Candido da Silva, C.C. de Melo Moura, Influence of artificial lights on the orientation of hatchlings of *Eretmochelys imbricata* in Pernambuco, Brazil, *Zoologia*. 34 (2017) 1–6. doi:10.3897/zoologia.34.e13727.
- [79] S. Paget, The Distribution of Secondary Growths in Cancer of the Breast, *Lancet*. 133 (1889) 571–573. doi:10.1016/S0140-6736(00)49915-0.
- [80] J.E. Moreau, K. Anderson, J.R. Mauney, T. Nguyen, D.L. Kaplan, M. Rosenblatt, Tissue-engineered bone serves as a target for metastasis of human breast cancer in a mouse model, *Cancer Res.* 67 (2007) 10304–10308. doi:10.1158/0008-5472.CAN-07-2483.
- [81] F.P. Seib, J.E. Berry, Y. Shiozawa, R.S. Taichman, D.L. Kaplan, Tissue engineering a surrogate niche for metastatic cancer cells, *Biomaterials*. 51 (2015) 313–319. doi:10.1016/j.biomaterials.2015.01.076.
- [82] C.Y. Ko, L. Wu, A.M. Nair, Y.T. Tsai, V.K. Lin, L. Tang, The use of chemokine-releasing tissue engineering scaffolds in a model of inflammatory response-mediated melanoma cancer metastasis, *Biomaterials*. 33 (2012) 876–885. doi:10.1016/j.biomaterials.2011.10.002.
- [83] S.M. Azarin, J. Yi, R.M. Gower, B.A. Aguado, M.E. Sullivan, A.G. Goodman, E.J. Jiang, S.S. Rao, Y. Ren, S.L. Tucker, V. Backman, J.S. Jeruss, L.D. Shea, In vivo capture and label-free detection of early metastatic cells, *Nat. Commun.* 6 (2015) 8094.

- doi:10.1038/ncomms9094.
- [84] A.C. Bellail, S.B. Hunter, D.J. Brat, C. Tan, E.G. Van Meir, Microregional extracellular matrix heterogeneity in brain modulates glioma cell invasion, *Int. J. Biochem. Cell Biol.* 36 (2004) 1046–1069. doi:10.1016/j.biocel.2004.01.013.
- [85] A. Jain, M. Betancur, G.D. Patel, C.M. Valmikinathan, V.J. Mukhatyar, A. Vakharia, S.B. Pai, B. Brahma, T.J. MacDonald, R. V. Bellamkonda, Guiding intracortical brain tumour cells to an extracortical cytotoxic hydrogel using aligned polymeric nanofibres, *Nat. Mater.* 13 (2014) 308–316. doi:10.1038/nmat3878.
- [86] S.J. Wang, W. Saadi, F. Lin, C. Minh-Canh Nguyen, N. Li Jeon, Differential effects of EGF gradient profiles on MDA-MB-231 breast cancer cell chemotaxis, *Exp. Cell Res.* 300 (2004) 180–189. doi:10.1016/j.yexcr.2004.06.030.
- [87] S.M.N. Rao, V.K. Lin, U. Tata, G. V. Raj, J.-T. Hsieh, K. Nguyen, J.-C. Chiao, Demonstration of Cancer Cell Migration Using a Novel Microfluidic Device, *J. Nanotechnol. Eng. Med.* 1 (2010) 21003. doi:10.1115/1.4001280.
- [88] Y. Zhou, P.H. Larsen, C. Hao, V.W. Yong, CXCR4 is a major chemokine receptor on glioma cells and mediates their survival, *J. Biol. Chem.* 277 (2002) 49481–49487. doi:10.1074/jbc.M206222200.
- [89] D. Zagzag, M. Esencay, O. Mendez, H. Yee, I. Smirnova, Y. Huang, L. Chiriboga, E. Lukyanov, M. Liu, E.W. Newcomb, Hypoxia- and Vascular Endothelial Growth Factor-Induced Stromal Cell-Derived Factor-1 $\alpha$ /CXCR4 Expression in Glioblastomas, *Am. J. Pathol.* 173 (2008) 545–560. doi:10.2353/ajpath.2008.071197.
- [90] V. Nand Yadav, D. Zamler, G.J. Baker, P. Kadiyala, A. Erdreich-Epstein, A.C. DeCarvalho, T. Mikkelsen, M.G. Castro, P.R. Lowenstein, CXCR4 increases in-vivo glioma perivascular invasion, and reduces radiation induced apoptosis: A genetic knockdown study, *Oncotarget.* 7 (2016) 83701–83719. doi:10.18632/oncotarget.13295.
- [91] V.A. Cuddapah, S. Robel, S. Watkins, H. Sontheimer, A neurocentric perspective on glioma invasion, *Nat. Rev. Neurosci.* 15 (2014) 455–465. doi:10.1038/nrn3765.
- [92] H. Peng, Y. Wu, Z. Duan, P. Ciborowski, J.C. Zheng, Proteolytic processing of SDF-1  $\alpha$  by matrix metalloproteinase-2 impairs CXCR4 signaling and reduces neural progenitor cell migration, *Protein Cell.* 3 (2012) 875–882. doi:10.1007/s13238-012-2092-8.
- [93] T. Adelita, R. Sessa, S. Won, G. Zenker, M. Porcionatto, Proteolytic processed form of CXCL12 abolishes migration and induces apoptosis in neural stem cells in vitro, *Stem Cell Res.* 22 (2017) 61–69. doi:10.1016/j.scr.2017.05.013.
- [94] H.K. Makadia, S.J. Siegel, Poly Lactic-co-Glycolic Acid (PLGA) as biodegradable controlled drug delivery carrier, *Polymers (Basel).* 3 (2011) 1377–1397. doi:10.3390/polym3031377.
- [95] M. Sokolsky-Papkov, K. Agashi, A. Olaye, K. Shakesheff, A.J. Domb, Polymer carriers for drug delivery in tissue engineering, *Adv. Drug Deliv. Rev.* 59 (2007) 187–206. doi:10.1016/j.addr.2007.04.001.
- [96] D. Ding, Q. Zhu, Recent advances of PLGA micro/nanoparticles for the delivery of biomacromolecular therapeutics, *Mater. Sci. Eng. C.* 92 (2018) 1041–1060. doi:10.1016/j.msec.2017.12.036.
- [97] M.K. Tran, A. Swed, F. Boury, Preparation of polymeric particles in CO<sub>2</sub> medium using non-toxic solvents: Formulation and comparisons with a phase separation method, *Eur. J. Pharm. Biopharm.* 82 (2012) 498–507. doi:10.1016/j.ejpb.2012.08.005.
- [98] D.S. Kohane, Microparticles and nanoparticles for drug delivery, *Biotechnol. Bioeng.* 96 (2007) 203–209. doi:10.1002/bit.21301.

- [99] W.W. Yang, E. Pierstorff, Reservoir-based polymer drug delivery systems, *J. Lab. Autom.* 17 (2012) 50–58. doi:10.1177/2211068211428189.
- [100] B.K. Lee, Y. Yun, K. Park, PLA micro- and nano-particles, *Adv. Drug Deliv. Rev.* 107 (2016) 176–191. doi:10.1016/j.addr.2016.05.020.
- [101] R. Singh, J.W.L. Jr, Nanoparticle-based targeted drug delivery, *Exp. Mol. Pathol.* 86 (2009) 215–223. doi:10.1016/j.yexmp.2008.12.004.
- [102] M. Kimura, K. Fukumoto, J. Watanabe, K. Ishihara, Hydrogen-bonding-driven spontaneous gelation of water-soluble phospholipid polymers in aqueous medium, *J. Biomater. Sci. Polym. Ed.* 15 (2004) 631–644. doi:10.1163/156856204323046898.
- [103] Z. Ren, Y. Zhang, Y. Li, B. Xu, W. Liu, Hydrogen bonded and ionically crosslinked high strength hydrogels exhibiting Ca<sup>2+</sup>-triggered shape memory properties and volume shrinkage for cell detachment, *J. Mater. Chem. B.* 3 (2015) 6347–6354. doi:10.1039/c5tb00781j.
- [104] P.L. Lu, J.Y. Lai, D.H.K. Ma, G.H. Hsiue, Carbodiimide cross-linked hyaluronic acid hydrogels as cell sheet delivery vehicles: Characterization and interaction with corneal endothelial cells, *J. Biomater. Sci. Polym. Ed.* 19 (2008) 1–18. doi:10.1163/156856208783227695.
- [105] M. Rafat, F. Li, P. Fagerholm, M. Griffith, M. Rafat, R. Munger, T. Matsuura, M.A. Watsky, N.S. Lagali, PEG-stabilized carbodiimide crosslinked collagen–chitosan hydrogels for corneal tissue engineering, *Biomaterials.* 29 (2008) 3960–3972. doi:10.1016/j.biomaterials.2008.06.017.
- [106] Z. Tian, W. Liu, G. Li, The microstructure and stability of collagen hydrogel cross-linked by glutaraldehyde, *Polym. Degrad. Stab.* 130 (2016) 264–270. doi:10.1016/j.polymdegradstab.2016.06.015.
- [107] E. Mirzaei B., A. Ramazani, M. Shafiee, M. Danaei, Studies on glutaraldehyde crosslinked chitosan hydrogel properties for drug delivery systems, *Int. J. Polym. Mater. Polym. Biomater.* 62 (2013) 605–611. doi:10.1080/00914037.2013.769165.
- [108] Q. Chai, Y. Jiao, X. Yu, Hydrogels for Biomedical Applications: Their Characteristics and the Mechanisms behind Them, *Gels.* 3 (2017) 1–15. doi:10.3390/gels3010006.
- [109] J. Li, D.J. Mooney, Designing hydrogels for controlled drug delivery, *Nat. Rev. Mater.* 1 (2016) 1–18. doi:10.1038/natrevmats.2016.71.
- [110] T.R. Hoare, D.S. Kohane, Hydrogels in drug delivery : Progress and challenges, *Polymer (Guildf).* 49 (2008) 1993–2007. doi:10.1016/j.polymer.2008.01.027.
- [111] S.R. Van Tomme, B.G. De Geest, K. Braeckmans, S.C. De Smedt, F. Siepmann, J. Siepmann, C.F. Van Nostrum, W.E. Hennink, Mobility of model proteins in hydrogels composed of oppositely charged dextran microspheres studied by protein release and fluorescence recovery after photobleaching, *J. Control. Release.* 110 (2005) 67–78. doi:10.1016/j.jconrel.2005.09.005.
- [112] E.L. Schneider, J. Henise, R. Reid, G.W. Ashley, D. V. Santi, Hydrogel Drug Delivery System Using Self-Cleaving Covalent Linkers for Once-a-Week Administration of Exenatide, *Bioconjug. Chem.* 27 (2016) 1210–1215. doi:10.1021/acs.bioconjchem.5b00690.
- [113] M. Sutter, J. Siepmann, W.E. Hennink, W. Jiskoot, Recombinant gelatin hydrogels for the sustained release of proteins, *J. Control. Release.* 119 (2007) 301–312. doi:10.1016/j.jconrel.2007.03.003.
- [114] P.C. Chen, D.S. Kohane, Y.J. Park, R.H. Bartlett, R. Langer, V.C. Yang, Injectable microparticle-gel system for prolonged and localized lidocaine release. II. In vivo anesthetic effects, *J. Biomed. Mater. Res. - Part A.* 70 (2004) 459–466. doi:10.1002/jbm.a.30101.
- [115] S.Q. Gao, T. Maeda, K. Okano, K. Palczewski, A microparticle/hydrogel combination

- drug-delivery system for sustained release of retinoids, *Investig. Ophthalmol. Vis. Sci.* 53 (2012) 6314–6323. doi:10.1167/iovs.12-10279.
- [116] M. Kim, Y. Kim, K. Gwon, G. Tae, Modulation of Cell Adhesion of Heparin-Based Hydrogel by Efficient Physisorption of Adhesive Proteins, *Macromol. Res.* 20 (2012) 271–276. doi:10.1007/s13233-012-0058-6.
- [117] B. Sarker, R. Singh, R. Silva, J.A. Roether, J. Kaschta, R. Detsch, D.W. Schubert, I. Cicha, A.R. Boccaccini, Evaluation of fibroblasts adhesion and proliferation on alginate-gelatin crosslinked hydrogel, *PLoS One.* 9 (2014) 1–12. doi:10.1371/journal.pone.0107952.
- [118] C. Shen, Y. Li, H. Wang, Q. Meng, Mechanically strong interpenetrating network hydrogels for differential cellular adhesion, *RSC Adv.* 7 (2017) 18046–18053. doi:10.1039/c7ra01271c.
- [119] A. Autissier, C. Le Visage, C. Pouzet, F. Chaubet, D. Letourneur, Fabrication of porous polysaccharide-based scaffolds using a combined freeze-drying/cross-linking process, *Acta Biomater.* 6 (2010) 3640–3648. doi:10.1016/j.actbio.2010.03.004.
- [120] K. Ochi, G. Chen, T. Ushida, S. Gojo, K. Segawa, H. Tai, K. Ueno, H. Ohkawa, T. Mori, A. Yamaguchi, Y. Toyama, J.I. Hata, A. Umezawa, Use of isolated mature osteoblasts in abundance acts as desired-shaped bone regeneration in combination with a modified poly-DL-lactic-co-glycolic acid (PLGA)-collagen sponge, *J. Cell. Physiol.* 194 (2003) 45–53. doi:10.1002/jcp.10185.
- [121] J.J. Yoon, T.G. Park, Degradation behaviors of biodegradable macroporous scaffolds prepared by gas foaming of effervescent salts, *J. Biomed. Mater. Res.* 55 (2001) 401–408. doi:10.1002/1097-4636(20010605)55:3<401::AID-JBM1029>3.0.CO;2-H.
- [122] H. Tai, M.L. Mather, D. Howard, W. Wang, L.J. White, J.A. Crowe, S.P. Morgan, A. Chandra, D.J. Williams, S.M. Howdle, K.M. Shakesheff, Control of pore size and structure of tissue engineering scaffolds produced by supercritical fluid processing, *Eur. Cells Mater.* 14 (2007) 64–77.
- [123] M.-K. Tran, A. Swed, B. Calvignac, K.-N. Dang, L.N. Hassani, T. Cordonnier, F. Boury, Preparation of polymeric particles in CO<sub>2</sub> medium using non-toxic solvents: discussions on the mechanism of particle formation, *J. Mater. Chem. B.* 3 (2015) 1573–1582. doi:10.1039/C4TB01319K.
- [124] W.F. McKay, S.M. Peckham, J.M. Badura, A comprehensive clinical review of recombinant human bone morphogenetic protein-2 (INFUSE® Bone Graft), *Int. Orthop.* 31 (2007) 729–734. doi:10.1007/s00264-007-0418-6.
- [125] S. Liu, Y. Liu, L. Jiang, Z. Li, S. Lee, C. Liu, J. Wang, J. Zhang, Recombinant human BMP-2 accelerates the migration of bone marrow mesenchymal stem cells via the CDC42/PAK1/LIMK1 pathway in vitro and in vivo, *Biomater. Sci.* 7 (2018) 362–372. doi:10.1039/c8bm00846a.
- [126] H.H. Luu, W.X. Song, X. Luo, D. Manning, J. Luo, Z.L. Deng, K.A. Sharff, A.G. Montag, R.C. Haydon, T.C. He, Distinct roles of bone morphogenetic proteins in osteogenic differentiation of mesenchymal stem cells, *J. Orthop. Res.* 25 (2007) 665–677. doi:10.1002/jor.20359.
- [127] S.Y. Chew, J. Wen, E.K.F. Yim, K.W. Leong, Sustained release of proteins from electrospun biodegradable fibers, *Biomacromolecules.* 6 (2005) 2017–2024. doi:10.1021/bm0501149.
- [128] Y.Z. Zhang, X. Wang, Y. Feng, J. Li, C.T. Lim, S. Ramakrishna, Coaxial electrospinning of (fluorescein isothiocyanate-conjugated bovine serum albumin)-encapsulated poly( $\epsilon$ -caprolactone) nanofibers for sustained release, *Biomacromolecules.* 7 (2006) 1049–1057. doi:10.1021/bm050743i.
- [129] H. Jiang, Y. Hu, P. Zhao, Y. Li, K. Zhu, Modulation of protein release from

- biodegradable core-shell structured fibers prepared by coaxial electrospinning, *J. Biomed. Mater. Res. - Part B Appl. Biomater.* 79 (2006) 50–57. doi:10.1002/jbm.b.30510.
- [130] S. Liu, M. Qin, C. Hu, F. Wu, T. Jin, W. Cui, S. Liu, C. Fan, C. Hu, Tendon healing and anti-adhesion properties of electrospun fibrous membranes containing bFGF loaded nanoparticles, *Biomaterials.* 34 (2013) 4690–4701. doi:10.1016/j.biomaterials.2013.03.026.
- [131] H. Qi, P. Hu, J. Xu, A. Wang, Encapsulation of drug reservoirs in fibers by emulsion electrospinning: Morphology characterization and preliminary release assessment, *Biomacromolecules.* 7 (2006) 2327–2330. doi:10.1021/bm060264z.
- [132] K.M. Woo, V.J. Chen, P.X. Ma, Nano-fibrous scaffolding architecture selectively enhances protein adsorption contributing to cell attachment, *J. Biomed. Mater. Res. - Part A.* 67 (2003) 531–537. doi:10.1002/jbm.a.10098.
- [133] C.C. Rider, B. Mulloy, Heparin, heparan sulphate and the TGF- Cytokine superfamily, *Molecules.* 22 (2017) 1–11. doi:10.3390/molecules22050713.
- [134] A. Utani, M. Nomizu, H. Matsuura, K. Kato, T. Kobayashi, U. Takeda, S. Aota, P.K. Nielsen, H. Shinkai, A Unique Sequence of the Laminin  $\alpha 3$  G Domain Binds to Heparin and Promotes Cell Adhesion through Syndecan-2 and -4, *J. Biol. Chem.* 276 (2001) 28779–28788. doi:10.1074/jbc.M101420200.
- [135] C.L. Casper, N. Yamaguchi, K.L. Kiick, J.F. Rabolt, Functionalizing electrospun fibers with biologically relevant macromolecules, *Biomacromolecules.* 6 (2005) 1998–2007. doi:10.1021/bm050007e.
- [136] S. Patel, K. Kurpinski, R. Quigley, H. Gao, S. Li, M.-M. Poo, B.S. Hsiao, S. Patel, Bioactive Nanofibers: Synergistic Effects of Nanotopography and Chemical Signaling on Cell Guidance, *Nano Lett.* 7 (2007) 2122–2128. doi:10.1021/nl071182z.
- [137] G. Wei, Q. Jin, W. V. Giannobile, P.X. Ma, The enhancement of osteogenesis by nano-fibrous scaffolds incorporating rhBMP-7 nanospheres, *Biomaterials.* 28 (2007) 2087–2096. doi:10.1016/j.biomaterials.2006.12.028.
- [138] P. Ye, Z.K. Xu, J. Wu, C. Innocent, P. Seta, Nanofibrous membranes containing reactive groups: Electrospinning from poly(acrylonitrile-co-maleic acid) for lipase immobilization, *Macromolecules.* 39 (2006) 1041–1045. doi:10.1021/ma0517998.
- [139] H. Jia, G. Zhu, B. Vugrinovich, W. Kataphinan, D.H. Reneker, P. Wang, Enzyme-carrying polymeric nanofibers prepared via electrospinning for use as unique biocatalysts, *Biotechnol. Prog.* 18 (2002) 1027–1032. doi:10.1021/bp020042m.
- [140] H.S. Yoo, T.G. Kim, T.G. Park, Surface-functionalized electrospun nanofibers for tissue engineering and drug delivery, *Adv. Drug Deliv. Rev.* 61 (2009) 1033–1042. doi:10.1016/j.addr.2009.07.007.
- [141] J.S. Choi, K.W. Leong, H.S. Yoo, In vivo wound healing of diabetic ulcers using electrospun nanofibers immobilized with human epidermal growth factor (EGF), *Biomaterials.* 29 (2008) 587–596. doi:10.1016/j.biomaterials.2007.10.012.
- [142] T.G. Kim, T.G. Park, Surface functionalized electrospun biodegradable nanofibers for immobilization of bioactive molecules, *Biotechnol. Prog.* 22 (2006) 1108–1113. doi:10.1021/bp060039t.
- [143] H.S. Yoo, T.G. Kim, T.G. Park, Surface-functionalized electrospun nanofibers for tissue engineering and drug delivery, *Adv. Drug Deliv. Rev.* 61 (2009) 1033–1042. doi:10.1016/j.addr.2009.07.007.
- [144] A. Szentivanyi, T. Chakradeo, H. Zernetsch, B. Glasmacher, Electrospun cellular microenvironments: Understanding controlled release and scaffold structure, *Adv. Drug Deliv. Rev.* 63 (2011) 209–220. doi:10.1016/j.addr.2010.12.002.
- [145] I. Keun Kwon, S. Kidoaki, T. Matsuda, Electrospun nano- to microfiber fabrics made

- of biodegradable copolyesters: Structural characteristics, mechanical properties and cell adhesion potential, *Biomaterials*. 26 (2005) 3929–3939. doi:10.1016/j.biomaterials.2004.10.007.
- [146] J. Du, P.L. Che, Z.Y. Wang, U. Aich, K.J. Yarema, Designing a binding interface for control of cancer cell adhesion via 3D topography and metabolic oligosaccharide engineering, *Biomaterials*. 32 (2011) 5427–5437. doi:10.1016/j.biomaterials.2011.04.005.
- [147] N. Zhang, Y. Deng, Q. Tai, B. Cheng, L. Zhao, Q. Shen, R. He, L. Hong, W. Liu, S. Guo, K. Liu, H.R. Tseng, B. Xiong, X.Z. Zhao, Electrospun TiO<sub>2</sub> nanofiber-based cell capture assay for detecting circulating tumor cells from colorectal and gastric cancer patients, *Adv. Mater.* 24 (2012) 2756–2760. doi:10.1002/adma.201200155.
- [148] X. Wang, B. Ding, B. Li, Biomimetic electrospun nanofibrous structures for tissue engineering, *Mater. Today*. 16 (2013) 229–241. doi:10.1016/j.mattod.2013.06.005.
- [149] S. Sankar, C.S. Sharma, S.N. Rath, S. Ramakrishna, Electrospun nanofibres to mimic natural hierarchical structure of tissues: application in musculoskeletal regeneration, *J. Tissue Eng. Regen. Med.* 12 (2018) e604–e619. doi:10.1002/term.2335.
- [150] Y. Su, Q. Su, W. Liu, M. Lim, J.R. Venugopal, X. Mo, S. Ramakrishna, S.S. Al-Deyab, M. El-Newehy, Controlled release of bone morphogenetic protein 2 and dexamethasone loaded in core-shell PLLACL-collagen fibers for use in bone tissue engineering, *Acta Biomater.* 8 (2012) 763–771. doi:10.1016/j.actbio.2011.11.002.
- [151] M. Rubert, J. Dehli, Y.F. Li, M.B. Taskin, R. Xu, F. Besenbacher, M. Chen, Electrospun PCL/PEO coaxial fibers for basic fibroblast growth factor delivery, *J. Mater. Chem. B*. 2 (2014) 8538–8546. doi:10.1039/c4tb01258e.
- [152] L. Tian, M.P. Prabhakaran, X. Ding, D. Kai, S. Ramakrishna, Emulsion electrospun vascular endothelial growth factor encapsulated poly(l-lactic acid-co- $\epsilon$ -caprolactone) nanofibers for sustained release in cardiac tissue engineering, *J. Mater. Sci.* 47 (2012) 3272–3281. doi:10.1007/s10853-011-6166-4.
- [153] Z.M. Huang, Y.Z. Zhang, M. Kotaki, S. Ramakrishna, A review on polymer nanofibers by electrospinning and their applications in nanocomposites, *Compos. Sci. Technol.* 63 (2003) 2223–2253. doi:10.1016/S0266-3538(03)00178-7.
- [154] T.J. Sill, H.A. von Recum, Electrospinning: Applications in drug delivery and tissue engineering, *Biomaterials*. 29 (2008) 1989–2006. doi:10.1016/j.biomaterials.2008.01.011.
- [155] D.H. Reneker, A.L. Yarin, Electrospinning jets and polymer nanofibers, *Polymer (Guildf)*. 49 (2008) 2387–2425. doi:10.1016/j.polymer.2008.02.002.
- [156] J. Doshi, D.H. Reneker, Electrospinning process and applications of electrospun fibers, *J. Electrostat.* 35 (1995) 151–160. doi:10.1016/0304-3886(95)00041-8.
- [157] Y.M. Shin, M.M. Hohman, M.P. Brenner, G.C. Rutledge, Electrospinning: A whipping fluid jet generates submicron polymer fibers, *Appl. Phys. Lett.* 78 (2001) 1149–1151. doi:10.1063/1.1345798.
- [158] K. Ziani, C. Henrist, C. Jérôme, A. Aqil, J.I. Maté, R. Cloots, Effect of nonionic surfactant and acidity on chitosan nanofibers with different molecular weights, *Carbohydr. Polym.* 83 (2011) 470–476. doi:10.1016/j.carbpol.2010.08.002.
- [159] M.S. Islam, M.R. Karim, Fabrication and characterization of poly(vinyl alcohol)/alginate blend nanofibers by electrospinning method, *Colloids Surfaces A Physicochem. Eng. Asp.* 366 (2010) 135–140. doi:10.1016/j.colsurfa.2010.05.038.
- [160] S.J. Liu, Y.C. Kau, C.Y. Chou, J.K. Chen, R.C. Wu, W.L. Yeh, Electrospun PLGA/collagen nanofibrous membrane as early-stage wound dressing, *J. Memb. Sci.* 355 (2010) 53–59. doi:10.1016/j.memsci.2010.03.012.
- [161] P. Katta, M. Alessandro, R.D. Ramsier, G.G. Chase, Continuous electrospinning of

- aligned polymer nanofibers onto a wire drum collector, *Nano Lett.* 4 (2004) 2215–2218. doi:10.1021/nl0486158.
- [162] S. Zhong, W.E. Teo, X. Zhu, R.W. Beerman, S. Ramakrishna, L.Y.L. Yung, An aligned nanofibrous collagen scaffold by electrospinning and its effects on in vitro fibroblast culture, *J. Biomed. Mater. Res. - Part A.* 79 (2006) 456–463. doi:10.1002/jbm.a.30870.
- [163] P. Kiselev, J. Rosell-Llompart, Highly aligned electrospun nanofibers by elimination of the whipping motion, *J. Appl. Polym. Sci.* 125 (2012) 2433–2441. doi:10.1002/app.36519.
- [164] H. Liu, Y. Lo Hsieh, Ultrafine fibrous cellulose membranes from electrospinning of cellulose acetate, *J. Polym. Sci. Part B Polym. Phys.* 40 (2002) 2119–2129. doi:10.1002/polb.10261.
- [165] Y. Wang, H. Shi, J. Qiao, Y. Tian, M. Wu, W. Zhang, Y. Lin, Z. Niu, Y. Huang, Electrospun tubular scaffold with circumferentially aligned nanofibers for regulating smooth muscle cell growth, *ACS Appl. Mater. Interfaces.* 6 (2014) 2958–2962. doi:10.1021/am405556x.
- [166] H. Wu, J. Fan, C.C. Chu, J. Wu, Electrospinning of small diameter 3-D nanofibrous tubular scaffolds with controllable nanofiber orientations for vascular grafts, *J. Mater. Sci. Mater. Med.* 21 (2010) 3207–3215. doi:10.1007/s10856-010-4164-8.
- [167] X.Y. Yuan, Y.Y. Zhang, C. Dong, J. Sheng, Morphology of ultrafine polysulfone fibers prepared by electrospinning, *Polym. Int.* 53 (2004) 1704–1710. doi:10.1002/pi.1538.
- [168] G. Zhu, L.Y. Zhao, L.T. Zhu, X.Y. Deng, W.L. Chen, Effect of Experimental Parameters on Nanofiber Diameter from Electrospinning with Wire Electrodes, *IOP Conf. Ser. Mater. Sci. Eng.* 230 (2017) 1–12. doi:10.1088/1757-899X/230/1/012043.
- [169] J.S. Lee, K.H. Choi, H. Do Ghim, S.S. Kim, D.H. Chun, H.Y. Kim, W.S. Lyoo, Role of molecular weight of atactic poly(vinyl alcohol) (PVA) in the structure and properties of PVA nanofabric prepared by electrospinning, *J. Appl. Polym. Sci.* 93 (2004) 1638–1646. doi:10.1002/app.20602.
- [170] V. Beachley, X. Wen, Effect of electrospinning parameters on the nanofiber diameter and length, *Mater. Sci. Eng. C.* 29 (2009) 663–668. doi:10.1016/j.msec.2008.10.037.
- [171] C. Meechaisue, R. Dubin, P. Supaphol, V.P. Hoven, J. Kohn, Electrospun mat of tyrosine-derived polycarbonate fibers for potential use as tissue scaffolding material, *J. Biomater. Sci. Polym. Ed.* 17 (2006) 1039–1056. doi:10.1163/156856206778365988.
- [172] S. Zargham, S. Bazgir, A. Tavakoli, A.S. Rashidi, R. Damerchely, The Effect of Flow Rate on Morphology and Deposition Area of Electrospun Nylon 6 Nanofiber, *J. Eng. Fiber. Fabr.* 7 (2012) 42–49. doi:10.1177/155892501200700414.
- [173] D. Rodoplu, M. Mutlu, Effects of Electrospinning Setup and Process Parameters on Nanofiber Morphology Intended for the Modification of Quartz Crystal Microbalance Surfaces, *J. Eng. Fiber. Fabr.* 7 (2012) 118–123. doi:10.1177/155892501200700217.
- [174] V. Milleret, B. Simona, P. Neuenschwander, H. Hall, Tuning Electrospinning Parameters For Production Of 3D-Fiber Fleeces With Increased Porosity For Soft Tissue Engineering Applications, *Eur. Cells Mater.* 21 (2011) 286–303. doi:10.22203/eCM.v021a22.
- [175] C. Zhang, X. Yuan, L. Wu, Y. Han, J. Sheng, Study on morphology of electrospun poly(vinyl alcohol) mats, *Eur. Polym. J.* 41 (2005) 423–432. doi:10.1016/j.eurpolymj.2004.10.027.
- [176] S.H. Chen, Y. Chang, K.R. Lee, J.Y. Lai, A three-dimensional dual-layer nano/microfibrous structure of electrospun chitosan/poly(d,l-lactide) membrane for the improvement of cytocompatibility, *J. Memb. Sci.* 450 (2014) 224–234.

- doi:10.1016/j.memsci.2013.08.007.
- [177] M. V. Someswararao, R.S. Dubey, P.S.V. Subbarao, S. Singh, Electrospinning process parameters dependent investigation of TiO<sub>2</sub> nanofibers, *Results Phys.* 11 (2018) 223–231. doi:10.1016/j.rinp.2018.08.054.
- [178] R. Ghelich, M.K. Rad, A.A. Youzbashi, Study on Morphology and Size Distribution of Electrospun NiO-GDC Composite Nanofibers, *J. Eng. Fiber. Fabr.* 10 (2015) 12–19.
- [179] H. Homayoni, S.A.H. Ravandi, M. Valizadeh, Electrospinning of chitosan nanofibers: Processing optimization, *Carbohydr. Polym.* 77 (2009) 656–661. doi:10.1016/j.carbpol.2009.02.008.
- [180] A.H. Hekmati, A. Rashidi, R. Ghazisaeidi, J.Y. Drean, Effect of needle length, electrospinning distance, and solution concentration on morphological properties of polyamide-6 electrospun nanowebs, *Text. Res. J.* 83 (2013) 1452–1466. doi:10.1177/0040517512471746.
- [181] J. Doshi, D.H. Reneker, Electrospinning process and applications of electrospun fibers, *J. Electrostat.* 35 (1995) 151–160. doi:10.1002/jcb.23036.
- [182] S. Huan, G. Liu, G. Han, W. Cheng, Z. Fu, Q. Wu, Q. Wang, Effect of experimental parameters on morphological, mechanical and hydrophobic properties of electrospun polystyrene fibers, *Materials (Basel)*. 8 (2015) 2718–2734. doi:10.3390/ma8052718.
- [183] R.M. Nezarati, M.B. Eifert, E. Cosgriff-Hernandez, Effects of Humidity and Solution Viscosity on Electrospun Fiber Morphology, *Tissue Eng. Part C Methods*. 19 (2013) 810–819. doi:10.1089/ten.tec.2012.0671.
- [184] N. Yuya, I. Kim, W. Kai, K. Byoung-Suhk, Morphology Controlled Electrospun Poly ( Vinyl Pyrrolidone ) Fibers : Effects of Organic Solvent and Relative Humidity., *J. Mater. Sci. Eng. with Adv. Technol.* 2 (2010) 97–112.
- [185] S. Megelski, J.S. Stephens, D. Bruce Chase, J.F. Rabolt, Micro- and nanostructured surface morphology on electrospun polymer fibers, *Macromolecules*. 35 (2002) 8456–8466. doi:10.1021/ma020444a.
- [186] A. Celebioglu, T. Uyar, Electrospun porous cellulose acetate fibers from volatile solvent mixture, *Mater. Lett.* 65 (2011) 2291–2294. doi:10.1016/j.matlet.2011.04.039.
- [187] G. Cadafalch Gazquez, V. Smulders, S. Veldhuis, P. Wieringa, L. Moroni, B. Boukamp, J. ten Elshof, Influence of Solution Properties and Process Parameters on the Formation and Morphology of YSZ and NiO Ceramic Nanofibers by Electrospinning, *Nanomaterials*. 7 (2017) 1–15. doi:10.3390/nano7010016.
- [188] X. Zong, K. Kim, D. Fang, S. Ran, B.S. Hsiao, B. Chu, Structure and process relationship of electrospun bioabsorbable nanofiber membranes, *Polymer (Guildf)*. 43 (2002) 4403–4412. doi:10.1016/S0032-3861(02)00275-6.
- [189] C. Mit-Uppatham, M. Nithitanakul, P. Supaphol, Ultrafine electrospun polyamide-6 fibers: Effect of solution conditions on morphology and average fiber diameter, *Macromol. Chem. Phys.* 205 (2004) 2327–2338. doi:10.1002/macp.200400225.
- [190] J. Zeng, A. Aigner, F. Czubyko, T. Kissel, J.H. Wendorff, A. Greiner, Poly ( vinyl alcohol ) Nanofibers by Electrospinning as a Protein Delivery System and the Retardation of Enzyme Release by Additional Polymer Coatings, *Biomacromolecules*. 6 (2005) 1484–1488. doi:10.1021/bm0492576.
- [191] S. Maretschek, A. Greiner, T. Kissel, Electrospun biodegradable nanofiber nonwovens for controlled release of proteins, *J. Control. Release*. 127 (2008) 180–187. doi:10.1016/j.jconrel.2008.01.011.
- [192] P. Gupta, G.L. Wilkes, Some investigations on the fiber formation by utilizing a side-by-side bicomponent electrospinning approach, *Polymer (Guildf)*. 44 (2003) 6353–6359. doi:10.1016/S0032-3861(03)00616-5.
- [193] I.C. Liao, S.Y. Chew, K.W. Leong, Aligned core-shell nanofibers delivering bioactive

- proteins, *Nanomedicine*. 1 (2006) 465–471. doi:10.2217/17435889.1.4.465.
- [194] J.S. Choi, S.H. Choi, H.S. Yoo, Coaxial electrospun nanofibers for treatment of diabetic ulcers with binary release of multiple growth factors, *J. Mater. Chem.* 21 (2011) 5258–5267. doi:10.1039/c0jm03706k.
- [195] I.C. Liao, S. Chen, J.B. Liu, K.W. Leong, Sustained viral gene delivery through core-shell fibers, *J. Control. Release*. 139 (2009) 48–55. doi:10.1016/j.jconrel.2009.06.007.
- [196] S. Safi, M. Morshed, S.A. Hosseini Ravandi, M. Ghiaci, Study of electrospinning of sodium alginate, blended solutions of sodium alginate/poly(vinyl alcohol) and sodium alginate/poly(ethylene oxide), *J. Appl. Polym. Sci.* 104 (2007) 3245–3255. doi:10.1002/app.25696.
- [197] J.W. Lu, Y.L. Zhu, Z.X. Guo, P. Hu, J. Yu, Electrospinning of sodium alginate with poly(ethylene oxide), *Polymer (Guildf)*. 47 (2006) 8026–8031. doi:10.1016/j.polymer.2006.09.027.
- [198] G. Kogan, L. Šoltés, R. Stern, P. Gemeiner, Hyaluronic acid: A natural biopolymer with a broad range of biomedical and industrial applications, *Biotechnol. Lett.* 29 (2007) 17–25. doi:10.1007/s10529-006-9219-z.
- [199] J. Li, A. He, C.C. Han, D. Fang, B.S. Hsiao, B. Chu, Electrospinning of hyaluronic acid (HA) and HA/ gelatin blends, *Macromol. Rapid Commun.* 27 (2006) 114–120. doi:10.1002/marc.200500726.
- [200] T.G. Kim, H.J. Chung, T.G. Park, Macroporous and nanofibrous hyaluronic acid/collagen hybrid scaffold fabricated by concurrent electrospinning and deposition/leaching of salt particles, *Acta Biomater.* 4 (2008) 1611–1619. doi:10.1016/j.actbio.2008.06.008.
- [201] E.K. Brenner, J.D. Schiffman, E.A. Thompson, L.J. Toth, C.L. Schauer, Electrospinning of hyaluronic acid nanofibers from aqueous ammonium solutions, *Carbohydr. Polym.* 87 (2011) 926–929. doi:10.1016/j.carbpol.2011.07.033.
- [202] Y. Ji, K. Ghosh, X.Z. Shu, B. Li, J.C. Sokolov, G.D. Prestwich, R.A. Clark, M.H. Rafailovich, Electrospun three-dimensional hyaluronic acid nanofibrous scaffolds, *Biomaterials*. 27 (2006) 3782–3792. doi:10.1016/j.biomaterials.2006.02.037.
- [203] Y. Liu, G. Ma, D. Fang, J. Xu, H. Zhang, J. Nie, Effects of solution properties and electric field on the electrospinning of hyaluronic acid, *Carbohydr. Polym.* 83 (2011) 1011–1015. doi:10.1016/j.carbpol.2010.08.061.
- [204] I.C. Um, D. Fang, B.S. Hsiao, A. Okamoto, B. Chu, Electro-Spinning and Electro-Blowing of Hyaluronic Acid, *Biomacromolecules*. 5 (2004) 1428–1436. doi:10.1021/bm034539b.
- [205] G.D. Prestwich, D.M. Marecak, J.F. Marecek, K.P. Vercruysse, M.R. Ziebell, Controlled chemical modification of hyaluronic acid: Synthesis, applications, and biodegradation of hydrazide derivatives, *J. Control. Release*. 53 (1998) 93–103. doi:10.1016/S0168-3659(97)00242-3.
- [206] X.Z. Shu, Y. Liu, Y. Luo, M.C. Roberts, G.D. Prestwich, Disulfide cross-linked hyaluronan hydrogels., *Biomacromolecules*. 3 (2002) 1304–11. <http://www.ncbi.nlm.nih.gov/pubmed/12425669>.
- [207] M.D. Shoulders, R.T. Raines, Collagen Structure and Stability, *Annu. Rev. Biochem.* 78 (2009) 929–958. doi:10.1146/annurev.biochem.77.032207.120833.
- [208] B.B. Brodsky, A. V Persikov, Molecular Structure of the Collagen Triple Helix, *Adv. Protein Chem.* 70 (2005) 301–309. doi:10.1016/S0065-3233(04)70009-1.
- [209] M.J. Fullana, G.E. Wnek, Electrospun collagen and its applications in regenerative medicine, *Drug Deliv. Transl. Res.* 2 (2012) 313–322. doi:10.1007/s13346-012-0087-x.
- [210] D.I. Zeugolis, S.T. Khew, E.S.Y. Yew, A.K. Ekaputra, Y.W. Tong, L.-Y.L. Yung,

- D.W. Hutmacher, C. Sheppard, M. Raghunath, Electro-spinning of pure collagen nano-fibres – Just an expensive way to make gelatin?, *Biomaterials*. 29 (2008) 2293–2305. doi:10.1016/j.biomaterials.2008.02.009.
- [211] M. Zhang, C. Ding, J. Yang, S. Lin, L. Chen, L. Huang, Study of interaction between water-soluble collagen and carboxymethyl cellulose in neutral aqueous solution, *Carbohydr. Polym.* 137 (2016) 410–417. doi:10.1016/j.carbpol.2015.10.098.
- [212] L. Huang, K. Nagapudi, P.R. Apkarian, E.L. Chaikof, Engineered collagen - PEO nanofibers and fabrics, *J. Biomater. Sci. Polym. Ed.* 12 (2001) 979–993. doi:10.1163/156856201753252516.
- [213] J.A. Matthews, G.E. Wnek, D.G. Simpson, G.L. Bowlin, Electrospinning of collagen nanofibers, *Biomacromolecules*. 3 (2002) 232–238. doi:10.1021/bm015533u.
- [214] L. Yang, C.F.C. Fitié, K.O. van der Werf, M.L. Bennink, P.J. Dijkstra, J. Feijen, Mechanical properties of single electrospun collagen type I fibers, *Biomaterials*. 29 (2008) 955–962. doi:10.1016/j.biomaterials.2007.10.058.
- [215] B. Dong, O. Arnoult, M.E. Smith, G.E. Wnek, Electrospinning of collagen nanofiber scaffolds from benign solvents, *Macromol. Rapid Commun.* 30 (2009) 539–542. doi:10.1002/marc.200800634.
- [216] Q. Jiang, N. Reddy, S. Zhang, N. Roscioli, Y. Yang, Water-stable electrospun collagen fibers from a non-toxic solvent and crosslinking system, *J. Biomed. Mater. Res. Part A*. 101A (2012) 1237–1247. doi:10.1002/jbm.a.34422.
- [217] B. Kundu, R. Rajkhowa, S.C. Kundu, X. Wang, Silk fibroin biomaterials for tissue regenerations, *Adv. Drug Deliv. Rev.* 65 (2013) 457–470. doi:10.1016/j.addr.2012.09.043.
- [218] Y. Qi, H. Wang, K. Wei, Y. Yang, R.Y. Zheng, I.S. Kim, K.Q. Zhang, A review of structure construction of silk fibroin biomaterials from single structures to multi-level structures, *Int. J. Mol. Sci.* 18 (2017). doi:10.3390/ijms18030237.
- [219] H.Y. Wang, Y.J. Wang, L.X. Zhou, L. Zhu, Y.Q. Zhang, Isolation and bioactivities of a non-sericin component from cocoon shell silk sericin of the silkworm *Bombyx mori*, *Food Funct.* 3 (2012) 150–158. doi:10.1039/c1fo10148j.
- [220] O. Hakimi, D.P. Knight, F. Vollrath, P. Vadgama, Spider and mulberry silkworm silks as compatible biomaterials, *Compos. Part B Eng.* 38 (2007) 324–337. doi:10.1016/j.compositesb.2006.06.012.
- [221] L.-D. Koh, H.-D. Yu, M.-Y. Han, C.-P. Teng, Y.-W. Zhang, Y.-W. Khin, X.-J. Loh, E. Ye, M. Low, Y. Cheng, S.-Y. Tee, Structures, mechanical properties and applications of silk fibroin materials, *Prog. Polym. Sci.* 46 (2015) 86–110. doi:10.1016/j.progpolymsci.2015.02.001.
- [222] S. Zarkoob, R.K. Eby, D.H. Reneker, S.D. Hudson, D. Ertley, W.W. Adams, Structure and morphology of electrospun silk nanofibers, *Polymer (Guildf)*. 45 (2004) 3973–3977. doi:10.1016/j.polymer.2003.10.102.
- [223] K. Ohgo, C. Zhao, M. Kobayashi, T. Asakura, Preparation of non-woven nanofibers of *Bombyx mori* silk, *Samia cynthia ricini* silk and recombinant hybrid silk with electrospinning method, *Polymer (Guildf)*. 44 (2002) 841–846. doi:10.1016/S0032-3861(02)00819-4.
- [224] H. Wang, Y. Zhang, H. Shao, X. Hu, Electrospun ultra-fine silk fibroin fibers from aqueous solutions, *J. Mater. Sci.* 40 (2005) 5359–5363. doi:10.1007/s10853-005-4332-2.
- [225] Y. Kishimoto, H. Morikawa, S. Yamanaka, Y. Tamada, Electrospinning of silk fibroin from all aqueous solution at low concentration, *Mater. Sci. Eng. C*. 73 (2017) 498–506. doi:10.1016/j.msec.2016.12.113.
- [226] S. Sun, S. Sun, X. Cao, R. Sun, The role of pretreatment in improving the enzymatic

- hydrolysis of lignocellulosic materials, *Bioresour. Technol.* 199 (2016) 49–58. doi:10.1016/j.biortech.2015.08.061.
- [227] M. Szymańska-Chargot, J. Cybulska, A. Zdunek, Sensing the structural differences in cellulose from apple and bacterial cell wall materials by Raman and FT-IR Spectroscopy, *Sensors*. 11 (2011) 5543–5560. doi:10.3390/s110605543.
- [228] P. Kulpinski, Cellulose nanofibers prepared by the N-methylmorpholine-N-oxide method, *J. Appl. Polym. Sci.* 98 (2005) 1855–1859. doi:10.1002/app.22123.
- [229] C.W. Kim, D.S. Kim, S.Y. Kang, M. Marquez, Y.L. Joo, Structural studies of electrospun cellulose nanofibers, *Polymer (Guildf)*. 47 (2006) 5097–5107. doi:10.1016/j.polymer.2006.05.033.
- [230] S.O. Han, J.H. Youk, K.D. Min, Y.O. Kang, W.H. Park, Electrospinning of cellulose acetate nanofibers using a mixed solvent of acetic acid/water: Effects of solvent composition on the fiber diameter, *Mater. Lett.* 62 (2007) 759–762. doi:10.1016/j.matlet.2007.06.059.
- [231] K.Y. Lee, L. Jeong, Y.O. Kang, S.J. Lee, W.H. Park, Electrospinning of polysaccharides for regenerative medicine, *Adv. Drug Deliv. Rev.* 61 (2009) 1020–1032. doi:10.1016/j.addr.2009.07.006.
- [232] S. Xu, J. Zhang, A. He, J. Li, H. Zhang, C.C. Han, Electrospinning of native cellulose from nonvolatile solvent system, *Polymer (Guildf)*. 49 (2008) 2911–2917. doi:10.1016/j.polymer.2008.04.046.
- [233] W.K. Son, J.H. Youk, T.S. Lee, W.H. Park, Electrospinning of ultrafine cellulose acetate fibers: Studies of a new solvent system and deacetylation of ultrafine cellulose acetate fibers, *J. Polym. Sci. Part B Polym. Phys.* 42 (2004) 5–11. doi:10.1002/polb.10668.
- [234] S. Tungprapa, T. Puangparn, M. Weerasombut, I. Jangchud, P. Fakum, S. Semongkhon, C. Meechaisue, P. Supaphol, Electrospun cellulose acetate fibers: Effect of solvent system on morphology and fiber diameter, *Cellulose*. 14 (2007) 563–575. doi:10.1007/s10570-007-9113-4.
- [235] M. Wang, L. Wang, Y. Huang, Electrospun hydroxypropyl methyl cellulose phthalate (HPMCP)/erythromycin fibers for targeted release in intestine, *J. Appl. Polym. Sci.* 106 (2007) 2177–2184. doi:10.1002/app.25666.
- [236] X. Wu, L. Wang, H. Yu, Y. Huang, Effect of solvent on morphology of electrospinning ethyl cellulose fibers, *J. Appl. Polym. Sci.* 97 (2005) 1292–1297. doi:10.1002/app.21818.
- [237] A. Frenot, M.W. Henriksson, P. Walkenström, Electrospinning of cellulose-based nanofibers, *J. Appl. Polym. Sci.* 103 (2007) 1473–1482. doi:10.1002/app.24912.
- [238] D. Elieh-Ali-Komi, M.R. Hamblin, Chitin and Chitosan: Production and Application of Versatile Biomedical Nanomaterials., *Int. J. Adv. Res.* 4 (2016) 411–427. doi:10.1002/nbm.3369.Three.
- [239] B.M. Min, S.W. Lee, J.N. Lim, Y. You, T.S. Lee, P.H. Kang, W.H. Park, Chitin and chitosan nanofibers: Electrospinning of chitin and deacetylation of chitin nanofibers, *Polymer (Guildf)*. 45 (2004) 7137–7142. doi:10.1016/j.polymer.2004.08.048.
- [240] J.D. Schiffman, L.A. Stulga, C.L. Schauer, Chitin and Chitosan: Transformations due to the electrospinning process, *Polym. Eng. Sci.* 49 (2009) 1918–1928. doi:10.1002/pen.21434.
- [241] K.E. Park, H.K. Kang, S.J. Lee, B.-M. Min, W.H. Park, Biomimetic Nanofibrous Scaffolds: Preparation and Characterization of PGA/Chitin Blend Nanofibers, *Biomacromolecules*. 7 (2006) 635–643. doi:10.1021/bm0509265.
- [242] M. Rinaudo, Chitin and chitosan: Properties and applications, *Prog. Polym. Sci.* 31 (2006) 603–632. doi:10.1016/j.progpolymsci.2006.06.001.

- [243] J. Nilsen-Nygaard, S.P. Strand, K.M. Vårum, K.I. Draget, C.T. Nordgård, Chitosan: Gels and interfacial properties, *Polymers (Basel)*. 7 (2015) 552–579. doi:10.3390/polym7030552.
- [244] X. Geng, O.H. Kwon, J. Jang, Electrospinning of chitosan dissolved in concentrated acetic acid solution, *Biomaterials*. 26 (2005) 5427–5432. doi:10.1016/j.biomaterials.2005.01.066.
- [245] B. Duan, C. Dong, X. Yuan, K. Yao, Electrospinning of chitosan solutions in acetic acid with poly(ethylene oxide), *J. Biomater. Sci. Polym. Ed.* 15 (2004) 797–811. doi:10.1163/156856204774196171.
- [246] S.M. Lemma, F. Bossard, M. Rinaudo, Preparation of pure and stable chitosan nanofibers by electrospinning in the presence of poly(ethylene oxide), *Int. J. Mol. Sci.* 17 (2016) 1–16. doi:10.3390/ijms17111790.
- [247] S.S. Ojha, D.R. Stevens, T.J. Hoffman, K. Stano, R. Klossner, M.C. Scott, W. Krause, L.I. Clarke, R.E. Gorga, Fabrication and characterization of electrospun chitosan nanofibers formed via templating with polyethylene oxide, *Biomacromolecules*. 9 (2008) 2523–2529. doi:10.1021/bm800551q.
- [248] L. Van Der Schueren, I. Steyaert, B. De Schoenmaker, K. De Clerck, Polycaprolactone/chitosan blend nanofibres electrospun from an acetic acid/formic acid solvent system, *Carbohydr. Polym.* 88 (2012) 1221–1226. doi:10.1016/j.carbpol.2012.01.085.
- [249] Z.Q. Feng, M.K. Leach, X.H. Chu, Y.C. Wang, T. Tian, X.L. Shi, Y.T. Ding, Z.Z. Gu, Electrospun chitosan nanofibers for hepatocyte culture, *J. Biomed. Nanotechnol.* 6 (2010) 658–666. doi:10.1166/jbn.2010.1159.
- [250] C. Kriegel, K.M. Kit, D.J. McClements, J. Weiss, Electrospinning of chitosan – poly (ethylene oxide) blend nanofibers in the presence of micellar surfactant solutions, *Polymer (Guildf)*. 50 (2009) 189–200. doi:10.1016/j.polymer.2008.09.041.
- [251] M. Dilamian, M. Montazer, J. Masoumi, Antimicrobial electrospun membranes of chitosan / poly (ethylene oxide) incorporating poly (hexamethylene biguanide) hydrochloride, *Carbohydr. Polym.* 94 (2013) 364–371. doi:10.1016/j.carbpol.2013.01.059.
- [252] M. Pakravan, M. Heuzey, A. Ajji, A fundamental study of chitosan / PEO electrospinning, *Polymer (Guildf)*. 52 (2011) 4813–4824. doi:10.1016/j.polymer.2011.08.034.
- [253] N. Bhattarai, D. Edmondson, O. Veiseh, F.A. Matsen, M. Zhang, Electrospun chitosan-based nanofibers and their cellular compatibility, *Biomaterials*. 26 (2005) 6176–6184. doi:10.1016/j.biomaterials.2005.03.027.
- [254] K. Desai, K. Kit, J. Li, S. Zivanovic, Morphological and surface properties of electrospun chitosan nanofibers, *Biomacromolecules*. 9 (2008) 1000–1006. doi:10.1021/bm701017z.
- [255] Q. He, Q. Ao, Y. Gong, X. Zhang, Preparation of chitosan films using different neutralizing solutions to improve endothelial cell compatibility, *J. Mater. Sci. Mater. Med.* 22 (2011) 2791–2802. doi:10.1007/s10856-011-4444-y.
- [256] P. Sangsanoh, P. Supaphol, Stability improvement of electrospun chitosan nanofibrous membranes in neutral or weak basic aqueous solutions, *Biomacromolecules*. 7 (2006) 2710–2714. doi:10.1021/bm060286l.
- [257] J.Y. Lai, Y.T. Li, T.P. Wang, In vitro response of retinal pigment epithelial cells exposed to chitosan materials prepared with different cross-linkers, *Int. J. Mol. Sci.* 11 (2010) 5256–5272. doi:10.3390/ijms11125256.
- [258] F.L. Mi, C.T. Huang, H.F. Liang, M.C. Chen, Y.L. Chiu, C.H. Chen, H.W. Sung, Physicochemical, antimicrobial, and cytotoxic characteristics of a chitosan film cross-

- linked by a naturally occurring cross-linking agent, aglycone geniposidic acid, *J. Agric. Food Chem.* 54 (2006) 3290–3296. doi:10.1021/jf0529868.
- [259] T. Yang, D. Nyiawung, A. Silber, J. Hao, L. Lai, S. Bai, Comparative Studies on Chitosan and Polylactic-co-glycolic Acid Incorporated Nanoparticles of Low Molecular Weight Heparin, *AAPS PharmSciTech.* 13 (2012) 1309–1318. doi:10.1208/s12249-012-9854-8.
- [260] B. Lu, X. Lv, Y. Le, Chitosan-Modified PLGA Nanoparticles for Control-Released Drug Delivery, *Polymers (Basel).* 11 (2019) 304. doi:10.3390/polym11020304.
- [261] Q. Min, J. Liu, J. Li, Y. Wan, J. Wu, Chitosan-Polylactide/Hyaluronic Acid Complex Microspheres as Carriers for Controlled Release of Bioactive Transforming Growth Factor- $\beta$ 1, *Pharmaceutics.* 10 (2018) 239. doi:10.3390/pharmaceutics10040239.
- [262] Y. Deng, J. Ren, G. Chen, G. Li, X. Wu, G. Wang, G. Gu, J. Li, Injectable in situ cross-linking chitosan-hyaluronic acid based hydrogels for abdominal tissue regeneration, *Sci. Rep.* 7 (2017) 2699–2711. doi:10.1038/s41598-017-02962-z.
- [263] N. Maeda, J. Miao, T.J. Simmons, J.S. Dordick, R.J. Linhardt, Composite polysaccharide fibers prepared by electrospinning and coating, *Carbohydr. Polym.* 102 (2014) 950–955. doi:10.1016/j.carbpol.2013.10.038.
- [264] A. Bignami, M. Hosley, D. Dahl, Hyaluronic acid and hyaluronic acid-binding proteins in brain extracellular matrix, *Anat. Embryol. (Berl).* 188 (1993) 419–433. doi:10.1007/BF00190136.

## **Chapter 2:**

# **Thesis aim and objectives**

## 2. THESIS AIM AND OBJECTIVES

The chemokine SDF-1 $\alpha$  is known to direct the migration of GBM cells by chemotaxis. GBM cells move up the SDF-1 $\alpha$  concentration gradient to invade surrounding healthy brain tissues. It is also a well-known fact that complete GBM tumor resection is often not achievable using current surgical procedures. The residual GBM cells in the brain can multiply to re-form the tumor, contributing to the worsening of the patients' clinical status and a high rate of mortality. With this in mind, **the project aimed to develop a polymer-based implant capable of sustainably releasing SDF-1 $\alpha$  that could be introduced into the resection cavity to attract the residual GBM cells to facilitate their selective killing** (Figure 2.1).

The following objectives have been identified to be crucial to the fulfilment of the aforementioned aim:

- To encapsulate SDF-1 $\alpha$  in polymer-based nanoparticles to form primary carriers of this chemokine
- To incorporate SDF-1 $\alpha$ -loaded nanoparticles into a nanofibrous scaffold to provide a secondary barrier to the SDF-1 $\alpha$  release process

The following two chapters of this thesis (Chapters 3 and 4) present and discuss the results related to these objectives.

Chapter 3 is titled “Encapsulation of SDF-1 $\alpha$  into Polymer-based Nanoparticles”. This chapter discusses on the preparation of uniform nanoparticles from PLGA and PEG-PLGA co-polymer to encapsulate SDF-1 $\alpha$ . Highlights of this chapter include the careful tailoring of the composition of the nanoparticles to obtain a good balance between SDF-1 $\alpha$  encapsulation efficiency and release capacity.

Chapter 4 is titled “Incorporation of SDF-1 $\alpha$ -loaded PLGA/PEG-PLGA Nanoparticles into Chitosan Nanofibers”. This chapter focuses on the preparation of nanoparticle-nanofiber composite scaffolds by electrospinning. Detailed discussions on the effect of different nanoparticle loads on the morphology of the electrospun fibers as well as the SDF-1 $\alpha$  release profile of the composite scaffolds were included in this part of the thesis.

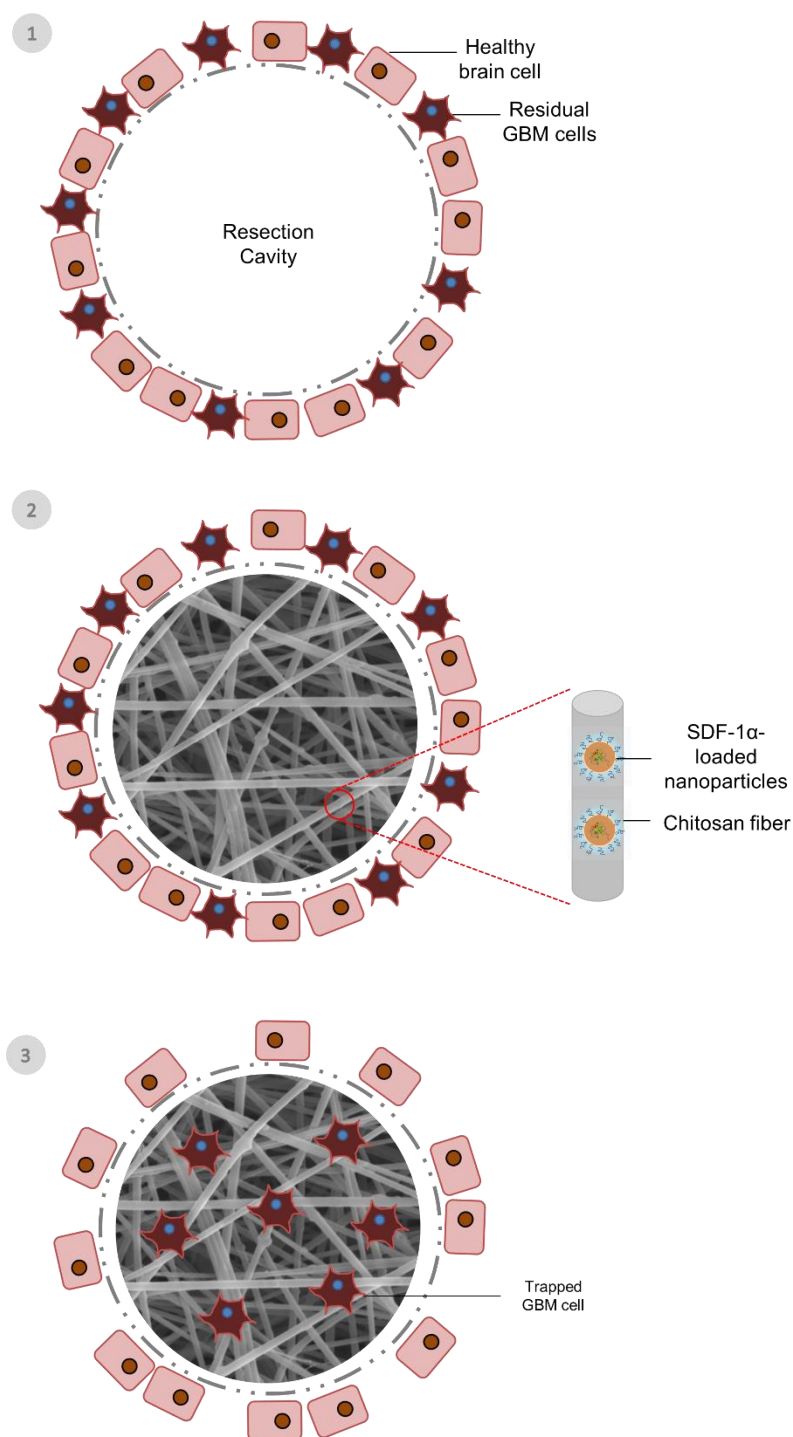


**Figure 2.1:** Schematic description of the aim of the project. Surgical resection of a GBM tumor often leaves behind residual GBM cells close to the resection cavity border (1). The implantation of an SDF-1 $\alpha$ -releasing scaffold into the resection cavity (2) may attract the residual GBM cells to localize them in a pre-defined space (3), facilitating their selective killing.



**Chapter 3:**  
**Encapsulation of SDF-1 $\alpha$**   
**into Polymer-based Nanoparticles**

### 3. ENCAPSULATION OF SDF-1 $\alpha$ INTO POLYMER-BASED NANOPARTICLES

---

#### 3.1. INTRODUCTION

This chapter concerns the design of a novel nanoparticle formulation process to encapsulate SDF-1 $\alpha$  as a first attempt to produce a biocompatible polymer-based vehicle capable of providing sustained release of this protein. Encapsulation of proteins into polymer-based nanoparticles is attractive in the sense that the encapsulation efficiency, release rate and the biocompatibility of the nanocarriers can be controlled at the level of the constituent polymers. It is possible to choose from a long list of polymers that offer a wide range of physicochemical properties to optimize these critical parameters. Of these, hydrophobic polymers such as PLGA and PCL are of significant interest as their relatively slow degradation rate in aqueous environments is likely to be useful in ensuring gradual drug release from the polymer matrix [1,2].

However, the process of formulating nanoparticles from hydrophobic polymers is often complicated by the toxicity of the organic solvents involved [3]. Due to the physical and chemical stress associated with the formulation process, denaturation of the encapsulated protein is also a common problem [4]. In addition, it is often challenging to obtain nanoparticles that can efficiently encapsulate proteins and are also able to subsequently release the protein load at the site of application. Another important issue regarding the use of polymer-based nanoparticles as protein carriers is their instability during storage. Freeze-drying is often required to prolong the shelf-life of nanoparticles formulated from polymers that are susceptible to hydrolysis [5]. However, freeze-drying can induce irreversible particle aggregation, which may affect the protein release profile of the formulation [6].

The work presented in this chapter was centered around achieving the first objective of this project, which is to encapsulate SDF-1 $\alpha$  into polymer-based nanoparticles to form primary carriers of this chemokine, while addressing the problems mentioned above.

Part of this chapter (Section 3.3.1) has been published in the form of an article titled “Development of a non-toxic and non-denaturing formulation process for encapsulation of SDF-1 $\alpha$  into PLGA/PEG-PLGA nanoparticles to achieve sustained release” in the European Journal of Pharmaceutics and Biopharmaceutics.

## 3.2. Summary of the results

Nanoparticles were formulated from a combination of PLGA and PEG-PLGA using a benign water-miscible organic solvent in the form of isosorbide dimethyl ether. Two different types of PLGA were investigated; one with uncapped carboxylic acid terminals (PLGA-COOH) and the other had capped terminals (PLGA-COOR). Thanks to the amphiphilic property of the PEG-PLGA co-polymer, the formation of stable nanoparticles can be induced by a simple phase separation process that took place readily at room temperature and pressure. In addition, proteins were precipitated prior to the encapsulation process to increase their structural stability and minimize denaturation. Changing between the two types of PLGA not only led to variations in the physicochemical characteristics of the nanoparticles (e.g. average size, width of size distribution, zeta-potential) but also the encapsulation efficiencies and release rates. After careful optimization, nanoparticles composed of PLGA-COOR and PEG-PLGA at a mass ratio of 67:33 (referred to as “Formulation 8” in Section 3.3.1) were identified to be a suitable carrier for SDF-1 $\alpha$ . These nanoparticles had an average size of  $259 \pm 8$  nm, a narrow size distribution (polydispersity index of  $0.19 \pm 0.01$ ) and a slightly negative zeta-potential ( $-2.9 \pm 0.2$  mV) when loaded with SDF-1 $\alpha$ . By buffering the pH of the aqueous phase used to induce the phase separation to a value close to the isoelectric point of SDF-1 $\alpha$ , a high encapsulation efficiency ( $75.5 \pm 2.2\%$ ) could be achieved. The nanoparticle formulation could provide SDF-1 $\alpha$  release over a 72-hour period when incubated in a buffer solution supplemented with a physiologically relevant salt concentration at pH 7.4. The released SDF-1 $\alpha$  molecules were verified to retain their biological activity using an *in vitro* bioassay. The nanoparticles were also found to exert negligible cytotoxicity on one human (Thp-1 macrophages) and one animal (NIH3T3 mouse fibroblasts) cell line. Finally, in the presence of hydroxypropyl- $\beta$ -cyclodextrin as a protective agent, the nanoparticles could be freeze-dried without detectable loss in the nanoparticle size uniformity.

### 3.3. RESULTS

#### 3.3.1. Publication 1: EJPB 125 (2018) 38-50

---

#### **Development of a non-toxic and non-denaturing formulation process for encapsulation of SDF-1 $\alpha$ into PLGA/PEG-PLGA nanoparticles to achieve sustained release**

Muhammad Haji Mansor<sup>a,b</sup>, Mathie Najberg<sup>a,c</sup>, Aurélien Contini<sup>a</sup>, Carmen Alvarez-Lorenzo<sup>c</sup>,  
Emmanuel Garcion<sup>a,\*</sup>, Christine Jérôme<sup>b,\*</sup>, Frank Boury<sup>a,#</sup>

<sup>a</sup>CRCINA, INSERM, Université de Nantes, Université d'Angers, Angers, France

<sup>b</sup>Center for Education and Research on Macromolecules (CERM), Université de Liège, Liège, Belgium

<sup>c</sup>Departamento de Farmacología, Farmacia y Tecnología Farmacéutica, R & D Pharma Group, Facultad de Farmacia, Universidade de Santiago de Compostela, Santiago de Compostela, Spain

\* Equivalent contribution

# Corresponding author.

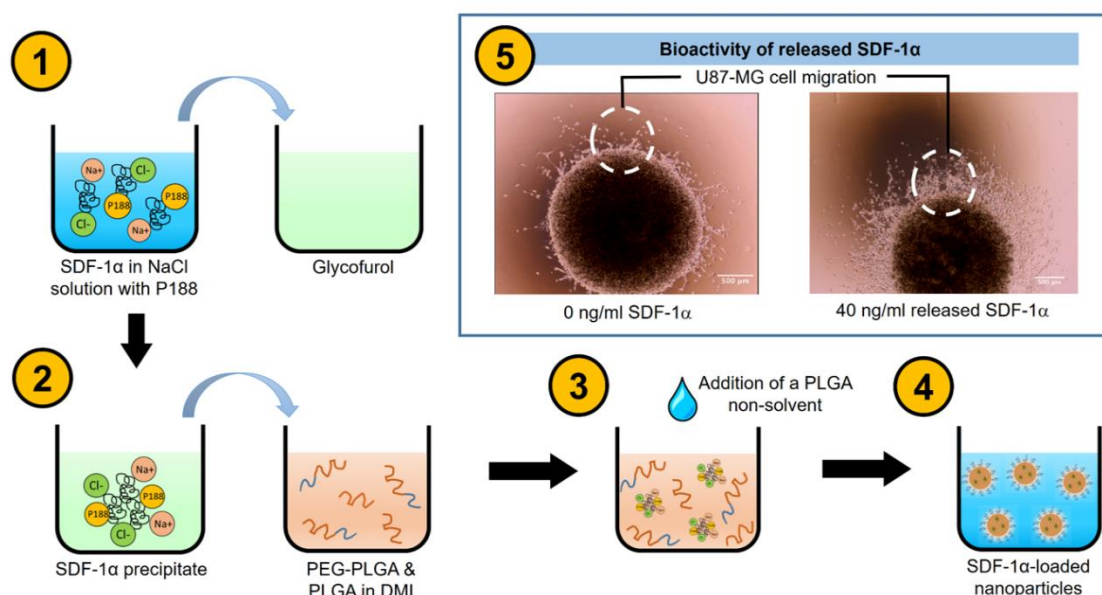
E-mail address: [frank.boury@univ-angers.fr](mailto:frank.boury@univ-angers.fr)

European Journal of Pharmaceutics and Biopharmaceutics 125 (2018) 38-50

<https://doi.org/10.1016/j.ejpb.2017.12.020>

## Abstract

Chemokines are known to stimulate directed migration of cancer cells. Therefore, the strategy involving gradual chemokine release from polymeric vehicles for trapping cancer cells is of interest. In this work, the chemokine stromal cell-derived factor-1 $\alpha$  (SDF-1 $\alpha$ ) was encapsulated into nanoparticles composed of poly(lactic-co-glycolic acid) (PLGA) and a polyethylene glycol (PEG)-PLGA co-polymer to achieve sustained release. SDF-1 $\alpha$ , and lysozyme as a model protein, were firstly precipitated to promote their stability upon encapsulation. A novel phase separation method utilizing a non-toxic solvent in the form of isosorbide dimethyl ether was developed for the individual encapsulation of SDF-1 $\alpha$  and lysozyme precipitates. Uniform nanoparticles of 200–250 nm in size with spherical morphologies were successfully synthesized under mild formulation conditions and conveniently freeze-dried in the presence of hydroxypropyl- $\beta$ -cyclodextrin as a stabilizer. The effect of PLGA carboxylic acid terminal capping on protein encapsulation efficiency and release rate was also explored. Following optimization, sustained release of SDF-1 $\alpha$  was achieved over a period of 72 h. Importantly, the novel encapsulation process was found to induce negligible protein denaturation. The obtained SDF-1 $\alpha$  nanocarriers may be subsequently incorporated within a hydrogel or other scaffolds to establish a chemokine concentration gradient for the trapping of glioblastoma cells.



## Keywords:

Stromal cell-derived factor-1 $\alpha$  (SDF-1 $\alpha$ ), Protein encapsulation, Polymeric nanoparticles, Sustained release

## 1. Introduction

Stromal cell-derived factor-1 $\alpha$  (SDF-1 $\alpha$ ) is a chemokine composed of 68 amino acids [7] that binds to its cognate receptor, C-X-C chemokine receptor type 4 (CXCR4) [8]. One of its important physiological functions is to retain high concentrations of CXCR4-expressing stem and progenitor cells within the bone marrow by creating a positive concentration gradient from the blood to this organ [9]. In the events of tissue damage, the SDF-1 $\alpha$  expression at the injury site is elevated [10–12] in a simultaneous fashion to the increased SDF-1 $\alpha$  degradation in the bone marrow [13,14] to allow mobilisation of the stem and progenitor cells and their subsequent chemoattraction to the site of damage. In addition to its roles in tissue repair and regeneration, SDF-1 $\alpha$ -mediated chemotaxis is also implicated in tumour metastases. CXCR4-expressing cancerous cells that are present in the blood or lymphatic circulation after getting dislodged from the primary tumour site can be chemoattracted to SDF-1 $\alpha$ -secreting sites such as the bone marrow [15], liver [16] and lymph nodes [17] for future metastatic growth. This pathological role of SDF-1 $\alpha$  has inspired the design of implants capable of creating a SDF-1 $\alpha$  concentration gradient for trapping CXCR4-expressing cancerous cells relevant to multiple types of malignant cancers such as glioblastoma (GBM) [18], gastric carcinoma [19] and small-cell lung cancer [20].

Due to its solubility and rapid diffusion in physiological media, a sustained delivery of SDF-1 $\alpha$  is a prerequisite for establishing its concentration gradient. Encapsulation of SDF-1 $\alpha$  into polymeric nanoparticles is a credible strategy for achieving a gradual SDF-1 $\alpha$  release at the site of application. In this regard, poly(lactic-co-glycolic acid) (PLGA) is a polymer of choice for nanoparticle formulations, owing to its biocompatibility, biodegradability and most importantly, its status as a Food and Drug Administration-approved pharmaceutical excipient [21]. However, due to its hydrophobicity, the formation of stable PLGA nanoparticles often necessitates the use of amphiphilic surfactants such as polyvinyl alcohol (PVA) [22,23] and poloxamer 188 (P188) [24] in the formulation process. Although these surfactants are innocuous when used in isolation, residual PVA and P188 bound to the PLGA nanoparticle surfaces have been reported to induce toxicities especially at nanoparticle concentrations exceeding 1 mg/mL [25], which are relevant to many local applications of PLGA-based nanoparticles. The development of a PLGA-based nanoparticle formulation process that avoids or reduces the need for surfactants is therefore in demand.

To encapsulate hydrophilic drugs in hydrophobic PLGA matrices, the double emulsion (water/oil/water) process is often preferred [26,27]. While this process is excellent for encapsulating small hydrophilic molecules, problems can arise with drugs of complex structures such as proteins. The first step of this process that involves emulsification of a protein solution in the polymer-containing organic phase can lead to adsorption of protein molecules to the water/organic solvent interface and their subsequent unfolding. The structural instability of dissolved proteins is actually exaggerated by their conformational flexibility that makes it possible for their hydrophobic pockets to be externalized to make contact with the organic phase upon emulsification [28]. Thus, a possible solution to promote protein stability during encapsulation is by minimizing their conformational mobility through the use of proteins in solid form. In this regard, techniques such as freeze-drying and spray-freeze-drying have been employed to produce fine protein particles for subsequent encapsulation [29,30]. However, these techniques themselves can induce substantial protein structural changes. On the other hand, proteins in solution can be precipitated by adding a water-miscible organic solvent [31]. This technique produces homogenous nano-sized protein particles without affecting protein structures and bioactivities, and therefore serves as a suitable protein treatment prior to encapsulation.

Currently, the encapsulation of proteins or peptides into PLGA nanoparticles typically involves the use of toxic halogenated solvents such as chloroform and dichloromethane as the polymer solvent [32–34]. Other common harmful PLGA solvents include acetonitrile [35], N-methylpyrrolidone [36], N,N-dimethylformamide and tetrahydrofuran [37]. These solvents belong to Class 2 according to the International Conference on Harmonization (ICH), which are harmful solvents that can pose serious threats to patient safety [38]. Less toxic solvents such as acetone [39], ethyl acetate [40] and dimethyl sulfoxide [36] are being increasingly used as alternatives. Nevertheless, they are still regarded as potential hazards to human health by the ICH. Differently, the safety of non-volatile water-miscible organic solvents such as glycofurol and isosorbide dimethyl ether (DMI) have been demonstrated *in vivo*. They have been recommended as solvents suitable for intravascular injections [41,42] due to their negligible toxicity. Thus, the use of these solvents for protein encapsulation into PLGA-based nanoparticles is well-motivated.

In the present study, an amphiphilic polyethylene glycol (PEG)-PLGA co-polymer was synthesized and used together with hydrophobic PLGA polymers to produce stable nanoparticles via a phase separation method without the use of conventional surfactants. In

addition, the non-toxic DMI was utilized as a solvent for the PLGA polymers and the PEG-PLGA co-polymer. To the best of our knowledge, this is the first example of the use of this benign solvent to produce PLGA/PEG-PLGA nanoparticles. PLGA with capped or uncapped carboxylic acid terminals were combined with the PEG-PLGA co-polymer at different proportions to produce nanoparticles of different size distributions and surface charges. The nanoparticles were then freeze-dried in the presence of three excipients to explore the possibility of obtaining nanocarriers with a prolonged shelf-life. Following the optimization of the PLGA/PEG-PLGA nanoparticle synthesis, lysozyme (14.3 kDa, isoelectric point: 11.35) was initially used as a model protein to optimize the encapsulation of SDF-1 $\alpha$  (8.0 kDa, isoelectric point: 10.5). To preserve the protein bioactivity throughout the formulation process, lysozyme and SDF-1 $\alpha$  precipitates were prepared by mixing respective protein solutions with glycofurol prior to encapsulation. Then, *in vitro* release of lysozyme and SDF-1 $\alpha$  from the PLGA/PEG-PLGA nanoparticles was studied. The bioactivity of the released SDF-1 $\alpha$  was subsequently assessed in terms of its capacity to induce migration of CXCR4-expressing human GBM cells (U87-MG). Finally, the cytocompatibility of the newly-developed nanoparticles was assessed *in vitro*.

## 2. Materials and methods

### 2.1. Materials

PLGA with capped carboxylic acid terminals and PEG-PLGA co-polymer were synthesised as described in Section 2.2.. PLGA 75:25 with uncapped terminals (Resomer® RG752H, Mw = 9850 Da, polydispersity index (PDI) = 2.4), lysozyme of chicken egg white, *Micrococcus lysodeikticus*, glycofurol (tetraglycol or tetrahydrofurfuryl alcohol polyethyleneglycol ether), isosorbide dimethyl ether (dimethyl isosorbide), dimethyl sulfoxide (DMSO), sodium chloride, poloxamer 188 (Lutrol® F68), glycine, sucrose, trehalose, 37% hydrochloric acid, 10 M sodium hydroxide, tris(hydroxymethyl)aminomethane (Tris) base (Trizma®) and agarose with low gelling temperature were obtained from Sigma-Aldrich (Saint Quentin Fallavier, France). DL-lactide (Purasorb® DL) and glycolide (Purasorb® G) were obtained from Purac Biomaterials, Frankfurt, Germany. Bovine serum albumin fraction V was obtained from Roche Diagnostics (Mannheim, Germany), human SDF-1 $\alpha$  from Miltenyi Biotech (Paris, France), hydroxypropyl- $\beta$ -cyclodextrin (Kleptose® HPBCD) from Roquette (Lestrem, France), Dulbecco's phosphate-buffered saline (Biowhittaker®) from Lonza (Verviers, Belgium), and Dulbecco's Modified Eagle's Medium (Gibco® DMEM) from Thermo Fisher Scientific

(Villebon sur Yvette, France). Ultrapure water dispensed from a Milli-Q® Advantage A10 system (Millipore, Paris, France) was used in all experiments.

## **2.2. Synthesis and characterization of PLGA with capped carboxylic acid terminals (PLGA-COOR) and PEG-PLGA co-polymer**

### **2.2.1. Synthesis**

The synthesis of PLGA-COOR was adapted from the ring-opening polymerization method described by Yoo and Park [43]. Briefly, a mixture of DL-lactide (Purasorb® DL) and glycolide (Purasorb® G) in the molar ratio of 3:1 was heated with the initiator benzyl alcohol to 140 °C under nitrogen atmosphere for complete melting. The use of this initiator would result in a benzyl group being the R-group in the PLGA-COOR product. Then, 0.04% (w/w) stannous octoate was added, and the reaction mixture was further heated to 180 °C. The temperature was maintained for 3 hours for polymerization to take place under static vacuum. The polymer was then recovered by dissolution in dichloromethane before precipitation in heptane. The precipitate was subsequently filtered and dried at 25 °C for 24 hours under vacuum. For the synthesis of PEG-PLGA co-polymer, the same procedure was adopted except that monomethoxy-PEG of number average molecular weight (Mn) of 5 kDa (Sigma-Aldrich) was used as an initiator instead of benzyl alcohol, and the precipitation of PEG-PLGA was carried out in diethyl ether chilled to -20 °C.

### **2.2.2. Characterization**

<sup>1</sup>H nuclear magnetic resonance (<sup>1</sup>H-NMR) spectra were recorded using a Bruker Avance® 400 apparatus (Bruker, Brussels, Belgium) to characterise the polymer/co-polymer composition and to estimate Mn. Deuterated DMSO and chloroform were used as solvents for PLGA-COOR and PEG-PLGA co-polymer respectively. Spectra were recorded at 400 MHz in the Fourier Transform mode at 25 °C with chemical shifts expressed in ppm with respect to the tetramethylsilane standard. The polymer/co-polymer was also characterized by size exclusion chromatography (SEC) using a Viscotek® TDA-305 equipment (Malvern, Worcestershire, UK). Polymer/co-polymer was dissolved in tetrahydrofuran at 5 mg/mL for elution at a flow rate of 1 mL/min at 45 °C. The weight-average molecular weight (Mw) and Mn were expressed with respect to polystyrene standards. The PDI of the polymer/co-polymer was subsequently obtained by calculating the ratio of Mw to Mn.

## **2.3. Preparation of lysozyme and SDF-1 $\alpha$ precipitates**

Proteins were precipitated using a technique adapted from Giteau et al. [31]. Briefly, lyophilized protein as provided by the supplier was dissolved in sodium chloride (NaCl) solution containing 20% (w/v) P188 as a protein protective agent. 25  $\mu$ L of the protein solution was then added to 975  $\mu$ L glycofurol in a 10 mL Nalgene® Oak Ridge High-Speed centrifuge tube (Thermo Fisher Scientific) prior to incubation in ice for 30 minutes. The optimal concentrations of protein and NaCl were investigated initially using lysozyme as a model protein. To evaluate the precipitation efficiency (PE), the formed suspension of protein precipitates was centrifuged at 12,800  $\times g$  for 30 minutes. The supernatant was carefully discarded and the pelleted protein precipitates were dissolved in 1 mL 0.05 M Tris-HCl buffer solution containing 0.1% (w/v) bovine serum albumin (BSA) and diluted for further quantification (see Section 2.7.). PE was calculated using Equation 1.

$$PE (\%) = \frac{\text{Mass of protein recovered after precipitation}}{\text{Initial mass of protein used as a starting material}} \times 100 \quad (\text{Equation 1})$$

#### 2.4. Preparation of lysozyme- and SDF-1 $\alpha$ -loaded nanoparticles

Nanoparticles were formed using a phase separation method adapted from Tran et al. [17]. Briefly, PLGA-COOR, PLGA-COOH and PEG-PLGA co-polymer were dissolved separately in DMI at 12% (w/v). The three polymer solutions were mixed in different proportions to give a total volume of 300  $\mu$ l. For protein encapsulation, 100  $\mu$ l protein precipitate suspension in glycofurol consisting of either 25  $\mu$ g lysozyme or 10  $\mu$ g SDF-1 $\alpha$  was added to the polymer solutions prior to magnetic stirring at 1300 rpm for 30 seconds. The theoretical drug loadings (DL), as calculated using Equation 2, were 0.07 % and 0.03 % for lysozyme and SDF-1 $\alpha$  respectively. For the synthesis of unloaded nanoparticles, the 100  $\mu$ l protein precipitates was replaced with an equal volume of glycofurol alone. Then, 100 $\mu$ l aqueous phase in the form of 0.05 M glycine-NaOH buffer solution was added under magnetic stirring to initiate phase separation. After 1 minute, another 500 $\mu$ l aqueous phase was added every 30 seconds for four times to enhance the phase separation process. The pH of the aqueous phase was varied to investigate the effect of protein solubility on encapsulation efficiencies. The formed nanoparticle suspension was diluted with water to 30 mL to allow diffusion of residual solvents out of the nanoparticles. After 1 hour, the nanoparticle suspension was centrifuged for 30 minutes at 10,000  $\times g$ . The supernatant was discarded and the nanoparticle pellet was re-suspended in water. The centrifugation was repeated once to complete the purification process and the resultant nanoparticle suspension was concentrated to a final volume of 1 mL.

$$DL (\%) = \frac{\text{Initial mass of protein used as a starting material}}{\text{Total mass of PLGA and PEG-PLGA}} \times 100 \quad (\text{Equation 2})$$

## 2.5. Freeze-drying of nanoparticles

After purification, 1 mL of nanoparticle suspension was transferred into a 20 mL glass vial. To ensure the stability of the nanoparticles throughout the freeze-drying process, 1 mL of cryoprotectant solution was added to the nanoparticle suspension to give a total volume of 2 mL and a final nanoparticle concentration of approximately 15 mg/mL. The cryoprotectants tested were HPBCD, trehalose and sucrose, at a final concentration of 5% (w/v). The vial was then immersed in liquid nitrogen (-196 °C) for 1 minute to freeze the nanoparticle-cryoprotectant mixture, and subsequently placed on the shelf of the freeze-dryer pre-cooled to -35 °C for 2 hours. The samples were subsequently lyophilized, alongside cryoprotectant-free nanoparticle samples as a control, in a Lyovax® GT freeze-dryer (Steris, Bordeaux, France) at -20 °C and 0.3 mbar for 16 hours. The nanoparticle size was measured (as described in 2.6.1.) before and after freeze-drying. The nanoparticles were assumed to be stable throughout the freeze-drying process if the ratio of final to initial size ( $S_f/S_i$ ) and polydispersity index ( $PDI_f/PDI_i$ ) is close to 1.

## 2.6. Nanoparticle characterization

### 2.6.1. Size distribution and zeta-potential

The nanoparticle size distribution was determined by a dynamic light scattering (DLS) technique whereas zeta-potentials were derived from electrophoretic mobility values using the Smoluchowski's approximation. Nanoparticle samples were prepared by dilution in water or 0.01 M NaCl solution for size and zeta-potential measurements respectively, to obtain concentrations suitable for analyses in a Nanosizer® ZS (Malvern) such that the attenuator value was in the range of 5 - 7. Each sample was measured in triplicate, with each measurement representing an average value of at least 10 runs. All measurements were made at 25°C under automatic mode. Besides average particle size, the DLS protocol of Nanosizer® ZS produced a PDI value ranging between 0 – 1 that estimates the width of the size distribution.

### 2.6.2. Scanning electron microscopy (SEM), transmission electron microscopy (TEM) and atomic force microscopy (AFM)

The nanoparticle morphology was visualised under SEM (JSM 6310F, JEOL, Paris, France), TEM (JEM 1400, JEOL, Paris, France) and AFM (AutoProbe CP-Research, Veeco Digital

Instruments, Santa Barbara, California, USA). A 2  $\mu\text{L}$  drop of purified nanoparticle suspension at a concentration of 200  $\mu\text{g}/\text{mL}$  was added onto the centre of a glass slide (for SEM and AFM) or carbon-coated nickel grid (for TEM), and left to dry overnight at room temperature. For SEM, the sample was coated with a gold layer of 5 nm thickness prior to observation while no coating was applied to TEM or AFM samples. For AFM, tapping mode (resonance frequency = 300 kHz) was used instead of contact mode to minimise sample damage upon observation.

For the observation of protein nanoprecipitates, the undiluted protein nanoprecipitate suspension was used to prepare samples for SEM, via the same procedure as the preparation of nanoparticle samples.

### 2.6.3. Protein encapsulation efficiency

Lyophilized protein-loaded nanoparticles, and unloaded nanoparticles as a control, were dissolved in 1 mL DMSO for 1 hour before the addition of 3 mL 0.01 M HCl. The solution was left to stand for another hour for protein extraction from the nanoparticle fragments. The samples were then diluted for use in protein quantification assays (see Section 2.7.). Encapsulation efficiency (EE) was calculated using Equation 3.

$$EE (\%) = \frac{\text{Mass of protein recovered from dissolved nanoparticles}}{\text{Initial mass of protein used as a starting material}} \times 100 \quad (\text{Equation 3})$$

## 2.7. Protein quantification

### 2.7.1. Quantification of lysozyme

Lysozyme was quantified using *Micrococcus lysodeikticus* cell suspension as a substrate as described by Morille et al. [44]. Briefly, 100  $\mu\text{L}$  lysozyme solution or sample was added to 2.9 mL suspension of *M. lysodeikticus* (0.015% (w/v)) in 0.05 M Tris-HCl buffer solution (pH 7.4). After 4 hours of incubation at 37°C, the absorbance was measured at 450 nm. For the construction of a standard curve, the concentration of lysozyme solutions used was between 100 - 1000 ng/mL. 0.05 M Tris-HCl buffer solution (pH 7.4) was used to prepare several dilutions of the samples to obtain absorbance readings that were within the standard curve range.

### 2.7.2. Quantification of SDF-1 $\alpha$

SDF-1 $\alpha$  was quantified using an enzyme-linked immunosorbent assay (ELISA) according to the supplier's instructions (R&D Systems, Lille, France). Briefly, SDF-1 $\alpha$  capture antibody solution was added to a Nunc Maxisorp® 96-well microplate (Thermo Fisher Scientific) and

incubated overnight to coat the wells. The microplate was then washed with 0.05% (w/v) Tween® 20 in phosphate-buffered saline (PBS) solution (pH 7.4), followed by a 1-hour incubation with PBS solution (pH 7.4) containing 1% (w/v) BSA to block the microplate. After washing, the kit standard and samples diluted in PBS (pH 7.4) containing 1% (w/v) BSA were added to the microplate for a 2-hour incubation. Then, the microplate was washed before addition of a detection antibody solution for another 2-hour incubation. The washing step was subsequently repeated prior to incubation with a streptavidin-horseradish peroxidase solution for 20 minutes. After the final wash, a substrate solution was added for another 20-minute incubation. Finally, 2 N sulphuric acid was added to terminate the enzymatic reaction followed by immediate measurement of absorbance at 450 nm. All incubations were done at room temperature.

## 2.8. Assessment of SDF-1 $\alpha$ bioactivity

The bioactivity of the precipitated and released SDF-1 $\alpha$  was assessed using the agarose drop migration assay as adapted from Milner et al. [45]. Briefly, U87-MG cells (American Tissue Culture Collection, Rockville, Maryland, USA), previously transfected to express CXCR4 receptor by Séhédic et al. [46], were seeded into a 24-well flat-bottomed culture plate (Nunc, Strasbourg, France) at a density of  $1 \times 10^5$  cells per well and cultured in medium supplemented with 10% foetal bovine serum (FBS) and 1% penicillin/streptomycin. The wells were previously treated with 500  $\mu$ L of a 10  $\mu$ g/mL poly-D-lysine hydrobromide (Sigma-Aldrich) solution for 15 minutes at 37 °C and washed three times with PBS prior to cell seeding. After 72 hours of incubation at 37 °C under a 5% CO<sub>2</sub> humidified atmosphere, the culture medium was removed and the cells were lysed by adding water (500  $\mu$ L per well) to cover the well surfaces with a thin cell-derived matrix. After 20 minutes, the wells were washed three times with PBS and allowed to air-dry. Then, 2  $\mu$ L of 1% (w/v) low gelling point agarose solution containing U87-MG cells at a density of  $50 \times 10^6$  cells/mL was dropped onto the centre of each well and allowed to gel at 4 °C for 15 minutes. At this point, 400  $\mu$ L of SDF-1 $\alpha$ -free medium or medium supplemented with 40 ng/mL native/precipitated/released SDF-1 $\alpha$  was added to the cell-laden agarose drops prior to incubation. After 72 hours, optical microscopic images of the plan view of each well were taken. Cell migration was estimated by measuring the distance between the furthest-migrating cells and the edge of the cell-laden agarose drop. Measurements were made on four sides (north, east, south and west) of the drop using ImageJ software and subsequently averaged to obtain a representative value of a drop. Three drops were prepared for each medium condition in each experiment.

## 2.9. *In vitro* protein release

Protein-loaded nanoparticles, and unloaded nanoparticles as a control, were suspended in 2 mL buffer solution containing 0.1% (w/v) BSA as a protein stabilizer and kept in a 2 mL centrifuge tube. The tube was incubated at 37°C in a shaking water bath (125 rpm). At pre-defined time intervals, the tube was centrifuged at  $8500 \times g$  for 30 minutes. 0.3 mL of the supernatant was collected and replaced with fresh buffer. The supernatant was stored at -20 °C until protein quantification (as described in Section 2.7 for lysozyme and SDF-1 $\alpha$ ) and biological activity assessment (as described in Section 2.8 for SDF-1 $\alpha$ ).

## 2.10. *In vitro* cytotoxicity of nanoparticles

*In vitro* cytotoxicity of unloaded PLGA/PEG-PLGA nanoparticles was evaluated using a resazurin-based assay adapted from Swed et al. [47]. NIH3T3 mouse fibroblast cell line was cultured at 37 °C and 5% CO<sub>2</sub> in medium supplemented with 10% FBS and 1% penicillin/streptomycin, and replaced every 3 days. The cells were seeded in a 96-well flat-bottomed culture plate (Nunc) at a density of  $5.5 \times 10^3$  cells/well in 100  $\mu$ L medium and incubated at 37 °C and 5% CO<sub>2</sub> for 24 h. At this point, 50  $\mu$ L of the old medium was replaced with an equal volume of nanoparticle-containing fresh medium, to obtain final nanoparticle concentrations of 0.01, 0.1, 1 and 10 mg/mL. As a negative control, cells incubated with the medium alone were prepared. After 48 h of incubation (72 h post-seeding) in the presence or absence of nanoparticles, the entire medium was replaced with 100  $\mu$ L fresh medium containing 44  $\mu$ M resazurin. The resazurin-containing medium was also added in three wells of the assay plates (without cells), which served as blank. The plate was incubated for another 3 h 30 m. Cell viability was estimated from the fluorescence intensity of the reduced product of resazurin, called resorufin, which was measured using a ClarioStar microplate fluorometer (BMG Labtech GmbH, Ortenberg, Germany) at 545 nm excitation and 600 nm emission. All readings were normalised to those obtained with the nanoparticle-untreated cells.

In addition to the PLGA/PEG-PLGA nanoparticles, two other types of nanoparticles, namely lipid nanocapsules (LNC) and polystyrene (PS) nanoparticles, were tested in this assay to obtain information on the relative safety of the newly-developed nanoparticles. LNC (average size = 122 nm, PDI = 0.088) were prepared using a phase inversion method as discussed by Heurtault et al. [48]. PS nanoparticles (average size = 285 nm, PDI = 0.175) were purchased from Sigma-Aldrich.

## 2.11. Statistical analysis

Data are presented as the mean value  $\pm$  standard deviation (SD) of at least three experiments ( $n \geq 3$ ). One-way ANOVA with post-Dunnett's multiple comparison test with a threshold P-value of 0.05 was used to investigate any significant difference between multiple groups of data. In the figures, \* indicates  $P \leq 0.05$ , \*\* indicates  $P \leq 0.01$ , \*\*\* indicates  $P \leq 0.001$  and \*\*\*\* indicates  $P \leq 0.0001$ .

### 3. Results and discussion

#### 3.1. Characterization of PLGA-COOR and PEG-PLGA co-polymer

$^1\text{H-NMR}$  spectrum of PLGA-COOR in Figure 1 revealed the presence of lactide units at 5.19 ppm and 1.46 ppm, glycolide units at 4.91 ppm, and benzyl capping groups at 7.37 ppm. Using the signal at 7.37 ppm as a reference for integration,  $M_n$  was calculated to be 5.5 kDa, with a lactide/glycolide molar percentage of 75/25. For the PEG-PLGA co-polymer, the signal at 3.64 ppm, which is characteristic of ethylene glycol units, indicated the successful co-polymerization of monomethoxy-PEG 5 kDa to the lactide and glycolide units. Using this signal as a reference, the  $M_n$  of the co-polymer was 30.7 kDa (PEG 5 kDa - PLGA 25.7 kDa) whereas the lactide/glycolide molar percentage was calculated to be 75/25. On the other hand, SEC analyses showed that the  $M_w/M_n$  values were 11.2/5.7 kDa (PDI = 2.0) and 44.1/21.0 kDa (PDI = 2.1) for PLGA-COOR and PEG-PLGA co-polymer respectively. The disparity between the PEG-PLGA  $M_n$  values calculated using these two techniques could be attributed to the amphiphilic nature of the co-polymer [44,49,50] that may have modified the hydrodynamic volume to prolong the retention time, which subsequently produced an underestimated  $M_n$  value using SEC.

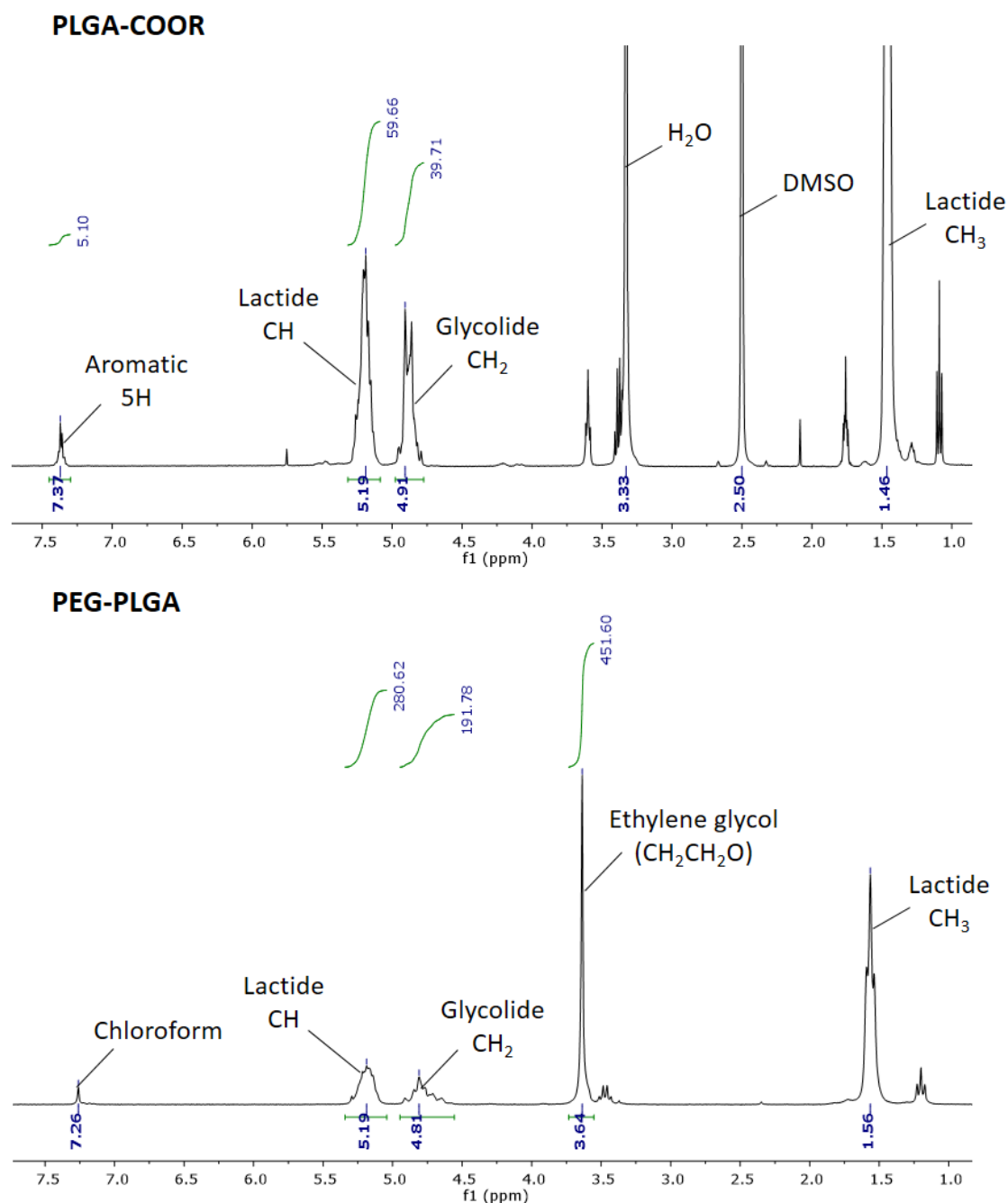


**Figure 1:**  $^1\text{H}$ -NMR of PLGA-COOR and PEG-PLGA co-polymer in deuterated DMSO and chloroform respectively.

### 3.2. Lysozyme and SDF-1 $\alpha$ precipitation

Due to the greater stability of proteins in their solid state, proteins dissolved in a salt solution containing P188 were precipitated through their addition to an organic solvent as a preparation for encapsulation. Glycofurol was the organic solvent of choice for two main reasons. Firstly, its water-miscibility enables an efficient separation of water from protein molecules to induce

precipitation. Secondly, it has been used to precipitate many proteins without causing their denaturation [31,44,51,52]. P188 was added due to its ability to refold any unfolded protein [53] and also to reduce protein adsorption to the hydrophobic PLGA following encapsulation, which in turn may allow for greater cumulative release [44,54]. To minimise any potential toxicity, the amount of P188 used to precipitate the amount of protein sufficient for one nanoparticle formulation was kept at 500  $\mu\text{g}$ . Proteins were initially dissolved in NaCl solution to neutralise the charged protein molecules and promote attractive hydrophobic interactions. The concentration of NaCl that would decrease the aqueous solubility of SDF-1 $\alpha$  without causing its denaturation was investigated using lysozyme as a model protein. Following precipitation, the amount of bioactive lysozyme was quantified using the *Micrococcus lysodeikticus* assay. As shown in Figure 2, 0.15 M NaCl resulted in a successful precipitation with a complete preservation of lysozyme bioactivity. Lower PE was obtained in the absence of NaCl, possibly due to the repulsion between charged protein molecules that hindered the formation of precipitates. On the other hand, PE decreased when the NaCl concentration was increased above 0.15 M. Although high concentrations of salt can reduce the aqueous solubility of a protein and facilitate precipitation, the excess charge neutralisation may simultaneously promote protein denaturation by allowing any unfolded protein molecules to spontaneously form aggregates and therefore preventing their re-folding [55]. On this basis, 0.15 M NaCl was used to precipitate SDF-1 $\alpha$ . The effect of protein concentrations on PE was also investigated. PE values were greater with higher lysozyme concentrations, due to greater tendencies for protein molecules to collide and interact with one another. Although 10 mg/mL or higher lysozyme concentrations were identified to result in a maximum PE, it was not possible to dissolve SDF-1 $\alpha$  in 0.15 M NaCl at these concentrations. Therefore, SDF-1 $\alpha$  was precipitated at 2.67 mg/mL, which was the highest concentration that could be achieved without the appearance of visible protein solids. Using ELISA, the PE was calculated to be  $91 \pm 5\%$ . More importantly, the bioactivity of the re-constituted SDF-1 $\alpha$  precipitates was not significantly different from the native SDF-1 $\alpha$  when tested using the agarose drop migration assay (Figure 6B,C).

Following the optimisation of precipitation conditions, the morphology of the precipitates was observed under SEM. The precipitates of both proteins were mostly spherical in shape (Figure 3). Furthermore, their size distributions (as estimated using the ImageJ software) were  $57 \pm 10$  nm and  $57 \pm 25$  nm for lysozyme and SDF-1 $\alpha$  respectively. The sub-100 nm sizes of the protein

precipitates make them ideal for subsequent encapsulation into the PLGA/PEG-PLGA nanoparticles.

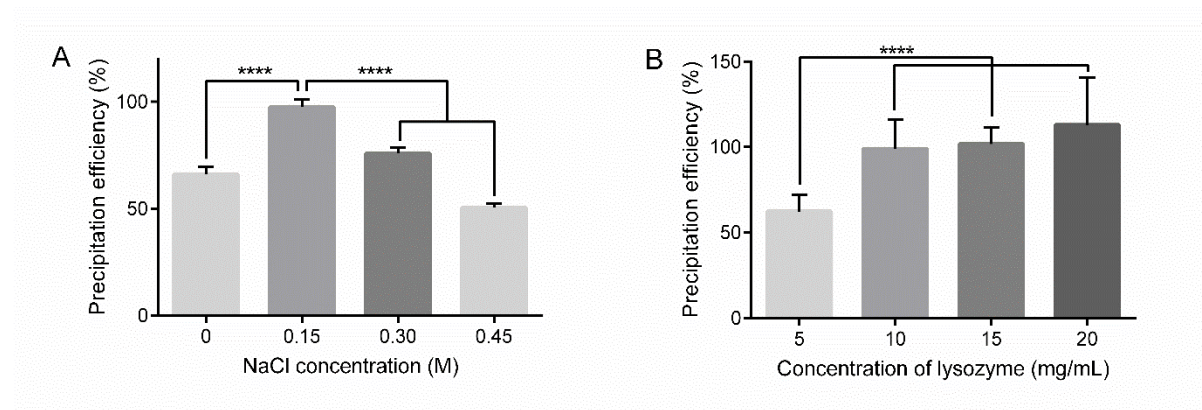


**Figure 2:** Effect of (A) NaCl and (B) lysozyme concentrations on lysozyme precipitation efficiency. For (A), lysozyme concentration was fixed at 10 mg/mL whereas NaCl concentration was fixed at 0.15 M for (B). Statistical analysis was conducted to investigate any significant difference ( $P \leq 0.05$ ) in comparison to 0.15 M NaCl or 5 mg/mL lysozyme concentration for (A) and (B) respectively. \*\*\*\* indicates  $P \leq 0.0001$ ,  $n = 3$  for each lysozyme precipitation condition.

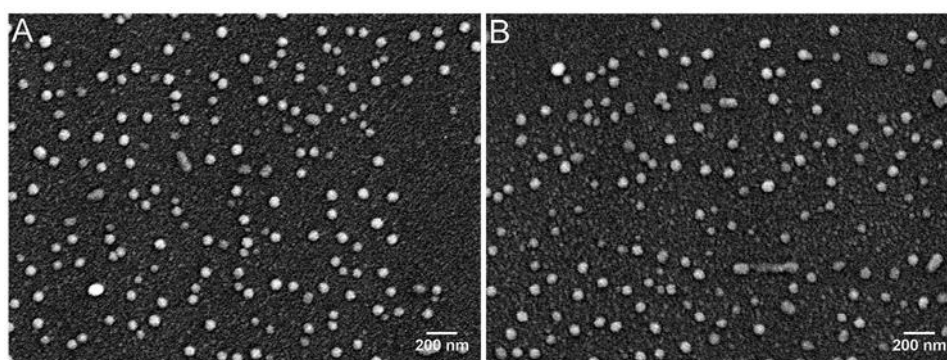


**Figure 3:** Scanning electron microscopy of (A) lysozyme and (B) SDF-1 $\alpha$  nanoprecipitates.

### 3.3. Preparation and characterization of lysozyme- and SDF-1 $\alpha$ -loaded nanoparticles

#### 3.3.1. Optimisation of PLGA/PEG-PLGA nanoparticle synthesis

Due to the amphiphilic behaviour of PEG-PLGA, it was predicted that uniform and stable nanoparticles can be obtained by mixing this co-polymer with the hydrophobic PLGA. Using this combination instead of the co-polymer alone can provide additional means for controlling the nanoparticle physicochemical properties that are critical for protein encapsulation and release, such as the size and zeta-potential, by varying the chemical constituents of the PLGA component such as the number of uncapped carboxylic acid groups.

The physicochemical characteristics of unloaded nanoparticles made from different combinations of PEG-PLGA co-polymer and PLGA polymers are shown in Table 1. No homogeneous nanoparticle suspension could be obtained in the absence of PEG-PLGA (Formulations 1 & 5) whereas the size and PDI values decreased as the PEG-PLGA proportion was increased when used in combination with either PLGA-COOH (Formulations 2 - 4) or PLGA-COOR (Formulations 6 - 8). These observations confirmed the critical nanoparticle-stabilizing roles of the co-polymer to compensate for the lack of use of surfactants such as PVA and P188. Furthermore, zeta-potential values generally became less negative with increasing PEG-PLGA proportion, which can be explained by the increasing density of PEG layer on the nanoparticle surface that shields the negatively-charged PLGA carboxylic acid groups [56]. Based on these observations and literature data [57], the synthesized nanoparticles can be thought of to possess a structure consisting of a hydrophilic PEG layer surrounding a hydrophobic PLGA core.

Upon substituting PLGA-COOH with an equal proportion of PLGA-COOR, the nanoparticle size increased and zeta-potential values became less negative (Formulations 2 vs. 6, 3 vs. 7 and 4 vs. 8), which suggested that PLGA terminal capping has an effect on nanoparticle properties. To confirm this, PLGA-COOH and PLGA-COOR were combined with a fixed proportion of PEG-PLGA that is sufficient to produce uniform nanoparticles (Formulation 9 and 10). Taking together the results obtained when only either PLGA-COOH or PLGA-COOR was combined with PEG-PLGA (Formulations 4 and 8), it was confirmed that the nanoparticle size increased as the PLGA-COOH was gradually replaced with PLGA-COOR. Simultaneously, the zeta-potential values also became less negative. The largest zeta-potential change was seen in alkaline conditions (pH 10) due to deprotonation of all uncapped carboxylic acid groups. The greater abundance of uncapped carboxylic acid terminals found in nanoparticles made of higher PLGA-COOH proportions may lead to higher inter-particle electrostatic repulsions, which prevent particle collusion and consequently reduce the average size.

**Table 1:** Average size, polydispersity index (PDI) and zeta-potential (ZP) of unloaded nanoparticle formulations. Data are presented as mean  $\pm$  SD, n = 3.

Formulation number	Proportion (%)			Average size (nm) <sup>a</sup>	Average PDI <sup>a</sup>	Average ZP (mV) <sup>b</sup>		
	PLGA-COOH	PLGA-COOR	PEG-PLGA			pH 4	pH 7	pH 10
1	100	0	0			n.d. <sup>c</sup>		
2	92	0	8	599 $\pm$ 20	0.46 $\pm$ 0.08	-16.6 $\pm$ 1.0	-20.7 $\pm$ 2.2	-28.0 $\pm$ 2.4
3	75	0	25	279 $\pm$ 3	0.17 $\pm$ 0.03	-9.9 $\pm$ 0.8	-12.1 $\pm$ 1.3	-15.7 $\pm$ 1.5
4	67	0	33	202 $\pm$ 3	0.08 $\pm$ 0.05	-6.6 $\pm$ 1.0	-8.9 $\pm$ 0.8	-9.8 $\pm$ 0.7
5	0	100	0			n.d. <sup>c</sup>		
6	0	92	8	>1000	1	-2.9 $\pm$ 0.5	-4.7 $\pm$ 0.4	-6.4 $\pm$ 0.6
7	0	75	25	691 $\pm$ 23	0.40 $\pm$ 0.05	-1.8 $\pm$ 0.1	-2.3 $\pm$ 0.3	-3.1 $\pm$ 0.4
8	0	67	33	255 $\pm$ 4	0.14 $\pm$ 0.04	-1.2 $\pm$ 0.2	-3.0 $\pm$ 0.6	-2.9 $\pm$ 0.2
9	33	33	33	215 $\pm$ 7	0.10 $\pm$ 0.03	-4.1 $\pm$ 0.2	-4.8 $\pm$ 0.5	-4.3 $\pm$ 0.3
10	17	50	33	236 $\pm$ 6	0.10 $\pm$ 0.02	-2.8 $\pm$ 0.4	-4.1 $\pm$ 0.6	-4.0 $\pm$ 0.4

<sup>a</sup> Purified nanoparticle suspension was diluted to 100  $\mu$ g/mL in water prior to measurement

<sup>b</sup> Purified nanoparticle suspension was diluted to 100  $\mu$ g/mL in 0.01 M NaCl and 0.1 M HCl or NaOH was used to adjust the pH of the suspension to pH 4, 7 or 10 prior to measurement

<sup>c</sup> n.d. = not determined, as no homogenous particle suspension was obtained

To ensure good colloidal stability, zeta potential values of greater than +30 mV or lower than -30 mV are generally regarded as ideal, as this ensures strong electrostatic repulsive forces between the nanoparticles [58]. In this work, the presence of the external PEG layer inevitably decreased the zeta potential magnitude of the PLGA/PEG-PLGA nanoparticles. Despite the loss in electrostatic stabilization, the nanoparticle suspension benefited from the steric stabilization conferred by the PEG chains. To verify this, Formulation 8 was suspended in 0.05 M Tris-HCl buffer (pH 7.4) containing 0.15 M NaCl at 1 mg/mL concentration and the suspension was kept at 37 °C. There were minimal changes in the average size of the nanoparticles after 20 days (Supplementary Figure 1A). Interestingly, the zeta-potential values became increasingly negative with time (Supplementary Figure 1B). It was likely that PEG-mediated steric repulsions provided the main stabilization force for freshly-produced nanoparticles. As the PLGA ester bonds gradually hydrolyzed to reveal more negatively-charged carboxylic acid terminals, the increasing magnitude of electrostatic repulsions prevented the formation of any aggregates.

### 3.3.2. Freeze-drying of PLGA/PEG-PLGA nanoparticles

Polyesters such as PLGA are prone to degradation by means of hydrolysis of the ester bonds, which may lead to leakage of the drug load encapsulated within polyester-based nanocarriers. Therefore, dehydration of PLGA-based nanoparticles, commonly by freeze-drying, is imperative to ensure their long-term stability. To protect the nanoparticles from freezing and

drying stresses, cryoprotectants should be added to the nanoparticle suspension before freezing. Disaccharides such as sucrose and trehalose, and oligosaccharides such as HPBCD have been shown to be excellent protectants [59]. Nevertheless, it is also important that the drying temperature is maintained below the collapse temperature ( $T_c$ ) of the protectant to prevent the collapse of the freeze-dried products [60], which may lead to prolonged nanoparticle reconstitution times [59,61] and higher residual humidity [62].

In this study, 5% (w/v) sucrose, trehalose and HPBCD with  $T_c$  of -32, -30 and -15 °C respectively [63,64] were used as protectants. The shelf temperature throughout the drying phase was fixed at -20 °C as this was the lowest temperature for water vaporization at 0.3 mbar, which was the lowest pressure achievable by the freeze-dryer used in this study. As predicted, the freeze-dried product containing either sucrose or trehalose appeared collapsed and required sonication for reconstitution while the non-collapsed HPBCD-stabilised product could be reconstituted completely by gentle agitation alone. The formulation collapse resulted in a decrease in the degree of porosity of the freeze-dried product, which subsequently reduced its surface area to volume ratio and hydration rate [62]. Nevertheless, all three protectants produced better results compared to that obtained from the lyophilization of nanoparticle suspension alone, confirming the protective roles of these excipients during freeze-drying.

Following reconstitution, the nanoparticle size and PDI were measured again to evaluate the protective effect of sucrose, trehalose and HPBCD. The highest protective effect, as demonstrated by the maximum preservation of nanoparticle size and PDI, was obtained with HPBCD (Table 2). It is likely that the volume shrinkage resulting from the collapse of the sucrose and trehalose matrices has reduced the distance of separation between the nanoparticles, allowing the PEG layers of neighbouring particles to interact and form stable crystalline bridges as reported in the literature [57,65]. Differently, in the presence of HPBCD, the PLGA/PEG-PLGA nanoparticles were easily freeze-dried, which may be convenient for long-term storage and transportation. In future work, the protective effects of sucrose and trehalose can be re-evaluated by setting the drying temperature to be lower than their respective  $T_c$  to minimise dependency on the relatively costly HPBCD.

**Table 2:** Characterization of PLGA/PEG-PLGA nanoparticles (Formulation 8) before and after freeze-drying without any cryoprotectant or with sucrose, trehalose or HPBCD. Data are presented as mean  $\pm$  SD, n = 3.

Protectant	Average size (nm)		Average PDI		S <sub>f</sub> /S <sub>i</sub>	PDI <sub>f</sub> /PDI <sub>i</sub>
	Before freeze-drying <sup>a</sup>	After freeze-drying <sup>b</sup>	Before freeze-drying <sup>a</sup>	After freeze-drying <sup>b</sup>		
-		n.d. <sup>c</sup>			n.d. <sup>c</sup>	
Sucrose	255 $\pm$ 8	308 $\pm$ 5	0.13 $\pm$ 0.01	0.22 $\pm$ 0.01	1.21	1.69
Trehalose	255 $\pm$ 8	266 $\pm$ 5	0.13 $\pm$ 0.01	0.19 $\pm$ 0.01	1.04	1.46
HPBCD		255 $\pm$ 3		0.14 $\pm$ 0.02	1.00	1.08

<sup>a</sup> Purified nanoparticle suspension was diluted to 100  $\mu$ g/mL in water prior to measurement

<sup>b</sup> Freeze-dried nanoparticles were re-suspended in 2 mL water and diluted to 100  $\mu$ g/mL in the same diluent prior to measurement

<sup>c</sup> n.d. = not determined, as the freeze-dried product could not be reconstituted completely even after 10 minutes sonication

### 3.3.3. Lysozyme and SDF-1 $\alpha$ encapsulation

#### 3.3.3.1. Effect of pH of the aqueous phase on encapsulation efficiencies

Protein molecules have smaller net electrical charge and thus lower aqueous solubility when the pH is buffered near the protein's isoelectric point (pI). This may decrease the leakage of protein into the aqueous phase during the formulation process to subsequently maximise encapsulation efficiency. The results shown in Table 3 supported this hypothesis as both lysozyme and SDF-1 $\alpha$  were encapsulated most successfully when the pH of the aqueous phase was buffered closest to their respective pI (lysozyme – 11.35; SDF-1 $\alpha$  – 10.5). In addition to a decrease in aqueous solubility, it is likely that the smaller net charge also attenuated the electrostatic repulsions between protein molecules to allow the protein load to be compacted, which can facilitate its entrapment within the nanoparticles [66,67]. For these reasons, the pH of the aqueous phase was always set to the protein's pI in subsequent encapsulations.

**Table 3:** Effect of pH of aqueous phase on encapsulation efficiencies of lysozyme. Data are presented as mean  $\pm$  SD, n = 3.

Formulation number	pH of aqueous phase <sup>a</sup>	Encapsulation efficiency (%)	
		Lysozyme	SDF-1a
4	8.4	18.0 $\pm$ 0.8	34.3 $\pm$ 3.7
	9.4	28.1 $\pm$ 1.7	79.7 $\pm$ 4.1
	10.4	66.0 $\pm$ 1.6	107.7 $\pm$ 1.5
	11.4	107.0 $\pm$ 3.6	-

<sup>a</sup> 0.05 M glycine-NaOH buffer solution was used as the aqueous phase

#### 3.3.3.2. Effect of PLGA carboxylic acid terminal capping on encapsulation efficiencies

Since both proteins and PLGA possess ionisable groups, electrostatic interactions can have a major influence on lysozyme and SDF-1 $\alpha$  encapsulation. Due to the complexity associated with protein charge modifications, the proportions of PLGA-COOH and PLGA-COOR were altered accordingly to vary the number of ionisable groups in the nanoparticles instead. The encapsulation of both proteins decreased slightly when PLGA-COOH was substituted with an equal amount of PLGA-COOR (Formulation 4 vs. 8 in Table 4). These results suggested that protein-polymer electrostatic interactions can influence the protein encapsulation efficiencies. Although protein leakage during the encapsulation process can be minimised by adjusting the pH of the aqueous phase to be similar to the protein's pI, proteins located close to the nanoparticle surface can be lost during subsequent purification stages when the nanoparticles were suspended in non-buffered water. This is especially true since the presence of the outer hydrophilic PEG layer can facilitate the access of water to the PLGA core to cause dissolution of any loosely-trapped proteins [68]. However, the strong electrostatic interactions between the negatively-charged carboxylic acid terminals, which are more abundant in PLGA-COOH than in PLGA-COOR, and the positively-charged basic proteins such as lysozyme and SDF-1 $\alpha$  can reduce protein loss. Interestingly, additional experiments with lysozyme (Formulation 9 and 10) and SDF-1 $\alpha$  (Formulation 10) produced similar results as Formulation 4. Considering the very low protein loading involved, it seems that the inclusion of a small proportion of PLGA-COOH is sufficient to ensure that the nanoparticles have an adequate number of carboxylic acid groups to interact with the protein molecules for maximum encapsulation efficiency.

**Table 4:** Effect of the PLGA-COOH proportion on encapsulation efficiencies of lysozyme and SDF-1 $\alpha$ . Data are presented as mean  $\pm$  SD, n = 3 and 4 for lysozyme and SDF-1 $\alpha$  respectively.

Formulation number	PLGA-COOH proportion (%)	Encapsulation efficiency (%)	
		Lysozyme	SDF-1a
4	67	107.0 $\pm$ 3.6	107.7 $\pm$ 1.5
8	0	89.6 $\pm$ 5.7	75.5 $\pm$ 2.2
9	33	108.2 $\pm$ 1.9	-
10	17	111.0 $\pm$ 3.9	104.0 $\pm$ 2.8

### 3.3.3.3. Physicochemical characteristics of protein-loaded nanoparticles

Protein encapsulation did not affect the size or zeta-potential of the nanoparticles regardless of the type of formulation or encapsulated protein (Table 5), possibly due to the low amount of protein being encapsulated. In terms of morphology, both the unloaded and SDF-1 $\alpha$ -loaded nanoparticles appeared similar under the vacuum condition of SEM or TEM (Figure 4). In addition, the image taken using AFM under a non-vacuum condition confirmed the consistent

appearance of the SDF-1 $\alpha$ -loaded nanoparticles regardless of the conditions under which the nanoparticles were observed and the differences in the sample treatment prior to observation.

**Table 5:** Average size, polydispersity index (PDI) and zeta-potential (ZP) of lysozyme and SDF-1 $\alpha$ -loaded nanoparticles. Data are presented as mean  $\pm$  SD, n = 3.

Formulation number	Encapsulated protein	Average size (nm) <sup>a</sup>	Average PDI <sup>a</sup>	Average ZP (mV) <sup>b</sup>
4	Lysozyme	202 $\pm$ 5	0.09 $\pm$ 0.01	-9.7 $\pm$ 0.8
	SDF-1 $\alpha$	197 $\pm$ 2	0.08 $\pm$ 0.01	-9.6 $\pm$ 0.7
8	Lysozyme	253 $\pm$ 5	0.17 $\pm$ 0.03	-3.3 $\pm$ 0.3
	SDF-1 $\alpha$	259 $\pm$ 8	0.19 $\pm$ 0.01	-2.9 $\pm$ 0.2

<sup>a</sup> Purified nanoparticle suspension was diluted to 100  $\mu$ g/mL in water prior to measurement

<sup>b</sup> Purified nanoparticle suspension was diluted to 100  $\mu$ g/mL in 0.01 M NaCl solution and the pH of the suspension was adjusted to pH 7 prior to measurement

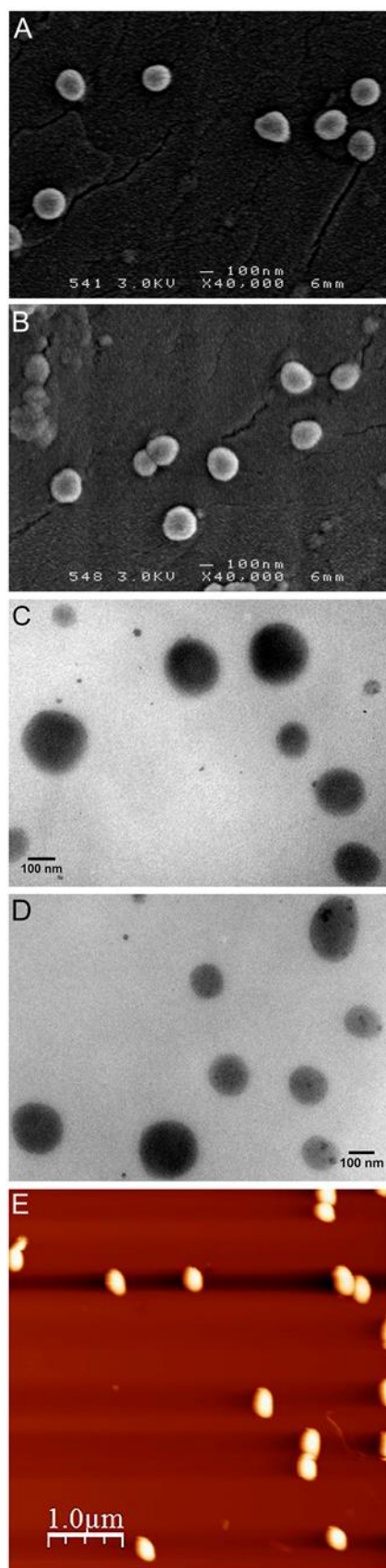


**Figure 4:** Morphology of PLGA/PEG-PLGA nanoparticles. SEM and TEM images of (A, C) unloaded and (B, D) SDF-1 $\alpha$ -loaded nanoparticles. (E) AFM image of SDF-1 $\alpha$ -loaded nanoparticles.

### 3.4. *In vitro* protein release

Protein release was studied by suspending the nanoparticles in a buffer solution followed by centrifugation at pre-defined time intervals to collect the supernatant for protein quantification. Initially, lysozyme release patterns in different buffer solutions was studied. At the physiologically-relevant pH 7.4 (0.05 M Tris-HCl buffer), the proportion of PLGA-COOH in the nanoparticles was shown to affect the extent of lysozyme release (Figure 5A). The highest release of encapsulated lysozyme was achieved with Formulation 8 (43%) whereas negligible protein release was observed with Formulation 4 even after 15 days. When a mixture of PLGA-COOH and PLGA-COOR was tested (Formulation 10), only 12% encapsulated lysozyme was successfully released. The lack of protein release from PLGA particles containing uncapped carboxylic end groups has been previously reported [44,47,69]. Concurrent measurement of zeta-potentials during the release study offered a possible explanation for this observation. Nanoparticles made from higher PLGA-COOH proportions had more negative zeta-potential values in the early stages of the release study (Figure 5B). At pH 7.4, these nanoparticles are expected to establish electrostatic interactions with the positively-charged lysozyme molecules ( $pI = 11.35$ ), which hinders their release. These interactions seem to be the governing factor for protein load entrapment, as no further protein release was observed despite the continuous degradation of PLGA matrices into acidic products, as inferred from the increasingly negative zeta-potential values of all the formulations, taking place throughout the release study period.

To confirm the obstructive effect of lysozyme-PLGA electrostatic interactions on lysozyme release, the study was repeated in release medium buffered to pH 4.0 (0.01 M citrate buffer). It can be hypothesised that the excess protons present in the release medium will neutralise the PLGA carboxylic acid groups, which in turn should trigger the release of lysozyme molecules. As expected, release of lysozyme was enhanced regardless of the nanoparticle's PLGA-COOH proportion (Figure 5C). However, incomplete release was still observed with Formulation 4, even after 30 days. It is likely that the high proportion of PLGA-COOH in this formulation led to incomplete neutralisation of the carboxylic acid groups, hindering complete lysozyme release. Besides pH, another factor that may affect lysozyme-PLGA electrostatic interactions is the concentration of cations in the release medium, as these ions can also displace lysozyme molecules from the PLGA carboxylic acid groups. As predicted, in the presence of 0.15 M sodium chloride, release of lysozyme at pH 7.4 was enhanced (Figure 5D), recording levels similar to those obtained at acidic pH. These release medium conditions were selected for subsequent SDF-1 $\alpha$  release study due to their physiological relevance.

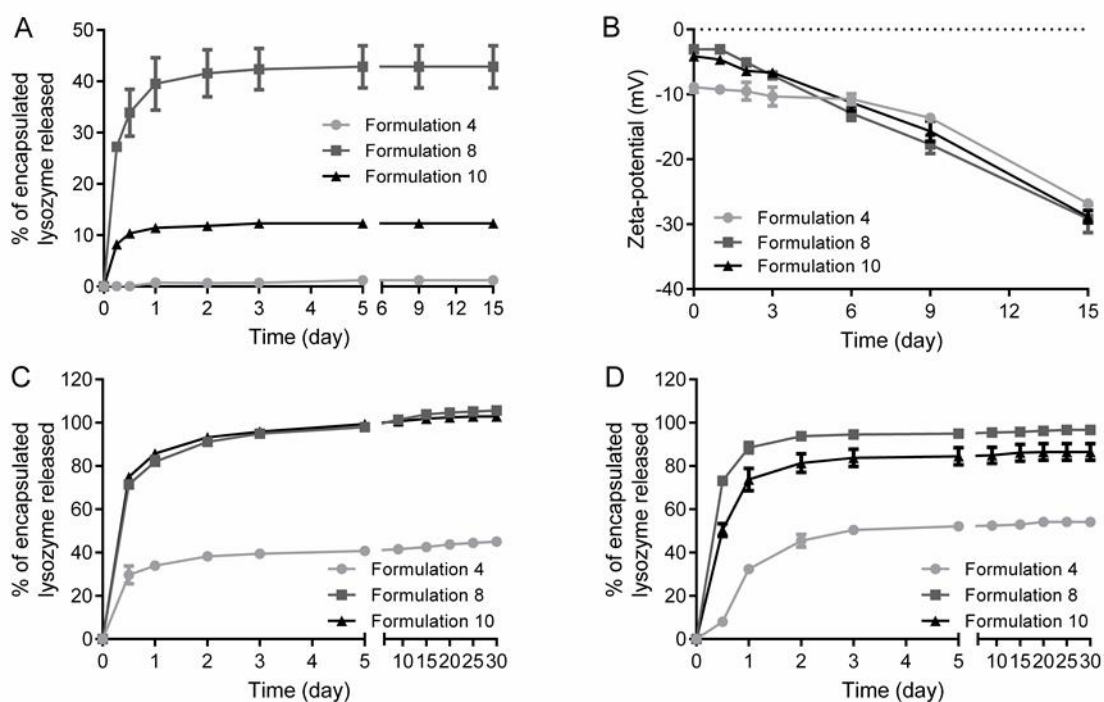


**Figure 5:** Release study of lysozyme. (A) Cumulative release of lysozyme in 0.05 M Tris-HCl buffer at pH 7.4 and (B) concurrent changes in the zeta-potential value of different nanoparticle formulations. Nanoparticle suspension was diluted 200-fold in 0.01 M NaCl solution and the pH was adjusted to pH 7 prior to zeta-potential measurement. (C) Cumulative lysozyme release in 0.01 M citrate buffer at pH 4.0 or (D) 0.05 M Tris-HCl buffer at pH 7.4 containing 0.15 M NaCl. Each data point with error bar represents mean  $\pm$  SD,  $n = 3$  for each formulation.

Interestingly, although the biphasic release pattern seen in lysozyme release study was reproduced, the release of SDF-1 $\alpha$  was reduced in all formulations (Figure 6A). After 30 days, the nanoparticles were lyophilized and dissolved to quantify the amount of unreleased SDF-1 $\alpha$  using ELISA. The sum of released SDF-1 $\alpha$  and the unreleased proportion, was equal to 95 – 98% of the total encapsulated SDF-1 $\alpha$  for all the studied formulations. SDF-1 $\alpha$  may establish stronger electrostatic interactions with PLGA carboxylic acid groups than lysozyme because of the greater percentage of basic amino acid residues in the SDF-1 $\alpha$  primary sequence, resulting in lower cumulative SDF-1 $\alpha$  releases. Despite the multiple literature-approved measures taken in this study to reduce protein-polymer interactions, including protein precipitation in the presence of poloxamer 188 [44] and use of more hydrophilic polymer materials [69] in the form of PEG-PLGA co-polymer, additional approaches such as protein PEGylation [70,71] should be considered in future work to obtain more complete protein release. Nevertheless, the bioactivity of SDF-1 $\alpha$  in the release sample collected up to 72 hours (after which further SDF-1 $\alpha$  release was negligible) was found to be similar to that of its native

counterpart when assessed using the agarose drop migration assay (Figure 6B,C), suggesting that the encapsulation process did not induce protein denaturation. In the context of patient safety, the preservation of protein bioactivity throughout formulation processes is imperative as denatured proteins tend to be more immunogenic than their native forms [72,73].

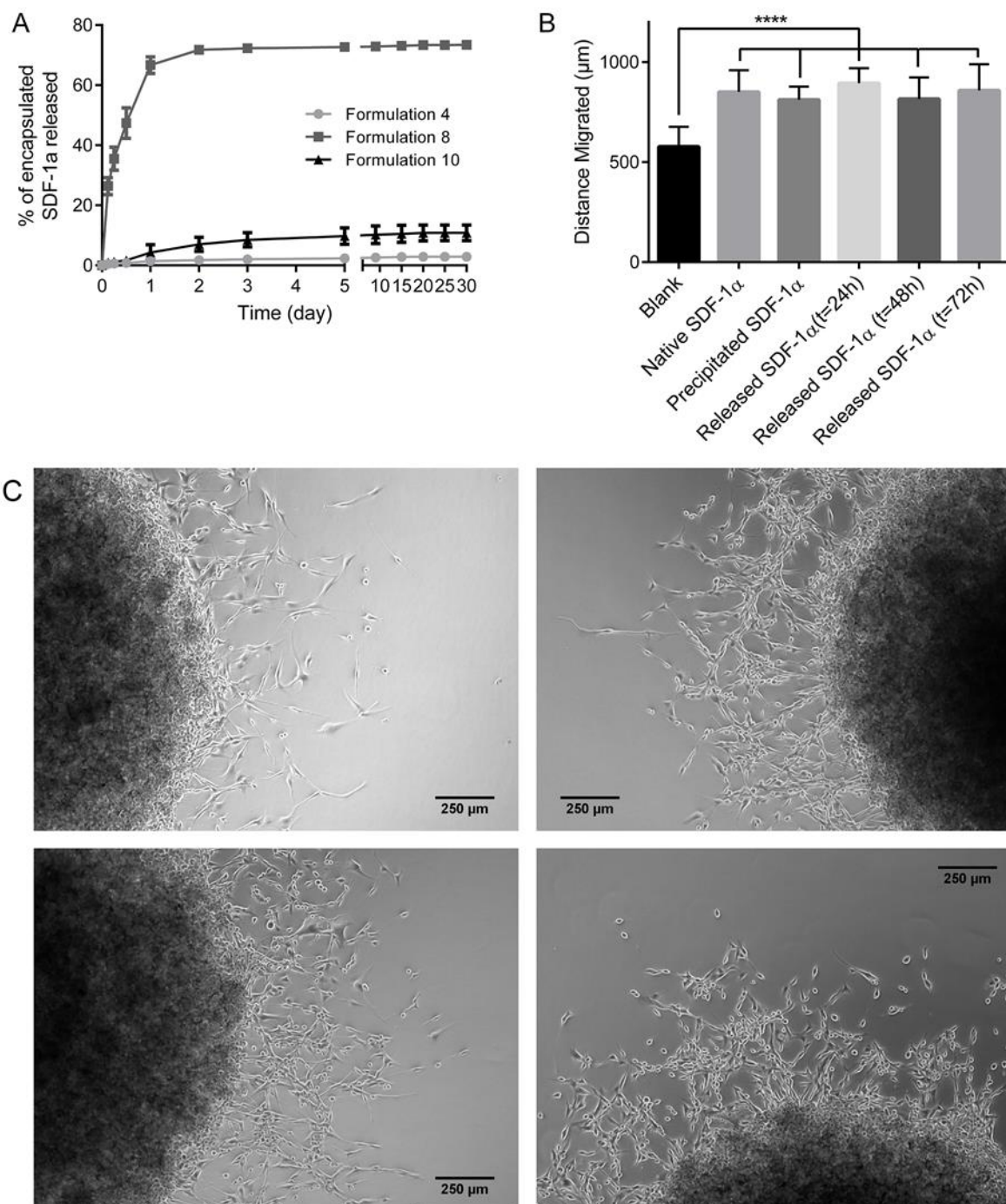


**Figure 6.** Release study of SDF-1 $\alpha$  and its biological activity assessment. (A) Cumulative release of SDF-1 $\alpha$  in 0.05 M Tris-HCl buffer at pH 7.4 containing 0.15 M NaCl. Each data point with error bar represents mean  $\pm$  SD,  $n = 4$  for each formulation. (B) Distance migrated by U87-MG cells induced by the culture medium alone (Blank), or supplemented with 40 ng/mL native, precipitated or released SDF-1 $\alpha$  collected from Formulation 8 at different time

points of the release study. Statistical analysis was conducted to investigate any significant difference ( $P \leq 0.05$ ) in comparison to the native SDF-1 $\alpha$ . \*\*\*\* indicates  $P \leq 0.0001$ ,  $n = 3$  for each type of SDF-1 $\alpha$  treatment. (C) Examples of optical microscopic images of U87-MG cell-laden agarose drops after 72 h treatment with culture medium alone (top left) or medium containing 40 ng/mL native (top right), precipitated (bottom left) or released SDF-1 $\alpha$  (bottom right).

The biphasic release patterns observed in lysozyme and SDF-1 $\alpha$  release studies were consistent with literature data on PEG-containing PLGA nanoparticles [67,74]. The initial burst release was due to the rapid liberation of proteins located adjacent to the nanoparticle surface, which was a consequence of the efflux of residual solvents during the purification step that drew most proteins away from the core of the nanoparticles. This stage was then followed by a slower release attributable to the diffusion of proteins from deeper parts of the nanoparticles. In relation to future work, the initial rapid SDF-1 $\alpha$  release is useful for establishing a concentration gradient within a hydrogel to immediately induce chemotaxis of cancer cells while the subsequent gradual release may be beneficial to maintain the established gradient. It was also observed that the cumulative release curves began to plateau after 72 hours. This relatively short duration of release was expected as the huge surface area to volume ratio of the nanoparticles contributed to a rapid protein release. However, as the SDF-1 $\alpha$ -loaded nanoparticles are intended in the future to be incorporated within a hydrogel and not suspended directly in physiological fluids, literature data suggested that the release duration can be prolonged [75], which would allow more time for cancer cells to migrate into the hydrogel/nanoparticle composite implant to be trapped.

### 3.5. *In vitro* cytotoxicity study

Due to the innocuous nature of the solvent used in the formulation process and the well-reported safety of PLGA, the newly-developed nanoparticles are expected to exhibit negligible cytotoxicity. To prove this, NIH3T3 mouse embryonic fibroblasts were treated with unloaded PLGA/PEG-PLGA nanoparticles (Formulation 8) for 48 hours. This cell line was chosen as it has been reported to be highly-sensitive to chemical-induced toxicities [76]. Alongside PLGA/PEG-PLGA nanoparticles, lipid nanocapsules (LNC) and polystyrene (PS) nanoparticles, which have been widely utilised in various pharmaceutical research, were tested to investigate the relative cytocompatibility of the newly-developed nanocarriers. The range of nanoparticle concentrations for cell treatment in this study was set to 0.01 - 10 mg/mL to assess the suitability of the PLGA/PEG-PLGA nanoparticles for both systemic and local drug delivery applications. In comparison to the two reference nanoparticles, the PLGA/PEG-PLGA

nanoparticles induced minimal cell deaths even at the highest concentration tested (Figure 7). In addition, the LNC was found to be the most toxic between the three types of nanoparticles at high concentrations. Two studies reported similar findings [77,78] and suggested that the high amount of surfactant (up to 2.8% (w/v)) required to stabilize the LNC formulation is responsible for the high toxicity due to the ability of the hydrophilic and hydrophobic components of surfactant molecules to interact with the phosphate groups and fatty acid tails of lipid bilayer respectively to cause disruption of cellular membranes [79]. On the other hand, the PS nanoparticles exhibited intermediate cytotoxicity, possibly due to the lower amount of surfactant used in their formulation (up to 0.5% (w/v)) as described by the manufacturer). Although one can speculate that the differences in the cytotoxicity can be attributed to other components of the three types of nanoparticles, as well as to differences in their physicochemical characteristics such as size and surface charge, the surfactant-free formulation process using non-toxic components developed in the present work can undoubtedly produce nanocarriers with excellent biocompatibility that are more suitable for local drug delivery applications compared to several other well-established alternatives.

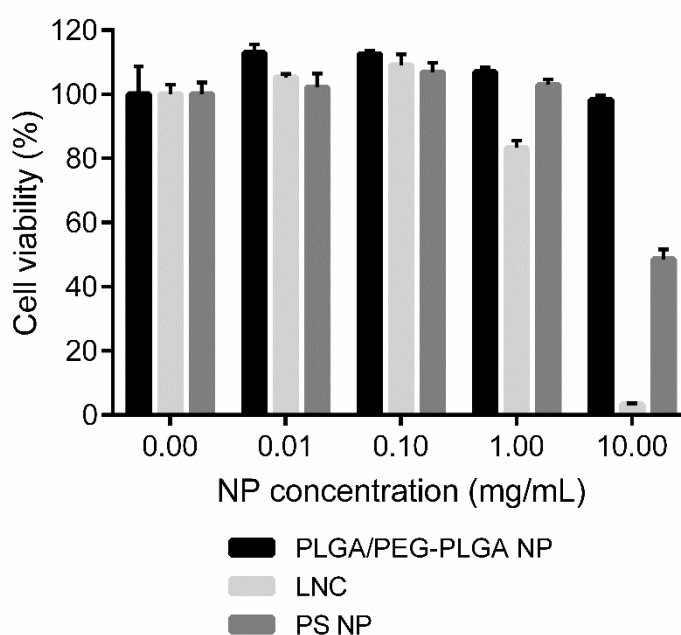


**Figure 7.** Effect of different concentrations of PLGA/PEG-PLGA nanoparticles (Formulation 8), lipid nanocapsules (LNC) and polystyrene (PS) nanoparticles on the viability of NIH3T3 cells after 48h incubation.  $n = 3$  for each nanoparticle treatment.

#### 4. Conclusion

This study reports on the development of novel SDF-1 $\alpha$  nanocarriers composed of PLGA and a PEG-PLGA co-polymer. Following optimization using lysozyme as a model protein, SDF-1 $\alpha$  was successfully precipitated and subsequently loaded into these nanoparticles under mild formulation conditions. SDF-1 $\alpha$  was also released in its bioactive conformation in a gradual fashion. Furthermore, by changing the number of uncapped carboxylic acid groups in the PLGA core, the novel formulation process allows the production of nanoparticles with different physicochemical properties that influence encapsulation efficiencies and the extent of protein release. In addition, the use of non-toxic polymers and solvents ensured the excellent biocompatibility of the synthesised nanoparticles. Thus, the novel SDF-1 $\alpha$  nanocarriers are promising for future cancer cell trapping applications and will be incorporated into a suitable hydrogel for studying chemotaxis of glioblastoma cells.

### **Acknowledgement**

Authors would like to thank the French Ministry of Higher Education and Research for their financial support (PhD Grant) and the National Funds for Scientific Research, Belgium (FNRS) for additional financial assistance. The authors are thankful for the European financial support (EACEA) in the frame of the NanoFar program, an Erasmus Mundus Joint Doctorate (EMJD) program in nanomedicine and pharmaceutical innovation. This work was also supported by “La Région Pays-de-la-Loire”, by the “Institut National de la Santé et de la Recherche Médicale” (INSERM), by the “University of Angers” and the “University of Liège” and by the “Cancéropôle Grand-Ouest” through the “glioblastoma” and “vectorization and radiotherapies” networks. E. Garcion is also a member of the LabEx IRON “Innovative Radiopharmaceuticals in Oncology and Neurology” as part of the French government “Investissements d’Avenir” program and head the PL-BIO 2014-2020 INCA (Institut National du Cancer) project MARENGO - “MicroRNA agonist and antagonist Nanomedicines for GliOblastoma treatment: from molecular programming to preclinical validation”. Finally, the authors thank Dr D. Séhédic for the kind provision of CXCR4-expressing U87-MG human glioblastoma cell line and R. Mallet and R. Perrot of the SCIAM (Common service for Imaging and microscopy analysis, Angers, France) for SEM and TEM analyses.

### **Appendix A. Supplementary material**

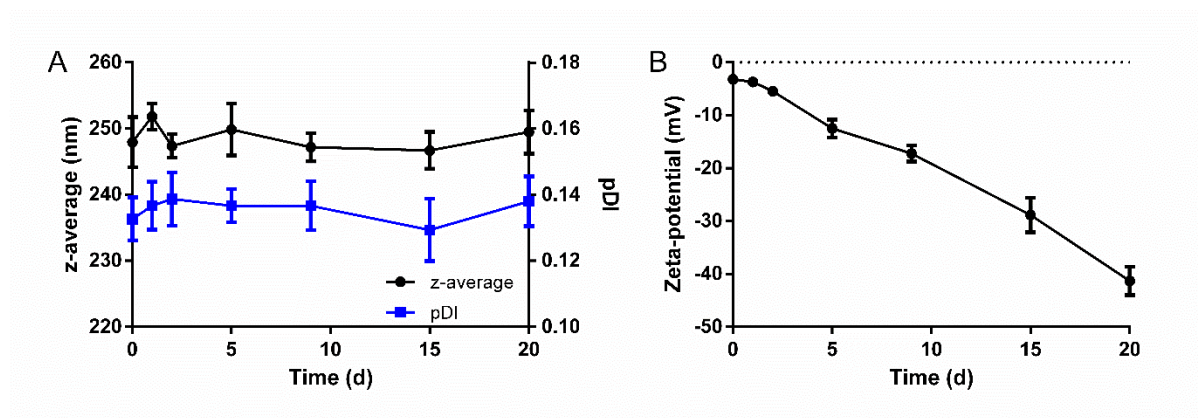


**Figure S1.** Changes in average size and pDI (A), and zeta potential (B) with time of incubation of 1 mg/mL PLGA/PEG-PLGA nanoparticles (Formulation 8) in 0.05 M Tris-HCl buffer (pH 7.4) at 37 °C. Each data point with error bar represents mean  $\pm$  SD,  $n = 3$ . For size and pDI measurement, nanoparticle suspension was diluted in water. For zeta-potential measurement, nanoparticle suspension was diluted in 0.01 M NaCl solution and the pH was adjusted to pH 7.

### 3.3.2. Unpublished results

In publication 1, the cytotoxicity of the developed PLGA/PEG-PLGA nanoparticles was evaluated using NIH3T3 mouse embryonic fibroblasts. Although no cytotoxicity was observed on this cell line, even at the highest nanoparticle concentration tested, it was imperative to establish that the PLGA/PEG-PLGA nanoparticles were compatible with cells that could be present in the human brain. Therefore, the cytotoxicity assay was also conducted on a human macrophage cell line known as Thp-1 macrophages. Under normal physiological circumstances, macrophages usually reside in the peripheral blood system as monocytes. However, they can be found ubiquitously in GBM tumors as they are free to cross the leaky BBB that is characteristic to the pathology of this disease [80]. Macrophages play important tumor suppressive roles that include production of pro-inflammatory cytokines and reactive oxygen species, especially when they are polarized towards the classical M1 phenotype [81]. Thus, it is crucial that these cells are not harmed by any of the active agents or excipients used in the treatment of GBM.

#### 3.3.2.1. Materials and Methods

To obtain Thp-1 macrophages, Thp-1 monocytes (TIB-202™, ATCC) were seeded in a 96-well flat-bottomed culture plate (Nunc) at a density of  $40 \times 10^3$  cells/well in 100  $\mu$ L complete Roswell Park Memorial Institute (RPMI) 1640 medium (Sigma-Aldrich) supplemented with 80 nM phorbol 12-myristate 13-acetate (PMA) (Sigma-Aldrich) and incubated at 37 °C and

5% CO<sub>2</sub> for 24 h. Following this, the pMA-containing medium was replaced with fresh pMA-free medium and the cells were incubated for another 24 hours. Then, the old medium was replaced with fresh medium containing unloaded nanoparticles at a concentration of 0.01, 0.1, 1 or 10 mg/mL. As a negative control, cells incubated with the medium alone were prepared. After 48 h of incubation (72 h post-seeding) in the presence or absence of nanoparticles, the entire medium was replaced with 100  $\mu$ L fresh medium containing 44  $\mu$ M resazurin. The resazurin-containing medium was also added in three wells of the assay plates (without cells), which served as blank. The plate was incubated for another 3 h 30 m. Cell viability was estimated from the fluorescence intensity of the reduced product of resazurin, called resorufin, which was measured using a ClarioStar microplate fluorometer (BMG Labtech GmbH, Ortenberg, Germany) at 545 nm excitation and 600 nm emission. All readings were normalized to those obtained with the nanoparticle-untreated cells.

In addition to the PLGA/PEG-PLGA nanoparticles, two other types of nanoparticles, namely lipid nanocapsules (LNC) and polystyrene (PS) nanoparticles, were tested in this assay to obtain information on the relative safety of the newly-developed nanoparticles. LNC (average size = 122 nm, PDI = 0.088) were prepared using a phase inversion method [48]. PS nanoparticles (average size = 285 nm, PDI = 0.175) were purchased from Sigma-Aldrich.

### **3.3.2.2. Results and Discussion**

As observed with the NIH3T3 cell line, PLGA/PEG-PLGA nanoparticles induced negligible cytotoxicity on Thp-1 macrophages across the tested range of concentration. This result provided another preliminary evidence of the safety of these nanoparticles as a vehicle to be used in local protein delivery applications.

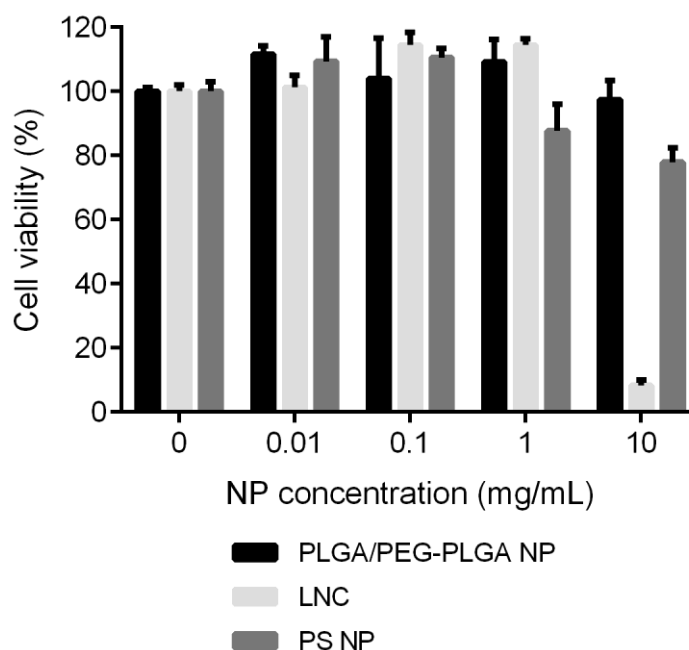


**Figure 3.1:** Effect of different concentrations of PLGA/PEG-PLGA nanoparticles (Formulation 8), lipid nanocapsules (LNC) and polystyrene (PS) nanoparticles on the viability of NIH3T3 cells after 48h incubation.  $n = 3$  for each nanoparticle treatment.

### 3.4. CONCLUSION OF CHAPTER 3

In this part of the study, a novel formulation process yielding uniform nanoparticles with high SDF-1 $\alpha$  encapsulation efficiency and good cytocompatibility was developed. PLGA was used as the main constituent polymer in the preparation of the nanoparticles due to its high versatility. It is a co-polymer of lactic acid and glycolic acid, meaning that its molecular chain always ends with a carboxyl group (Figure 3.2) that provides a site for chemical conjugation or physical interaction with other polymers or protein molecules. For example, PLGA can be conjugated with a hydrophilic polymer such as PEG to form an amphiphilic di-block (as produced in this study) or tri-block co-polymer [52] that may be used as a replacement for surfactant molecules, which are often needed in the preparation of micro/nanoparticle formulations. When uncapped, the carboxyl groups can also interact electrostatically with basic protein molecules to contribute to high encapsulation efficiencies. Being a hydrophobic polymer, PLGA degrades slowly in an aqueous environment [82]. This property is thought to be valuable in preparing polymer-based carriers that are intended to provide sustained protein release. The lactide component of PLGA is actually more hydrophobic than the glycolide residue as the former bears a methyl side group. Having a high lactide-to-glycolide ratio is therefore useful in slowing down the hydrolytic degradation of PLGA [83].

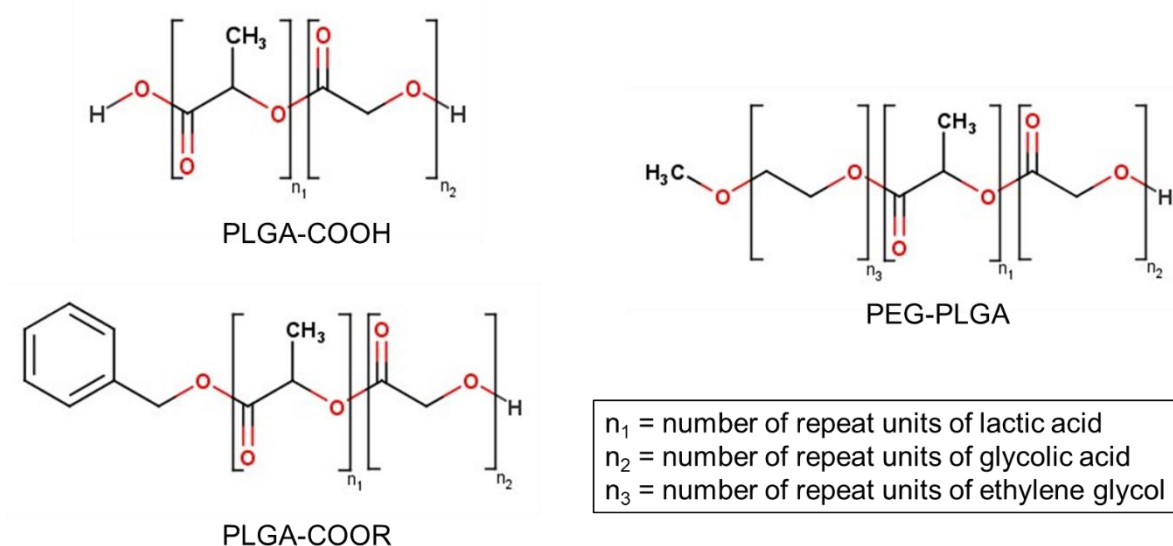


**Figure 3.2:** Chemical structures of the PLGA-COOH, PLGA-COOR and PEG-PLGA used in this work.

The PLGA-COOH, PLGA-COOR and PEG-PLGA used in this study all had a lactide-to-glycolide ratio of 75:25. With these, it was expected that the formulated nanoparticles would have a slow degradation rate. In fact, the degradation time of PLGA 75:25 has been reported to be in the order of several months [84,85]. Despite this, the formulated nanoparticles were shown to release most of their protein load very rapidly (approximately 72 hours) when incubated in appropriate release media. While the particle degradation rate may appear to be an important determinant of the release kinetics, this is not the only factor that controls the rate of diffusion of water molecules into the polymer matrix and the subsequent dissolution of the protein load [86]. Diffusion of organic solvents out of the polymer matrix during the extraction step have often led to the formation of nanoparticles with a porous internal structure (Figure 3.3) [87]. These pores could increase the total surface area accessible to the release medium and speed up the dissolution of the protein molecules that were surface-adsorbed or only partially embedded in the polymer matrix. This explains why a huge burst release was seen with the developed nanoparticle system. In addition, the porous internal structure could also reduce the distance of diffusion required for the embedded protein molecules to escape from the polymer matrix, thus shortening the overall duration of protein release.

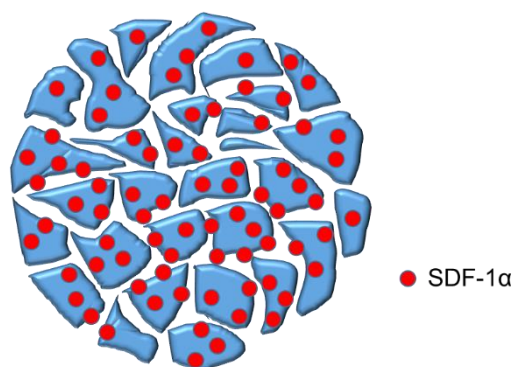


**Figure 3.3:** Proposed structure of the SDF-1 $\alpha$ -loaded PLGA/PEG-PLGA nanoparticles developed in this study.

The rapid protein release from the nanoparticles is likely to provide only a short window of time for the chemotactic attraction of GBM cells in the brain. GBM are known to be very invasive and can penetrate diffusively into the surrounding brain parenchyma. An autopsy study showed that infiltrating GBM cells could be found as far as 14 mm away from the tumor border outlined using magnetic resonance imaging (MRI) [88]. As surgical resection of GBM is generally defined by the contrast-enhanced areas in MRI, these infiltrating GBM cells were often unremoved from the brain and could subsequently multiply to re-form the tumor. In fact, 96% of GBM recurrence occurred within 20 mm from the MRI-defined tumor border [89]. Although no information on the *in vivo* migration speed of GBM cells has been published so far, a recent *in vitro* study investigating the three-dimensional migratory behavior of GBM cells seeded into micro-chambers within a collagen hydrogel estimated a migration speed of between 245 to 720  $\mu\text{m}/\text{day}$  across the four GBM cell lines tested [90]. Using the two-dimensional agarose drop migration assay, we observed that U87-MG cells migrated at a speed of 284  $\mu\text{m}/\text{day}$  when incubated in a medium supplemented with SDF-1 $\alpha$ . Although these values may not necessarily reflect the *in vivo* behavior of GBM cells, they still provide valuable insights into the migration capacity of these cells. With regards to the *in vivo* trapping of GBM cells, a slower migration rate is expected as the cells would have to make their way through the dense peritumoral matrices [91] in order to be recruited into the SDF-1 $\alpha$ -releasing scaffold implanted into the resection cavity. Regardless, if we assume that GBM cells migrate at the maximum speed observed *in vitro* (720  $\mu\text{m}/\text{day}$ ), it may still take approximately 20 days for the GBM cells located 14 mm away from the resection border to be recruited into the tumor trap. This estimation provides a reasonable explanation on why scaffolds capable of providing sustained release of SDF-1 $\alpha$  are very much needed to increase the likelihood of trapping the entire residual GBM cell population post-surgery. The development of such scaffolds was furthered

by incorporating the developed SDF-1 $\alpha$ -loaded nanoparticles into chitosan nanofibers as discussed in the next chapter.

### 3.5. REFERENCES

- [1] N. Kamaly, B. Yameen, J. Wu, O.C. Farokhzad, Degradable Controlled-Release Polymers and Polymeric Nanoparticles: Mechanisms of Controlling Drug Release, *Chem. Rev.* 116 (2016) 2602–2663. doi:10.1021/acs.chemrev.5b00346.
- [2] H.M. Mansour, M.J. Sohn, A. Al-Ghananeem, P.P. DeLuca, Materials for pharmaceutical dosage forms: Molecular pharmaceuticals and controlled release drug delivery aspects, *Int. J. Mol. Sci.* 11 (2010) 3298–3322. doi:10.3390/ijms11093298.
- [3] D.K. Sahana, G. Mittal, V. Bhardwaj, M.N.V.R. Kumar, PLGA nanoparticles for oral delivery of hydrophobic drugs: Influence of organic solvent on nanoparticle formation and release behavior in vitro and in vivo using estradiol as a model drug, *J. Pharm. Sci.* 97 (2008) 1530–1542. doi:10.1002/jps.21158.
- [4] F. Wu, T. Jin, Polymer-Based Sustained-Release Dosage Forms for Protein Drugs, Challenges, and Recent Advances, *AAPS PharmSciTech.* 9 (2008) 1218–1229. doi:10.1208/s12249-008-9148-3.
- [5] W. Abdelwahed, G. Degobert, S. Stainmesse, H. Fessi, Freeze-drying of nanoparticles: Formulation, process and storage considerations, *Adv. Drug Deliv. Rev.* 58 (2006) 1688–1713. doi:10.1016/j.addr.2006.09.017.
- [6] A. Saez, M. Guzmán, J. Molpeceres, M.R. Aberturas, Freeze-drying of polycaprolactone and poly(D,L-lactic-glycolic) nanoparticles induce minor particle size changes affecting the oral pharmacokinetics of loaded drugs, *Eur. J. Pharm. Biopharm.* 50 (2000) 379–387. doi:10.1016/S0939-6411(00)00125-9.
- [7] M. De La Luz Sierra, F. Yang, M. Narazaki, O. Salvucci, D. Davis, R. Yarchoan, H.H. Zhang, H. Fales, G. Tosato, Differential processing of stromal-derived factor-1alpha and stromal-derived factor-1beta explains functional diversity., *Blood.* 103 (2004) 2452–2459. doi:10.1182/blood-2003-08-2857.
- [8] M. Janowski, Functional diversity of SDF-1 splicing variants., *Cell Adh. Migr.* 3 (2009) 243–249.
- [9] T. Sugiyama, H. Kohara, M. Noda, T. Nagasawa, Maintenance of the Hematopoietic Stem Cell Pool by CXCL12-CXCR4 Chemokine Signaling in Bone Marrow Stromal Cell Niches, *Immunity.* 25 (2006) 977–988. doi:10.1016/j.immuni.2006.10.016.
- [10] T. Kitaori, H. Ito, E.M. Schwarz, R. Tsutsumi, H. Yoshitomi, S. Oishi, M. Nakano, N. Fujii, T. Nagasawa, T. Nakamura, Stromal cell-derived factor 1/CXCR4 signaling is critical for the recruitment of mesenchymal stem cells to the fracture site during skeletal repair in a mouse model, *Arthritis Rheum.* 60 (2009) 813–823. doi:10.1002/art.24330.
- [11] J. Deng, Z.M. Zou, T.L. Zhou, Y.P. Su, G.P. Ai, J.P. Wang, H. Xu, S.W. Dong, Bone marrow mesenchymal stem cells can be mobilized into peripheral blood by G-CSF in vivo and integrate into traumatically injured cerebral tissue, *Neurol. Sci.* 32 (2011) 641–651. doi:10.1007/s10072-011-0608-2.
- [12] Y. Kimura, M. Komaki, K. Iwasaki, M. Sata, Y. Izumi, I. Morita, Recruitment of bone marrow-derived cells to periodontal tissue defects, *Front. Cell Dev. Biol.* 2 (2014) 1–6. doi:10.3389/fcell.2014.00019.
- [13] J.-P. Lévesque, J. Henry, Y. Takamatsu, P.J. Simmons, L.J. Bendall, Disruption of the CXCR4 / CXCL12 chemotactic interaction during ..., *J. Clin. Invest.* 110 (2003) 187–196. doi:10.1172/JCI200315994.Introduction.
- [14] L. Marquez-Curtis, A. Jalili, K. Deiteren, N. Shirvaikar, A.-M. Lambeir, A. Janowska-Wieczorek, Carboxypeptidase M Expressed by Human Bone Marrow Cells Cleaves the C-Terminal Lysine of Stromal Cell-Derived Factor-1 $\alpha$ : Another Player in Hematopoietic Stem/Progenitor Cell Mobilization?, *Stem Cells.* 26 (2008) 1211–1220.

- doi:10.1634/stemcells.2007-0725.
- [15] A.M. Roccaro, A. Sacco, W.G. Purschke, M. Moschetta, C. Maasch, D. Zboralski, S. Zöllner, S. Vonhoff, P. Maiso, M.R. Reagan, S. Lonardi, M. Ungari, D. Eulberg, A. Kruschinski, A. Vater, G. Rossi, I.M. Ghobrial, *Therapy*, 9 (2014) 118–128. doi:10.1016/j.celrep.2014.08.042.SDF-1.
- [16] R. Matsusue, H. Kubo, S. Hisamori, K. Okoshi, H. Takagi, K. Hida, K. Nakano, A. Itami, K. Kawada, S. Nagayama, Y. Sakai, Hepatic stellate cells promote liver metastasis of colon cancer cells by the action of SDF-1/CXCR4 axis., *Ann. Surg. Oncol.* 16 (2009) 2645–53. doi:10.1245/s10434-009-0599-x.
- [17] J.-P. Zhang, W.-G. Lu, F. Ye, H.-Z. Chen, C.-Y. Zhou, X. Xie, Study on CXCR4/SDF-1 $\alpha$  axis in lymph node metastasis of cervical squamous cell carcinoma., *Int. J. Gynecol. Cancer.* 17 (2007) 478–83. doi:10.1111/j.1525-1438.2007.00786.x.
- [18] C.B. Stevenson, M. Ehtesham, K.M. McMillan, J.G. Valadez, M.L. Edgeworth, R.R. Price, T.W. Abel, K.Y. Mapara, R.C. Thompson, CXCR4 expression is elevated in glioblastoma multiforme and correlates with an increase in intensity and extent of peritumoral T2-weighted magnetic resonance imaging signal abnormalities, *Neurosurgery.* 63 (2008) 560–569. doi:10.1227/01.NEU.0000324896.26088.EF.
- [19] B.-C. Zhao, Z.-J. Wang, W.-Z. Mao, H.-C. Ma, J.-G. Han, B. Zhao, H.-M. Xu, CXCR4/SDF-1 axis is involved in lymph node metastasis of gastric carcinoma., *World J. Gastroenterol.* 17 (2011) 2389–96. doi:10.3748/wjg.v17.i19.2389.
- [20] M. Burger, A. Glodek, T. Hartmann, A. Schmitt-Gräff, L.E. Silberstein, N. Fujii, T.J. Kipps, J.A. Burger, Functional Expression of CXCR4 (CD184) on Small-Cell Lung Cancer Cells Mediates Migration, Integrin Activation, and Adhesion to Stromal Cells, *Oncogene.* 22 (2003) 8093–8101. doi:10.1038/sj.onc.1207097.
- [21] F. Danhier, E. Ansorena, J.M. Silva, R. Coco, A. Le Breton, V. Pr at, PLGA-based nanoparticles: An overview of biomedical applications, *J. Control. Release.* 161 (2012) 505–522. doi:10.1016/j.jconrel.2012.01.043.
- [22] R.M. Mainardes, R.C. Evangelista, PLGA nanoparticles containing praziquantel: Effect of formulation variables on size distribution, *Int. J. Pharm.* 290 (2005) 137–144. doi:10.1016/j.ijpharm.2004.11.027.
- [23] X. Song, Y. Zhao, W. Wu, Y. Bi, Z. Cai, Q. Chen, Y. Li, S. Hou, PLGA nanoparticles simultaneously loaded with vincristine sulfate and verapamil hydrochloride: Systematic study of particle size and drug entrapment efficiency, *Int. J. Pharm.* 350 (2008) 320–329. doi:10.1016/j.ijpharm.2007.08.034.
- [24] M.K. Tran, A. Swed, F. Boury, Preparation of polymeric particles in CO<sub>2</sub> medium using non-toxic solvents: Formulation and comparisons with a phase separation method, *Eur. J. Pharm. Biopharm.* 82 (2012) 498–507. doi:10.1016/j.ejpb.2012.08.005.
- [25] N. Grabowski, H. Hillaireau, J. Vergnaud, N. Tsapis, M. Pallardy, S. Kerdine-R omer, E. Fattal, Surface coating mediates the toxicity of polymeric nanoparticles towards human-like macrophages, *Int. J. Pharm.* 482 (2015) 75–83. doi:10.1016/j.ijpharm.2014.11.042.
- [26] E. Cohen-Sela, M. Chorny, N. Koroukhov, H.D. Danenberg, G. Golomb, A new double emulsion solvent diffusion technique for encapsulating hydrophilic molecules in PLGA nanoparticles, *J. Control. Release.* 133 (2009) 90–95. doi:10.1016/j.jconrel.2008.09.073.
- [27] J. Liu, Z. Qiu, S. Wang, L. Zhou, S. Zhang, A modified double-emulsion method for the preparation of daunorubicin-loaded polymeric nanoparticle with enhanced *in vitro* anti-tumor activity, *Biomed. Mater.* 5 (2010) 65002. doi:10.1088/1748-

- 6041/5/6/065002.
- [28] U. Bilati, E. Allémann, E. Doelker, Strategic approaches for overcoming peptide and protein instability within biodegradable nano- and microparticles, *Eur. J. Pharm. Biopharm.* 59 (2005) 375–388. doi:10.1016/j.ejpb.2004.10.006.
- [29] A. Sánchez, B. Villamayor, Y. Guo, J. McIver, M.J. Alonso, Formulation strategies for the stabilization of tetanus toxoid in poly(lactide-co-glycolide) microspheres, *Int. J. Pharm.* 185 (1999) 255–266. doi:10.1016/S0378-5173(99)00178-7.
- [30] J. Wang, K.M. Chua, C.H. Wang, Stabilization and encapsulation of human immunoglobulin G into biodegradable microspheres, *J. Colloid Interface Sci.* 271 (2004) 92–101. doi:10.1016/j.jcis.2003.08.072.
- [31] A. Giteau, M.C. Venier-Julienne, S. Marchal, J.L. Courthaudon, M. Sergent, C. Montero-Menei, J.M. Verdier, J.P. Benoit, Reversible protein precipitation to ensure stability during encapsulation within PLGA microspheres, *Eur. J. Pharm. Biopharm.* 70 (2008) 127–136. doi:10.1016/j.ejpb.2008.03.006.
- [32] B. Mukherjee, K. Santra, G. Pattnaik, S. Ghosh, Preparation, characterization and in-vitro evaluation of sustained release protein-loaded nanoparticles based on biodegradable polymers, *Int. J. Nanomedicine.* 3 (2008) 487–496. doi:10.2147/IJN.S3938.
- [33] T. Feczko, J. Tóth, G. Dósa, J. Gyenis, Optimization of protein encapsulation in PLGA nanoparticles, *Chem. Eng. Process. Process Intensif.* 50 (2011) 757–765. doi:10.1016/j.cep.2011.06.008.
- [34] X. Jiang, H. Lin, D. Jiang, G. Xu, X. Fang, L. He, M. Xu, B. Tang, Z. Wang, D. Cui, F. Chen, H. Geng, Co-delivery of VEGF and bFGF via a PLGA nanoparticle-modified BAM for effective contracture inhibition of regenerated bladder tissue in rabbits, *Sci. Rep.* 6 (2016) 20784. doi:10.1038/srep20784.
- [35] M. Morales-Cruz, G.M. Flores-Fernández, M. Morales-Cruz, E.A. Orellano, J.A. Rodríguez-Martínez, M. Ruiz, K. Griebenow, Two-step nanoprecipitation for the production of protein-loaded PLGA nanospheres, *Results Pharma Sci.* 2 (2012) 79–85. doi:10.1016/j.rinphs.2012.11.001.
- [36] U. Bilati, E. Allémann, E. Doelker, Development of a nanoprecipitation method intended for the entrapment of hydrophilic drugs into nanoparticles, *Eur. J. Pharm. Sci.* 24 (2005) 67–75. doi:10.1016/j.ejps.2004.09.011.
- [37] L. Tang, J. Azzi, M. Kwon, M. Mounayar, R. Tong, Q. Yin, R. Moore, N. Skartsis, T.M. Fan, R. Abdi, J. Cheng, Immunosuppressive Activity of Size-Controlled PEG-PLGA Nanoparticles Containing Encapsulated Cyclosporine A, *J. Transplant.* 2012 (2012) 1–9. doi:10.1155/2012/896141.
- [38] EMEA, ICH guideline Q3C (R6) on impurities: guideline for residual solvents, 2003. [http://www.ema.europa.eu/docs/en\\_GB/document\\_library/Scientific\\_guideline/2011/03/WC500104258.pdf](http://www.ema.europa.eu/docs/en_GB/document_library/Scientific_guideline/2011/03/WC500104258.pdf).
- [39] A. Yang, L. Yang, W. Liu, Z. Li, H. Xu, X. Yang, Tumor necrosis factor alpha blocking peptide loaded PEG-PLGA nanoparticles: Preparation and in vitro evaluation, *Int. J. Pharm.* 331 (2007) 123–132. doi:10.1016/j.ijpharm.2006.09.015.
- [40] J. Coleman, A. Lowman, Biodegradable Nanoparticles for Protein Delivery: Analysis of Preparation Conditions on Particle Morphology and Protein Loading, Activity and Sustained Release Properties, *J. Biomater. Sci. Polym. Ed.* ahead-of-p (2012) 1–23. doi:10.1163/092050611X576648.
- [41] O. Dudeck, O. Jordan, K.T. Hoffmann, A.F. Okuducu, K. Tesmer, T. Kreuzer-Nagy, D.A. Rüfenacht, E. Doelker, R. Felix, Organic solvents as vehicles for precipitating liquid embolics: A comparative angiototoxicity study with superselective injections of swine rete mirabile, *Am. J. Neuroradiol.* 27 (2006) 1900–1906.

- [42] A. Boongird, N. Nasongkla, S. Hongeng, N. Sukdawong, W. Sa-Nguanruang, N. Larbcharoensub, Biocompatibility study of glycofurol in rat brains, *Exp. Biol. Med.* 236 (2011) 77–83. doi:10.1258/ebm.2010.010219.
- [43] H.S. Yoo, T.G. Park, Biodegradable polymeric micelles composed of doxorubicin conjugated PLGA – PEG block copolymer, *J. Control. Release.* 70 (2001) 63–70.
- [44] M. Morille, T. Van-Thanh, X. Garric, J. Cayon, J. Coudane, D. Noël, M.C. Venier-Julienne, C.N. Montero-Menei, New PLGA-P188-PLGA matrix enhances TGF- $\beta$ 3 release from pharmacologically active microcarriers and promotes chondrogenesis of mesenchymal stem cells, *J. Control. Release.* 170 (2013) 99–110. doi:10.1016/j.jconrel.2013.04.017.
- [45] R. Milner, G. Edwards, C. Streuli, C. Ffrench-Constant, A role in migration for the alpha V beta 1 integrin expressed on oligodendrocyte precursors., *J. Neurosci.* 16 (1996) 7240–7252.
- [46] D. Séhédic, I. Chourpa, C. Tétaud, A. Griveau, C. Loussouarn, S. Avril, C. Legendre, N. Lepareur, D. Wion, F. Hindré, F. Davodeau, E. Garcion, Locoregional Confinement and Major Clinical Benefit of  $^{188}\text{Re}$ -Loaded CXCR4-Targeted Nanocarriers in an Orthotopic Human to Mouse Model of Glioblastoma, *Theranostics.* 7 (2017) 4517–4536. doi:10.7150/thno.19403.
- [47] A. Swed, T. Cordonnier, A. Dénarnaud, C. Boyer, J. Guicheux, P. Weiss, F. Boury, Sustained release of TGF- $\beta$ 1 from biodegradable microparticles prepared by a new green process in CO<sub>2</sub> medium, *Int. J. Pharm.* 493 (2015) 357–365. doi:10.1016/j.ijpharm.2015.07.043.
- [48] B.J.P. Heurtault B., Saulnier P., Pech B., Proust J.E., A novel phase inversion -based process for the preparation of lipid nanocarrier, *Pharm. Res.* 19 (2002) 875–880.
- [49] F. Li, S. Li, M. Vert, Synthesis and rheological properties of polylactide/poly(ethylene glycol) multiblock copolymers, *Macromol. Biosci.* 5 (2005) 1125–1131. doi:10.1002/mabi.200500143.
- [50] A. Harrane, A. Leroy, H. Nouailhas, X. Garric, J. Coudane, B. Nottelet, PLA-based biodegradable and tunable soft elastomers for biomedical applications, *Biomed. Mater.* 6 (2011) 65006. doi:10.1088/1748-6041/6/6/065006.
- [51] A. Swed, T. Cordonnier, A. Dénarnaud, C. Boyer, J. Guicheux, P. Weiss, F. Boury, Sustained release of TGF- $\beta$ 1 from biodegradable microparticles prepared by a new green process in CO<sub>2</sub> medium, *Int. J. Pharm.* 493 (2015) 357–365. doi:10.1016/j.ijpharm.2015.07.043.
- [52] S. Kandalam, L. Sindji, G.J.-R. Delcroix, F. Violet, X. Garric, E.M. André, P.C. Schiller, M.-C. Venier-Julienne, A. des Rieux, J. Guicheux, C.N. Montero-Menei, Pharmacologically active microcarriers delivering BDNF within a hydrogel: Novel strategy for human bone marrow-derived stem cells neural/neuronal differentiation guidance and therapeutic secretome enhancement, *Acta Biomater.* (2016). doi:10.1016/j.actbio.2016.11.030.
- [53] D. Mustafi, C.M. Smith, M.W. Makinen, R.C. Lee, Multi-block poloxamer surfactants suppress aggregation of denatured proteins, *Biochim. Biophys. Acta - Gen. Subj.* 1780 (2008) 7–15. doi:10.1016/j.bbagen.2007.08.017.
- [54] A. Paillard-Giteau, V.T. Tran, O. Thomas, X. Garric, J. Coudane, S. Marchal, I. Chourpa, J.P. Benoît, C.N. Montero-Menei, M.C. Venier-Julienne, Effect of various additives and polymers on lysozyme release from PLGA microspheres prepared by an s/o/w emulsion technique, *Eur. J. Pharm. Biopharm.* 75 (2010) 128–136. doi:10.1016/j.ejpb.2010.03.005.
- [55] S. James, J.J. McManus, Thermal and solution stability of lysozyme in the presence of sucrose, glucose, and trehalose, *J. Phys. Chem. B.* 116 (2012) 10182–10188.

- doi:10.1021/jp303898g.
- [56] N. Pirooznia, S. Hasannia, A. Lotfi, M. Ghanei, Encapsulation of Alpha-1 antitrypsin in PLGA nanoparticles: In Vitro characterization as an effective aerosol formulation in pulmonary diseases, *J. Nanobiotechnol.* 10 (2012) 20. doi:10.1186/1477-3155-10-20.
- [57] F. De Jaeghere, E. Allémann, J. Feijen, T. Kissel, E. Doelker, R. Gurny, Freeze-drying and lyopreservation of diblock and triblock poly(lactic acid)-poly(ethylene oxide) (PLA-PEO) copolymer nanoparticles., *Pharm. Dev. Technol.* 5 (2000) 473–483. doi:10.1081/PDT-100102031.
- [58] S. Honary, F. Zahir, Effect of Zeta Potential on the Properties of Nano - Drug Delivery Systems - A Review (Part 2), *Trop. J. Pharm. Al Res.* 12 (2013) 265–273. doi:10.4314/tjpr.v12i2.19.
- [59] W. Abdelwahed, G. Degobert, H. Fessi, Investigation of nanocapsules stabilization by amorphous excipients during freeze-drying and storage, *Eur. J. Pharm. Biopharm.* 63 (2006) 87–94. doi:10.1016/j.ejpb.2006.01.015.
- [60] W. Abdelwahed, G. Degobert, S. Stainmesse, H. Fessi, Freeze-drying of nanoparticles: Formulation, process and storage considerations, *Adv. Drug Deliv. Rev.* 58 (2006) 1688–1713. doi:10.1016/j.addr.2006.09.017.
- [61] M. Sameti, G. Bohr, M.N. V Ravi Kumar, C. Kneuer, U. Bakowsky, M. Nacken, H. Schmidt, C.M. Lehr, Stabilisation by freeze-drying of cationically modified silica nanoparticles for gene delivery, *Int. J. Pharm.* 266 (2003) 51–60. doi:10.1016/S0378-5173(03)00380-6.
- [62] S.M. Patel, T. Doen, M.J. Pikal, Determination of End Point of Primary Drying in Freeze-Drying Process Control, *AAPS PharmSciTech.* 11 (2010) 73–84. doi:10.1208/s12249-009-9362-7.
- [63] W. Abdelwahed, G. Degobert, H. Fessi, A pilot study of freeze drying of poly(epsilon-caprolactone) nanocapsules stabilized by poly(vinyl alcohol): Formulation and process optimization, *Int. J. Pharm.* 309 (2006) 178–188. doi:10.1016/j.ijpharm.2005.10.003.
- [64] G. Yang, K. Gilstrap, A. Zhang, L.X. Xu, X. He, Collapse temperature of solutions important for lyopreservation of living cells at ambient temperature, *Biotechnol. Bioeng.* 106 (2010) 247–259. doi:10.1002/bit.22690.
- [65] F. De Jaeghere, E. Allémann, J.C. Leroux, W. Stevels, J. Feijen, E. Doelker, R. Gurny, Formulation and lyoprotection of poly(Lactic acid-co-ethylene oxide) nanoparticles: Influence on physical stability and In vitro cell uptake, *Pharm. Res.* 16 (1999) 859–866. doi:10.1023/A:1018826103261.
- [66] N. Shamim, L. Hong, K. Hidajat, M.S. Uddin, Thermosensitive-polymer-coated magnetic nanoparticles: Adsorption and desorption of Bovine Serum Albumin, *J. Colloid Interface Sci.* 304 (2006) 1–8. doi:10.1016/j.jcis.2006.08.047.
- [67] M.J. Santander-Ortega, N. Csaba, L. González, D. Bastos-González, J.L. Ortega-Vinuesa, M.J. Alonso, Protein-loaded PLGA-PEO blend nanoparticles: Encapsulation, release and degradation characteristics, *Colloid Polym. Sci.* 288 (2010) 141–150. doi:10.1007/s00396-009-2131-z.
- [68] T. Morita, Y. Sakamura, Y. Horikiri, T. Suzuki, H. Yoshino, Protein encapsulation into biodegradable microspheres by a novel S/O/W emulsion method using poly(ethylene glycol) as a protein micronization adjuvant, *J. Control. Release.* 69 (2000) 435–444. doi:10.1016/S0168-3659(00)00326-6.
- [69] L.J. White, G.T.S. Kirby, H.C. Cox, R. Qodratnama, O. Qutachi, F.R.A.J. Rose, K.M. Shakesheff, Accelerating protein release from microparticles for regenerative medicine applications, *Mater. Sci. Eng. C.* 33 (2013) 2578–2583. doi:10.1016/j.msec.2013.02.020.
- [70] I.J. Castellanos, W. Al-Azzam, K. Criebenow, Effect of the covalent modification with

- poly(ethylene glycol) on  $\alpha$ -chymotrypsin stability upon encapsulation in poly(lactic-co-glycolic) microspheres, *J. Pharm. Sci.* 94 (2005) 327–340. doi:10.1002/jps.20243.
- [71] K.D. Hinds, K.M. Campbell, K.M. Holland, D.H. Lewis, C.A. Piché, P.G. Schmidt, PEGylated insulin in PLGA microparticles. In vivo and in vitro analysis, *J. Control. Release.* 104 (2005) 447–460. doi:10.1016/j.jconrel.2005.02.020.
- [72] S. Hermeling, D.J.A. Crommelin, H. Schellekens, W. Jiskoot, Structure-immunogenicity relationships of therapeutic proteins, *Pharm. Res.* 21 (2004) 897–903. doi:10.1023/B:PHAM.0000029275.41323.a6.
- [73] C. Maas, S. Hermeling, B. Bouma, W. Jiskoot, M.F.B.G. Gebbink, A role for protein misfolding in immunogenicity of biopharmaceuticals, *J. Biol. Chem.* 282 (2007) 2229–2236. doi:10.1074/jbc.M605984200.
- [74] J. Park, P.M. Fong, J. Lu, K.S. Russell, C.J. Booth, W.M. Saltzman, T.M. Fahmy, PEGylated PLGA nanoparticles for the improved delivery of doxorubicin, *Nanomedicine Nanotechnology, Biol. Med.* 5 (2009) 410–418. doi:10.1016/j.nano.2009.02.002.
- [75] J. Liu, S.M. Zhang, P.P. Chen, L. Cheng, W. Zhou, W.X. Tang, Z.W. Chen, C.M. Ke, Controlled release of insulin from PLGA nanoparticles embedded within PVA hydrogels, *J. Mater. Sci. Mater. Med.* 18 (2007) 2205–2210. doi:10.1007/s10856-007-3010-0.
- [76] M. Xia, R. Huang, K.L. Witt, N. Southall, J. Fostel, M.H. Cho, A. Jadhav, C.S. Smith, J. Inglese, C.J. Portier, R.R. Tice, C.P. Austin, Compound cytotoxicity profiling using quantitative high-throughput screening, *Environ. Health Perspect.* 116 (2008) 284–291. doi:10.1289/ehp.10727.
- [77] C. Maupas, B. Moulari, A. Béduneau, A. Lamprecht, Y. Pellequer, Surfactant dependent toxicity of lipid nanocapsules in HaCaT cells, *Int. J. Pharm.* 411 (2011) 136–141. doi:10.1016/j.ijpharm.2011.03.056.
- [78] G. Le Roux, H. Moche, A. Nieto, J.P. Benoit, F. Nessler, F. Lagarce, Cytotoxicity and genotoxicity of lipid nanocapsules, *Toxicol. Vitro.* 41 (2017) 189–199. doi:10.1016/j.tiv.2017.03.007.
- [79] M. Partearroyo, H. Ostolaza, Surfactant-induced cell toxicity and cell lysis: a study using B16 melanoma cells, *Biochem. ....* (1990) 1323–1328. doi:10.1016/0006-2952(90)90399-6.
- [80] D. Hambarzumyan, D.H. Gutmann, H. Kettenmann, The role of microglia and macrophages in glioma maintenance and progression, *Nat. Neurosci.* 19 (2015) 20–27. doi:10.1038/nn.4185.
- [81] S.R. Nielsen, M.C. Schmid, Macrophages as Key Drivers of Cancer Progression and Metastasis, *Mediators Inflamm.* 2017 (2017) 1–11. doi:10.1155/2017/9624760.
- [82] Konstantinos Avgoustakis, Polylactic-Co-Glycolic Acid (PLGA), *Encycl. Biomater. Biomed. Eng.* 1 (2005) 1–11. doi:10.1081/E-EBBE-120013950.
- [83] H.K. Makadia, S.J. Siegel, Poly Lactic-co-Glycolic Acid (PLGA) as biodegradable controlled drug delivery carrier, *Polymers (Basel).* 3 (2011) 1377–1397. doi:10.3390/polym3031377.
- [84] R. Guarecuco, J. Lu, K.J. McHugh, J.J. Norman, L.S. Thapa, E. Lydon, R. Langer, A. Jaklenec, Immunogenicity of pulsatile-release PLGA microspheres for single-injection vaccination, *Vaccine.* 36 (2018) 3161–3168. doi:10.1016/j.vaccine.2017.05.094.
- [85] J.C. Middleton, A.J. Tipton, Synthetic biodegradable polymers as orthopedic devices, *Biomaterials.* 21 (2000) 2335–2346. doi:10.1016/S0142-9612(00)00101-0.
- [86] B.D. Ulery, L.S. Nair, C.T. Laurencin, Biomedical applications of biodegradable polymers, *J. Polym. Sci. Part B Polym. Phys.* 49 (2011) 832–864. doi:10.1002/polb.22259.

- [87] J. Zhao, C.S. Liu, Y. Yuan, X.Y. Tao, X.Q. Shan, Y. Sheng, F. Wu, Preparation of hemoglobin-loaded nano-sized particles with porous structure as oxygen carriers, *Biomaterials*. 28 (2007) 1414–1422. doi:10.1016/j.biomaterials.2006.10.012.
- [88] T. Yamahara, Y. Numa, T. Oishi, T. Kawaguchi, T. Seno, A. Asai, K. Kawamoto, Morphological and flow cytometric analysis of cell infiltration in glioblastoma: A comparison of autopsy brain and neuroimaging, *Brain Tumor Pathol.* 27 (2010) 81–87. doi:10.1007/s10014-010-0275-7.
- [89] L.E. Gaspar, B.J. Fisher, D.R. Macdonald, D. V. Leber, E.C. Halperin, S.C. Schold, J.G. Cairncross, Supratentorial malignant glioma: Patterns of recurrence and implications for external beam local treatment, *Int. J. Radiat. Oncol. Biol. Phys.* 24 (2010) 55–57. doi:10.1016/0360-3016(92)91021-e.
- [90] W. Diao, X. Tong, C. Yang, F. Zhang, C. Bao, H. Chen, L. Liu, M. Li, F. Ye, Q. Fan, J. Wang, Z.C. Ou-Yang, Behaviors of Glioblastoma Cells in in Vitro Microenvironments, *Sci. Rep.* 9 (2019) 1–9. doi:10.1038/s41598-018-36347-7.
- [91] C. Wang, X. Tong, F. Yang, Bioengineered 3D brain tumor model to elucidate the effects of matrix stiffness on glioblastoma cell behavior using peg-based hydrogels, *Mol. Pharm.* 11 (2014) 2115–2125. doi:10.1021/mp5000828.

**Chapter 4:**  
**Incorporation of SDF-1 $\alpha$ -loaded  
PLGA/PEG-PLGA Nanoparticles into  
Chitosan Nanofibers**

## 4. INCORPORATION OF SDF-1 $\alpha$ -LOADED PLGA/PEG-PLGA NANOPARTICLES INTO CHITOSAN NANOFIBERS

### 4.1. INTRODUCTION

In the previous chapter, nanoparticles loaded with SDF-1 $\alpha$  were successfully produced from a combination of PLGA and PEG-PLGA using a non-toxic and non-denaturing phase separation method. The nanoparticles had high SDF-1 $\alpha$  encapsulation efficiencies and good cytocompatibility. However, one significant disadvantage of the developed nanoparticle system was its incapability to provide sustained release of SDF-1 $\alpha$ , which is perceived to be crucial for providing a sufficient time window for the post-surgical recruitment of GBM cells. The fast release of SDF-1 $\alpha$  can be attributed to the rapid dissolution of the protein load as a result of free penetration of solvent molecules into the porous structure of the nanoparticles.

To restrict the access of solvent molecules to the protein load in the nanoparticles, and thus reduce the initial burst and prolong the short duration of release typically seen with PLGA-based nanoparticles, incorporation of the protein-loaded nanoparticles into an appropriate scaffold may be a useful strategy. The external scaffold may present an additional barrier to the diffusion of protein and solvent molecules to slow down the release process, especially when the scaffold phase consists of materials with high degree of crystallinity and low water solubility. Gentile *et al.* incorporated parathyroid hormone (PTH)-loaded PLGA nanoparticles into porous chitosan/gelatin scaffolds by freeze-drying the nanoparticles in a chitosan/gelatin blend solution. They observed a reduction in the percentage of the protein load released in the first 48 hours from 75 to 15% upon incorporation of the nanoparticles into the porous scaffold [1]. Similarly, Asghar *et al.* observed sustained protein release over a period of 30 days after embedding BSA-loaded PLGA nanoparticles into porous collagen scaffolds [2].

This chapter concerns the fulfillment of the second objective of this thesis, which is to incorporate the SDF-1 $\alpha$ -loaded nanoparticles developed in the previous chapter into chitosan-based nanofibrous scaffolds to provide a secondary barrier to the SDF-1 $\alpha$  release process. As discussed briefly at the end of Section 1.3.3.5, chitosan was the material of choice for making nanofibrous scaffolds due to its cationic property that permit electrostatic interactions with PLGA-based nanoparticles during processing. Electrospinning was the preferred processing technique as it can reliably produce fibrous scaffolds with a range of fiber diameter that correlates to the size scale of the fibrous ECM network, which may help to provide relevant structural and potentially mechanical cues for cell adhesion and migration, and subsequently

facilitates the trapping of GBM cells. After the optimization of the electrospinning step, the cytotoxicity and biocompatibility of the generated nanofibrous scaffolds were also evaluated using suitable *in vitro* and *in vivo* assays.

Part of this chapter (Section 4.3.1) will be submitted for publication in the form of an article titled “Development of nanoparticle-containing nanofibrous scaffolds to achieve sustained release of SDF-1 $\alpha$ ” in the Journal of Materials Chemistry B.

## 4.2. SUMMARY OF THE RESULTS

SDF-1 $\alpha$ -loaded PLGA/PEG-PLGA nanoparticles were successfully co-electrospun with chitosan in the presence of the fiber-forming additive PEO. Up to 10 mg of nanoparticles could be loaded into nanofibers electrospun from a mixture of 110 mg chitosan and 15 mg PEO. The presence of the nanoparticles within the nanofibers was verified using FTIR spectroscopy, SEM and TEM. After electrospinning, the amino groups of chitosan could be deprotonated to turn the nanofibers water-stable by treating the electrospun scaffold with 0.1 M NaOH. The deprotonation process did not significantly affect the nanofibrous morphology or the integrity of the nanoparticles. The deprotonated nanofibers bearing the SDF-1 $\alpha$ -loaded nanoparticles could provide sustained release of the chemokine for up to 5 weeks. For the same period of time, the scaffold also did not degrade significantly when incubated in buffer solutions supplemented with physiologically-relevant concentration of lysozyme, the main enzyme known to digest chitosan. Furthermore, the nanofibrous morphology of the scaffold could support the attachment of U87-MG cells. All these point towards excellent potential for the scaffold to function as an efficient trap for glioblastoma cells. In terms of safety, the scaffold was shown to be highly cytocompatible with NIH3T3 fibroblasts, Thp-1 macrophages as well as the primary astrocytes extracted from the brain of newborn rats. These encouraging *in vitro* results called for the assessment of the scaffold's biocompatibility in animals. Thus, the scaffold was implanted into the brain of healthy rats using a customized surgical procedure and followed up. The results of a short-term study (7 days) revealed that the scaffold could induce a strong immune response at the site of implantation. However, the animals did not show any signs of distress throughout the follow-up period. The long-term study (100 days) to obtain more information regarding possible chronic inflammation and tissue integration of the scaffold is currently underway.

## 4.3. RESULTS

### 4.3.1. Publication 2 (to be submitted to the Journal of Materials Chemistry B)

---

#### **Development of nanoparticle-containing nanofibrous scaffolds to achieve sustained release of SDF-1 $\alpha$**

Muhammad Haji Mansor<sup>a,b</sup>, Mathie Najberg<sup>a,c</sup>, Jean-Michel Thomassin<sup>b</sup>, Carmen Alvarez-Lorenzo<sup>c</sup>, Emmanuel Garcion<sup>a</sup>, Christine Jérôme<sup>b</sup>, Frank Boury<sup>a,#</sup>

<sup>a</sup>CRCINA, INSERM, Université de Nantes, Université d'Angers, Angers, France

<sup>b</sup>Center for Education and Research on Macromolecules (CERM), CESAM RU, University of Liège, Liège, Belgium

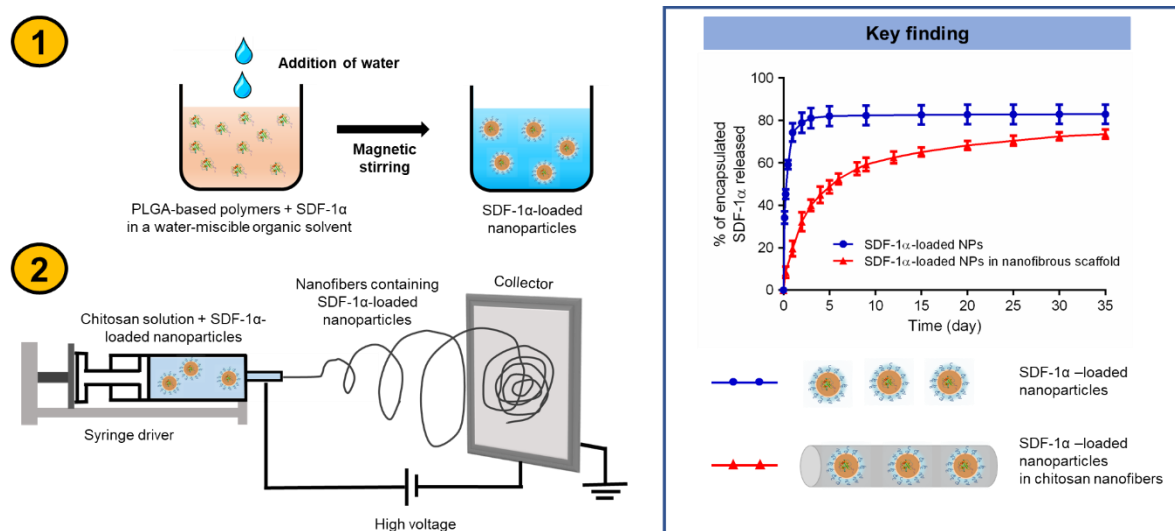
<sup>c</sup>Departamento de Farmacología, Farmacia y Tecnología Farmacéutica, R & D Pharma Group, Facultad de Farmacia, and Health Research Institute of Santiago de Compostela (IDIS), Universidade de Santiago de Compostela, Santiago de Compostela, Spain

# Corresponding author.

E-mail address: [frank.boury@univ-angers.fr](mailto:frank.boury@univ-angers.fr)

## Abstract

Chemokines such as stromal cell-derived factor-1 $\alpha$  (SDF-1 $\alpha$ ) regulate the migration of cancer cells. In vivo, cancer cells can spread from their primary tumor site by migrating up an SDF-1 $\alpha$  concentration gradient, facilitating their local invasion and metastasis. Therefore, the implantation of SDF-1 $\alpha$ -releasing scaffolds can be a useful strategy to trap cancer cells expressing the receptor for SDF-1 $\alpha$ . In this work, SDF-1 $\alpha$  was encapsulated into poly(lactic-co-glycolic acid) (PLGA)-based nanoparticles and subsequently electrospun with chitosan to produce nanofibrous scaffolds intended for trapping glioblastoma (GBM) cells. The encapsulated SDF-1 $\alpha$  maintained its biological activity after the electrospinning process and the scaffolds could provide sustained release of SDF-1 $\alpha$  for at least 5 weeks. Using a mouse fibroblast cell line, we showed that the scaffolds possessed high cytocompatibility. Furthermore, the nanofibrous structure of the scaffolds provided excellent anchoring sites to support the adhesion of human GBM cells. The scaffolds also demonstrated slow degradation kinetics, which may be useful in maximizing the time window for trapping GBM cells. As surgical resection does not permit a complete removal of GBM tumors, our results support future implantation of these scaffolds into the walls of the resection cavity to attract and trap the residual GBM cells in the brain.



## Keywords:

Stromal cell-derived factor-1 $\alpha$  (SDF-1 $\alpha$ ), Poly(lactic-co-glycolic acid) (PLGA), Sustained release, Electrospinning, Chitosan, Nanofibrous scaffold

## 1. Introduction

Stromal cell-derived factor-1 $\alpha$  (SDF-1 $\alpha$ ) is a 68-amino-acid chemokine [3] with a strong binding affinity to the C-X-C chemokine receptor type 4 (CXCR4) [4]. One of its prominent physiological functions is to induce the migration of CXCR4-expressing stem and progenitor cells from the bone marrow towards a site of injury to initiate the process of tissue repair and recovery [5]. The directed migration is an effect of an elevated SDF-1 $\alpha$  expression at the injury site [6–8] and the simultaneous increase in SDF-1 $\alpha$  degradation in the bone marrow [9,10] that creates a positive SDF-1 $\alpha$  concentration gradient towards the site needing repair. In addition to its role in tissue regeneration, SDF-1 $\alpha$ -induced chemotaxis also mediates the spreading of cancer cells that escaped their respective primary tumor sites. CXCR4-expressing cancer cells have been shown to penetrate the blood or lymphatic circulation and subsequently be chemoattracted to SDF-1 $\alpha$ -secreting organs such as the liver [11], bone marrow [12] and lymph nodes [13] for future metastatic colonization. Even in non-metastasizing cancers, the chemotactic effect of SDF-1 $\alpha$  can support tumor progression by facilitating the invasion of cancer cells into proximal healthy tissues [14]. The significant influence of SDF-1 $\alpha$  on the migration of cancer cells has motivated the design of implants capable of releasing this chemokine to create a local concentration gradient that may attract CXCR4-expressing cancer cells relevant to many types of cancers including glioblastoma (GBM) [15], melanoma [16] and breast cancer [17].

Like other peptides and proteins, SDF-1 $\alpha$  is water-soluble and thus can move rapidly through a physiological fluid compartment [18]. Therefore, to establish and maintain a local concentration gradient of SDF-1 $\alpha$ , sustained delivery of this chemokine from a fixed source is necessary. In this regard, encapsulation into nanocarriers composed of biodegradable polymers such as poly-(lactic-co-glycolic acid) (PLGA) is a reasonable strategy to achieve gradual SDF-1 $\alpha$  release at the intended site of delivery. PLGA, having a hydrophobic molecular backbone that terminates with an ionizable carboxyl group (Figure 1), is known to form strong interactions with non-polar or positively-charged residues in proteins to facilitate the encapsulation of these molecules. However, we have previously shown that the duration of SDF-1 $\alpha$  release from PLGA-based nanoparticles was relatively brief. The release profile was characterized by a steep initial release curve that levels out shortly afterwards due to the high surface area to volume ratio of the polymer-based nanoparticles [19]. In addition, nanoparticles tend to spread away from the initial site of application, making it difficult to establish a concentration gradient of the released drug molecules. Considering these shortcomings, we

postulate that SDF-1 $\alpha$ -loaded nanoparticles should be embedded within a suitable scaffold to slow down the SDF-1 $\alpha$  release process and to prevent them from moving away from the initial site of administration.

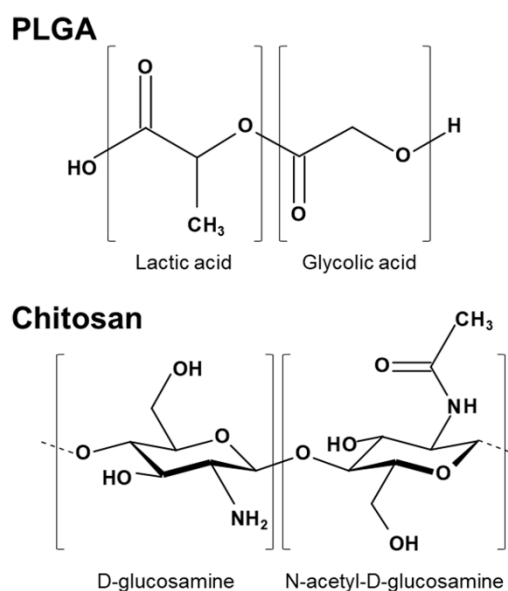


**Figure 1:** Chemical structures of PLGA (top) and chitosan (bottom) showing their respective monomers.

Currently, there are multiple types of scaffold within which drug-loaded carriers can be confined. These structures can provide an additional barrier to the drug diffusion process and may subsequently contribute to a longer duration of drug release from the primary carrier into the local environment. These include physically and chemically cross-linked hydrogels [20–22], scaffolds prepared by the freeze-drying process [23,24] and those derived from a direct compression of the drug-loaded carriers [25]. However, these confining matrices usually lack the nanofibrous structures typically found in native human extracellular matrices (ECM). In relation to our objective, it is important to develop scaffolds with structures mirroring those of the ECM in order to promote the adhesion and retention of cancer cells. A convenient way of producing nanofibrous scaffolds is to use a technique called electrospinning [26,27]. Using this approach, many natural and synthetic materials can be used to produce ECM-mimetic nanofibrous scaffolds that may be loaded with drug molecules or drug-loaded carriers. Among these, chitosan, a polymer consisting of D-glucosamine and N-acetyl-D-glucosamine as monomers (Figure 1), has been an outstanding material for making electrospun scaffolds to be used in a variety of biomedical applications due to its excellent biocompatibility [28–30]. As it carries weakly-basic amino groups, chitosan is insoluble in aqueous solutions of

physiological pH. However, in dilute acid solutions such as 1 M acetic acid, the amino groups are protonated, making the chitosan molecules soluble and thus feasible for electrospinning [31]. In addition, the positively-charged amino groups may facilitate the interaction between the chitosan molecules and the negatively-charged SDF-1 $\alpha$ -loaded PLGA-based nanoparticles, opening up the possibility for a successful co-electrospinning process. However, the use of chitosan alone cannot guarantee the generation of defect-free nanofibers under mild conditions [32–35]. Studies have shown that the strong electrostatic repulsion between positively-charged chitosan molecules prevents sufficient chain entanglement that is necessary for nanofiber formation [36]. Thus, a small amount of high molecular weight and neutral polymers such as polyethylene oxide (PEO) is usually added to a chitosan solution to promote chain entanglement by virtue of the formation of hydrogen bonds between the ether oxygen of PEO and the amino hydrogen of chitosan [37]. Furthermore, the electrospinning of chitosan and many other materials often involves challenging conditions, including the use of high voltage to draw fibers from the material solution, which may compromise the structural integrity of protein molecules pre-incorporated into the solubilized material. Therefore, we hypothesize that by pre-encapsulating SDF-1 $\alpha$  molecules into PLGA-based nanoparticles, their denaturation during processing may be minimized.

In the present study, SDF-1 $\alpha$  was encapsulated into nanoparticles composed of PLGA and a polyethylene glycol (PEG)-PLGA co-polymer. The SDF-1 $\alpha$ -loaded nanoparticles were then dispersed in a chitosan solution in the presence of the fiber-forming additive PEO and subsequently electrospun to produce nanoparticle-containing nanofibrous scaffolds. After electrospinning, the charged chitosan amino groups within the nanofibers were deprotonated to improve the scaffold stability in physiological media. Following this, the *in vitro* release of the model protein lysozyme as well as SDF-1 $\alpha$  from the scaffolds was studied. The bioactivity of the released SDF-1 $\alpha$  was subsequently evaluated by assessing its capacity to induce the migration of CXCR4-expressing human GBM cells (U87-MG). Finally, after studying their degradation profiles, the scaffolds' ability to retain U87-MG cells as well as their cytocompatibility was assessed *in vitro* to evaluate the appropriateness of their use in future *in vivo* studies.

## 2. Materials and Methods

### 2.1. Materials

Ester-capped PLGA ( $M_n = 5.5$  kDa) and PEG-PLGA copolymer ( $M_{nPEG} = 5$  kDa,  $M_{nPLGA} = 25.7$  kDa) were synthesized using a ring-opening polymerization method as described elsewhere [19]. Glycofurol (Tetraglycol BioXtra®), isosorbide dimethyl ether, poloxamer 188 (Lutrol® F68), sodium chloride, lysozyme from hen egg white, glycine, 10 M sodium hydroxide, dimethyl sulfoxide, Tris base (Trizma®), 37% hydrochloric acid, *Micrococcus lysodeikticus*, low gelling point agarose and PEO (average  $M_v \sim 2$  MDa) were obtained from Sigma-Aldrich (Saint Quentin Fallavier, France). Human SDF-1 $\alpha$  (research grade) was purchased from Miltenyi Biotech (Paris, France), chitosan with a degree of deacetylation of  $\sim 80\%$  (Chitocentials®) from Heppe Medical Chitosan GmbH (Halle, Germany), 1x Dulbecco's phosphate-buffered saline (Biowhittaker®) from Lonza (Verviers, Belgium), bovine serum albumin fraction V from Roche Diagnostics GmbH (Mannheim, Germany) and high glucose Dulbecco's Modified Eagle's Medium (Gibco®) from Thermo Fisher Scientific (Villebon sur Yvette, France). Deionized water supply was obtained from a Milli-Q® Advantage A10 system (Millipore, Paris, France).

## 2.2. Preparation and characterization of protein-loaded nanoparticles

### 2.2.1. Preparation of protein-loaded nanoparticles

Protein-loaded nanoparticles were prepared as described previously [19]. Briefly, the lyophilized model protein lysozyme and SDF-1 $\alpha$  as provided by their respective manufacturers were separately dissolved in 0.15 M sodium chloride (NaCl) solution containing 20% (w/v) poloxamer 188 at a concentration of 10 and 2.67 mg/mL respectively. After that, 975  $\mu$ L of glycofurol was added to 25  $\mu$ L of the protein solution and the mixture was subsequently incubated in ice for 30 minutes to induce the formation of protein precipitates. Then, 100  $\mu$ L of the protein precipitate dispersion containing either 25  $\mu$ g lysozyme or 10  $\mu$ g SDF-1 $\alpha$  was mixed with 100  $\mu$ L of each of 12% (w/v) solutions of PLGA and PEG-PLGA in isosorbide dimethyl ether (total volume after mixing = 300  $\mu$ L). Using Equation (1), the theoretical drug loadings (DL) for lysozyme and SDF-1 $\alpha$  were calculated to be 0.10% and 0.04% respectively. For the synthesis of unloaded nanoparticles, the 100  $\mu$ L protein precipitate dispersion was replaced with an equal volume of glycofurol alone. Then, 2.1 mL of 0.05 M glycine-sodium hydroxide (NaOH) buffer solution was added gradually under magnetic stirring to initiate the formation of nanoparticles that encapsulate the protein load. The pH of the buffer solution was set to 11.35 and 10.40 for the encapsulation of lysozyme and SDF-1 $\alpha$  respectively. The formed nanoparticle dispersion was subsequently diluted with excess deionized water and centrifuged

for 30 min at 10,000 x g. The supernatant was then discarded and replaced with an equal volume of deionized water. The centrifugation was repeated once and after subsequent removal of the supernatant, the purified nanoparticle dispersion was stored at a concentration of approximately 40 mg/mL in 0.5 mL volume in deionized water at 4 °C until use.

$$DL (\%) = \frac{\text{Initial mass of protein used as a starting material}}{\text{Total mass of PLGA and PEG-PLGA}} \times 100 \quad \text{Equation 1}$$

### 2.2.2. Characterization of protein-loaded nanoparticles

The morphology of the nanoparticles was visualized using scanning electron microscopy (SEM) (JSM 6310F, JEOL, Paris, France). The purified nanoparticle dispersion was initially diluted 200-fold with deionized water to a concentration of approximately 200 µg/mL. Then, 2 µL of the dispersion was added onto a glass slide and left overnight to dry at room temperature. Prior to observation, a gold coating of 5 nm thickness was deposited onto the nanoparticle sample.

The size distribution of the nanoparticles was determined using a dynamic light scattering (DLS) method whereas zeta-potentials were derived from the electrophoretic mobility values using the Smoluchowski's approximation in a Nanosizer® ZS (Malvern, Worcestershire, UK). Initially, the purified nanoparticle dispersion was diluted with either deionized water or 0.01 M NaCl solution for size and zeta-potential measurements respectively to obtain optimal nanoparticle concentrations for analyses such that the attenuator values were in the range of 5–7. Each sample was measured three times, with one measurement representing the average value of at least 10 runs. All measurements were conducted at 25 °C under the automatic mode. In addition to the average particle size, the DLS protocol of Nanosizer® ZS generated a polydispersity index (PDI) ranging from 0 to 1 that estimates the width of the size distribution. For the assessment of protein encapsulation efficiencies, the protein-loaded nanoparticles were initially lyophilized for 16 hours alongside the unloaded nanoparticles that served as a control. Then, the nanoparticles were dissolved in 1 mL of dimethyl sulfoxide. After 1 hour, 3 mL of 0.01 M hydrochloric acid (HCl) was added to extract the protein load from the polymer-based components of the nanoparticles. The samples were then diluted appropriately prior to assessment using the protein quantification assays described in Section 2.7. The encapsulation efficiency (EE) was calculated using Equation (2).

$$EE (\%) = \frac{\text{Mass of protein recovered from dissolved nanoparticles}}{\text{Initial mass of protein used as a starting material}} \times 100 \quad \text{Equation 2}$$

## 2.3. Preparation and characterization of nanoparticle-containing nanofibrous scaffolds

### 2.3.1. Preparation of nanoparticle-containing nanofibrous scaffolds

To prepare nanofibrous scaffolds containing protein-loaded nanoparticles, 11 mg of PEO was initially added to 0.5 mL of nanoparticle dispersion in deionized water. The nanoparticle concentration was varied between approximately 10 and 40 mg/mL to determine the maximum mass of nanoparticles that can be loaded into the nanofibrous scaffolds. After that, the nanoparticles/PEO mixture was added to 1.7 mL of 6.5% (w/v) chitosan solution in 1 M acetic acid. Based on this, the theoretical nanoparticle load in the nanofibrous scaffold to be synthesized ranged from 4.0 – 14.2% w/w (5 – 20 mg nanoparticles per 110 mg chitosan and 11 mg PEO). The materials were then mixed at room temperature using a laboratory magnetic stirrer set to 100 rpm for 2 hours. For the preparation of nanofibrous scaffolds carrying unencapsulated protein molecules, the PEO was dissolved in 0.5 mL deionized water containing either 25  $\mu$ g lysozyme or 10  $\mu$ g SDF-1 $\alpha$  to match the protein load in the nanoparticles prior to mixing with the 6.5% (w/v) chitosan solution. The homogenized materials were subsequently transferred into a 10 mL HSW SOFT-JECT® disposable plastic syringe (Henke-Sass, Wolf GmbH, Tuttlingen, Germany) with a luer slip tip that was fixed with a 21 G x 1½ inch blunt-ended needle. The syringe was then left to stand for another 2 hours for degassing.

For the electrospinning step, the syringe containing the protein-loaded nanoparticles, PEO and chitosan was carefully mounted onto a syringe driver (KD Scientific, Holliston, MA, USA) with the tip of the needle positioned 17 cm away from the collector plate. The syringe driver was used to control the flow rate of the materials at 0.78 mL/hour. To produce nanofibers, a Spellman SL10® high voltage generator (Spellman High Voltage Electronics Corp., Hauppauge, NY, USA) was used to apply a potential difference of 30 kV between the needle and the collector plate for 165 minutes. The nanofibers were deposited onto a piece of aluminum foil covering the collector plate to facilitate the subsequent retrieval of the electrospun scaffold.

### 2.3.2. Characterization of nanoparticle-containing nanofibrous scaffolds

The thickness of the nanofibrous scaffolds were measured using a Kaefer Dial Gauge (Kaefer Messuhrenfabrik GmbH, Villingen-Schwenningen, Germany).

The composition of the nanofibrous scaffolds was determined using attenuated total reflectance-Fourier transform infrared (ATR-FTIR) spectroscopy. ATR-FTIR spectra were recorded using a Nicolet iS5® spectrometer (Thermo Fisher Scientific) with a spectral resolution of 4 cm<sup>-1</sup>.

The morphology of the nanofibrous scaffolds was observed using SEM (JSM 840A, JEOL) and transmission electron microscopy (TEM) (JEM 1400, JEOL). For SEM, the nanofibrous scaffolds were coated with a 5 nm platinum layer prior to observation. Fiber diameter measurements were then performed using the ImageJ software (NIH, USA) on 30 randomly-selected fibers in a SEM image. Three SEM images were analyzed for each sample. For TEM, nanofibers were collected on a copper grid (Gilder Grids, Grantham, UK) placed in front of the collector plate for about 3 seconds during the electrospinning process and observed without any coating.

To investigate whether the electrospinning process contributes to any protein denaturation, 2 mL of 1 M acetic acid solution was added to the nanofibrous scaffolds to dissolve the nanofibers and subsequently release the protein-loaded nanoparticles. After 1 hour, 4 mL of 1 M NaOH solution was added gradually to increase the basicity of the mixture (to pH>13) to induce the precipitation of the chitosan molecules as well as the dissolution of the nanoparticles. After another 1-hour incubation, the mixture was centrifuged at 9,500 x g for 30 minutes to spin down the chitosan precipitates. 2 mL of the supernatant was kept for use in the protein quantification assays described in Section 2.7.

#### **2.4. Stabilization of the nanofibrous scaffolds**

To reduce the solubility of the nanofibrous scaffolds in physiological media, the charged amino groups of chitosan in the nanofibers were deprotonated [38,39]. To achieve this, the nanofibrous scaffolds were treated sequentially with absolute ethanol for 5 minutes and then 0.1 M NaOH for 30 seconds, followed by three times washing with 0.1x phosphate-buffered saline (PBS). The scaffolds were then dried under reduced pressure for 16 h.

#### **2.5. *In vitro* scaffold degradation study**

Stabilized nanofibrous scaffolds were cut into quarters of approximately 25 mg in mass. The scaffold pieces were then incubated separately in 2 mL of 0.05 M Tris-HCl buffer solution (pH 7.4) supplemented with 0.15 M NaCl, 20 µg/mL lysozyme and 1 mg/mL bovine serum albumin (BSA) at 37 °C. At each pre-defined time point, three scaffold pieces were removed from their

respective buffer solution and dried under reduced pressure for 16 h. The dried scaffold pieces were then weighed, and the % of scaffold mass degraded throughout the incubation period was calculated using Equation (3).

$$\% \text{ of scaffold mass degraded} = \frac{\text{mass before incubation} - \text{mass after incubation}}{\text{mass before incubation}} \times 100\% \quad \text{Equation 3}$$

## 2.6. *In vitro* protein release study

The *in vitro* protein release study was conducted on the protein-loaded nanoparticles, nanofibrous scaffolds loaded with unencapsulated protein molecules and protein-loaded nanoparticles incorporated into a nanofibrous scaffold. Protein-free nanoparticles and nanofibrous scaffolds were used as controls. All nanofibrous scaffolds were stabilized prior to use. Nanoparticles and whole scaffolds were incubated separately in 2 mL of 0.05 M Tris-HCl buffer solution (pH 7.4) supplemented with 0.15 M NaCl and 1 mg/mL BSA at 37 °C. At each pre-defined time point, 1.5 mL of the buffer solution was collected and replaced with fresh buffer. For the nanoparticle samples, the dispersion was centrifuged at 9,500 x g for 30 minutes to spin down the nanoparticles and 1.5 mL of the supernatant was subsequently collected and replaced with fresh buffer. The quantification of protein molecules in the collected samples was conducted as described in Section 2.7.

## 2.7. Protein quantification

### 2.7.1. Quantification of lysozyme

Lysozyme was quantified using the turbidity reduction assay as described by Hassani and colleagues [40]. Briefly, 100  $\mu$ L of lysozyme-containing sample was added to 2.9 mL of 0.015% (w/v) *Micrococcus lysodeikticus* suspension in 0.05 M Tris-HCl buffer solution (pH 7.4). The assay mixture was then incubated at 37°C to allow the lysozyme molecules to lyse the *M. lysodeikticus* cell walls. After 4 hours, the absorbance at 450 nm was measured. To construct a standard curve, lysozyme solutions of concentration ranging from 100 to 1000 ng/mL were also assayed. Each sample was diluted with 0.05 M Tris-HCl buffer solution (pH 7.4) by several dilution factors to obtain absorbance readings that were within the standard curve range.

### 2.7.2. Quantification of SDF-1 $\alpha$

SDF-1 $\alpha$  was quantified using an enzyme-linked immunosorbent assay (ELISA) as per supplier's instructions (R&D Systems, Lille, France). Briefly, a Nunc Maxisorp® 96-well

microplate (Thermo Fisher Scientific) was incubated overnight with SDF-1 $\alpha$  capture antibody solution to coat the wells. The plate was then washed with 0.05% (w/v) Tween® 20 in 1x PBS (pH 7.4). To prevent any non-specific protein binding during sample incubation stage, the plate was subsequently incubated with 10 mg/mL BSA solution in 1x PBS (pH 7.4) for 1 hour. After washing, SDF-1 $\alpha$ -containing samples and the provided SDF-1 $\alpha$  standard pre-diluted with 10 mg/mL BSA solution in 1x PBS (pH 7.4) were added to the wells for a 2-hour incubation. Following another wash, the wells were incubated with detection antibody solution for 2 hours. The plate was washed again prior to a 20-minute incubation with streptavidin-horseradish peroxidase solution. The final washing step was carried out and the plate was then incubated with the substrate solution for another 20 minutes. The enzymatic reaction was subsequently terminated by adding 1 M sulfuric acid solution and the absorbance at 450 nm was immediately measured. All incubations were done at room temperature.

## 2.8. Assessment of SDF-1 $\alpha$ bioactivity

SDF-1 $\alpha$  bioactivity was assessed using an agarose drop migration assay [41]. Initially, constitutively CXCR4-expressing U87-MG cells, as produced by S h edic and colleagues [42], were seeded into a 24-well flat-bottomed culture plate (Nunc, Strasbourg, France) at a density of  $1 \times 10^5$  cells per well and incubated with Dulbecco's Modified Eagle's (DME) medium supplemented with 10% fetal bovine serum (FBS) and 1% penicillin/streptomycin. To enhance cell adhesion, each well was previously treated with 500  $\mu$ L of 10  $\mu$ g/mL poly-D-lysine hydrobromide (Sigma-Aldrich) solution for 15 minutes and subsequently washed with 1x PBS three times. After 72 hours of incubation, the medium was replaced with deionized water to lyse the cells. The wells were washed with 1x PBS after 20 minutes and the thin cell-derived matrices coating the well surfaces were left to air-dry under laminar flow. Next, 2  $\mu$ L of 1% (w/v) solution of low gelling point agarose containing  $1 \times 10^5$  CXCR4-expressing U87-MG cells was deposited onto the center of each well and the plate was kept at 4  $^\circ$ C for 15 minutes for the gelation step. Then, the cell-loaded agarose drop was covered with 400  $\mu$ L of DME medium (FBS-free, 1% penicillin/streptomycin) with or without 40 ng/mL SDF-1 $\alpha$ . After 72 hours of incubation, the plan view of each well was captured using an optical microscope and a built-in camera (AxioCam® ICm 1, Zeiss, Jena, Germany). The cell migration distance was estimated by measuring the distance between the edge of the drop and the cell front on four distinct sides of the drop using the ImageJ software. The measurements were subsequently averaged to obtain a representative migration distance in each well. Three drops were assayed

for each medium condition in each experiment. All incubations were done at 37 °C and 5% CO<sub>2</sub>.

## **2.9. *In vitro* cytocompatibility and cell adhesion assays**

To exclude any potential proliferative effect of the protein load that may reduce the reliability of the study results, only the nanofibrous scaffold loaded with blank nanoparticles and unloaded nanofibrous scaffold were evaluated in these assays. The nanofibrous scaffolds were cut into circular pieces of 10 mm in diameter and approximately 0.6 mg in mass to promote ease of handling. All incubations were done at 37 °C and 5% CO<sub>2</sub> and the medium used was always supplemented with 10% FBS and 1% penicillin/streptomycin.

### **2.9.1. *In vitro* cytocompatibility assay**

The *in vitro* cytocompatibility of the nanofibrous scaffolds was assessed using the “scaffold extract” method adapted from Wang and colleagues [43]. Five scaffold pieces were placed in a well of a 24-well flat-bottomed culture plate (Nunc) containing 400 µL of DME medium and incubated for 24 hours to produce the scaffold extract. Simultaneously, NIH3T3 cells (CRL-1658™, ATCC, Rockville, Maryland, USA) were seeded in a 96-well flat-bottomed culture plate (Nunc) at a density of 5500 cells/well in 100 µL of DME medium and incubated for 24 hours. Then, the medium on the cells was replaced with 100 µL of the scaffold extract and the cells were incubated for another 24 hours. As a positive control, 100 µL of fresh medium was used in place of the scaffold extract. 10 µL of WST-1 reagent (Sigma-Aldrich) was subsequently added into each well. After 2 hours of incubation, the number of viable cells was estimated from the absorbance of the cleaved product of the tetrazolium salts in the WST-1 reagent, called formazan, which was measured at 450 nm using a ClarioStar® microplate reader (BMG Labtech GmbH, Ortenberg, Germany). To estimate the background absorbance, the WST-1 reagent was also added to wells containing either the scaffold extract or fresh medium alone without any cells. All background-corrected absorbance values were normalized to those of the positive control.

### **2.9.2. *In vitro* cell adhesion assay**

The cell adhesion capacity of the nanofibrous scaffolds was studied using U87-MG cells (HTB-14™, ATCC). Initially, 25 µL of DME medium containing 10,000 cells was deposited on top of a scaffold piece placed in a well of a 48-well flat-bottomed culture plate (Nunc). As a positive control, the same number of cells was added to a well without any scaffold. After 1

hour of incubation, another 275  $\mu\text{L}$  of medium was added into the wells and the plate was incubated for another 3 hours to allow the cells to adhere to the scaffold or well surfaces. Then, the wells were washed with 1x PBS three times to remove any loosely-attached cells. After another 24 hours of incubation in 300  $\mu\text{L}$  of fresh medium, the cell viability on the scaffold was evaluated using WST-1 reagent as described in Section 2.9.1. To ensure that the cells that reacted with the WST-1 reagent were those that were attached to the scaffolds and not of any colonies that formed on the well surface underneath, the scaffolds were transferred into new wells containing 300  $\mu\text{L}$  of fresh medium before adding 30  $\mu\text{L}$  of WST-1 reagent. To determine the background absorbance, the reagent was also added to cell-free wells containing DME medium with or without a scaffold piece. For the absorbance measurement, 100  $\mu\text{L}$  of medium was transferred from each well to a 96-well plate 2 hours after the addition of WST-1 reagent.

### 2.10. Statistical analysis

All data were expressed as the mean  $\pm$  standard deviation of at least three experiments ( $n \geq 3$ ). When applicable, one-way ANOVA with Dunnett's post-hoc test with a significance level of 0.05 was employed to detect any statistically significant difference existing between multiple data groups. In the figures, \* indicates  $P \leq 0.05$ , \*\* indicates  $P \leq 0.01$ , \*\*\* indicates  $P \leq 0.001$  and \*\*\*\* indicates  $P \leq 0.0001$ .

## 3. Results

### 3.1. Characterization of protein-loaded nanoparticles

Nanoparticles were produced from PLGA and PEG-PLGA co-polymer using a phase separation process to encapsulate the protein of interest. The synthesized nanoparticles were mostly spherical (Figure 2) and uniform in size, as indicated by the low PDI values of the nanoparticle formulations (Table 1), regardless of the type of protein encapsulated. The slightly negative zeta-potential values can be explained by the presence of the hydrophilic PEG layer on the surface of the nanoparticles that shields the negatively-charged carboxyl groups carried by the hydrophobic PLGA forming the nanoparticle core. The nanoparticles were also highly-efficient in encapsulating lysozyme and SDF-1 $\alpha$ .

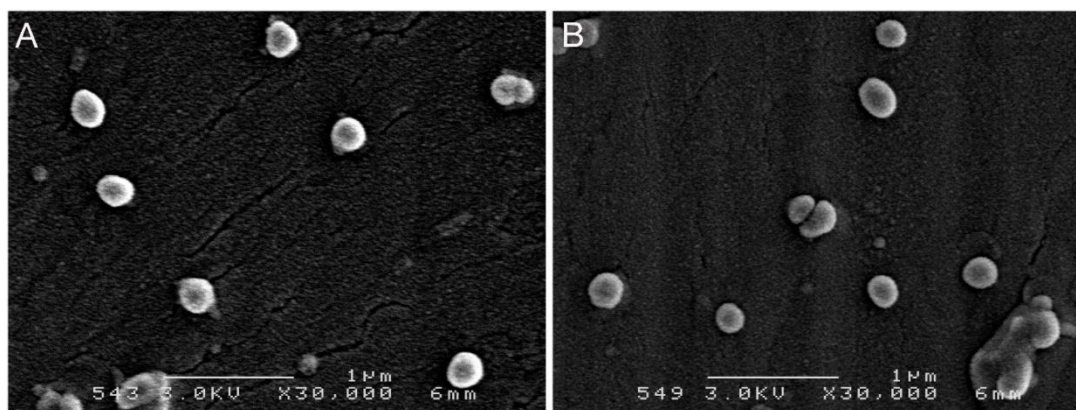


**Figure 2:** Scanning electron microscopy of (A) lysozyme-loaded and (B) SDF-1 $\alpha$ -loaded nanoparticles.

**Table 1:** Average size, polydispersity index (PDI), zeta-potential (ZP) and encapsulation efficiencies of lysozyme-loaded and SDF-1 $\alpha$ -loaded nanoparticle formulations.

Encapsulated protein	Average size (nm) <sup>a</sup>	Average PDI <sup>a</sup>	Average ZP (mV) <sup>b</sup>	Encapsulation efficiency (%)
Lysozyme	244 $\pm$ 11	0.14 $\pm$ 0.01	- 4.1 $\pm$ 0.7	96 $\pm$ 5
SDF-1 $\alpha$	238 $\pm$ 8	0.12 $\pm$ 0.01	- 3.5 $\pm$ 0.6	87 $\pm$ 5

<sup>a</sup> Purified nanoparticle dispersion was diluted to 100  $\mu$ g/mL in deionized water prior to measurement

<sup>b</sup> Purified nanoparticle dispersion was diluted to 100  $\mu$ g/mL in 0.01 M NaCl solution and the pH was adjusted to pH 7 prior to measurement

## 3.2. Characterization of nanoparticle-containing nanofibrous scaffolds

### 3.2.1. Co-electrospinnability of chitosan and protein-loaded nanoparticles

The electrospinning process produced flat scaffolds of approximately 40  $\mu$ m thick after 165 minutes (Figure 3A). The presence of nanoparticles in the scaffolds was initially confirmed using ATR-FTIR spectroscopy. ATR-FTIR spectra of scaffolds loaded with different concentration of nanoparticles revealed the presence of a peak at 1758  $\text{cm}^{-1}$  (Figure 3B), which is characteristic of the ester bonds present in the PLGA component of the nanoparticle. In addition, as the nanoparticle load in the scaffolds was increased, the height of this peak increased proportionately.

To gain an insight into the effect of different nanoparticle loads on the morphology of the electrospun nanofibers, SEM and TEM images of the scaffolds were recorded. SEM images revealed the presence of the nanoparticles within the nanofibers as “bulges” that were visible along their lengths (Figure 3C), and these features became increasingly apparent as the nanoparticle load was increased from 4.0 to 14.2% w/w. Further observation using TEM confirmed the presence of spherical nanoparticles within these “bulges” (Figure 3D).

Interestingly, at the highest nanoparticle load tested (14.2% w/w), the nanofibers were found to be thinner (Table 2) and cut at random points. Therefore, the maximum load of protein-loaded nanoparticles in the nanofibrous scaffolds for further experiments was limited to 7.6% (w/w) (10 mg nanoparticles per 121 mg chitosan-PEO mixture) to preserve good co-electrospinnability.

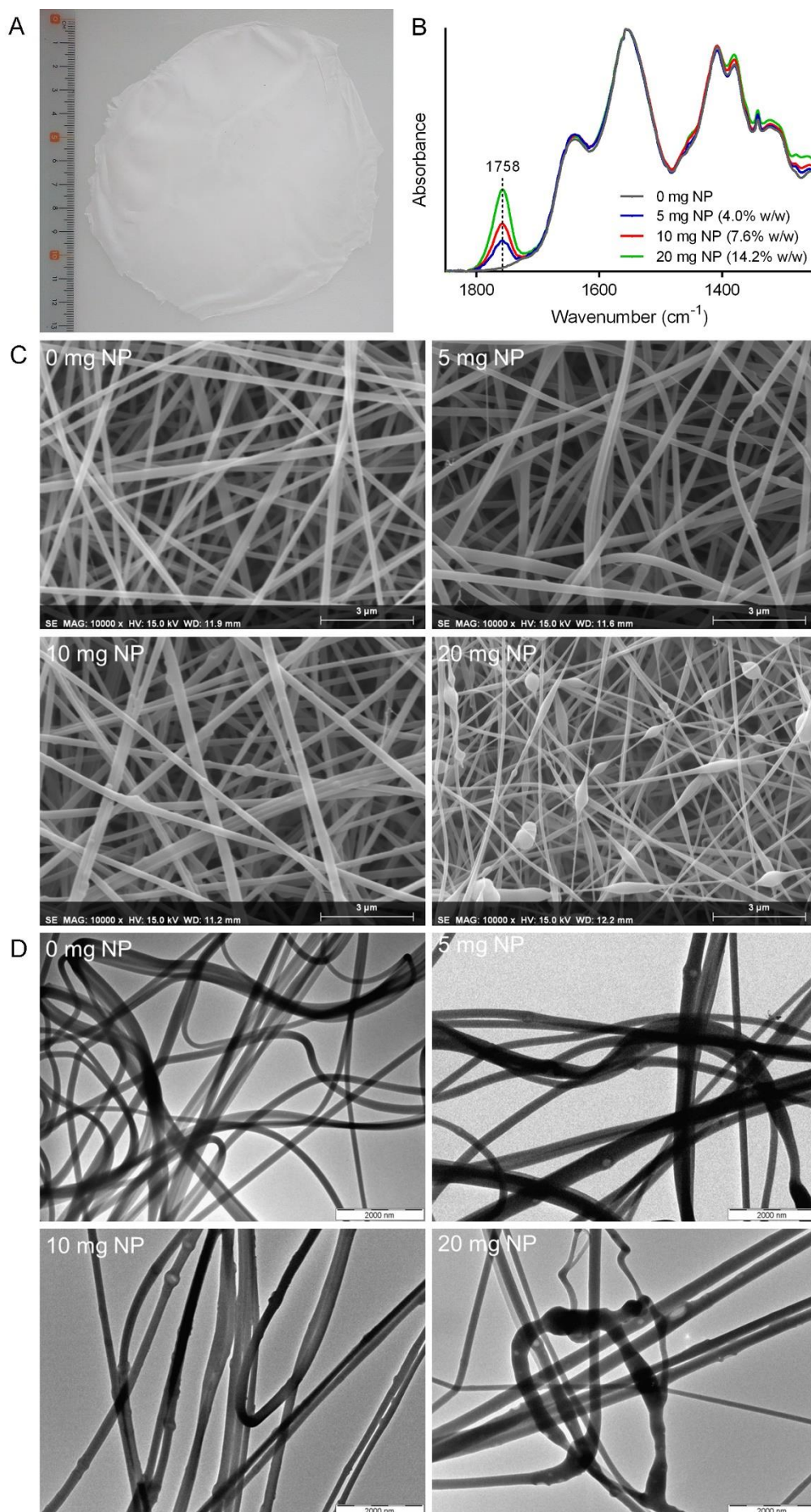


**Figure 3:** (A) An example of nanofibrous scaffolds produced from the electrospinning process. The scale placed on the left displayed length in centimeters. (B) ATR-FTIR spectra of nanofibrous scaffolds with different nanoparticle loads. For each spectrum, the absorbance values were normalized to their corresponding highest absorbance value, which was recorded at  $1557\text{ cm}^{-1}$ , to permit height comparison of the peak at  $1758\text{ cm}^{-1}$ . (C) Scanning and (D) transmission electron microscopy of nanofibrous scaffolds with different nanoparticle loads.

**Table 2:** Fiber diameter of nanofibrous scaffolds with different nanoparticle loads.

Nanoparticle load	Fiber diameter before stabilization (nm) <sup>a</sup>	Fiber diameter after stabilization (nm) <sup>a</sup>
0 mg	$249 \pm 49$	$263 \pm 42$
5 mg (4.0% w/w)	$244 \pm 52$	-
10 mg (7.6% w/w)	$251 \pm 46$	$261 \pm 45$
20 mg (14.0% w/w)	$150 \pm 43$	-

<sup>a</sup> Only the parts of the nanofibers that were free of the “bulges” were measured

### 3.2.2. Effect of electrospinning on the biological activity of protein molecules

Using the turbidity reduction assay,  $93 \pm 6\%$  of the lysozyme molecules extracted from the nanofibrous scaffold containing lysozyme-loaded nanoparticles remained biologically active. This fraction decreased to  $58 \pm 4\%$  when the lysozyme molecules were directly mixed with chitosan prior to electrospinning, highlighting the importance of lysozyme encapsulation into the nanoparticles on the preservation of its bioactivity. It was also confirmed that the denaturation of the unencapsulated lysozyme molecules occurred mainly during the electrospinning process and not during their extraction from the nanofibrous scaffold, as there was negligible loss in their biological activity after successive incubations in 1 M acetic acid solution, which was used to dissolve the chitosan/PEO nanofibers, and 1 M NaOH solution, which was the solvent for the PLGA/PEG-PLGA nanoparticles.

To investigate whether SDF-1 $\alpha$  was also susceptible to electrospinning-induced denaturation, nanofibrous scaffolds containing either unencapsulated SDF-1 $\alpha$  molecules or SDF-1 $\alpha$ -loaded nanoparticles were prepared. Using ELISA, there was no difference in the % recovery of SDF-1 $\alpha$  from both types of scaffolds ( $94 \pm 5\%$  and  $92 \pm 4\%$  from scaffolds loaded with unencapsulated SDF-1 $\alpha$  molecules and those containing SDF-1 $\alpha$ -loaded nanoparticles respectively). When the biological activity of the recovered SDF-1 $\alpha$  molecules were assessed using the agarose drop migration assay, the distance of migration of CXCR4-expressing U87-MG cells induced by the SDF-1 $\alpha$  molecules that was electrospun unencapsulated was similar

to that induced by their encapsulated counterpart (Figure 5C), suggesting that SDF-1 $\alpha$  was more resistant to electrospinning-induced denaturation than lysozyme.

### 3.2.3. Stabilization of nanoparticle-containing nanofibrous scaffolds

The changes in the composition of the nanoparticle-containing nanofibrous scaffolds after the stabilization step were investigated using ATR-FTIR spectroscopy (Figure 4A). The procedure successfully deprotonated the chitosan amino groups as evidenced by the appearance of a peak at 1592  $\text{cm}^{-1}$ , which correlated to the N-H stretching of the  $\text{NH}_2$  groups. The neutralization of the chitosan amino groups was accompanied by the disappearance of the peaks at 1557 and 1406  $\text{cm}^{-1}$  originating from the asymmetric and symmetric stretching of the carboxylate component of acetate ions. In addition, the neutralization procedure increased the visibility of several chitosan characteristic peaks that were partially masked by the presence of the acetate ions. These include the trio of peaks at 1420, 1377 and 1322  $\text{cm}^{-1}$  that represented  $\text{CH}_2$  bending,  $\text{CH}_3$  deformation and  $\text{CH}$  bending/ $\text{CH}_2$  wagging respectively [44,45]. However, the peak at 1758  $\text{cm}^{-1}$  that is characteristic of an ester bond as mentioned earlier remained visible after the stabilization procedure, suggesting that the PLGA/PEG-PLGA nanoparticles were not significantly degraded by the 0.1 M NaOH neutralizing solution.

Using SEM, some degree of swelling can be observed in the stabilized nanofibers. However, the scaffold retained its overall nanofibrous morphology (Figure 4B).

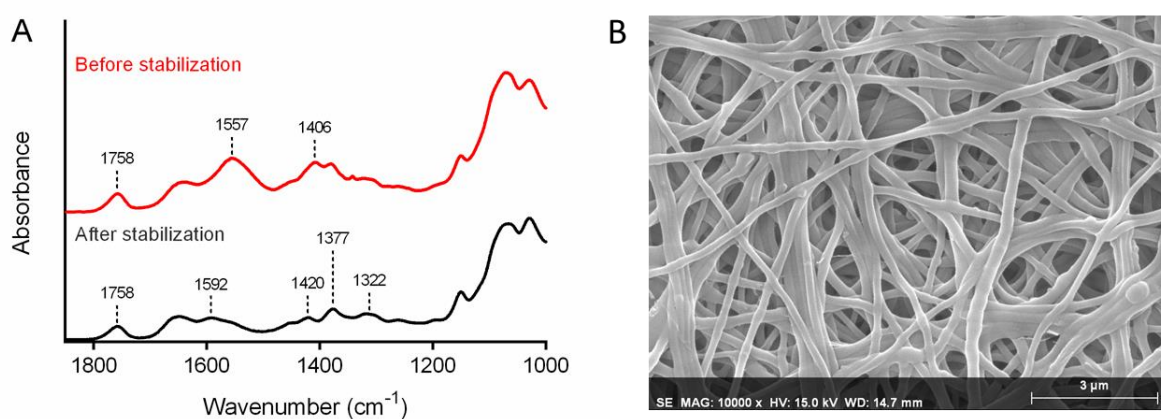


**Figure 4:** (A) ATR-FTIR spectra of a nanofibrous scaffold containing 10 mg NP load (7.6% w/w) before and after stabilization. (B) Scanning electron microscopy of the stabilized nanoparticle-containing nanofibrous scaffold.

## 3.3. *In vitro* protein release study

### 3.3.1. *In vitro* lysozyme release

The release of lysozyme from (i) the lysozyme-loaded nanoparticles, (ii) the nanofibrous scaffold loaded with unencapsulated lysozyme molecules and (iii) the lysozyme-loaded nanoparticles incorporated into a nanofibrous scaffold is shown in Figure 5A. Consistent with our previous finding, a steep initial release curve that plateaued after 3 days was obtained in the first case. A similar release profile was also observed in the second case, indicating that a direct dispersion of lysozyme molecules within the nanofibrous scaffold did not prevent the huge initial burst release. After 6 hours, 39% of the bioactive unencapsulated lysozyme load was released. Then, the release tailed off drastically between 6 and 120 hours and became negligible thereafter. Interestingly, in the third case, a more sustained release profile was observed. The scaffold loaded with lysozyme-loaded nanoparticles released only 11% of its bioactive lysozyme load after 6 hours. This was followed by gradual release that persisted up to day 35.

### 3.3.2. *In vitro* SDF-1 $\alpha$ release

SDF-1 $\alpha$  release profiles were similar to those observed with lysozyme, with the nanofibrous scaffold containing SDF-1 $\alpha$ -loaded nanoparticles providing sustained release up to day 35 (Figure 5B).

The bioactivity of the SDF-1 $\alpha$  molecules released from the nanofibrous scaffolds was assessed using the agarose drop migration assay. Release samples on day 4 from the nanofibrous scaffold loaded with unencapsulated SDF-1 $\alpha$  molecules and day 20 from the nanofibrous scaffold containing SDF-1 $\alpha$ -loaded nanoparticles were tested. These time points were chosen because the decrease in release rate and the periodic refreshment of the release medium caused the amount of SDF-1 $\alpha$  collected after these time points to be insufficient to achieve the optimal working concentration for the migration assay. SDF-1 $\alpha$  molecules released from both scaffolds induced similar distances of CXCR4-expressing U87-MG cell migration compared to their pristine counterpart (Figure 5C), suggesting that their biological activity was retained during the release process regardless of whether they were encapsulated into nanoparticles or not.

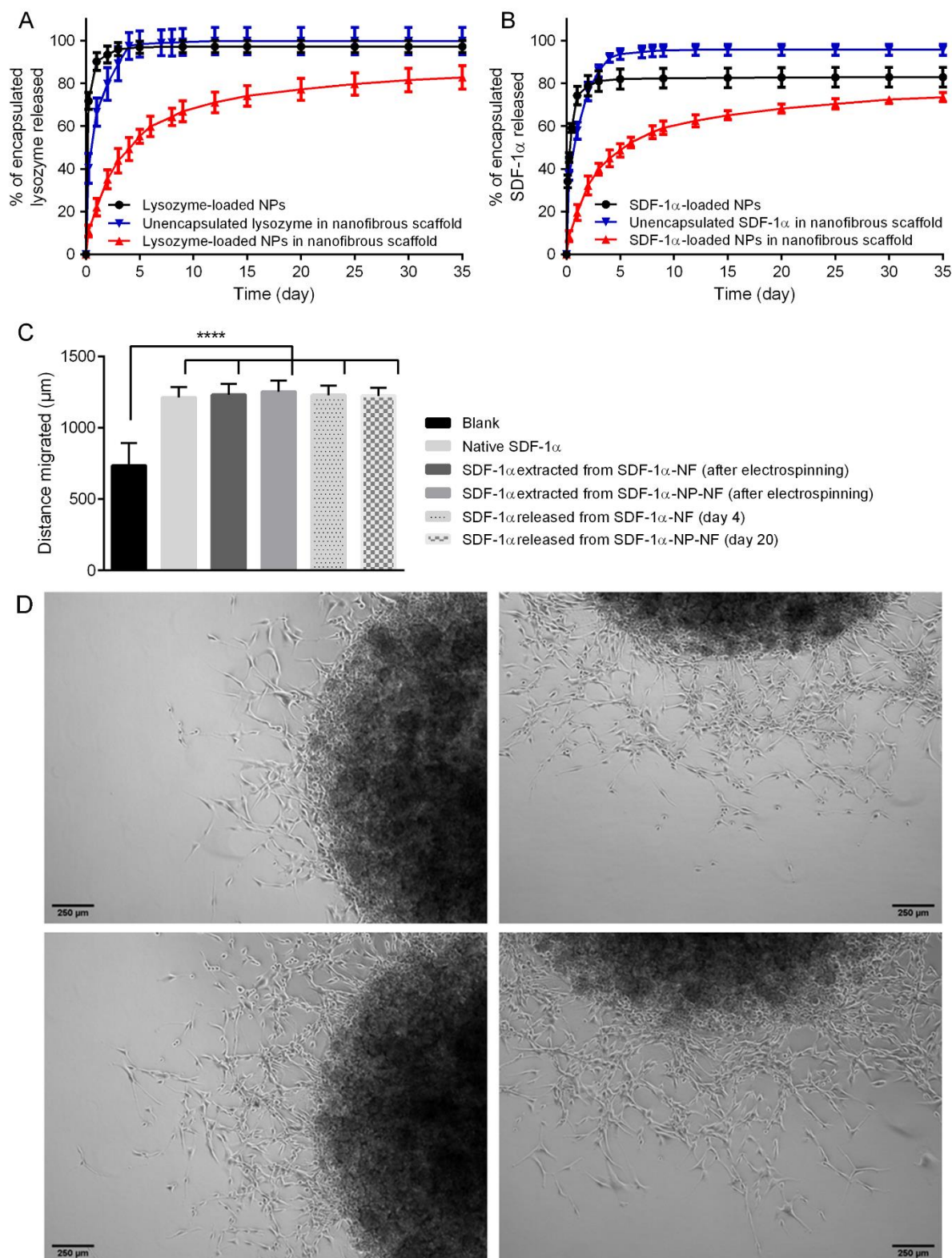


**Figure 5:** (A) Cumulative release of lysozyme with respect to the amount of bioactive lysozyme retrievable from each sample (as quantified using the turbidity reduction assay). (B) Cumulative release of SDF-1 $\alpha$  with respect to the amount of SDF-1 $\alpha$  retrievable from each sample (as quantified using ELISA). (C) The distance of migration of CXCR4-expressing U87-MG cells induced by the SDF-1 $\alpha$ -free medium (Blank), and medium supplemented with 40 ng/mL SDF-1 $\alpha$  (native SDF-1 $\alpha$  or those extracted after electrospinning/released from

nanofibrous scaffolds carrying either unencapsulated SDF-1 $\alpha$  molecules (SDF-1 $\alpha$ -NF) or SDF-1 $\alpha$ -loaded nanoparticles (SDF-1 $\alpha$ -NP-NF). Statistical analysis was conducted to detect any significant difference ( $P \leq 0.05$ ) between the multiple data groups. \*\*\*\* indicates  $P \leq 0.0001$ . (D) Representative images of CXCR4-expressing U87-MG cell-loaded agarose drops after 72-hour incubation with SDF-1 $\alpha$ -free medium (top left) or medium containing 40 ng/mL native SDF-1 $\alpha$  (top right) or SDF-1 $\alpha$  extracted after electrospinning (bottom left)/released (bottom right) from the nanofibrous scaffold containing SDF-1 $\alpha$ -loaded nanoparticles.

### 3.4. Scaffold degradation study

The degradation of the nanofibrous scaffolds was assessed by monitoring the loss of scaffold mass throughout their incubation in a buffer solution supplemented with chitosan-degrading lysozyme. The degradation profiles were similar regardless of whether the scaffolds were loaded with blank nanoparticles or not. Despite losing over 10% of their original mass after 5 weeks of incubation (Figure 6A), the scaffolds retained their nanofibrous structure as observed under SEM (Figure 6B).

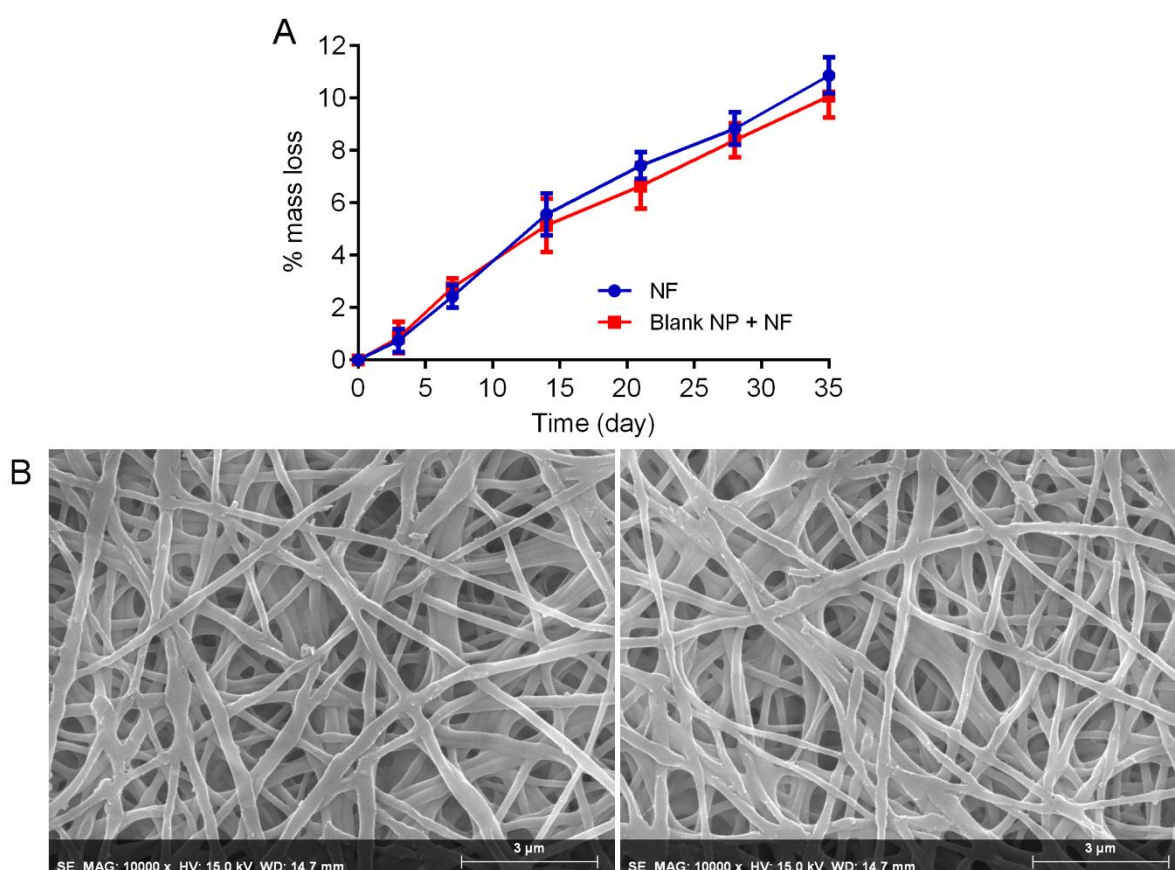


**Figure 6:** (A) Percentage of original scaffold mass degraded with time of incubation in 0.05 M Tris-HCl buffer solution (pH 7.4) supplemented with 20  $\mu$ g/mL lysozyme for the unloaded nanofibrous scaffolds (NF) and those loaded with 10 mg blank NP (Blank NP + NF). (B) SEM images of the unloaded nanofibrous scaffold (left) and the one loaded with 10 mg blank NP (right) after 5 weeks of incubation.

### 3.5. *In vitro* cytocompatibility and cell adhesion study

After a 24-hour treatment with medium pre-incubated with nanofibrous scaffolds loaded with blank nanoparticles or not, no cytotoxicity was observed (Figure 7A), indicating that the leachables from both scaffold types were well-tolerated by the NIH3T3 cells. In addition to their excellent cytocompatibility, the scaffolds were also capable of retaining U87-MG cells cultured on them. Although there were fewer cells on the scaffolds compared to the number of cells adhered to the cell culture plate surface after the same adhesion time (Figure 7B), U87-MG cells could spread well on the scaffold surface by extending their pseudopodia to maximize cell-scaffold interactions (Figure 7C,D).

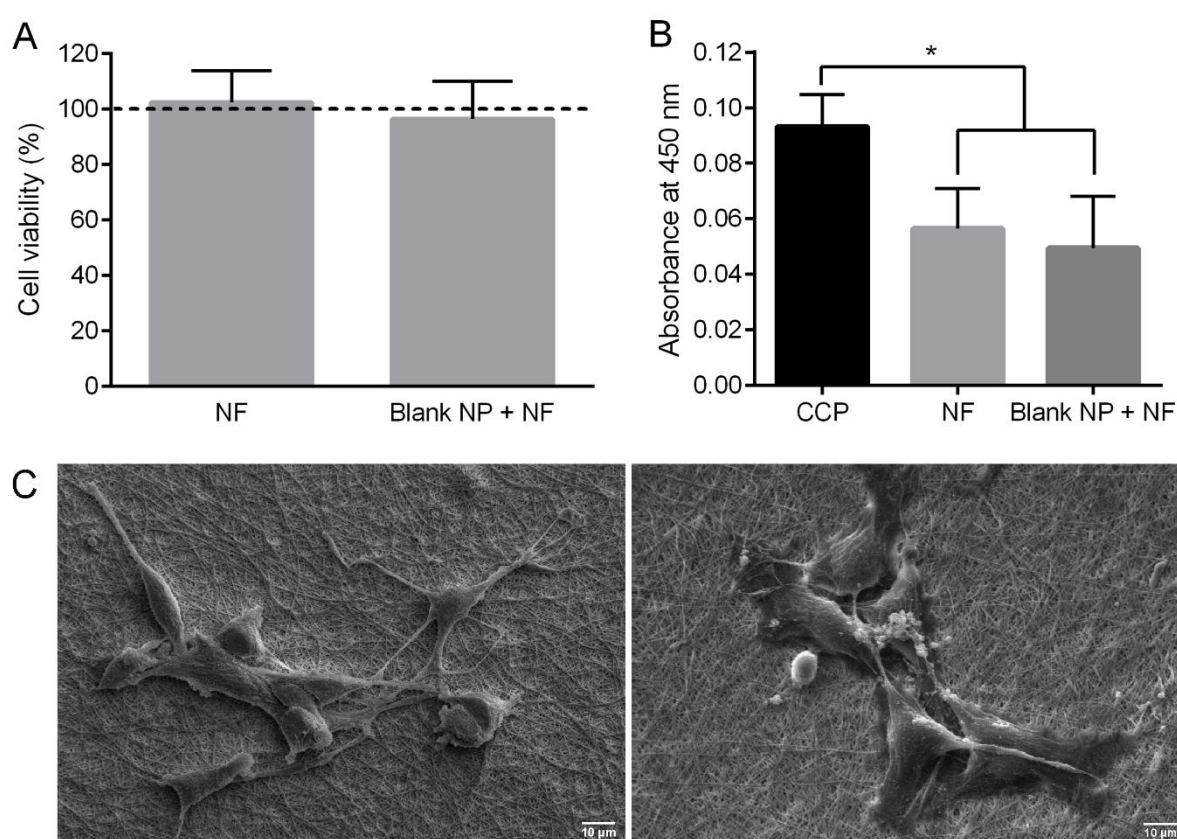


**Figure 7:** (A) % viability of NIH3T3 cells treated with medium pre-incubated with either unloaded nanofibrous scaffolds (NF) or those loaded with 10 mg blank NP (Blank NP + NF) normalized to the viability of cells treated with fresh medium (control). (B) Absorbance at 450 nm proportional to the number of U87-MG cells attached to the surface of cell culture plate (CCP), NF and Blank NP + NF. Statistical analysis was conducted to detect any significant difference ( $P \leq 0.05$ ) between the multiple data groups. \* indicates  $P \leq 0.05$ . (C) SEM images showing the morphology of U87-MG cells attached to the surface of NF (left) and Blank NP + NF (right).

## 4. Discussion

Chemokines such as SDF-1 $\alpha$  can mobilize cancer cells from their respective primary tumor locations towards proximal or distant colonizable sites by making them migrate up the chemokine concentration gradient. The implantation of SDF-1 $\alpha$ -secreting scaffolds therefore opens up the possibility of trapping these cells for subsequent selective killing procedures. This approach is highly relevant for treating cancers capable of metastasis, as the SDF-1 $\alpha$ -secreting scaffolds can divert the cancer cells away from their conventional metastatic niches and disrupt the natural cancer progression. More importantly, for cancers with high rates of local relapse due to an incomplete primary tumor removal such as glioblastoma, the trapping strategy can be used to eradicate the residual cancer cells and therefore prevent tumor recurrence. Recently, it was reported that a chemoattractant-loaded membrane could attract glioblastoma cells *in vitro*, despite the presence of several limitations that might have impaired the trapping capacity of the device, including short duration of chemoattractant release [61]. In this work, we developed scaffolds capable of providing sustained release of SDF-1 $\alpha$  in its bioactive form with excellent cytocompatibility and capacity to interact with human glioblastoma cells, which are intended for future implantation into the tumor resection cavity in the brain.

To achieve sustained SDF-1 $\alpha$  release, the chemokine was encapsulated into biodegradable PLGA/PEG-PLGA nanoparticles, which were subsequently incorporated into nanofibrous scaffolds by electrospinning. Regarding the first step, the use of an amphiphilic co-polymer and the straightforward phase separation technique in this study yielded particles of mostly uniform shape and size that favor their incorporation into nanofibrous scaffolds. For the subsequent electrospinning process, chitosan was the material of choice for making the nanofibrous scaffolds due to its unique physicochemical properties. Up to a nanoparticle load of 10 mg (7.6% (w/w)), uniform chitosan nanofibers can be obtained in the presence of PEO at a concentration of approximately 8.8% of the total PEO/chitosan mass in the electrospinning mixture. The requirement for such a low concentration of the biologically-inert PEO ensures that the electrospun scaffolds were predominantly characterized by the useful biological properties of chitosan, including excellent cancer cell adhesion [46] and slow biodegradation [47], which was subsequently proven in our *in vitro* studies. However, when the nanoparticle load was increased to 20 mg, beaded nanofibers of smaller diameter were produced. It was likely that the large number of negatively-charged nanoparticles interacting with the positively-charged chitosan molecules reduced the hydrogen bond interactions and chain entanglement between the chitosan and PEO molecules, leading to the formation of thin fibers with beaded morphology as reported in the literature [33]. Despite this, we have shown that our

electrospinning setup can ensure uniform incorporation of up to 10 mg of nanoparticles into a nanofibrous scaffold made of 110 mg of chitosan and 11 mg of PEO that is likely to be critical for sustained SDF-1 $\alpha$  release. As long as this nanoparticle loading limit is not exceeded, the developed method can also produce uniform nanofibers capable of providing a robust anchoring platform that is suitable for the adhesion of glioblastoma cells.

As described earlier, the electrospinning step involves the use of high voltage to generate nanofibers. A strong electric field is needed to induce repulsions between the charged components in a polymer solution to overcome the surface tension of the liquid that is necessary for the Taylor cone formation and subsequent fiber deposition on the collector plate [48]. This harsh processing condition presents a significant barrier to the incorporation of protein molecules into electrospun scaffolds. Using lysozyme as a model protein, we have shown that high voltage can denature more than 40% of the protein molecules that were electrospun directly without any prior encapsulation step. In contrast, the electrospinning process inflicted negligible loss of biological activity on lysozyme molecules that were pre-encapsulated into nanoparticles. The protective effect of protein encapsulation may be explained by the immobilization of the protein molecules within the polymer matrix of the nanoparticles. In an electric field, dipole moments arising from individual domains within a protein molecule will be forced to align themselves along the applied field [49–51]. The movement of the polarized domains can alter the overall protein structure that may result in a loss of biological activity [52–54], particularly for enzymes such as lysozyme with a sensitive substrate binding site [55,56]. Differently, encapsulated lysozyme molecules have limited conformational mobility due to their steric and electrostatic interactions with the polymer constituents of the nanoparticle, preventing them from undergoing structural changes that can compromise their enzymatic activity. However, we also observed that SDF-1 $\alpha$  retained its biological activity after the electrospinning process regardless of whether it was encapsulated or not. Although it was not possible to accurately quantify the proportion of bioactive SDF-1 $\alpha$  due to the semi-quantitative nature of the agarose drop migration assay, it is probable that SDF-1 $\alpha$  is more resistant to electrospinning-induced denaturation than lysozyme. This could be due to the difference in the secondary structure of these two proteins. Based on the information from Protein Data Bank (PDB 1DPX; PDB 2KEE), lysozyme possesses seven helices as opposed to two of SDF-1 $\alpha$ . Helical domains are characterized by large net dipole moments due to their unidirectionally-aligned peptide dipoles [57,58], making them very reactive to an external electric field. In fact, lysozyme has been reported to unfold irreversibly upon exposure to an

electric field of a strength as low as  $300 \text{ V m}^{-1}$  [56]. Considering the much stronger electric field applied in this study, it is plausible that lysozyme unfolded more extensively than SDF-1 $\alpha$  when these proteins were electrospun unencapsulated.

After neutralizing the charged amino groups in the nanofibrous scaffolds to improve their stability in physiological media, we observed that scaffolds containing SDF-1 $\alpha$ -loaded nanoparticles can sustain the release of SDF-1 $\alpha$  for a longer duration than SDF-1 $\alpha$ -loaded nanoparticles alone and scaffolds containing unencapsulated SDF-1 $\alpha$  molecules. This may be explained by the two-stepped process involved in the release of SDF-1 $\alpha$  from the scaffolds containing SDF-1 $\alpha$ -loaded nanoparticles. SDF-1 $\alpha$  molecules would have to first diffuse out of the nanoparticles into the nanofibers before they could be released into the surrounding medium. The first stage of the diffusion process is likely to be rate-limiting as the positively-charged SDF-1 $\alpha$  molecules would have to overcome their electrostatic interactions with the negatively-charged carboxyl groups of PLGA in the nanoparticles [59]. These interactions can be disrupted by cations such as  $\text{Na}^+$  [60] that were present at a physiologically-relevant concentration in the release medium on the condition that they first have to diffuse through the nanofiber to make contact with the nanoparticles. Based on this assumption, it was not expected that SDF-1 $\alpha$  release could still be observed immediately after incubation in the release medium. A potential explanation for this observation is that some large nanoparticles that were not completely embedded in the nanofibers, as visualized under SEM and TEM, were releasing part of their SDF-1 $\alpha$  load immediately upon direct contact with the release medium. This stage of minimal burst release was then followed by the two-staged diffusion of SDF-1 $\alpha$  from the parts of the nanoparticles that were better embedded in the nanofibers as discussed above, contributing to gradual SDF-1 $\alpha$  release. In fact, the 5-week SDF-1 $\alpha$  release period observed in this work is likely to provide a longer time window for glioblastoma cell trapping compared to the 2-day protein release duration achieved with the chemoattractant-loadable membranes developed by Autier and colleagues for a similar purpose [61].

To study the degradation of the nanofibrous scaffolds, lysozyme was the enzyme of choice as chitosan is hydrolyzed *in vivo* mainly via the action of this enzyme [62]. However, despite the exposure to lysozyme at a concentration comparable to the cerebrospinal fluid lysozyme levels of  $1 - 14 \text{ }\mu\text{g/mL}$  [63,64], the nanofibrous scaffolds remained mostly intact at the end of the degradation study. The slow degradation rate can be explained by the high degree of deacetylation ( $\sim 80\%$ ) of the chitosan used to prepare the scaffolds. As lysozyme degrades chitosan by targeting its acetylated residues [65], the degradation rate generally decreases with

an increasing degree of chitosan deacetylation [66,67]. The high stability of the scaffolds will be beneficial for holding the SDF-1 $\alpha$ -loaded nanoparticles in place during the gradual SDF-1 $\alpha$  release process to permit the establishment of a local SDF-1 $\alpha$  concentration gradient that is necessary for the chemotactic attraction of glioblastoma cells. In addition, the scaffolds' nanofibrous feature was observed to be unaffected by their slow degradation rates. It has been well-reported that surface structure significantly influences the extent of cell adhesion, and scaffolds with three-dimensional nanofibrous topography retain cancer cells to a greater degree than two-dimensional flat films [68]. As such, the highly-robust nanofibrous structure suggests that our scaffolds can provide an excellent cell-anchoring platform to retain the attracted glioblastoma cells until the subsequent killing step. Despite this, there was minimal cell infiltration into the scaffolds due to the compact arrangement of the nanofibers. In the future, should it become necessary to increase cell infiltration into the scaffolds to improve their cell trapping capacity, post-electrospinning treatments such as ultrasonication may be used to loosen the dense fiber network and increase pore size [69]. Furthermore, slow-degrading chitosan scaffolds have also been reported to be more biocompatible than their fast-degrading counterparts due to the slower production of pro-inflammatory degradation products [70]. This property, coupled with the absence of cytotoxic leachables from the scaffolds observed in our cytocompatibility study, may help to diminish the risk of an unfavorable immune or toxicological response during the several weeks of implantation period that will be necessary for maximizing the trapping of glioblastoma cells.

## 5. Conclusion

This study reports on the development of chitosan-based nanofibrous scaffolds containing SDF-1 $\alpha$ -loaded PLGA-based nanoparticles to achieve sustained release of SDF-1 $\alpha$ . To the best of our knowledge, this is the first example of the use of such a composite polymer-based vehicle for local delivery of protein molecules. Thus, the usability of these scaffolds in delivering proteins of similar physicochemical characteristics to SDF-1 $\alpha$  should be explored. More importantly, as the scaffolds demonstrated excellent *in vitro* cytocompatibility and capacity to support the adhesion of glioblastoma cells, it is justifiable to proceed to the *in vivo* assessment of their safety profile. Ultimately, after the removal of the bulk tumor from the brain, the implantation of the scaffolds into the tumor resection cavity seems to hold great promise as an efficient cancer cell trap for the residual glioblastoma cells.

## Acknowledgement

Authors would like to thank R. Mallet and R. Perrot of the SCIAM (Common Service for Imaging and Microscopy Analysis, Angers, France) as well as V. Pitrebois and M. Dejeneffe of CERM for SEM and TEM analyses. This work was supported by the “Institut National de la Santé et de la Recherche Médicale” (INSERM), the University of Angers (Angers, France), the University of Liege (Liege, Belgium), MINECO [SAF2017-83118-R], Agencia Estatal de Investigación (AEI) Spain, and FEDER. It is also related to the regional program BILBO "Bioimplants for Bone Regeneration" funded by the consortium Bioregate, an Excellent Center in Regenerative Medicine, "NanoFar+ International Strategy Network in Nanomedicine" funded by La Région Pays-de-la-Loire, LabEx IRON “Innovative Radiopharmaceuticals in Oncology and Neurology” as part of the French government “Investissements d’Avenir” program, the INCa (Institut National du Cancer) MARENGO consortium “MicroRNA agonist and antagonist Nanomedicines for GliOblastoma treatment: from molecular programming to preclinical validation” through the PL-BIO 2014-2020 grant and the MuMoFRaT project “Multi-scale Modeling & simulation of the response to hypo-Fractionated Radiotherapy or repeated molecular radiation Therapies” supported by La Région Pays-de-la-Loire and the Cancéropôle Grand-Ouest (tumor targeting and radiotherapy network). Muhammad Haji Mansor and Mathie Najberg were Ph.D. students involved in the Erasmus Mundus Joint Doctorate program for Nanomedicine and Pharmaceutical Innovation (EMJD NanoFar) funded by the European Agency EACEA. Muhammad Haji Mansor received a doctoral fellowship from the University of Angers while Mathie Najberg received a fellowship from La Région Pays-de-la-Loire.

---

### 4.3.2. Unpublished results

In publication 2, the cytotoxicity of the nanofibrous scaffolds were assessed using the “scaffold extract” method. This approach assumes that cytotoxicity can arise only from the leachable elements of the scaffolds and does not address other mechanisms of cytotoxicity such as contact-induced cytotoxicity. Using this method alone may lead to an overestimation of the cytocompatibility of the scaffolds. Therefore, additional cytotoxicity assessments were conducted by incubating the scaffolds directly on top of cell monolayers to obtain more accurate cytocompatibility data. The direct incubation of the scaffolds with the cells was allowed for up to 72 hours, in contrast to the shorter 24-hour limit tested in publication 2. Furthermore, two additional cell lines in the form of Thp-1 macrophages and primary astrocytes were also assayed to assess the compatibility of the scaffolds with cells that are more

relevant to the physiology of the brain. Finally, in addition to the *in vitro* assessments, *in vivo* studies were also conducted by implanting the scaffolds into the brain of healthy rats to assess the potential toxicity/immunogenicity of the scaffolds as well as their tendency to degrade in the brain environment.

#### 4.3.2.1. Materials and methods

##### 4.3.2.1.a. *In vitro* cytocompatibility assay (direct contact)

Contact-induced cytotoxicity of the nanofibrous scaffolds was assessed using NIH3T3 mouse fibroblasts, human Thp-1 macrophages and rat primary astrocytes. Assays were conducted in 24-well cell culture plates (well diameter = 15.6 mm). All incubations were done at 37 °C and 5% CO<sub>2</sub> and DME medium supplemented with 10% FBS and 1% penicillin/streptomycin was used throughout the assay unless stated otherwise.

Cells were prepared accordingly prior to the 24 or 72-hour period of incubation with the scaffolds. NIH3T3 cells were seeded at a density of 40 x 10<sup>3</sup> and 10 x 10<sup>3</sup> cells/well for the 24 and 72-hour assay respectively and incubated in 500 µL medium 24 hours before use. To obtain Thp-1 macrophages, Thp-1 monocytes (TIB-202™, ATCC) were seeded at a density of 200 x 10<sup>3</sup> cells and 50 x 10<sup>3</sup> cells/well for the 24 and 72-hour assay respectively. The Thp-1 monocytes were incubated in 500 µL complete Roswell Park Memorial Institute (RPMI) 1640 medium (Sigma-Aldrich) supplemented with 80 nM phorbol 12-myristate 13-acetate (PMA) (Sigma-Aldrich) for 24 h to induce their differentiation into macrophages. Following this, the pMA-containing medium was replaced with fresh complete RPMI medium (without PMA) and the cells were incubated for another 24 hours before use. Pure cultures of newborn rat primary astrocytes were prepared from extracts of cerebral cortex using the mechanical dissociation method as originally described [71]. Brain extract was homogenized, lyophilized and reconstituted in cell culture medium before being added to the 24-well plate. The medium was refreshed twice weekly for two weeks to obtain highly-pure cultures of primary astrocytes.

Prior to incubation with the cells, the nanofibrous scaffolds were cut into circular pieces of 10 or 14 mm in diameter, which correlated to a 2-fold difference in surface areas (79 vs. 154 mm<sup>2</sup>). The scaffold pieces were washed with 1x PBS three times and incubated in the cell culture medium for 15 minutes before being deposited onto the cell monolayer prepared in the 24-well plate. Wells without scaffolds acted as control. After 24 or 72 hours of incubation, the medium in each well was replaced with 500 µL fresh medium containing 44 µM resazurin. To estimate the background fluorescence, the resazurin-containing medium was also added into three

empty wells of the assay plate (without any cells). The plate was incubated for another 2 h. Cell viability was estimated from the fluorescence intensity of the reduced product of resazurin, called resorufin, which was measured using a ClarioStar microplate fluorometer (BMG Labtech GmbH, Ortenberg, Germany) at 545 nm excitation and 600 nm emission. All background-corrected fluorescence intensity values were normalized to those obtained with the control wells.

#### **4.3.2.1.b. *In vivo* implantation of nanofibrous scaffolds into rat brain cortex**

Fischer female rats aged 8-10 weeks were obtained from Janvier Labs (Le Genest-Saint-Isle, France). The protocol was approved by the Ethical Committee for Animal Experimentation of Région Pays de la Loire (authorization number #2015.20). Animals were anesthetized by intraperitoneal injection of a mixture of ketamine (100 mg/kg) and xylazine (13 mg/kg) and positioned in a Kopf stereotaxic instrument. A 10 mm-long incision was made along the midline to create access to the surface of the skull. Following this, a burr hole was drilled into the skull using a high-speed drill to expose the brain tissues underneath. A portion of the brain cortex was then cut using a biopsy punch device and subsequently removed using vacuum suction to create a cavity that was approximately 3 mm wide and 2 mm deep. To facilitate the scaffold implantation process, the nanofibrous scaffolds (containing 10 mg blank nanoparticles) were rolled and cut into cylinders with a similar dimension as the cavity in the brain. In fact, the dimension of the cylinders was slightly different between the short-term and the long-term studies. For the short-term study, the cylinders were 2 mm wide and 2 mm tall. After observing that the scaffolds did not swell significantly upon implantation into the cavity, larger cylinders (3 mm wide and 2.5 mm tall) were used for the long-term study (Figure 4.1A). Following the implantation of the scaffold into the cavity (Figure 4.1B), the wound was sutured, and the rats were allowed to awaken without any further intervention. All rats became fully conscious and active between 1 and 2 hours after surgery and did not display any sign of distress. In control rats, the same surgical procedure was also performed, but no scaffold was implanted. Two groups of rats were set up non-concurrently: one group, consisted of 6 rats (3 implanted with scaffolds and 3 controls), was intended for the short-term study (sacrificed after 7 days) while the other group, consisted of 8 rats (4 implanted with scaffolds and 4 controls), was intended for the long-term follow-up (sacrificed after 100 days).



**Figure 4.1:** (A) The dimension of the scaffolds used in the short-term (left pair) and long-term (right pair) *in vivo* biocompatibility studies. (B) The left image shows the global view of the surgical setup for the opening of the skull of an anesthetized animal to enable scaffold implantation while the right image provides an enlarged view of the cavity (with the implanted scaffold).

#### 4.3.2.1.c. *In vivo* MRI

MRI analysis was performed on D1 and D7 for the short-term study and D7, D50 and D100 for the long-term study, with a Bruker Biospec 70/20 system operating at 7 T, under isoflurane (0.5% 1 L/min O<sub>2</sub>) anesthesia, with the monitoring of respiratory parameters. T2-weighted images were acquired with a multispin echo sequence [FOV = 35 x 35 mm, 7 axial 0.8 mm slices (gap = 0.3 mm), matrix 256 x 256, TR = 2 s, 25 TE = 8, 16, 24, . . .200 ms, one average]. The volume of the scaffolds was measured by manually drawing the region of interest on the generated T2 maps.

#### 4.3.2.1.d. Histological analysis

Histological analysis of the brain tissues was performed at one week and 100 days after implantation of the nanofibrous scaffolds. At each of these two time points, the rats implanted

with the scaffold as well as the control rats were sacrificed. The removed brains were fixed in formalin for 10 days. After that, the brains were cut into sections of 30  $\mu\text{m}$  thickness and stained with hematoxylin, phloxin and saffron.

#### 4.3.2.2. Results and Discussion

##### 4.3.2.2.a. *In vitro* cytocompatibility of nanofibrous scaffolds

Regardless of the surface area, both types of nanofibrous scaffolds (with and without blank nanoparticles) were not highly toxic on any of the three cell lines tested (Figure 4.2). This result was not surprising considering the well-reported biocompatibility of chitosan-based constructs [72–75]. At the 24-hour limit, the lowest % viability recorded was 80% and this value decreased to 68% at the 72-hour limit. These figures were recorded when the larger-sized (154  $\text{mm}^2$ ) nanoparticle-free scaffolds were put in contact with NIH3T3 fibroblasts, which are known to be highly sensitive to chemical induce-toxicities [76]. It is worth mentioning that among the three cell lines tested, the brain-resident primary astrocytes appeared to be the most resistant against any toxic effects of the scaffolds. This observation provides early evidence for the safe use of the nanofibrous scaffolds in the brain.

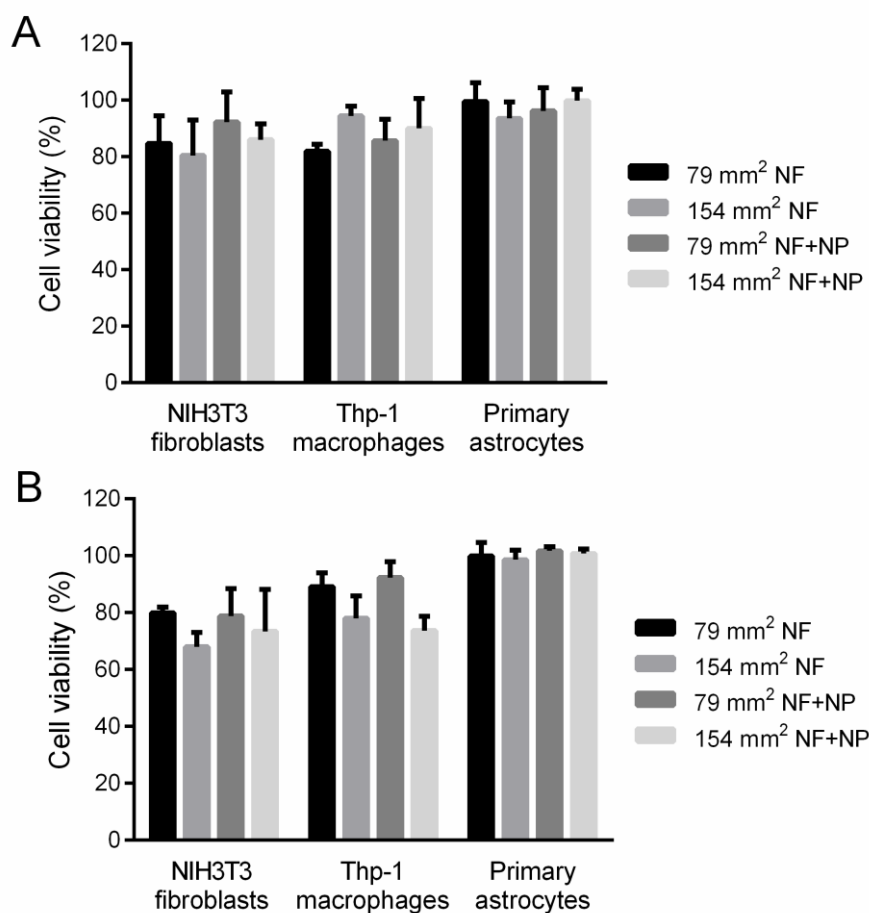


**Figure 4.2:** Effect of different size of unloaded nanofibrous scaffolds (NF) and those loaded with 10 mg blank NP (NF+NP) on the viability of NIH3T3 cells, Thp-1 macrophages and primary astrocytes after (A) 24-hour and (B) 72-hour incubation.

#### 4.3.2.2.b. *In vivo* degradation and biocompatibility of nanofibrous scaffolds

At the time of writing, only the results from the short-term *in vivo* study were available for analysis and discussion. The results for the long-term study will be presented upon the completion of the follow-up period.

By monitoring the changes in the scaffold volume using MRI (Figure 4.3), it can be inferred that the nanofibrous scaffolds did not suffer significant degradation during the 7-day implantation period. This observation is well in line with the slow degradation rate of the scaffolds seen previously *in vitro*. Based on these results, the scaffolds may support prolonged duration of GBM cell trapping by acting as a stable reservoir for gradual SDF-1 $\alpha$  release as well as by serving as a durable matrix to retain the recruited cells. The latter contribution is especially important as premature scaffold degradation may increase the risk of GBM cells



[80]. This explained why such a dense population of PMNs was seen at the implantation site as well as within the scaffolds (Figure 4.4). In the absence of an implanted scaffold, the extent of infiltration of PMNs into the resection cavity was much less (Figure 4.5). This suggests that it was the present of foreign materials that contributed to the strong immune response, not the tissue injuries inflicted by the surgical procedure. The main purpose of PMNs during early stages of inflammation is to clean up the implantation site [79]. In control rats, they rapidly phagocytosed the dead cells and debris at the surgical site and disappeared afterwards due to their short life-span [81]. However, in the implanted rats, PMNs were continuously being recruited to the site of implantation as they were unable to phagocytose the large foreign bodies [82]. Alongside PMNs, circulating monocytes can also infiltrate the site of inflammation as part of the innate immune response. As these group of cells leave the circulation and enter the tissues, they differentiate into macrophages [80]. Furthermore, lymphocytes can also be recruited during the course of an inflammatory cascade, marking the start of the adaptive immune response [78,82]. Both macrophages and lymphocytes were present in the histological samples prepared from both the implanted and control rats, especially at the border of the resection cavity where network of blood vessels from which these cells originate can be located.

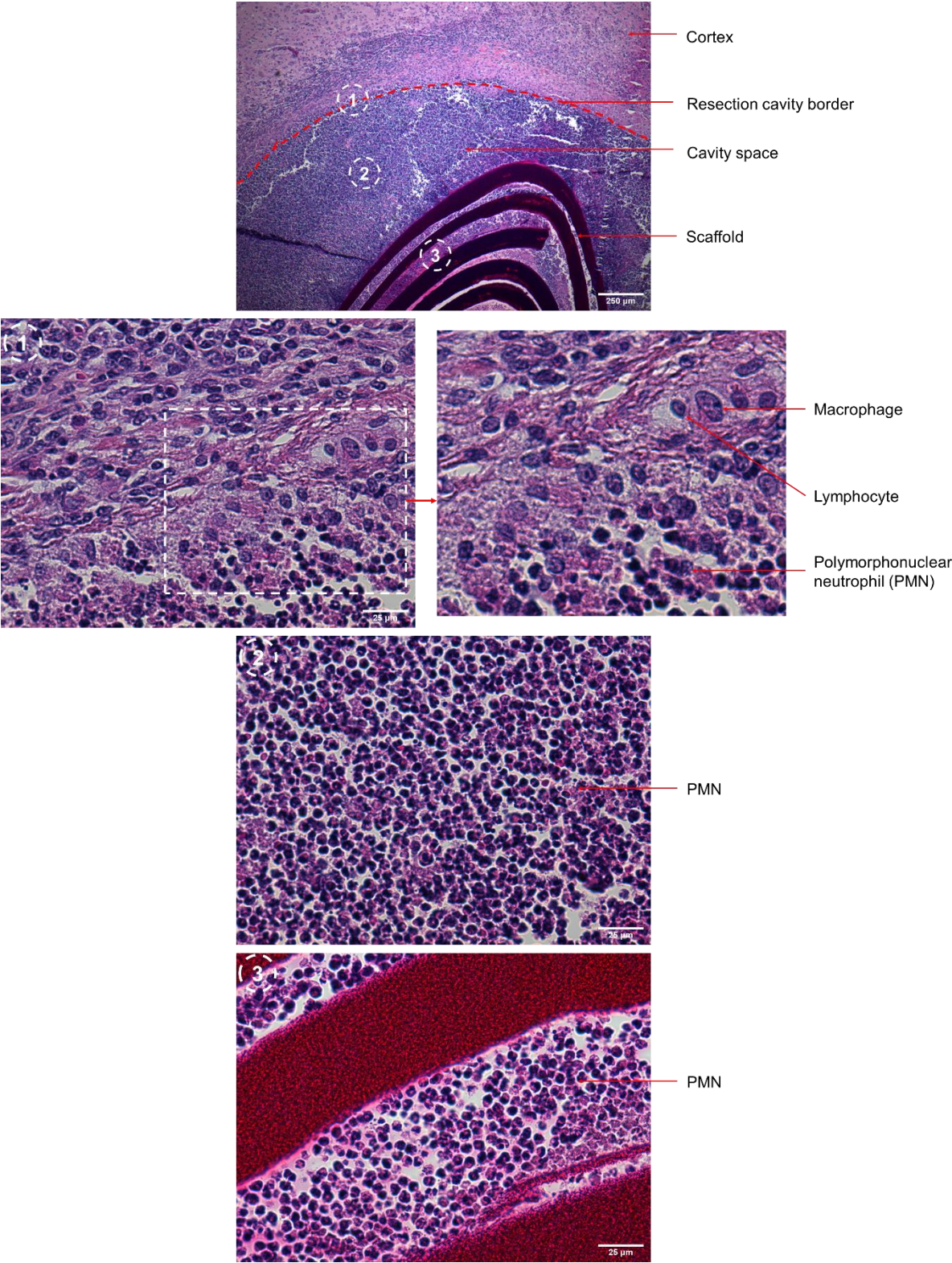


**Figure 4.4:** Histological sections of the brain of rats implanted with nanofibrous scaffolds. The top image provides a global overview of the scaffold implanted into the cavity created in the cortex. Lower images are magnifications of the region at the border of the resection cavity (1), the cavity space (2) and the inside of the implanted scaffold (3). Polymorphonuclear neutrophils (characterized by their multi-lobed, dark-stained nuclei) could be seen to

extensively infiltrate the cavity space as well as the implanted scaffold. Lymphocytes (round nuclei) and macrophages (characterized by their large size) were present near the cavity border.

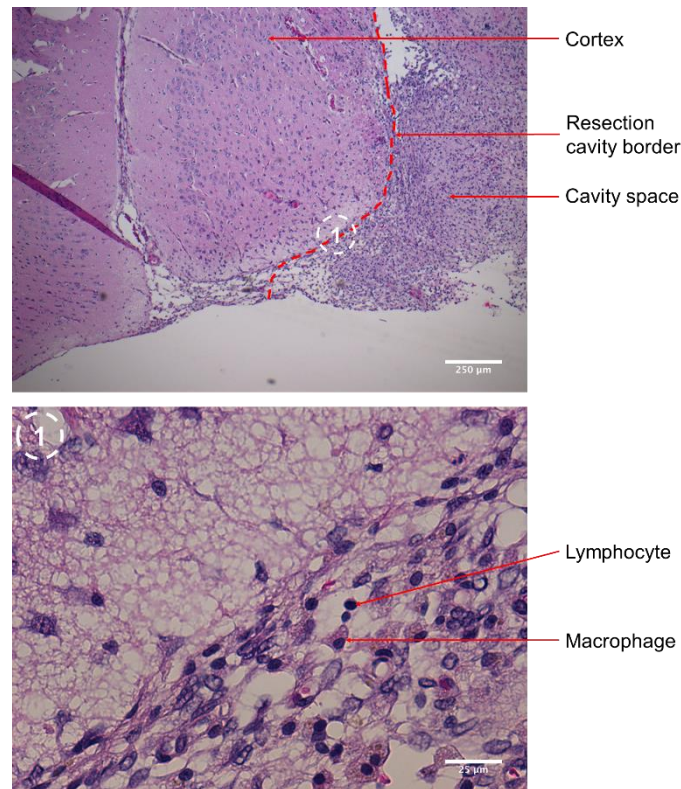


**Figure 4.5:** Histological sections of the brain of rats subjected to the surgical procedure without any scaffold implantation. The top image provides an overview of the resection cavity created in the cortex while the lower image is a magnification of the region at the border of the resection cavity.

Despite the strong immune response induced by the scaffolds, all implanted rats did not show any signs of deterioration during the 7-day study period. However, it is worth noting that the extensive infiltration of PMNs at the implantation site may hint for future recruitment and activation of fibroblasts, which are capable of depositing Type I and Type III collagen to facilitate tissue repair [80]. The presence of a slow-degrading implant at the site of injury may interfere with the repair process and induce excessive collagen secretion from the fibroblasts and immune cells such as the M1 macrophages [79]. This can then lead to formation of fibrotic tissues that encapsulate the entire implant [79,80]. Should this happen, cell infiltration into the implant will diminish, compromising the GBM cell trapping capacity of the scaffold. However, little can be concluded until the results from the long-term follow-up are made available.

#### 4.4. CONCLUSION OF CHAPTER 4

In this part of the study, SDF-1 $\alpha$ -loaded PLGA/PEG-PLGA nanoparticles were incorporated into chitosan nanofibers by electrospinning to obtain scaffolds that could provide sustained SDF-1 $\alpha$  release. Chitosan was used as the main constituent polymer in the preparation of the nanofibrous scaffolds for several reasons. First, it is readily soluble in mildly-acidic polar solvents such as dilute organic acid solutions. Using these solvents, the PLGA/PEG-PLGA nanoparticles could retain their integrity when dispersed in the chitosan solution prior to co-electrospinning. Solubilization of chitosan in acidic solvents is mediated by the protonation of the weakly-basic amino groups present in this polymer. The cationic property of solubilized chitosan can permit electrostatic interactions with the negatively-charged PLGA/PEG-PLGA nanoparticles to facilitate the production of nanoparticle-loaded nanofibers, further justifying the use of chitosan as a polymer for electrospinning in this work. More importantly, nanofibers made from chitosan can be turned water-stable using a simple deprotonation treatment without the use of any chemical cross-linker. The stabilized chitosan nanofibers, as shown in this work, degrade slowly to prolong the duration of SDF-1 $\alpha$  release and thus the time window for GBM cell trapping.

For a scaffold to function optimally as a GBM cell trap *in vivo*, it should support the adhesion of GBM cells that have been recruited by chemotaxis. We observed that U87-MG cells seeded on the chitosan-based scaffolds developed in this study could adhere well to the scaffolds' nanofibrous surface. The large surface area afforded by the fibrous topography is known to be useful for promoting cell-scaffold interactions. However, despite their excellent capacity in supporting cell attachment, cell infiltration into electrospun constructs have often been reported to be poor. This problem has been well-documented in tissue engineering and regenerative applications of electrospun scaffolds. The sub-micron pores and densely compacted fibers in these scaffolds can present significant barriers to cell infiltration, preventing the integration of the scaffold into host tissues post-implantation. The same issue may limit the GBM cell trapping capacity of electrospun scaffolds. Cell migration through a three-dimensional matrix is governed by the capacity of the cells to remodel the matrix as well as their deformability. Cancer cells often express high levels of matrix metalloproteinases (MMPs) to digest ECM components such as collagen and laminin to facilitate their invasion into surrounding healthy tissues. Considering that chitosan is not a native constituent of the ECM, it is unlikely that cancer cells such as those of GBM can enzymatically degrade chitosan-based scaffolds to infiltrate these constructs. On the other hand, the importance of matrix remodeling in the

migration of cancer cells becomes less significant when the pore size of the matrix exceeds  $7 \mu\text{m}^2$ . Cancer cells such as fibrosarcoma cells have been shown to be able to undergo deformation to migrate through these spaces [83]. As mentioned in publication 2, post-electrospinning treatments such as ultrasonication may help to loosen up the densely compacted fibers and thus increase the porosity of electrospun scaffolds. Gas foaming is another potentially useful treatment for this purpose. Electrospun scaffolds can be mechanically kneaded with particles of carbonate salts such as  $\text{NH}_4\text{HCO}_3$ . Subsequent treatment of the scaffolds with warm water generates  $\text{CO}_2$  gas that flushes through the scaffolds to increase their porosity [84]. The use of custom-made collectors has also been demonstrated to be useful in producing electrospun scaffolds with a lower degree of fiber packing. A hemispherical dish internally decorated with metal probes has been utilized to overcome the high fiber packing density issue associated with conventional flat collectors. The improved collector design could result in the production of electrospun scaffolds with an uncompressed, cotton ball-like structure [85].

Apart from increasing the cell penetrability of the scaffold, a simpler way to augment GBM cell trapping capacity is to increase the total surface area of the scaffold available for cell attachment. In the *in vivo* biocompatibility study associated with this work, flat electrospun chitosan scaffolds were rolled into cylinders before being implanted into the brain cortex. This approach increased the surface area for cell contact as cells could access the interior of the scaffolds by migrating from either the top or bottom of the construct. Histological analyses of the brain tissues extracted from the sacrificed rats revealed extensive colonization of the scaffold by neutrophils that were recruited during the course of the post-surgical immune response. The high number of recruited immune cells may possibly compete against other cells for spaces inside the scaffold, potentially reducing the number of tumor cells that can be trapped by the implant. Should this be the case, it may be useful to further expand the colonizable volume of the scaffold by increasing the scaffold porosity using the techniques mentioned above.

To conclude, chitosan-based nanofibrous scaffolds that could incorporate different amount of SDF-1 $\alpha$ -loaded PLGA/PEG-PLGA nanoparticles were successfully developed in this part of the study. The scaffolds could provide sustained SDF-1 $\alpha$  release that will be crucial for the chemotaxis of GBM cells. Furthermore, the scaffolds demonstrated excellent *in vitro* and *in vivo* compatibility, thus fulfilling the requirement for further *in vivo* studies to evaluate their capacity to recruit GBM cells.

## 4.5. REFERENCES

- [1] P. Gentile, V.K. Nandagiri, R. Pabari, J. Daly, C. Tonda-Turo, G. Ciardelli, Z. Ramtoola, Influence of parathyroid hormone-loaded plga nanoparticles in porous scaffolds for bone regeneration, *Int. J. Mol. Sci.* 16 (2015) 20492–20510. doi:10.3390/ijms160920492.
- [2] W. Asghar, M. Islam, A.S. Wadajkar, Y. Wan, A. Ilyas, K.T. Nguyen, S.M. Iqbal, PLGA micro- and nanoparticles loaded into gelatin scaffold for controlled drug release, *IEEE Trans. Nanotechnol.* 11 (2012) 546–553. doi:10.1109/TNANO.2012.2183004.
- [3] M. De La Luz Sierra, F. Yang, M. Narazaki, O. Salvucci, D. Davis, R. Yarchoan, H.H. Zhang, H. Fales, G. Tosato, Differential processing of stromal-derived factor-1alpha and stromal-derived factor-1beta explains functional diversity., *Blood.* 103 (2004) 2452–2459. doi:10.1182/blood-2003-08-2857.
- [4] Y. Kofuku, C. Yoshiura, T. Ueda, H. Terasawa, T. Hirai, S. Tominaga, M. Hirose, Y. Maeda, H. Takahashi, Y. Terashima, K. Matsushima, I. Shimada, Structural basis of the interaction between chemokine stromal cell-derived factor-1/CXCL12 and its G-protein-coupled receptor CXCR4, *J. Biol. Chem.* 284 (2009) 35240–35250. doi:10.1074/jbc.M109.024851.
- [5] M.Z. Ratajczak, M. Kucia, R. Reza, M. Majka, A. Janowska-Wieczorek, J. Ratajczak, Stem cell plasticity revisited: CXCR4-positive cells expressing mRNA for early muscle, liver and neural cells “hide out” in the bone marrow, *Leukemia.* 18 (2004) 29–40. doi:10.1038/sj.leu.2403184.
- [6] T. Kitaori, H. Ito, E.M. Schwarz, R. Tsutsumi, H. Yoshitomi, S. Oishi, M. Nakano, N. Fujii, T. Nagasawa, T. Nakamura, Stromal cell-derived factor 1/CXCR4 signaling is critical for the recruitment of mesenchymal stem cells to the fracture site during skeletal repair in a mouse model, *Arthritis Rheum.* 60 (2009) 813–823. doi:10.1002/art.24330.
- [7] F. Knerlich-Lukoschus, B. Von Der Ropp-Brenner, R. Lucius, H.M. Mehdorn, J. Held-Feindt, Chemokine expression in the white matter spinal cord precursor niche after force-defined spinal cord contusion injuries in adult rats, *Glia.* 58 (2010) 916–931. doi:10.1002/glia.20974.
- [8] J. Deng, Z.M. Zou, T.L. Zhou, Y.P. Su, G.P. Ai, J.P. Wang, H. Xu, S.W. Dong, Bone marrow mesenchymal stem cells can be mobilized into peripheral blood by G-CSF in vivo and integrate into traumatically injured cerebral tissue, *Neurol. Sci.* 32 (2011) 641–651. doi:10.1007/s10072-011-0608-2.
- [9] L. Marquez-Curtis, A. Jalili, K. Deiteren, N. Shirvaikar, A.-M. Lambeir, A. Janowska-Wieczorek, Carboxypeptidase M Expressed by Human Bone Marrow Cells Cleaves the C-Terminal Lysine of Stromal Cell-Derived Factor-1 $\alpha$ : Another Player in Hematopoietic Stem/Progenitor Cell Mobilization?, *Stem Cells.* 26 (2008) 1211–1220. doi:10.1634/stemcells.2007-0725.
- [10] F. Jin, Q. Zhai, L. Qiu, H. Meng, D. Zou, Y. Wang, Q. Li, Z. Yu, J. Han, Q. Li, B. Zhou, Degradation of BM SDF-1 by MMP-9: The role in G-CSF-induced hematopoietic stem/progenitor cell mobilization, *Bone Marrow Transplant.* 42 (2008) 581–588. doi:10.1038/bmt.2008.222.
- [11] J. Kim, T. Mori, S.L. Chen, F.F. Amersi, S.R. Martinez, C. Kuo, R.R. Turner, X. Ye, A.J. Bilchik, D.L. Morton, D.S.B. Hoon, Chemokine receptor CXCR4 expression in patients with melanoma and colorectal cancer liver metastases and the association with disease outcome, *Ann. Surg.* 244 (2006) 113–120. doi:10.1097/01.sla.0000217690.65909.9c.

- [12] A.M. Roccaro, A. Sacco, W.G. Purschke, M. Moschetta, K. Buchner, C. Maasch, D. Zboralski, S. Zöllner, S. Vonhoff, Y. Mishima, P. Maiso, M.R. Reagan, S. Lonardi, M. Ungari, F. Facchetti, D. Eulberg, A. Kruschinski, A. Vater, G. Rossi, S. Klussmann, I.M. Ghobrial, SDF-1 inhibition targets the bone marrow niche for cancer therapy, *Cell Rep.* 9 (2014) 118–128. doi:10.1016/j.celrep.2014.08.042.
- [13] M. Katsura, F. Shoji, T. Okamoto, S. Shimamatsu, F. Hirai, G. Toyokawa, Y. Morodomi, T. Tagawa, Y. Oda, Y. Maehara, Correlation between CXCR4/CXCR7/CXCL12 chemokine axis expression and prognosis in lymph-node-positive lung cancer patients, *Cancer Sci.* 109 (2018) 154–165. doi:10.1111/cas.13422.
- [14] D. Zagzag, M. Esencay, O. Mendez, H. Yee, I. Smirnova, Y. Huang, L. Chiriboga, E. Lukyanov, M. Liu, E.W. Newcomb, Hypoxia- and Vascular Endothelial Growth Factor-Induced Stromal Cell-Derived Factor-1 $\alpha$ /CXCR4 Expression in Glioblastomas, *Am. J. Pathol.* 173 (2008) 545–560. doi:10.2353/ajpath.2008.071197.
- [15] A. do Carmo, I. Patricio, M.T. Cruz, H. Carvalheiro, C.R. Oliveira, M.C. Lopes, CXCL12/CXCR4 promotes motility and proliferation of glioma cells, *Cancer Biol. Ther.* 9 (2010) 56–65. doi:10.5214/ans.0972-7531.1017207.
- [16] G. O’Boyle, I. Swidenbank, H. Marshall, C.E. Barker, J. Armstrong, S.A. White, S.P. Fricker, R. Plummer, M. Wright, P.E. Lovat, Inhibition of CXCR4-CXCL12 chemotaxis in melanoma by AMD11070, *Br. J. Cancer.* 108 (2013) 1634–1640. doi:10.1038/bjc.2013.124.
- [17] T. Sobolik, Y. -j. Su, S. Wells, G.D. Ayers, R.S. Cook, A. Richmond, CXCR4 drives the metastatic phenotype in breast cancer through induction of CXCR2 and activation of MEK and PI3K pathways, *Mol. Biol. Cell.* 25 (2014) 566–582. doi:10.1091/mbc.E13-07-0360.
- [18] W.M. Pardridge, Drug transport in brain via the cerebrospinal fluid, *Fluids Barriers CNS.* 8 (2011) 7–10. doi:10.1186/2045-8118-8-7.
- [19] M. Haji Mansor, M. Najberg, A. Contini, C. Alvarez-Lorenzo, E. Garcion, C. Jérôme, F. Boury, Development of a Non-toxic and Non-denaturing Formulation Process for Encapsulation of SDF-1 $\alpha$  into PLGA/PEG-PLGA Nanoparticles to Achieve Sustained Release, *Eur. J. Pharm. Biopharm.* 125 (2018) 38–50. doi:10.1016/j.ejpb.2017.12.020.
- [20] H. Zhang, Y. Tian, Z. Zhu, H. Xu, X. Li, D. Zheng, W. Sun, Efficient antitumor effect of co-drug-loaded nanoparticles with gelatin hydrogel by local implantation, *Sci. Rep.* 6 (2016) 1–14. doi:10.1038/srep26546.
- [21] R.J. Ono, A.L.Z. Lee, Z.X. Voo, S. Venkataraman, B.W. Koh, Y.Y. Yang, J.L. Hedrick, Biodegradable Strain-Promoted Click Hydrogels for Encapsulation of Drug-Loaded Nanoparticles and Sustained Release of Therapeutics, *Biomacromolecules.* 18 (2017) 2277–2285. doi:10.1021/acs.biomac.7b00377.
- [22] A.L.Z. Lee, Z.X. Voo, W. Chin, R.J. Ono, C. Yang, S. Gao, J.L. Hedrick, Y.Y. Yang, Injectable Coacervate Hydrogel for Delivery of Anticancer Drug-Loaded Nanoparticles in vivo, *ACS Appl. Mater. Interfaces.* 10 (2018) 13274–13282. doi:10.1021/acsami.7b14319.
- [23] S. Pulavendran, G. Thiyagarajan, Three-dimensional scaffold containing EGF incorporated biodegradable polymeric nanoparticles for stem cell based tissue engineering applications, *Biotechnol. Bioprocess Eng.* 16 (2011) 393–399. doi:10.1007/s12257-009-3155-4.
- [24] P. Gentile, V.K. Nandagiri, R. Pabari, J. Daly, C. Tonda-Turo, G. Ciardelli, Z. Ramtoola, Influence of parathyroid hormone-loaded plga nanoparticles in porous scaffolds for bone regeneration, *Int. J. Mol. Sci.* 16 (2015) 20492–20510. doi:10.3390/ijms160920492.
- [25] L. Du, S. Yang, W. Li, H. Li, S. Feng, R. Zeng, B. Yu, L. Xiao, H.Y. Nie, M. Tu,

- Scaffold composed of porous vancomycin-loaded poly(lactide-co-glycolide) microspheres: A controlled-release drug delivery system with shape-memory effect, *Mater. Sci. Eng. C*. 78 (2017) 1172–1178. doi:10.1016/j.msec.2017.04.099.
- [26] Z.M. Huang, Y.Z. Zhang, M. Kotaki, S. Ramakrishna, A review on polymer nanofibers by electrospinning and their applications in nanocomposites, *Compos. Sci. Technol.* 63 (2003) 2223–2253. doi:10.1016/S0266-3538(03)00178-7.
- [27] Q.P. Pham, U. Sharma, A.G. Mikos, Electrospinning of polymeric nanofibers for tissue engineering applications: a review., *Tissue Eng.* 12 (2006) 1197–211. doi:10.1089/ten.2006.12.1197.
- [28] G. Ma, Y. Liu, C. Peng, D. Fang, B. He, J. Nie, Paclitaxel loaded electrospun porous nanofibers as mat potential application for chemotherapy against prostate cancer, *Carbohydr. Polym.* 86 (2011) 505–512. doi:10.1016/j.carbpol.2011.04.082.
- [29] M.E. Frohbergh, A. Katsman, G.P. Botta, P. Lazarovici, C.L. Schauer, U.G.K. Wegst, P.I. Lelkes, Electrospun hydroxyapatite-containing chitosan nanofibers crosslinked with genipin for bone tissue engineering, *Biomaterials*. 33 (2012) 9167–9178. doi:10.1016/j.biomaterials.2012.09.009.
- [30] Z. Xie, C.B. Paras, H. Weng, P. Punnakitikashem, L.C. Su, K. Vu, L. Tang, J. Yang, K.T. Nguyen, Dual growth factor releasing multi-functional nanofibers for wound healing, *Acta Biomater.* 9 (2013) 9351–9359. doi:10.1016/j.actbio.2013.07.030.
- [31] M. Rinaudo, G. Pavlov, J. Desbrières, Influence of acetic acid concentration on the solubilization of chitosan, *Polymer (Guildf)*. 40 (1999) 7029–7032. doi:10.1016/S0032-3861(99)00056-7.
- [32] X. Geng, O.H. Kwon, J. Jang, Electrospinning of chitosan dissolved in concentrated acetic acid solution, *Biomaterials*. 26 (2005) 5427–5432. doi:10.1016/j.biomaterials.2005.01.066.
- [33] C. Kriegel, K.M. Kit, D.J. McClements, J. Weiss, Electrospinning of chitosan – poly (ethylene oxide ) blend nanofibers in the presence of micellar surfactant solutions, *Polymer (Guildf)*. 50 (2009) 189–200. doi:10.1016/j.polymer.2008.09.041.
- [34] M. Dilamian, M. Montazer, J. Masoumi, Antimicrobial electrospun membranes of chitosan / poly (ethylene oxide ) incorporating poly ( hexamethylene biguanide ) hydrochloride, *Carbohydr. Polym.* 94 (2013) 364–371. doi:10.1016/j.carbpol.2013.01.059.
- [35] K. Ziani, C. Henrist, C. Jérôme, A. Aqil, J.I. Maté, R. Cloots, Effect of nonionic surfactant and acidity on chitosan nanofibers with different molecular weights, *Carbohydr. Polym.* 83 (2011) 470–476. doi:10.1016/j.carbpol.2010.08.002.
- [36] B.M. Min, S.W. Lee, J.N. Lim, Y. You, T.S. Lee, P.H. Kang, W.H. Park, Chitin and chitosan nanofibers: Electrospinning of chitin and deacetylation of chitin nanofibers, *Polymer (Guildf)*. 45 (2004) 7137–7142. doi:10.1016/j.polymer.2004.08.048.
- [37] M. Pakravan, M. Heuzey, A. Aji, A fundamental study of chitosan / PEO electrospinning, *Polymer (Guildf)*. 52 (2011) 4813–4824. doi:10.1016/j.polymer.2011.08.034.
- [38] Q. He, Q. Ao, Y. Gong, X. Zhang, Preparation of chitosan films using different neutralizing solutions to improve endothelial cell compatibility, *J. Mater. Sci. Mater. Med.* 22 (2011) 2791–2802. doi:10.1007/s10856-011-4444-y.
- [39] V.T. Tchemtchoua, G. Atanasova, A. Aqil, P. Filée, N. Garbacki, O. Vanhooetghem, C. Deroanne, A. Noël, C. Jérôme, B. Nusgens, Y. Poumay, A. Colige, Development of a Chitosan Nanofibrillar Scaffold for Skin Repair and Regeneration, *Biomacromolecules*. 12 (2011) 3194–3204. doi:10.1021/bm200680q.
- [40] L.N. Hassani, F. Hindré, T. Beuvier, B. Calvignac, N. Lautram, A. Gibaud, F. Boury, Lysozyme encapsulation into nanostructured CaCO<sub>3</sub> microparticles using a

- supercritical CO<sub>2</sub> process and comparison with the normal route, *J. Mater. Chem. B.* 1 (2013) 4011–4019. doi:10.1039/c3tb20467g.
- [41] R. Milner, G. Edwards, C. Streuli, C. Ffrench-Constant, A role in migration for the alpha V beta 1 integrin expressed on oligodendrocyte precursors., *J. Neurosci.* 16 (1996) 7240–7252. doi:10.1523/JNEUROSCI.16-22-07240.1996.
- [42] D. Séhédic, I. Chourpa, C. Tétaud, A. Griveau, C. Loussouarn, S. Avril, C. Legendre, N. Lepareur, D. Wion, F. Hindré, F. Davodeau, E. Garcion, Locoregional Confinement and Major Clinical Benefit of <sup>188</sup>Re-Loaded CXCR4-Targeted Nanocarriers in an Orthotopic Human to Mouse Model of Glioblastoma, *Theranostics.* 7 (2017) 4517–4536. doi:10.7150/thno.19403.
- [43] M.O. Wang, J.M. Etheridge, J.A. Thompson, C.E. Vorwald, D. Dean, J.P. Fisher, Evaluation of the In Vitro Cytotoxicity of Cross-Linked Biomaterial, *Biomacromolecules.* 14 (2013) 1321–1329. doi:10.1021/bm301962f.
- [44] Y. Dong, C. Xu, J. Wang, M. Wang, Y. Wu, Y. Ruan, Determination of degree of substitution for N-acylated chitosan using IR spectra, *Sci. China, Ser. B Chem.* 44 (2001) 216–224. doi:10.1007/BF02879541.
- [45] S.E. Noriega, A. Subramanian, Consequences of Neutralization on the Proliferation and Cytoskeletal Organization of Chondrocytes on Chitosan-Based Matrices, *Int. J. Carbohydr. Chem.* 2011 (2011) 1–13. doi:10.1155/2011/809743.
- [46] H.K. Dhiman, A.R. Ray, A.K. Panda, Characterization and evaluation of chitosan matrix for in vitro growth of MCF-7 breast cancer cell lines, *Biomaterials.* 25 (2004) 5147–5154. doi:10.1016/j.biomaterials.2003.12.025.
- [47] C. Cunha-Reis, K. Tuzlakoglu, E. Baas, Y. Yang, A. El Haj, R.L. Reis, Influence of porosity and fibre diameter on the degradation of chitosan fibre-mesh scaffolds and cell adhesion, *J. Mater. Sci. Mater. Med.* 18 (2007) 195–200. doi:10.1007/s10856-006-0681-x.
- [48] S. Ramakrishna, K. Fujihara, W.E. Teo, T. Yong, Z. Ma, R. Ramaseshan, Electrospun nanofibers: Solving global issues, *Mater. Today.* 9 (2006) 40–50. doi:10.1016/S1369-7021(06)71389-X.
- [49] D.R. Ripoll, J.A. Vila, H.A. Scheraga, On the orientation of the backbone dipoles in native folds, *Proc. Natl. Acad. Sci.* 102 (2005) 7559–7564. doi:10.1073/pnas.0502754102.
- [50] P. Ojeda-May, M.E. Garcia, Electric field-driven disruption of a native  $\beta$ -sheet protein conformation and generation of a helix-structure, *Biophys. J.* 99 (2010) 595–599. doi:10.1016/j.bpj.2010.04.040.
- [51] L.J. Martin, B. Akhavan, M.M.M. Bilek, Electric fields control the orientation of peptides irreversibly immobilized on radical-functionalized surfaces, *Nat. Commun.* 9 (2018) 357–367. doi:10.1038/s41467-017-02545-6.
- [52] F. Toschi, F. Lugli, F. Biscarini, F. Zerbetto, Effects of electric field stress on a  $\beta$ -amyloid peptide, *J. Phys. Chem. B.* 113 (2009) 369–376. doi:10.1021/jp807896g.
- [53] W. Zhao, R. Yang, Effect of high-intensity pulsed electric fields on the activity, conformation and self-aggregation of pepsin, *Food Chem.* 114 (2009) 777–781. doi:10.1016/j.foodchem.2008.10.016.
- [54] X. Wang, Y. Li, X. He, S. Chen, J.Z.H. Zhang, Effect of strong electric field on the conformational integrity of insulin, *J. Phys. Chem. A.* 118 (2014) 8942–8952. doi:10.1021/jp501051r.
- [55] W. Zhao, R. Yang, Experimental study on conformational changes of lysozyme in solution induced by pulsed electric field and thermal stresses, *J. Phys. Chem. B.* 114 (2010) 503–510. doi:10.1021/jp9081189.
- [56] I. Bekard, D.E. Dunstan, Electric field induced changes in protein conformation, *Soft*

- Matter. 10 (2014) 431–437. doi:10.1039/c3sm52653d.
- [57] A. Wada, The alpha-helix as an electric macro-dipole, *Adv. Biophys.* 9 (1976) 1–63.
- [58] W.G.J. Hol, The role of the  $\alpha$ -helix dipole in protein function and structure, *Prog. Biophys. Mol. Biol.* 45 (1985) 149–195. doi:10.1016/0079-6107(85)90001-X.
- [59] S.C. Balmert, A.C. Zmolek, A.J. Glowacki, T.D. Knab, S.N. Rothstein, J.M. Wokpetah, M. V. Fedorchak, S.R. Little, Positive charge of “sticky” peptides and proteins impedes release from negatively charged PLGA matrices, *J. Mater. Chem. B.* 3 (2015) 4723–4734. doi:10.1039/c5tb00515a.
- [60] M.M. Pakulska, I. Elliott Donaghue, J.M. Obermeyer, A. Tuladhar, C.K. McLaughlin, T.N. Shendruk, M.S. Shoichet, Encapsulation-free controlled release: Electrostatic adsorption eliminates the need for protein encapsulation in PLGA nanoparticles, *Sci. Adv.* 2 (2016) e1600519–e1600528. doi:10.1126/sciadv.1600519.
- [61] L. Autier, A. Clavreul, M.L. Cacicedo, F. Franconi, L. Sindji, A. Rousseau, R. Perrot, C.N. Montero-Menei, G.R. Castro, P. Menei, A new glioblastoma cell trap for implantation after surgical resection, *Acta Biomater.* 84 (2018) 268–279. doi:10.1016/j.actbio.2018.11.027.
- [62] K.M. Vårum, M.M. Myhr, R.J.N. Hjerde, O. Smidsrød, In vitro degradation rates of partially N-acetylated chitosans in human serum, *Carbohydr. Res.* 299 (1997) 99–101. doi:10.1016/S0008-6215(96)00332-1.
- [63] J. Newman, A.S. Josephson, A. Cacatian, A. Tsang, Spinal-fluid lysozyme in the diagnosis of central-nervous-system tumors, *Lancet.* 304 (1974) 756–757. doi:10.1016/S0140-6736(74)90946-5.
- [64] A. Constantopoulos, K. Antonakakis, N. Matsaniotis, Z. Kapsalakis, Spinal Fluid Lysozyme in the Diagnosis of Central Nervous System Tumours, *Neurochirurgia (Stuttg.)* 19 (1976) 169–171. doi:10.1055/s-0028-1090407.
- [65] H. Sashiwa, H. Saimoto, Y. Shigemasa, R. Ogawa, S. Tokura, Lysozyme susceptibility of partially deacetylated chitin, *Int. J. Biol. Macromol.* 12 (1990) 295–296. doi:10.1016/0141-8130(90)90016-4.
- [66] D. Ren, H. Yi, W. Wang, X. Ma, The enzymatic degradation and swelling properties of chitosan matrices with different degrees of N-acetylation, *Carbohydr. Res.* 340 (2005) 2403–2410. doi:10.1016/j.carres.2005.07.022.
- [67] T. Freier, H.S. Koh, K. Kazazian, M.S. Shoichet, Controlling cell adhesion and degradation of chitosan films by N-acetylation, *Biomaterials.* 26 (2005) 5872–5878. doi:10.1016/j.biomaterials.2005.02.033.
- [68] J. Du, P.L. Che, Z.Y. Wang, U. Aich, K.J. Yarema, Designing a binding interface for control of cancer cell adhesion via 3D topography and metabolic oligosaccharide engineering, *Biomaterials.* 32 (2011) 5427–5437. doi:10.1016/j.biomaterials.2011.04.005.
- [69] J. Wu, Y. Hong, Enhancing cell infiltration of electrospun fibrous scaffolds in tissue regeneration, *Bioact. Mater.* 1 (2016) 56–64. doi:10.1016/j.bioactmat.2016.07.001.
- [70] K. Tomihata, Y. Ikada, In vitro and in vivo degradation of films of chitin and its deacetylated derivatives, *Biomaterials.* 18 (1997) 567–575. doi:10.1016/S0142-9612(96)00167-6.
- [71] K.D. McCarthy, J. De Vellis, Preparation of separate astroglial and oligodendroglial cell cultures from rat cerebral tissue, *J Cell Biol.* 85 (1980) 890–902.
- [72] E.A. Mayerberger, R.M. Street, R.M. McDaniel, M.W. Barsoum, C.L. Schauer, Antibacterial properties of electrospun  $\text{Ti}_3\text{C}_2\text{T}_z$  (MXene)/chitosan nanofibers, *RSC Adv.* 8 (2018) 35386–35394. doi:10.1039/C8RA06274A.
- [73] X. Wang, J. Guan, X. Zhuang, Z. Li, S. Huang, J. Yang, C. Liu, F. Li, F. Tian, J. Wu, Z. Shu, Exploration of Blood Coagulation of N -Alkyl Chitosan Nanofiber Membrane

- in Vitro, *Biomacromolecules*. 19 (2018) 731–739. doi:10.1021/acs.biomac.7b01492.
- [74] B. Tyliszczak, A. Drabczyk, S. Kudłacik-Kramarczyk, K. Bialik-Wąs, A. Sobczak-Kupiec, In vitro cytotoxicity of hydrogels based on chitosan and modified with gold nanoparticles, *J. Polym. Res.* 24 (2017). doi:10.1007/s10965-017-1315-3.
- [75] S. Saravanan, N. Sareen, E. Abu-El-Rub, H. Ashour, G.L. Sequiera, H.I. Ammar, V. Gopinath, A.A. Shamaa, S.S.E. Sayed, M. Moudgil, J. Vadivelu, S. Dhingra, Graphene Oxide-Gold Nanosheets Containing Chitosan Scaffold Improves Ventricular Contractility and Function After Implantation into Infarcted Heart, *Sci. Rep.* 8 (2018) 15069. doi:10.1038/s41598-018-33144-0.
- [76] M. Xia, R. Huang, K.L. Witt, N. Southall, J. Fostel, M.H. Cho, A. Jadhav, C.S. Smith, J. Inglese, C.J. Portier, R.R. Tice, C.P. Austin, Compound cytotoxicity profiling using quantitative high-throughput screening, *Environ. Health Perspect.* 116 (2008) 284–291. doi:10.1289/ehp.10727.
- [77] R.M. Boehler, J.G. Graham, L.D. Shea, Tissue engineering tools for modulation of the immune response, *Biotechniques*. 51 (2011) 239–254. doi:10.2144/000113754.
- [78] L. Chen, H. Deng, H. Cui, J. Fang, Z. Zuo, J. Deng, Y. Li, X. Wang, L. Zhao, Inflammatory responses and inflammation-associated diseases in organs, *Oncotarget*. 9 (2018) 7204–7218. doi:10.18632/oncotarget.23208.
- [79] B.O. Ode Boni, L. Lamboni, T. Souho, M. Gauthier, G. Yang, Immunomodulation and cellular response to biomaterials: the overriding role of neutrophils in healing, *Mater. Horizons*. (2019). doi:10.1039/c9mh00291j.
- [80] E. Mariani, G. Lisignoli, R.M. Borzì, L. Pulsatelli, Biomaterials: Foreign bodies or tuners for the immune response?, *Int. J. Mol. Sci.* 20 (2019). doi:10.3390/ijms20030636.
- [81] McCracken JM, Allen LAH, Regulation of Human Neutrophil Apoptosis and Lifespan in Health and Disease, *J. Cell Death*. 7 (2014) 15–23. doi:10.4137/JCD.S11038.RECEIVED.
- [82] A. Vishwakarma, N.S. Bhise, M.B. Evangelista, J. Rouwkema, M.R. Dokmeci, A.M. Ghaemmaghami, N.E. Vrana, A. Khademhosseini, Engineering Immunomodulatory Biomaterials To Tune the Inflammatory Response, *Trends Biotechnol.* 34 (2016) 470–482. doi:10.1016/j.tibtech.2016.03.009.
- [83] K. Wolf, M. te Lindert, M. Krause, S. Alexander, J. te Riet, A.L. Willis, R.M. Hoffman, C.G. Figdor, S.J. Weiss, P. Friedl, Physical limits of cell migration: Control by ECM space and nuclear deformation and tuning by proteolysis and traction force, *J. Cell Biol.* 201 (2013) 1069–1084. doi:10.1083/jcb.201210152.
- [84] Y.H. Lee, J.H. Lee, I.G. An, C. Kim, D.S. Lee, Y.K. Lee, J. Do Nam, Electrospun dual-porosity structure and biodegradation morphology of Montmorillonite reinforced PLLA nanocomposite scaffolds, *Biomaterials*. 26 (2005) 3165–3172. doi:10.1016/j.biomaterials.2004.08.018.
- [85] B.A. Blakeney, A. Tambralli, J.M. Anderson, A. Andukuri, D.J. Lim, D.R. Dean, H.W. Jun, Cell infiltration and growth in a low density, uncompressed three-dimensional electrospun nanofibrous scaffold, *Biomaterials*. 32 (2011) 1583–1590. doi:10.1016/j.biomaterials.2010.10.056.



# **Chapter 5:**

## **General discussion, conclusion and perspectives**

---

## 5. GENERAL DISCUSSION, CONCLUSION AND PERSPECTIVES

---

### 5.1. GENERAL DISCUSSION

The term glioblastoma multiforme was first coined by Harvey Cushing and Percival Bailey in 1926 when the pair analyzed and stratified 414 cases of tumors involving the glial cells of the brain, or gliomas [1]. Nowadays, commonly referred to as glioblastoma (GBM), these tumors continue to be a conundrum among clinicians and researchers alike. As GBM can progress very rapidly, surgical procedure has been established as the first-line treatment for this disease due to its utility in immediately reducing the bulk tumor volume and curbing its aggressiveness. In fact, this approach has retained its gold standard status since the 1970s. That said, it is worth noting that surgical resection of brain tumors has been explored and optimized since 1879 [2]. However, genuine optimism in the curing potential of this procedure only emerged nearly a century later. The rising expectation was driven by the huge advancements made in the field of *in vivo* imaging, as computerized tomography (CT) scanning and magnetic resonance imaging (MRI) made their debut in 1972 and 1973 respectively [3,4]. Despite this, achieving complete tumor resection to cure GBM remains an elusive goal. In 1950, Ernest Sachs stated that “the greatest stumbling block in the cure of glioblastomas has been the difficulty of finding the limits of an infiltrating tumor” [5]. Due to their unbound invasiveness, GBM can invade into surrounding brain parenchyma, extending its frontier in multiple directions. Consequently, GBM often adopts an octopus-like shape that cannot be accurately defined by conventional imaging platforms such as CT scan and MRI, thus reducing the potential of achieving complete tumor resection by surgery [6].

To kill the residual tumor cells, adjuvant treatments in the form of radiotherapy and chemotherapy are administered post-surgery. Bundling these treatments altogether, the median survival of GBM patients post-diagnosis can only be stretched to approximately 15 months [7]. The poor prognosis is driven by a small subpopulation of residual tumor cells that survive the cytotoxic effect of the post-surgical treatments and subsequently multiply to form a tumor with even more aggressive phenotypes [8]. The incomplete killing of the residual tumor cells can be due to resistance developed against the employed treatments [9,10] or evasion as a result of anatomical barriers [11]. To make things worse, the poorly selective mechanisms of action of chemoradiation therapies can often result in extensive damage to the healthy brain tissues that they come into contact with [6]. Patients are worsening off not only from the recurrence of the

tumor, but also because of the side effects of the treatments they received. Therefore, we were motivated to explore the strategy of recruiting the residual tumor cells into a well-defined location to facilitate more selective and complete eradication of this cell population.

Tumor cells can migrate in response to chemokine concentration gradients, a biological process referred to as chemotaxis, as they disseminate into local and distant healthy tissues. GBM cells are no exception to this process. These cells are known to migrate towards, and subsequently along, the blood vessel structures in the brain. This migration pattern is driven by an increased expression of SDF-1 $\alpha$  chemokine in the endothelial cells lining the blood vessels [12]. The released SDF-1 $\alpha$  can bind to and activate the CXCR4 receptors on the surface of invading GBM cells to cause them to migrate up the chemokine concentration gradients, which indirectly leads to their recruitment to the blood vessels [13,14]. As such, implantation of SDF-1 $\alpha$ -releasing scaffolds into the resection cavity following the removal of the bulk tumor could be a promising strategy to attract the residual GBM cells for their selective killing. It should be mentioned that these cells can reside more than one centimeter away from the resection cavity border. Therefore, prolonged release of SDF-1 $\alpha$  will be crucial to expand the time window for their chemotactic recruitment. With this in mind, this thesis aimed to develop scaffolds that can provide sustained delivery of bioactive SDF-1 $\alpha$  and the experimental work were centered on the following two objectives:

- To encapsulate SDF-1 $\alpha$  in polymer-based nanoparticles to form primary carriers of this chemokine
- To incorporate SDF-1 $\alpha$ -loaded nanoparticles into a nanofibrous scaffold to provide a secondary barrier to the SDF-1 $\alpha$  release process

### **Objective 1: To prepare SDF-1 $\alpha$ -loaded polymer-based nanoparticles**

Polymer-based nanoparticles have been used as delivery vehicles for a wide range of protein molecules. Nanoparticles can be conveniently prepared from a wide range of polymers using several formulation processes that include phase separation, solvent evaporation and spray-drying. Despite their widespread use, none of these nanoparticle formulation processes can be readily used to encapsulate all types of protein. Often, the formulation process has to be carefully chosen according to the physicochemical properties of the protein to be encapsulated. Apart from identifying the right formulation process to go with, another important thing to consider is choosing the right type of polymer. Strictly speaking, these decisions should be

made hand-in-hand as the chosen polymer materials must be compatible with the selected formulation process. From here, various parameters related to the process and the polymer materials should be fine-tuned to achieve desirable encapsulation efficiencies and release rates.

In this work, a combination of PLGA and PEG-PLGA were used to prepare nanoparticles using a phase separation method. The classical phase separation process for encapsulating protein molecules into PLGA-based nanoparticles begins with solubilization of protein molecules in an aqueous solvent, which is then dispersed in a PLGA-containing organic phase (e.g. dichloromethane) to form a water-in-oil (W/O) emulsion. Following this step, an organic solvent that is non-solvent to PLGA (e.g. silicon oil) is gradually introduced to extract the PLGA solvent and decrease the PLGA solubility. The phase separation of the polymer from its solution contributes to the formation of polymer-rich liquid phase (coacervate) around the inner protein-containing aqueous phase. As more and more non-solvent is added, the coacervate solidifies to produce protein-loaded particles [15–17]. An obvious drawback of this method is the requirement for a large volume of organic solvent to induce phase separation. To counter this, isosorbide dimethyl ether (DMI) was used to dissolve PLGA and PEG-PLGA. DMI is a non-halogenated and non-volatile solvent with an excellent *in vivo* safety profile [18]. More importantly, it is a water-miscible solvent, meaning that the phase separation step can be triggered using aqueous solvents such as water. The use of such a benign solvent and the significant reduction in the total volume of organic solvents involved help prevent the need for any special equipment or facility to protect the operators or their surroundings. Overall, the formulation process was intentionally designed to be simple such that it could be performed without requiring no more than a beaker and a magnetic stirrer to ensure that it can be set up and reproduced easily in any lab.

Another important modification introduced in this work was the precipitation of protein molecules prior to their encapsulation. This helped eliminate the need to emulsify protein solution in the polymer phase, a process that can often lead to unfolding of protein molecules at the water-oil interface. *In vivo*, protein molecules are folded in such a way that their hydrophobic residues are protected from the aqueous environments. However, they can undergo conformational rearrangements when exposed to an oil-water interface in order to achieve the state of lowest free energy. The hydrophobic residues could become exposed and interact with the oil phase, altering the three-dimensional conformation of a protein and potentially disrupting its biological functions [19]. When precipitated, protein molecules have more limited conformational mobility, making them less likely to unfold when exposed to

organic solvents. We showed that by dispersing SDF-1 $\alpha$  precipitates in PLGA solutions prior to the phase separation process, the protein could be encapsulated with no detectable loss of biological activity. We also observed that parameters such as protein concentration and ionic strength can affect the efficiency of the precipitation process in terms of the amount and bioactivity of the precipitates generated. Therefore, should the developed formulation process be used to encapsulate other types of protein in the future, it will be essential to re-optimize the precipitation parameters.

Despite the evident simplicity of the formulation process, there are many parameters that may influence the final protein encapsulation efficiency. As protein molecules generally have high aqueous solubility, they tend to partition into the aqueous phase during the phase separation process, resulting in poor encapsulation efficiencies. This problem was mitigated by buffering the pH of the aqueous phase close to the isoelectric point (pI) of the protein being encapsulated. In so doing, the net charge of the protein molecules that came into contact with the buffer solution will be close to zero, rendering the protein less water-soluble. As SDF-1 $\alpha$  has a pI of 10.5, mildly-basic glycine buffer solutions were used during the phase separation step. Apart from changing the pH, the protein solvation capacity of the aqueous phase may also be deprived by adding salts or other additives. Salts such as ammonium sulfate and hydrophilic polymers such as PEG, when added to an aqueous solvent, can interact with water molecules, which would otherwise be available for solvation of protein molecules [20,21]. Thus, they could also be useful to reduce protein leakage from the organic phase during the phase separation step.

In addition to process-related parameters, the properties of the polymer used can also influence encapsulation efficiency. We showed that better encapsulation could be achieved by using PLGA with uncapped, thus ionizable, carboxylic terminals. However, it was clear that relying merely on the electrostatic interactions between the negatively-charged carboxyl groups and the positively-charged protein molecules to boost encapsulation efficiency could later lead to a bigger problem in the form of incomplete protein release. The high number of carboxyl groups in nanoparticles composed of uncapped PLGA could strongly interact with the protein molecules to inhibit their release. Therefore, we decided to use PLGA with capped terminals and trade encapsulation efficiency for more complete protein release. With Formulation 8 (67% capped PLGA, 33% PEG-PLGA), the encapsulation efficiency for SDF-1 $\alpha$  was 76% and more than 70% of the protein load was released at the end of the 30-day release study period (Figure 5.1A). The lack of totally complete SDF-1 $\alpha$  release could be explained by the hydrolysis of the PLGA ester bonds that generated ionizable carboxyl groups, which could then interact strongly

with SDF-1 $\alpha$  molecules. The gradual hydrolysis of ester bonds was evident from the increasingly negative zeta-potential values of Formulation 8 measured during the release study (Figure 5.1B). In the early stages of the release study, the small number of negatively-charged carboxyl groups might have been neutralized by the cations present in the release medium (e.g. sodium ions), permitting the release of the protein load. However, due to the autocatalytic nature of the hydrolysis reaction, the number of carboxyl groups could have increased steeply afterwards. Even if only a small fraction of these interacted with the encapsulated SDF-1 $\alpha$  molecules, it could hinder further SDF-1 $\alpha$  release. In the future, the use of more hydrophobic polymers such as PLA, which are less prone to hydrolysis, may be useful to slow down the generation of ionizable carboxyl groups and obtain more complete SDF-1 $\alpha$  release.

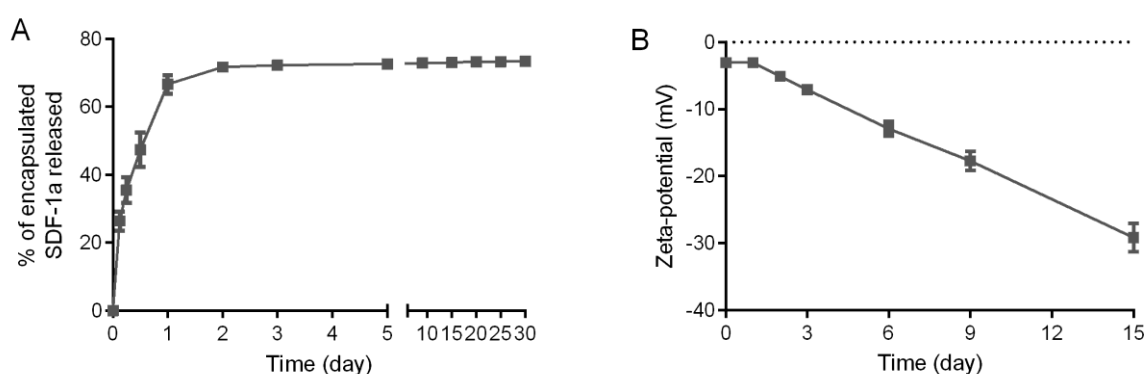


**Figure 5.1:** (A) The SDF-1 $\alpha$  release profile and (B) the change in the zeta-potential of Formulation 8 (67% capped PLGA, 33% PEG-PLGA) during the *in vitro* release study.

Due to the tendency of PLGA to undergo hydrolysis, it is important to store PLGA-based nanoparticles in dry state. Lyophilization, or freeze-drying, is a commonly used technique for removing water from aqueous dispersions of PLGA-based nanoparticles. As this technique can exert significant physical stresses on the nanoparticles, disaccharides or oligosaccharides are usually added to the nanoparticle dispersion to form a spacing matrix to prevent aggregation of the nanoparticles. However, it should be noted that the performance of these so-called “protectants” can vary between different publications. We noticed that many of these publications either did not state the exact details (e.g. temperature and pressure) of the freeze-drying conditions or failed to justify why a certain set of conditions was chosen. In this work, we showed clearly that the success of freeze-drying, in terms of maintaining the size and polydispersity of the nanoparticles, is dependent on the drying temperature being lower than the collapse temperature of the added protectant. Thus, it is important to choose a protectant species with a high collapse temperature or set the drying temperature to be as low as possible

to obtain the best results. This brief yet effective investigation generated useful knowledge for lyophilization of other polymer-based nanoparticles in the future.

### **Objective 2: To incorporate SDF-1 $\alpha$ -loaded nanoparticles into chitosan-based nanofibers**

As the SDF-1 $\alpha$ -loaded nanoparticles themselves provide only transient SDF-1 $\alpha$  release, they were subsequently incorporated into chitosan-based nanofibers by electrospinning to prolong the release duration. Chitosan was the polymer of choice for the electrospinning process due to its unique physicochemical properties. Owing to its weakly-basic nature, chitosan can be solubilized in mildly acidic solvents such as dilute solutions of acetic acid, which do not degrade PLGA-based nanoparticles. Upon dissolution, the protonated amino groups in chitosan can interact with the negatively-charged PLGA carboxyl groups to facilitate the incorporation of SDF-1 $\alpha$ -loaded nanoparticles into chitosan nanofibers. The electrospun nanofibers can be turned water stable by treating them with a dilute solution of inorganic base such as sodium hydroxide to deprotonate the chitosan amino groups. The stabilized chitosan nanofibers degrade slowly in an aqueous environment, holding the SDF-1 $\alpha$ -loaded nanoparticles in place during the SDF-1 $\alpha$  release process. This is likely useful for creating and maintaining SDF-1 $\alpha$  concentration gradients that are essential for the chemotaxis of GBM cells.

We observed that the incorporation of SDF-1 $\alpha$ -loaded nanoparticles into nanofibers actually helped to slow down SDF-1 $\alpha$  release from the nanoparticles. As mentioned above, the release of SDF-1 $\alpha$  can occur freely when the cations in the release media neutralized any ionized carboxyl groups in the nanoparticles. However, the free access of the release media to the nanoparticles can also contribute to the hydrolysis of the PLGA ester bonds, generating high number of ionized carboxyl groups that can restrict further release of the encapsulated SDF-1 $\alpha$ . This explains the short duration of SDF-1 $\alpha$  release seen in the case of bare nanoparticles. By incorporating these nanoparticles in chitosan nanofibers, the influx of release media into the nanoparticles can be slowed down, preventing the initial burst release and fast increase in the number of ionized carboxyl groups, both of which lead to more sustained SDF-1 $\alpha$  release. We also observed that SDF-1 $\alpha$  molecules that were loaded directly into chitosan nanofibers were released rapidly after incubation in an appropriate release media. As both SDF-1 $\alpha$  and chitosan were positively-charged under the electrospinning condition, it was likely that the SDF-1 $\alpha$  molecules partitioned themselves close to the surface of the electrospun nanofibers and thus, could be washed away immediately by the release media. The rapid release of bare SDF-1 $\alpha$  and the slow liberation of its encapsulated counterpart from the chitosan nanofibers

offer a possibility of tailoring the rate of SDF-1 $\alpha$  delivery at the site of implantation to maximize the extent of GBM cell recruitment.

Apart from having the optimal SDF-1 $\alpha$  release rate, for an implant to work as a trap for the GBM cells, it is important that it remains stable at the implantation site for a certain period of time to provide ample opportunity for the cells to migrate into it. We observed that the developed nanofibrous scaffolds possess excellent *in vitro* and *in vivo* stability. In fact, the scaffolds were mostly intact when retrieved from the rat brains at the end of the 7-day *in vivo* study period. This raises the question on whether the scaffolds will eventually be degraded if they are left in the animals for a longer duration. Thus, the results from the ongoing 100-day study should be analyzed and further *in vivo* studies may be conducted to obtain an estimation on the time required to have the scaffolds fully degraded and to document any adverse events that may arise from the prolonged period of implantation. Alternatively, the chitosan used in this study could be replaced with one of its water-soluble derivatives to speed up the degradation rate of the scaffolds. However, such a drastic approach may require re-optimization of the electrospinning process and introduce the need for post-electrospinning cross-linking treatments, both of which could affect the SDF-1 $\alpha$  release profile of the scaffold.

During the period of GBM cell recruitment, it is important that the implanted scaffold does not induce any adverse toxicological effects that may worsen patients' clinical conditions. As such, scaffolds with excellent biocompatibility are highly desirable. We observed that rats implanted with the developed scaffolds as part of the 100-day biocompatibility study are alive and do not show any signs of toxicity at the time of writing. However, we also observed that the scaffolds could induce extensive recruitment of immune cells to the resection cavity. As chitosan is foreign to the human body, the strong inflammatory response to the implanted scaffold is not entirely unexpected. This response, however, may be exploited to facilitate the killing of any recruited GBM cells. To achieve this, we need to link our existing strategy with immunotherapy. Immunotherapy refers to the treatment of diseases, including cancers, through modulation of the patient's immune system. The clinical significance of this type of treatment has been growing steadily over the last decade. Arguably, the most important players within this area of treatment are programmed cell death protein 1 (PD-1) inhibitors, which first entered the anti-cancer market in late 2014 through the approval of Bristol-Myers Squibb's Opdivo® in Japan. PD-1 is a protein that is expressed on the surface of T-lymphocytes that functions to down-regulate the immune system and suppress inflammatory activity [22]. Although it plays important roles in preventing autoimmune diseases, it can also hinder T-lymphocytes from

killing tumor cells [23,24]. In fact, T-lymphocyte exhaustion is a hallmark of GBM. A recent study reported that T-lymphocytes isolated from GBM patients are characterized by an elevated expression of multiple immune checkpoints, including PD-1 [25]. Thus, future incorporation of immunotherapeutic agents such as PD-1 inhibitors into the scaffold developed in this work could be useful to stimulate *in situ* killing of the chemoattracted GBM cells by the co-recruited immune cells.

## 5.2. CONCLUSION AND PERSPECTIVES

In this thesis, chitosan-based nanofibrous scaffolds containing SDF-1 $\alpha$ -loaded PLGA-based nanoparticles were developed as a means of achieving sustained release of SDF-1 $\alpha$ . Careful selection of polymer materials ensured that the developed scaffolds could provide continuous release of bioactive SDF-1 $\alpha$  for up to 5 weeks. The possibility of loading SDF-1 $\alpha$  into both the nanoparticle and the nanofiber compartments of the composite vehicles also means that the rate of SDF-1 $\alpha$  delivery could be carefully controlled to optimize the chemotactic recruitment of GBM cells. In addition, the scaffolds were also shown to have excellent *in vivo* biocompatibility.

Considering their promising SDF-1 $\alpha$  release and safety performance, it is justifiable to proceed to the *in vivo* assessment of the GBM cell trapping efficacy of the developed scaffolds. To do this, it will be essential to develop a suitable preclinical GBM resection model. GBM cells can be injected into the brain of athymic nude animals through a cranial opening to induce tumor formation. After a certain period of time, the tumor can be resected from the brain to create a cavity into which the SDF-1 $\alpha$ -releasing scaffold can be implanted. The resection could be performed as per the biopsy punch method used in our *in vivo* biocompatibility study. Several factors should be considered to make sure that the pre-clinical model closely represents the clinical situation of GBM. First, the GBM cells injected into the brain should facilitate the formation of a tumor that reflects the genetic and proteomic profile of clinical GBM. Commercially-available U87-MG has been the preferred GBM cell line as these cells can consistently form tumor within 1-2 weeks post-inoculation [26]. However, the formed tumor lacks the invasive phenotype that is typical of clinical GBM. In addition, U87-MG cells also lack the expression of CXCR4, making them less likely to respond to SDF-1 $\alpha$  gradients. The absence of CXCR4 expression in these cells may also explain the benign nature of the formed tumor as CXCR4 is well-known for their prominent role in facilitating the invasion of GBM. To counter these two issues, CXCR4-positive U87-MG cells, as used in the agarose drop

migration assay, may be used during the tumor formation step. This said, it is important to consider the potential negative impact of the transfection procedure on the tumor forming ability of U87-MG cells. Apart from the complexities associated with forming clinically-relevant tumors, there are also several challenges associated with the tumor resection step. It is important to consider for how long the tumor should be allowed to grow. If the tumor exceeds a certain size, the animals may deteriorate rapidly and die prematurely after the tumor resection step. On the other hand, the tumor should be allowed to grow long enough such that when it is resected, the cavity is adequately large to accommodate a reasonable volume of the SDF-1 $\alpha$ -releasing scaffold.

In addition to developing a suitable disease model, it will also be important to study the pharmacokinetic of exogenous SDF-1 $\alpha$  upon introduction into the brain. The distribution of exogenous SDF-1 $\alpha$  released from the implanted scaffold in the brain should be monitored to have a better assessment of the possibility of recruiting GBM cells that are distant from the border of the resection cavity. This could be achieved by labelling native SDF-1 $\alpha$  molecules with fluorescent probes prior to incorporation into the scaffold. Dutta *et al.* encapsulated AlexaFluor-647-conjugated SDF-1 $\alpha$  into PLGA nanoparticles and studied the distribution of the protein after intracortical injection of the nanoparticles in mice. After 7 days, the animals were sacrificed, and brain tissues were sliced for viewing under fluorescence microscopy. They observed modest local diffusion of SDF-1 $\alpha$  in the cortical parenchyma, where most of the released SDF-1 $\alpha$  were localized within 400  $\mu$ m from the injection site. They hypothesized that the presence of negatively-charged molecules such as hyaluronic acid and heparan sulfate in the cortical ECM may hinder the diffusion of highly basic proteins such as SDF-1 $\alpha$  [27]. However, it should be noted that there may be appreciable difference between the density of ECM in an intact brain and that in a brain with surgical injuries. Post-surgical inflammatory responses often lead to the release of proteases from activated immune cells that can lead to degradation and remodeling of the ECM in the regions surrounding the site of surgery [28,29]. The remodeling of the brain tissue structure may create a more permissive environment for SDF-1 $\alpha$  diffusion.

Equally important as studying the intracortical distribution of exogenous SDF-1 $\alpha$  is investigating the pharmacodynamic effects of this protein on the brain. Sustained delivery of exogenous SDF-1 $\alpha$  to an intact brain has been reported to induce endogenous SDF-1 $\alpha$  production in cells residing close to the site of delivery. There was also weaker upregulation in SDF-1 $\alpha$  expression in more distant tissues [27]. Should the same response take place in a brain

with residual GBM, the dose of SDF-1 $\alpha$  incorporated into the scaffold should be reduced accordingly as the establishment of SDF-1 $\alpha$  gradients for chemotactic recruitment of GBM cells could be also be contributed by the subsequent upregulation of endogenous SDF-1 $\alpha$  expression.

The SDF-1 $\alpha$ -releasing scaffolds developed in this work are intended to serve as early tools to assess the feasibility of using chemokine and chemotaxis to recruit GBM cells. As the chemotactic attraction of GBM cells relies strongly on the establishment and maintenance of chemokine concentration gradients, the development of a vehicle that is capable of providing sustained chemokine release has been the main goal of this thesis. It is not the intention of this work to unequivocally identify the most effective chemokine molecule for selective trapping of GBM cells. The decision to use SDF-1 $\alpha$  was made mainly based on its well-documented involvement in the regulation of GBM cell migration. As such, it is probable that SDF-1 $\alpha$  may not be the most suitable chemokine for this purpose. To our knowledge, there is no publication discussing the effect of exogenous SDF-1 $\alpha$  on GBM cells. In fact, there is only one known research conducted to investigate the effect of exogenous SDF-1 $\alpha$  in a healthy brain. The group concluded that sustained exposure to exogenous SDF-1 $\alpha$  can cause gradual decrease of CXCR4 receptor expression in the brain [27]. The same observation is unlikely to happen in the case of GBM, as GBM cells are heavily dependent on the SDF-1 $\alpha$ /CXCR4 axis to maintain their proliferative and invasive phenotypes [30,31]. However, cancer cells in general are known for their capacity to switch to other signaling pathways to maintain their survival and growth when needed. Thus, it is important to confirm that the chemotactic effect of exogenous SDF-1 $\alpha$  on GBM cells is not prone to any mechanisms of desensitization. This could be done by exposing CXCR4-positive GBM cells to gradients of SDF-1 $\alpha$  using a Boyden chamber setup or a suitable microfluidic device and quantifying the change, if there will be any, in the level of CXCR4 receptor expression.

In addition to potential receptor downregulation issues, there are also concerns regarding the selectivity of SDF-1 $\alpha$ -mediated chemotaxis. GBM cells are known to overexpress CXCR4 receptors to benefit from the pro-migratory and trophic effects of SDF-1 $\alpha$  as mentioned above [32]. However, these receptors are also expressed, albeit to a lower extent than that seen in GBM cells, in many types of cells in the brain, including neural stem/progenitor cells, glial cells and microglia [33–35]. Therefore, it is probable that these cells may also be recruited upon implantation of an SDF-1 $\alpha$ -releasing scaffold into the brain. Although this unintended effect may seem acceptable considering the potential clinical benefits of recruiting GBM cells,

it is still desirable to try to increase the selectivity of this approach to distinguish it from the poorly selective nature of existing treatments. Apart from SDF-1 $\alpha$ , bradykinin is another chemokine known to be involved in the homing of GBM cells to the blood vessels. After it is secreted from the vascular endothelial cells, bradykinin binds to the bradykinin B2 receptor (B2R) on GBM cells, leading to downstream changes in cell shape and volume that facilitate migration of the cells through the dense brain ECM [36]. A preclinical study revealed that inhibition of B2R could reduce the vascular association of GBM cells from 77% to 19% [37]. Due to its proven role in directing GBM cell migration, bradykinin presents itself as an interesting chemokine to replace, or be used together with, SDF-1 $\alpha$  to induce more potent and selective chemotactic effects on GBM cells.

Another question that needs to be addressed to improve the feasibility of the tumor trapping approach as a treatment for GBM is how long the implanted scaffold should be left inside the brain to allow complete recruitment of the residual GBM cells. To begin answering this question, it is important to conduct a preclinical study to monitor the migration of GBM cells into the implanted scaffold. GBM cells can be labelled using appropriate tumor cell tagging peptides that are conjugated with a fluorophore. These fluorescent imaging agents are thus useful in distinguishing a tumor from the surrounding healthy tissues. One of the most promising GBM cell labelling agents is BLZ-100 that is currently developed by Blaze Bioscience. BLZ-100 is composed of a synthetic form of the chlorotoxin peptide that is covalently bound to the near-infrared (NIR) fluorophore indocyanine green [38,39]. When administered intravenously several hours before a surgery, BLZ-100 can cross the blood-brain barrier to bind and label GBM cells, facilitating more complete and precise resection of the tumor [40,41]. Although this agent is useful for intraoperative visualization of the tumor, it offers little value for post-operative tracking of the residual GBM cells. This is because NIR fluorophores such as indocyanine green emit light in the wavelength range of 700 – 900 nm, which is prone to tissue scattering and autofluorescence issues [42]. As such, *in vivo* brain imaging using NIR fluorophores have a limited penetration depth of 1 – 2 mm and most unfortunately, it requires craniotomy to produce images with good resolutions. To overcome these problems, contrast agents that emit light of longer wavelengths can be used. Hong *et al.* demonstrated that through-skull imaging of the brain can be achieved by using single-walled carbon nanotubes (SWNT) that have intrinsic photoluminescence in the 1.3–1.4  $\mu\text{m}$  wavelength range [43]. Coupling SWNT to the peptide component of BLZ-100 may produce an imaging agent that is useful for real-time tracking of the migration of GBM cells into an

implanted scaffold. Apart from this, the use of established *in vivo* imaging techniques such as MRI and  $\mu$ CT scan for this purpose should also be explored.

After developing a method to monitor the progression of the trapping process, it will be essential to identify the most effective way to kill the recruited GBM cells. It may be tempting to suggest direct removal of the cell-laden scaffold to achieve an immediate eradication of the disease. However, this approach will necessitate an additional surgery, a requirement that may be very difficult to fulfil especially in patients who are terminally ill. A less invasive solution would be to use stereotactic radiotherapy (SRT). SRT is a treatment where radiation beam is directed to a well-defined spot, usually the tumor site, from many different angles around the body. The procedure ensures the targeted site receives a much higher dose of radiation than the surrounding tissues [44,45]. Thus, SRT seems to be a suitable tool to achieve selective killing of the trapped GBM cells.

Further down the development timeline, it will be essential to develop a diagnostic tool that can be used to identify patient subpopulations that are most suitable to receive the developed treatment. Information on the biological features of GBM, including proteomic profiles and density of ECM, will have to be gathered accurately as this can greatly influence the success rate of post-surgical trapping of residual GBM cells. Overexpression of CXCR4 and lower ECM densities may predict more successful recruitment of GBM cell by SDF-1 $\alpha$ -releasing scaffolds. Conventionally, biological characterization of GBM can only be done after the surgery as a small portion of the resected tumor is sent to the pathology lab for analysis. This may prevent timely provision of the information required to decide whether or not a tumor trap should be implanted into the resected brain. As such, efforts should be made to identify alternative sources of information to help inform the decision.

To conclude, the work conducted within this thesis has resulted in the development of a tool that can be used in the subsequent proof-of-concept stage of the tumor trapping strategy. From the physicochemical perspective, the work also helped progress the field of nanomedicine and drug delivery by generating new polymer-based platforms for local delivery of therapeutic proteins. The next step will be to address relevant biological challenges that may impede the tumor trapping efficacy and selectivity of the developed scaffolds. Close collaboration between the physicochemists, biologists, and other preclinical researchers will be essential to answer preliminary questions regarding the feasibility of the tumor trapping strategy as a treatment for GBM. Beyond that, inputs from neurosurgeons and patient group representatives will have to

be sought to assess the adoptability of this approach in the clinic. Overall, this thesis may serve as a starting point for the development of a novel clinical tool to answer the century-old conundrum of GBM.

### 5.3. REFERENCES

- [1] J. Bianco, C. Bastiancich, A. Jankovski, A. des Rieux, V. Pr at, F. Danhier, On glioblastoma and the search for a cure: where do we stand?, *Cell. Mol. Life Sci.* 74 (2017) 2451–2466. doi:10.1007/s00018-017-2483-3.
- [2] M. Macmillan, Localization and William Macewen’s early brain surgery part II: The cases, *J. Hist. Neurosci.* 14 (2005) 24–56. doi:10.1080/09647040590881793.
- [3] J. Ambrose, Computerized transverse axial scanning (tomography): II. Clinical application, *Br. J. Radiol.* 46 (1973) 1023–1047. doi:10.1259/0007-1285-46-552-1023.
- [4] P.C. Lauterbur, Image formation by induced local interactions: Examples employing nuclear magnetic resonance, *Nature.* 242 (1973) 190–191. doi:10.1038/242190a0.
- [5] E. Sachs, The Problem of the Glioblastomas, *J. Neurosurg.* 7 (1950) 185–189. doi:10.3171/jns.1950.7.3.0185.
- [6] C. Bastiancich, P. Danhier, V. Pr at, F. Danhier, Anticancer drug-loaded hydrogels as drug delivery systems for the local treatment of glioblastoma, *J. Control. Release.* 243 (2016) 29–42. doi:10.1016/j.jconrel.2016.09.034.
- [7] R. Stupp, W.P. Mason, M.J. van den Bent, M. Weller, B. Fisher, M.J.B. Taphoorn, K. Belanger, A.A. Brandes, C. Marosi, U. Bogdahn, J. Curschmann, R.C. Janzer, S.K. Ludwin, T. Gorlia, A. Allgeier, D. Lacombe, J.G. Cairncross, E. Eisenhauer, R.O. Mirimanoff, Radiotherapy plus Concomitant and Adjuvant Temozolomide for Glioblastoma, *N. Engl. J. Med.* 352 (2005) 987–996. doi:10.1056/NEJMoa043330.
- [8] T. Ichikawa, Y. Otani, K. Kurozumi, I. Date, Phenotypic Transition as a Survival Strategy of Glioma, *Neurol. Med. Chir. (Tokyo).* 56 (2016) 387–395. doi:10.2176/nmc.ra.2016-0077.
- [9] S.Y. Lee, Temozolomide resistance in glioblastoma multiforme, *Genes Dis.* 3 (2016) 198–210. doi:10.1016/j.gendis.2016.04.007.
- [10] J.P. Sheehan, M.E. Shaffrey, B. Gupta, J. Larner, J.N. Rich, D.M. Park, Improving the radiosensitivity of radioresistant and hypoxic glioblastoma, *Futur. Oncol.* 6 (2010) 1591–1601. doi:10.2217/fon.10.123.
- [11] M.C. de Gooijer, N.A. de Vries, T. Buckle, L.C.M. Buil, J.H. Beijnen, W. Boogerd, O. van Tellingen, Improved Brain Penetration and Antitumor Efficacy of Temozolomide by Inhibition of ABCB1 and ABCG2, *Neoplasia.* 20 (2018) 710–720. doi:10.1016/j.neo.2018.05.001.
- [12] S. Rao, R. Sengupta, E.J. Choe, B.M. Woerner, E. Jackson, T. Sun, J. Leonard, D. Piwnica-Worms, J.B. Rubin, CXCL12 mediates trophic interactions between endothelial and tumor cells in glioblastoma, *PLoS One.* 7 (2012). doi:10.1371/journal.pone.0033005.
- [13] D. Zagzag, M. Esencay, O. Mendez, H. Yee, I. Smirnova, Y. Huang, L. Chiriboga, E. Lukyanov, M. Liu, E.W. Newcomb, Hypoxia- and Vascular Endothelial Growth Factor-Induced Stromal Cell-Derived Factor-1 $\alpha$ /CXCR4 Expression in Glioblastomas, *Am. J. Pathol.* 173 (2008) 545–560. doi:10.2353/ajpath.2008.071197.
- [14] S. Kenig, M.B.D. Alonso, M.M. Mueller, T.T. Lah, Glioblastoma and endothelial cells cross-talk, mediated by SDF-1, enhances tumour invasion and endothelial proliferation by increasing expression of cathepsins B, S, and MMP-9, *Cancer Lett.* 289 (2010) 53–61. doi:10.1016/j.canlet.2009.07.014.
- [15] V.R. Sinha, A. Trehan, Biodegradable microspheres for protein delivery., *J. Control. Release.* 90 (2003) 261–280. doi:10.1016/S0168-3659(03)00194-9.
- [16] H.K. Makadia, S.J. Siegel, Poly Lactic-co-Glycolic Acid (PLGA) as biodegradable controlled drug delivery carrier, *Polymers (Basel).* 3 (2011) 1377–1397. doi:10.3390/polym3031377.

- [17] D. Ding, Q. Zhu, Recent advances of PLGA micro/nanoparticles for the delivery of biomacromolecular therapeutics, *Mater. Sci. Eng. C*. 92 (2018) 1041–1060. doi:10.1016/j.msec.2017.12.036.
- [18] O. Dudeck, O. Jordan, K.T. Hoffmann, A.F. Okuducu, K. Tesmer, T. Kreuzer-Nagy, D.A. Rüfenacht, E. Doelker, R. Felix, Organic solvents as vehicles for precipitating liquid embolics: A comparative angiotoxicity study with superselective injections of swine rete mirabile, *Am. J. Neuroradiol.* 27 (2006) 1900–1906.
- [19] U. Bilati, E. Allémann, E. Doelker, Strategic approaches for overcoming peptide and protein instability within biodegradable nano- and microparticles, *Eur. J. Pharm. Biopharm.* 59 (2005) 375–388. doi:10.1016/j.ejpb.2004.10.006.
- [20] T.J. Gibson, K. Mccarty, I.J. Mcfadyen, E. Cash, P. Dalmonte, K.D. Hinds, A.A. Dinerman, J.C. Alvarez, D.B. Volkin, Application of a high-throughput screening procedure with PEG-induced precipitation to compare relative protein solubility during formulation development with IgG1 monoclonal antibodies, *J. Pharm. Sci.* 100 (2011) 1009–1021. doi:10.1002/jps.22350.
- [21] A.P. Yamniuk, N. Ditto, M. Patel, J. Dai, P. Sejwal, P. Stetsko, M.L. Doyle, Application of a kosmotrope-based solubility assay to multiple protein therapeutic classes indicates broad use as a high-throughput screen for protein therapeutic aggregation propensity, *J. Pharm. Sci.* 102 (2013) 2424–2439. doi:10.1002/jps.23618.
- [22] J.L. Riley, PD-1 signaling in primary T cells, *Immunol. Rev.* 229 (2009) 114–125. doi:10.1111/j.1600-065X.2009.00767.x.
- [23] J. Gong, A. Chehrazi-Raffle, S. Reddi, R. Salgia, Development of PD-1 and PD-L1 inhibitors as a form of cancer immunotherapy: A comprehensive review of registration trials and future considerations, *J. Immunother. Cancer.* 6 (2018) 1–18. doi:10.1186/s40425-018-0316-z.
- [24] J.A. Seidel, A. Otsuka, K. Kabashima, Anti-PD-1 and Anti-CTLA-4 Therapies in Cancer: Mechanisms of Action, Efficacy, and Limitations, *Front. Oncol.* 8 (2018) 1–14. doi:10.3389/fonc.2018.00086.
- [25] K. Woroniecka, P. Chongsathidkiet, K. Rhodin, H. Kemeny, C. Dechant, S. Harrison Farber, A.A. Elsamadicy, X. Cui, S. Koyama, C. Jackson, L.J. Hansen, T.M. Johanns, L. Sanchez-Perez, V. Chandramohan, Y.R.A. Yu, D.D. Bigner, A. Giles, P. Healy, G. Dranoff, K.J. Weinhold, G.P. Dunn, P.E. Fecci, T-cell exhaustion signatures vary with tumor type and are severe in glioblastoma, *Clin. Cancer Res.* 24 (2018) 4175–4186. doi:10.1158/1078-0432.CCR-17-1846.
- [26] J. Bianco, C. Bastiancich, N. Joudiou, B. Gallez, A. des Rieux, F. Danhier, Novel model of orthotopic U-87 MG glioblastoma resection in athymic nude mice, *J. Neurosci. Methods.* 284 (2017) 96–102. doi:10.1016/j.jneumeth.2017.04.019.
- [27] D. Dutta, K. Hickey, M. Salifu, C. Fauer, C. Willingham, S.E. Stabenfeldt, Spatiotemporal presentation of exogenous SDF-1 with PLGA nanoparticles modulates SDF-1/CXCR4 signaling axis in the rodent cortex, *Biomater. Sci.* 5 (2017) 1640–1651. doi:10.1039/c7bm00489c.
- [28] A.D. Gaudet, P.G. Popovich, Extracellular matrix regulation of inflammation in the healthy and injured spinal cord, *Exp. Neurol.* 258 (2014) 24–34. doi:10.1016/j.expneurol.2013.11.020.
- [29] N. George, H.M. Geller, Extracellular matrix and traumatic brain injury, *J. Neurosci. Res.* 96 (2018) 573–588. doi:10.1002/jnr.24151.
- [30] R. Würth, A. Bajetto, J.K. Harrison, F. Barbieri, T. Florio, CXCL12 modulation of CXCR4 and CXCR7 activity in human glioblastoma stem-like cells and regulation of the tumor microenvironment., *Front. Cell. Neurosci.* 8 (2014) 144. doi:10.3389/fncel.2014.00144.

- [31] V. Nand Yadav, D. Zamler, G.J. Baker, P. Kadiyala, A. Erdreich-Epstein, A.C. DeCarvalho, T. Mikkelsen, M.G. Castro, P.R. Lowenstein, CXCR4 increases in-vivo glioma perivascular invasion, and reduces radiation induced apoptosis: A genetic knockdown study, *Oncotarget*. 7 (2016) 83701–83719. doi:10.18632/oncotarget.13295.
- [32] C.B. Stevenson, M. Ehtesham, K.M. McMillan, J.G. Valadez, M.L. Edgeworth, R.R. Price, T.W. Abel, K.Y. Mapara, R.C. Thompson, CXCR4 expression is elevated in glioblastoma multiforme and correlates with an increase in intensity and extent of peritumoral T2-weighted magnetic resonance imaging signal abnormalities, *Neurosurgery*. 63 (2008) 560–569. doi:10.1227/01.NEU.0000324896.26088.EF.
- [33] A. Guyon, CXCL12 chemokine and its receptors as major players in the interactions between immune and nervous systems, *Front. Cell. Neurosci*. 8 (2014) 1–10. doi:10.3389/fncel.2014.00065.
- [34] J. Lipfert, V. Ödemis, D.C. Wagner, J. Boltze, J. Engele, CXCR4 and CXCR7 form a functional receptor unit for SDF-1/CXCL12 in primary rodent microglia, *Neuropathol. Appl. Neurobiol*. 39 (2013) 667–680. doi:10.1111/nan.12015.
- [35] S.-Y. Ho, T.-Y. Ling, H.-Y. Lin, J.T.-J. Liou, F.-C. Liu, I.-C. Chen, S.-W. Lee, Y. Hsu, D.-M. Lai, H.-H. Liou, SDF-1/CXCR4 Signaling Maintains Stemness Signature in Mouse Neural Stem/Progenitor Cells, *Stem Cells Int*. 2017 (2017) 1–14. doi:10.1155/2017/2493752.
- [36] V.A. Cuddapah, S. Robel, S. Watkins, H. Sontheimer, A neurocentric perspective on glioma invasion, *Nat. Rev. Neurosci*. 15 (2014) 455–465. doi:10.1038/nrn3765.
- [37] V. Montana, H. Sontheimer, Bradykinin Promotes the Chemotactic Invasion of Primary Brain Tumors, *J. Neurosci*. 31 (2011) 4858–4867. doi:10.1523/jneurosci.3825-10.2011.
- [38] P. V. Butte, A. Mamelak, J. Parrish-Novak, D. Drazin, F. Shweikeh, P.R. Gangalum, A. Chesnokova, J.Y. Ljubimova, K. Black, Near-infrared imaging of brain tumors using the Tumor Paint BLZ-100 to achieve near-complete resection of brain tumors, *Neurosurg. Focus*. (2014) E1. doi:10.3171/2013.11.FOCUS13497.
- [39] J. Parrish-Novak, K. Byrnes-Blake, N. Lalayeva, S. Burlison, J. Fidel, R. Gilmore, P. Gayheart-Walsten, G.A. Bricker, W.J. Crumb, K.S. Tarlo, S. Hansen, V. Wiss, E. Malta, W.S. Dernell, J.M. Olson, D.M. Miller, Nonclinical Profile of BLZ-100, a Tumor-Targeting Fluorescent Imaging Agent, *Int. J. Toxicol*. 36 (2017) 104–112. doi:10.1177/1091581817697685.
- [40] G. Cohen, S.R. Burks, J.A. Frank, Chlorotoxin—A multimodal imaging platform for targeting glioma tumors, *Toxins (Basel)*. 10 (2018) 1–12. doi:10.3390/toxins10120496.
- [41] C.G. Patil, D.G. Walker, D.M. Miller, P. Butte, B. Morrison, D.S. Kittle, S.J. Hansen, K.L. Nufer, K.A. Byrnes-blake, L.L. Lin, K. Pham, J. Perry, J. Parrish-novak, L. Ishak, Phase 1 Safety, Pharmacokinetics, and Fluorescence Imaging Study of Tozuleristide (BLZ-100) in Adults With Newly Diagnosed or Recurrent Gliomas, *Neurosurgery*. 0 (2019) 1–9. doi:10.1093/neuros/nyz004.
- [42] F. Ding, Y. Zhan, X. Lu, Y. Sun, Recent advances in near-infrared II fluorophores for multifunctional biomedical imaging, *Chem. Sci*. 9 (2018) 4370–4380. doi:10.1039/c8sc01153b.
- [43] G. Hong, S. Diao, J. Chang, A.L. Antaris, C. Chen, B. Zhang, S. Zhao, D.N. Atochin, P.L. Huang, K.I. Andreasson, C.J. Kuo, Through-skull fluorescence imaging of the brain in a new near-infrared window, *Nat. Photonics*. 8 (2014) 723–730. doi:10.1038/nphoton.2014.166.
- [44] C. Nieder, A.L. Grosu, L.E. Gaspar, Stereotactic radiosurgery (SRS) for brain

- metastases: A systematic review, *Radiat. Oncol.* 9 (2014) 1–9. doi:10.1186/1748-717X-9-155.
- [45] F. Müller-Riemenschneider, A. Bockelbrink, I. Ernst, C. Schwarzbach, C. Vauth, J.M.G. von der Schulenburg, S.N. Willich, Stereotactic radiosurgery for the treatment of brain metastases, *Radiother. Oncol.* 91 (2009) 67–74. doi:10.1016/j.radonc.2008.12.001.

# Annexes

**ANNEX 1: Review article accepted for publication in Frontiers in Pharmacology (date of acceptance: 15<sup>th</sup> of July 2019)**

---

**Reversing the tumor target: Establishment of a tumor trap**

Mathie Najberg<sup>1,2</sup>, Muhammad Haji Mansor<sup>1,3</sup>, Frank Boury<sup>1</sup>, Carmen Alvarez-Lorenzo<sup>2</sup>,  
Emmanuel Garcion<sup>1\*</sup>

<sup>1</sup>CRCINA, INSERM, Université de Nantes, Université d'Angers, Angers, France

<sup>2</sup>Departamento de Farmacología, Farmacia y Tecnología Farmacéutica, R + D Pharma Group (GI-1645), Facultad de Farmacia, Universidade de Santiago de Compostela, Santiago de Compostela, Spain

<sup>3</sup>Center for Education and Research on Macromolecules (CERM), Université de Liège, Liège, Belgium

\*Corresponding author

Email address: [emmanuel.garcion@univ-angers.fr](mailto:emmanuel.garcion@univ-angers.fr)

## Abstract

Despite the tremendous progress made in the field of cancer therapy in recent years, certain solid tumors still cannot be successfully treated. Alongside classical treatments in the form of chemotherapy and/or radiotherapy, targeted treatments such as immunotherapy that cause fewer side effects emerge as new options in the clinics. However, these alternative treatments may not be useful for treating all types of cancers, especially for killing infiltrative and circulating tumor cells (CTCs). Recent advances pursue the trapping of these cancer cells within a confined area to facilitate their removal for therapeutic and diagnostic purposes. A good understanding of the mechanisms behind tumor cell migration may drive the design of traps that mimic natural tumor niches and guide the movement of the cancer cells. To bring this trapping idea into reality, strong efforts are being made to create structured materials that imitate myelinated fibers, blood vessels, or pre-metastatic niches and incorporate chemical cues such as chemoattractants or adhesive proteins. In this review, the different strategies used (or could be used) to trap tumor cells are described and relevant examples of their performance are analyzed.

**Keywords:** Tumor cell migration, Tumor trap, Biomimetic trap, Cancer therapy, Premetastatic niche recruitment

## 1. Introduction

For many decades, surgery, radiotherapy and chemotherapy have served as the mainstay trident in the fight against cancer (Figure 1 Scheme I). During this period, the prognosis of many types of cancer has been significantly improved [1–4]. However, the widespread use of these treatments has also uncovered several major limitations. For example, the feasibility of surgery is very much dependent on the localization and the size of the tumor. The procedure is also contraindicated in patients with poor clinical performance. As for radiotherapy and chemotherapy, these treatments are often implicated with serious side effects that, in some cases, may outweigh their potential therapeutic benefits. Moreover, these treatments lack the capacity to prevent metastases, which are responsible for roughly 90% of cancer-associated deaths [5].

Numerous studies in the quest of improving cancer treatments are driven by the concept of “magic bullet” (Figure 1 Scheme II-2) put forward by the German scientist Paul Ehrlich [6]. If radio- and chemotherapy are considered as weapons of mass destruction, Ehrlich’s strategy can be regarded as the sniper of cancer therapy. This concept is mainly based on the idea of increasing the bioavailability and specificity of vector-associated active agents in the body, while limiting their premature degradation and toxicity. In the context of anti-cancer approaches, the success of selective therapies depends on the discovery of targeting elements that, when coupled with active ingredients and/or diagnostic cues, enable the recognition of well-characterized molecules, cells or tissues. For example, Adcetris<sup>®</sup> targets the antigen CD30 in the treatment of Hodgkin's lymphoma, and Kadcyla<sup>®</sup> targets HER2, which is present in about 20% of breast cancer patients [7]. Nevertheless, the discovery of appropriate targets that are specific to tumor cells remains a challenging task, despite the significant advancements made in the field of genomics and proteomics in recent decades.

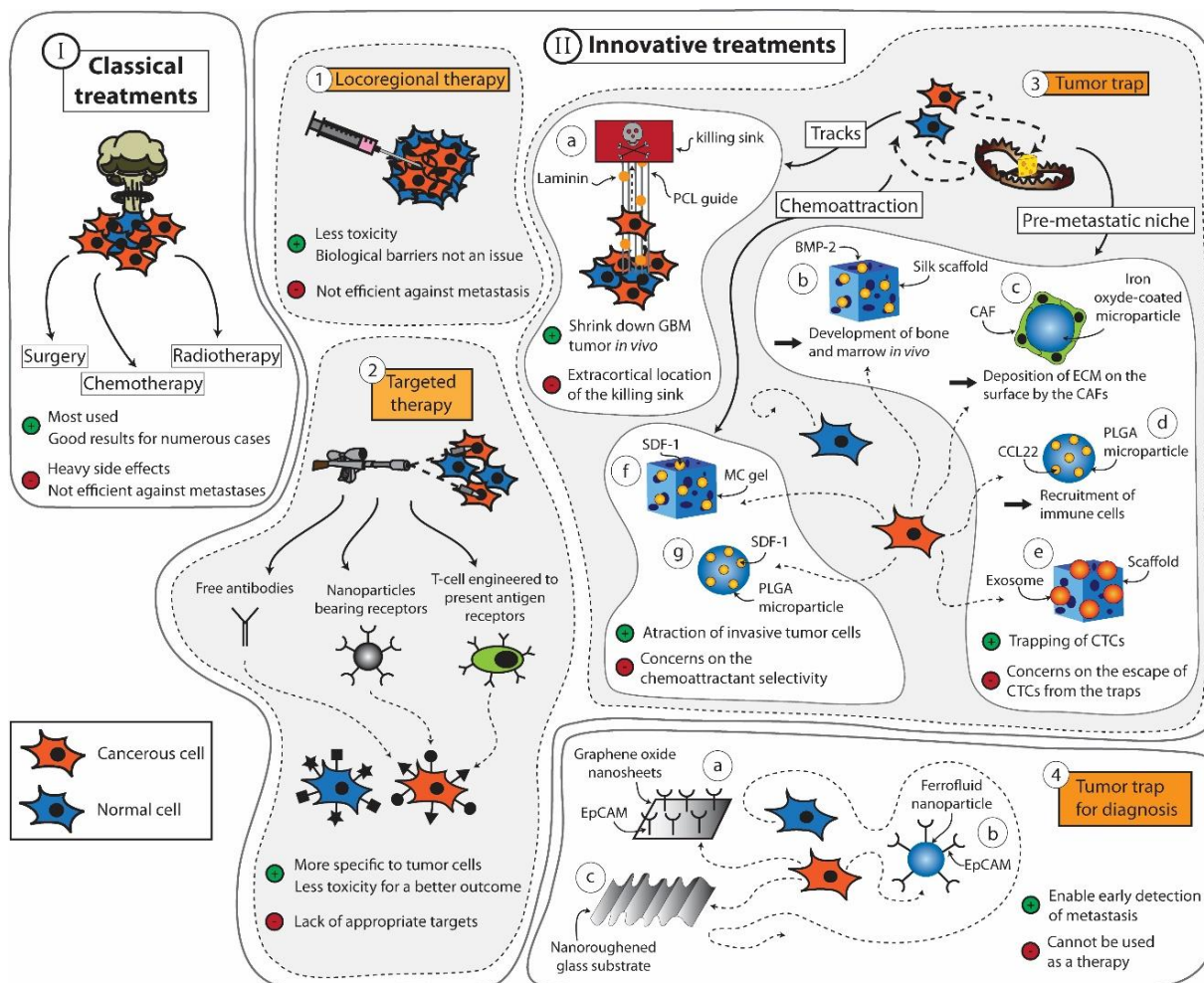


**Figure 1:** Summary of the strategies that can be applied to fight cancers. (Scheme I) The classical treatments used for cancers are surgery, chemotherapy and radiotherapy. (Scheme II) Innovative treatments include (1) locoregional therapy, (2) targeted therapy and (3) tumor traps, among others. Tumor traps can be designed to take advantage of the migration pathways used by the tumor cells. It includes the use of tracks ((a) system developed by Jain *et al.* [8] using aligned PCL fibers coated with laminin). Tumor traps can be designed as synthetic pre-metastatic niches ((b) system developed by Seib *et al.* [9] using a silk scaffold loaded with bone morphogenic protein 2 (BMP-2) capable of developing bone and marrow *in vivo*, (c) system developed by De Vlieghere *et al.* [10] using iron oxide-coated microparticles encapsulating cancer-associated fibroblasts (CAFs) that deposit continuously ECM on the surface, (d) system developed by Azarin *et al.* [11] using poly(lactide-co-glycolic acid) (PLGA) through the induction of the immune system by the CCL22 chemokine, and (e) system developed by De la Fuente *et al.* [12] using a 3D scaffold loaded with exosomes). Finally, tumor traps can use chemoattractive molecule ((f) system developed by Giarra *et al.* [13] using a methylcellulose (MC) thermo-responsive hydrogel loaded with stromal derived factor-1 (SDF-1), and (g) the system developed by Haji Mansor *et al.* [14] using SDF-1 encapsulated in PLGA nanoparticles). (4) Tumor traps can also be used for the early detection of metastasis ((a) system developed by Yoon *et al.* [15] using graphene oxide nanosheets, (b) CELLSEARCH<sup>®</sup> CTC test [16] is a device using ferrofluid nanoparticles with EpCAM antibodies, and (c) system developed by Chen *et al.* [17] using a nanoroughened glass substrate).

Fortunately, a plethora of new therapies are being regularly approved for the treatment of cancer. Among them is the use of locoregional therapies (Figure 1 Scheme II-1) which includes Nanotherm<sup>®</sup> (MagForce) that involves injection of magnetic nanoparticles inside the tumor or into the resection cavity. A magnetic field is then applied to generate heat via the nanoparticles and kill the cancerous cells locally [18]. It is currently licensed in Europe for the treatment of brain tumors and has received FDA approval in February 2018 to be used in clinical trials involving prostate cancer patients [19]. Another example is Optune<sup>®</sup> (Novocure Ltd), a tumor-treating field (TTF) device composed of electrodes that can be placed on the patients' scalp and connected to a generator to deliver a low intensity electric field of 200 kHz [20]. It is believed to exert anti-cancer effects by disrupting the division of tumor cells [21]. The device has been approved for the treatment of glioblastoma and shown to increase the median survival from 15 months to 21 months when used on top of the standard treatments for this cancer [22]. However, many countries and insurance companies do not cover the cost of this treatment and the clinical adoption of this technology remains limited due to concerns regarding the lack of understanding of the device's exact mechanism of action. Moreover, some skepticism exists toward the legitimacy of the device approval process due to the poor consideration of any placebo effects during the clinical trial phase [23].

Among the numerous classes of novel anti-cancer treatments entering the market, cancer immunotherapy is arguably the one that is currently attracting the highest level of attention (Figure 1 Scheme II-2). This class of treatment aims to treat cancer through artificial stimulation of the patient's immune system [24]. The most cutting-edge subset of this type of treatment is the chimeric antigen receptor (CAR) T-cell immunotherapy, which involves harvesting T-cells from a patient and genetically modifying these cells to express a receptor that can bind to a tumor antigen before injecting them back into the patient [25]. CAR-T cell immunotherapy made its debut in the clinic in August 2017 when Kymriah<sup>®</sup> (Novartis) was approved by the FDA for the treatment of B-cell acute lymphoblastic leukemia (BCALL) [26]. This was followed by the approval of Yescarta<sup>®</sup> (Gilead Sciences) in October the same year for the treatment of diffuse large B-cell lymphoma [27]. Both Kymriah<sup>®</sup> and Yescarta<sup>®</sup> exert their effects by targeting CD19 antigen [28]. However, there are numerous ongoing clinical studies that explore the feasibility of targeting other antigens including PD-L1 (ClinicalTrials.gov Identifier NCT03672305, NCT03198052, NCT03330834), EpCAM (ClinicalTrials.gov Identifier NCT03013712, NCT03563326, NCT02729493), and CD123 (ClinicalTrials.gov Identifier NCT03796390, NCT02937103, NCT03672851). Many of these

trials also attempt to evaluate the efficacy of CAR-T cell immunotherapy against solid tumors to expand its indication beyond certain blood cancers. More comprehensive reviews on the current status and future directions of CAR T-cell immunotherapy as well as other subsets of cancer immunotherapy such as immune checkpoint inhibitors and cancer vaccines can be found elsewhere [29–31].

Despite the continuous increase in the number of novel anti-cancer treatments entering the clinic, local recurrence in previously healthy tissues seen in many cases of solid tumors remains an unsolved conundrum among clinicians and researchers alike. Development of new therapies for *in situ* control of the disease, while avoiding the problems of biological barriers and systemic toxicity, still proves to be a formidable task. Thus, in parallel to the innovative approaches mentioned above, the idea of trapping infiltrative or circulating tumor cells (CTCs) within a confined area to facilitate their removal for therapeutic or diagnostic purposes has risen (Figure 1 Scheme II-3,4). Over the last years, this concept has developed progressively. The aim is two-fold: (a) to avoid the uncontrolled dissemination of tumor cells and (b) to efficiently prevent the phenomenon of epithelial-mesenchymal transition (EMT) or development of metastases. The concept is largely inspired by the “ecological trap” theory [32]. By considering cancers as ecosystems, it is possible to develop tumor traps not only for the infiltrative tumor cells, but also for the CTCs that are responsible for metastasis. However, imitating the traditional features of a natural habitat or niche for tumor cells and directing their migration pathways presents numerous physical and biological challenges. The focus of this review will be on understanding the mechanisms of tumor cell migration and how this knowledge can be used to capture them, keeping in mind that different tumors are likely to utilize different mechanisms.

## 2. Migration of tumor cells

Tumor cells must cover a great distance on their journey to form metastases (Figure 2). The first step of the process is to migrate away from the primary tumor. Tumor cells can follow aligned tracks [33], or gradients of chemoattractant in solution (chemotaxis) [34] or fixed on a substrate (haptotaxis) [35] through the extracellular matrix (ECM). The second step is to intravasate into the bloodstream or the lymphatic system in which the tumor cells will transit through the circulation. Third, cells extravasate to secondary tissues once they reach a location where they can adhere to the walls of the vessel [36]. The fourth and final step deals with the

formation of a secondary tumor. This only occurs if the environment is favorable to tumor growth [37].

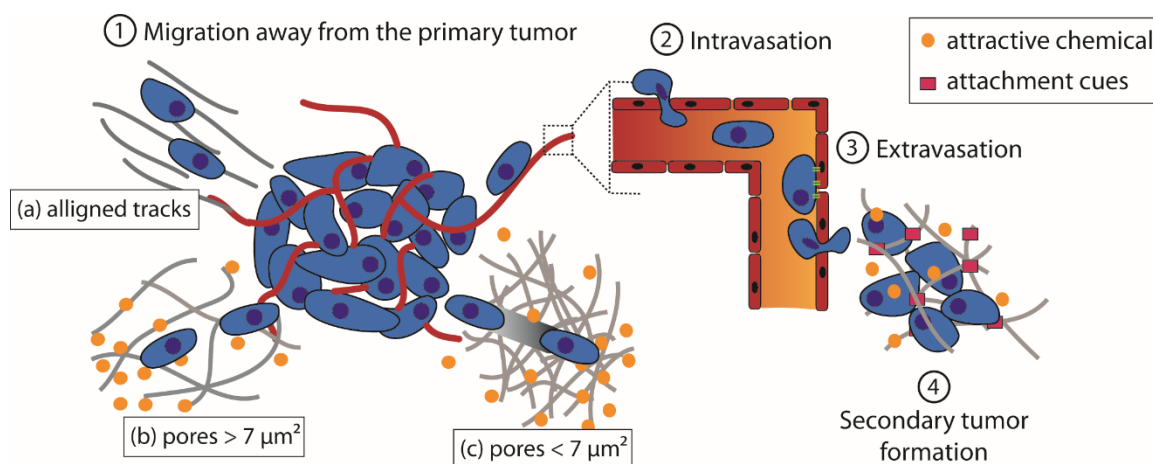


**Figure 2:** Schematic representation of theorized paths of cancer metastasis (1) Migration away from the primary tumor; tumor cells can follow (a) aligned tracks, or (b) gradients of chemoattractant in solution (chemotaxis) or fixed on a substrate (haptotaxis) through the ECM. Matrix degradation is not needed if the pore size is more than  $7 \mu\text{m}^2$  (b), otherwise, matrix metalloproteinase (MMP)-dependent ECM remodeling is essential (c). (2) Intravasation of tumor cells into the blood or lymphatic stream and (3) subsequent extravasation. (4) If the environment is favorable, a secondary tumor grows.

The different strategies implemented to mislead these cells into a trap are described in the following sections. These strategies exploit the current knowledge on cancer cell migration and metastasis and the specificities of each type of tumor.

## 2.1. Migration away from the primary tumor

The physical interactions between the ECM and cancer cells play a key role in allowing the cells to start migrating. Cancer cells may undergo an EMT to acquire a motile phenotype [38]. This translates into the loss of intracellular adhesion molecules such as E-cadherin and cytokeratins, resulting in detachment of the cells from the primary tumor, and an overexpression of MMP on their surface that allows the cells to digest laminin and collagen IV to progress in the dense ECM [38]. These changes are thought to be related to the stiffness of the matrix around the tumor, which is of higher values than that of normal tissues [39–42]. For example, the stiffness of GBM tissues is of  $\sim 25$  kPa while normal brain tissues have a stiffness of 0.1 to 1 kPa [43]. Wang *et al.* investigated the effect of matrix stiffness on GBM cells and found that an increase in matrix rigidity could induce an upregulation of MMP-1, Hras, RhoA and ROCK1 [43], which are involved in increasing cell motility [44–47]. Another physical

factor that governs the dissemination of cancer cells is the architecture of the extracellular environment, which includes pores of a diameter ranging from less than 1  $\mu\text{m}$  to 20  $\mu\text{m}$  [48]. Matrix degradation is usually required for cancer cell migration to occur when the cross-sectional area of the interfibrillar pore is less than 7  $\mu\text{m}^2$ , which corresponds to about 10% of the nuclear cross-section of cancer cells [49]. Above this value, cells can undergo deformation to migrate through the ECM.

Apart from the porosity of the ECM, the spatial arrangement of the matrix fibers near the primary tumor sites can also influence the motility of tumor cells; aligned fibers offer tracks that are more conducive to migration [50,51]. These tracks are found along the ECM fibers in the interstitial space, between the muscle and nerve fibers, and along or within the vasculature of organs, among others [52]. Moreover, it has been observed that leader tumor cells are able to align collagen fibers to assist the migration of the following cells [53]. In addition to creating the required physical space, these tracks also facilitate cancer cell migration by providing relevant molecular guidance. For example, cancer cells can be guided towards laminin and hyaluronan molecules in the ECM by their integrins and CD44 receptors respectively, and also via haptotaxis by chemokines and growth factors immobilized along the tracks [52,54]. Jain *et al.* took inspirations from these biological phenomena and designed a scaffold to guide GBM cells toward a killing sink in an extracortical location (Figure 1 Scheme II-3-a) [8]. They utilized aligned poly-L-lysine and laminin-coated polycaprolactone (PCL) nanofibers (10  $\mu\text{m}$  thick) encased in a PCL / polyurethane support (2.4 mm diameter) to imitate the white matter tracts [55,56]. The killing sink was composed of a collagen-based hydrogel conjugated to the chemotherapeutic agent cyclophosphamide. With this approach, the tumor mass of induced GBM in mice could be reduced. However, despite the positive results, this strategy as itself has limited clinical appeals as the establishment of an extracortical sink in human patients may invite numerous technical difficulties. Instead, exploiting the local (intracortical) migration of the cancer cells may be a more translatable strategy to develop an efficient tumor trap for this cancer.

## 2.2. Intravasation and tumor cell circulation

Tumor cells can circulate through the blood and lymphatic vessels on their journey to form a secondary tumor distant from the primary site [57]. This requires the cells to intravasate by passing through the endothelial cell junctions. Intravasation into the blood vessels occurs frequently due to the leaky nature of tumor vasculature. In addition, it has been observed *in*

*in vivo* that metastatic cells are able to polarize toward blood vessels. A possible explanation to this phenomenon is that these cells have an increased expression of epidermal growth factor (EGF) and/or colony-stimulating factor 1 (CSF-1) receptors. Thus, they migrate toward a gradient of EGF or CSF-1 released by the macrophages lining the blood vessels [58,59]. However, it is still easier for tumor cells to enter the lymphatic system as the surrounding ECM network is easier to penetrate and that the endothelial junctions are looser [60]. Either route can lead to blood vessel dissemination since the lymphatic circulation drains into the blood. As the lymphatic fluid is filtered by the lymph nodes, tumor cells are invariably invading them, starting with the nearest [61].

Once in the blood circulation, the trajectory of the tumor cells is influenced by the blood flow, the diameter of the blood vessels and the intercellular adhesion force [37]. Two mechanisms can lead to the arrest of a CTC: physical occlusion and cell adhesion (Figure 3). Physical occlusion occurs when the diameter of the blood vessel is smaller or equal to the one of the CTC (usually around 10  $\mu\text{m}$ ). This has been observed in the brain by real-time imaging in a mouse model [62]. Adhesion of CTCs to the vessel walls occurs when there is a balance between the adhesion force and the shear force exerted inside the blood vessel [63]. When the shear force increases, the collisions between cells and the vessel wall increases, which in turn enhances the likelihood of cell adhesion. However, if the shear force is too high, turbulences may prevent the adhesion.

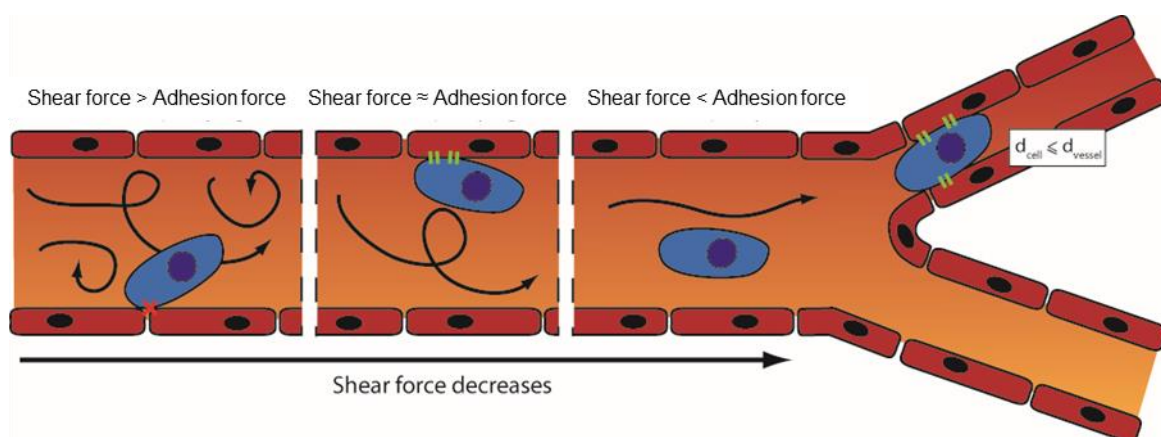


**Figure 3:** Mechanisms of arrest of a CTC: the influence of the shear force and the blood vessel diameter on the site of CTC extravasation.

It is therefore possible to capture CTCs by designing a device with strong adhesive cues. Yoon *et al.* [15] designed a microfluidic device consisting of graphene oxide nanosheets fixed onto a patterned gold surface to capture CTCs in early-stage cancer for analytical purposes (Figure

1 Scheme II-4-a). The nanosheets were functionalized with epithelial cell adhesion molecule (EpCAM) antibody to capture CTCs. Blood samples were retrieved from healthy donors and mixed with labeled human breast cancer cell lines MCF-7 and Hs-578T and the human prostate cancer cell line PC-3. This microfluidic device captured more than 70% of the cancer cells in the prepared blood sample with high specificity. A similar principle was also implemented in the design of CELLSEARCH<sup>®</sup> CTC Test, the first and only clinically validated and FDA approved blood test for enumerating CTCs [64]. It allows for early assessment of patient prognosis as well as follow up of the patient. The test constitutes the use of ferrofluid nanoparticles with EpCAM antibodies that bind to CTCs (Figure 1 Scheme II-4-b). Once magnetically separated from the rest of the blood sample, cells are stained to discriminate CTCs from leukocytes that can co-present in the sample. Working within the same domain of research, Chen *et al.* [17] designed a nanoroughened glass substrate to capture CTCs based on their stronger adhesion capacity compared to normal blood cells (Figure 1 Scheme II-4-c). Such a working principle makes this device useful for capturing CTCs regardless of their surface marker expression profile, which is known to vary according to the type of cancer, patient demographics and the state of the disease. It is indeed well-discussed in the literature that the EMT process may lead to reduction in the EpCAM expression in CTC [65]. The capture of CTC using EpCAM antibody alone may lead to an underestimation of the CTC number in the blood. With this device, more than 80% of cancer cells in whole blood samples from mice with induced breast cancer or lung cancer were captured independently of their EpCAM expression. Based on these findings, it is evident that a number of approaches can be adopted to capture CTCs to enable early detection of metastasis although most of them are still far from translation to the clinic.

### 2.3. Extravasation and secondary tumor formation

At the end of their time in blood circulation, the CTCs that survived and adhered to the blood vessel walls extravasate and a fraction of these proceeds to form a secondary tumor. It has been shown experimentally that only about 0.01% of the cells in the circulation system eventually contribute to metastatic colonization [66]. The location at which they stop and grow into a secondary tumor is not believed to be randomly-determined, and the reasons driving the selection of a particular site are still being investigated. In 1889, Paget *et al.* hypothesized that metastasizing cancer cells are like seeds that can only grow in the proper soil [67]. Indeed, it has been observed that invasive cancer cells tend to migrate toward certain preferred sites of metastasis; a phenomenon that has been coined as “tissue tropism” [9]. More recent studies

revealed that the formation of certain microenvironments termed as pre-metastatic niches is crucial to the subsequent formation of metastatic tumors. These microenvironments consist of inflammatory immune cells, stromal cells, ECM proteins, tumor-secreted exosomes and homing factors [68]. Tumor-secreted exosomes are sent to prime the niche at a target organ (often lungs, liver, brain, bone and lymph nodes) by attracting bone marrow-derived cells (BMDCs) as well as increasing the proliferation of fibroblast-like stromal cells [69]. BMDCs include CD11b<sup>+</sup> myeloid cells, myeloid-derived suppressor cells, neutrophils, tumor-associated macrophages and regulatory T cells. They are known to create an attractive site for metastasizing cells and the presence of VEGFR1-positive BMDCs can serve as a predictor for the arrival of tumor cells [70]. Moreover, the establishment of a pre-metastatic niche is associated with an increased secretion of inflammatory cytokines and chemokines [71–73]. The increasing understanding of the pre-metastatic niches and their roles in welcoming metastatic dissemination has inspired scientists to create synthetic niches as a means to trap migrating cancer cells.

### **2.3.1. Creation of a synthetic pre-metastatic niche to trap CTCs**

Many different strategies have been explored to engineer pre-metastatic niches. For example, Seib *et al.* [9] developed a tumor trap for the metastasizing cells of breast and prostate cancer by imitating the red bone marrow microenvironment (Figure 1 Scheme II-3-b). The strategy was adopted based on the knowledge that the bone was the preferred site of colonization in more than 60% cases of metastasis for primary breast cancer and 73% for primary prostate cancer [74]. Evidence shows that red bone marrow attracts migrating cancer cells via chemotaxis with stromal derived factor-1 (SDF-1) [75] and CXCL16 [76]. It also provides adhesion sites that interact with tumor cell surface molecules such as annexin2 [77], growth arrest-specific 6 (GASP-6) [78], CD44 [79], integrins (such as VLA-4, VLA-5 and LFA-1) and cadherins. Moreover, the bone marrow microenvironment is composed of osteoblasts, osteoclasts, stromal cells, stem cells and mineralized bone marrow surrounded by a rich vascular bed, making it a perfect site for tumor growth [80]. To imitate the red bone marrow, Seib *et al.* designed a silk fibroin scaffold loaded with bone morphogenetic protein 2 (BMP-2) capable of developing bone and marrow *in vivo*. After implantation into the mammary fat pads of mice with induced breast or prostate tumor, no effect on the primary tumor growth was observed. However, metastatic growth could be seen taking place in the functionalized scaffolds, suggesting that it is possible to lure metastasizing cells into a trap by imitating the bone marrow microenvironment. A similar strategy was adopted by Bersani *et al.* [81]. They

utilized a polyacrylamide hydrogel coated with bone marrow stromal cells (BMSCs), which was able to capture metastasizing cells of prostate cancer.

De Vlieghere *et al.* [10] took a slightly different approach to mimic a pre-metastatic niche by developing traps made of iron oxide-coated microparticles encapsulating metabolically active CAFs (Figure 1 Scheme II-3-c). The CAFs continuously deposited ECM composed of type I collagen and tenascin C, among others, creating an adhesive environment for disseminated cancer cells. The microparticles were implanted into the peritoneal cavities of mice with induced ovarian cancer. 24 hours after the implantation, the microparticles were magnetically removed and the adhesion of cancer cells on the microparticles was assessed. The treatment led to a delay in peritoneal metastasis and prolonged the animal survival.

Another variation in the strategy for recruiting metastasizing cancer cells was presented by Azarin *et al.* [11]. They developed a microporous scaffold from poly(lactide-co-glycolic acid) (PLGA) scaffold for *in vivo* capture of metastasizing breast cancer cells through the induction of a local immune response (Figure II-3-d). Indeed, it has been shown that immune cells are implicated in tumor cell recruitment [82,83]. Here, they have either recruited immune cells into the scaffold by grafting the chemokine CCL22, which is known to induce migration of immune cells but not tumor cells, or incorporated the Gr1<sup>hi</sup>CD11b<sup>+</sup> immune cells directly into the PLGA scaffold. By doing this, they were able to reduce the number of breast cancer cells that metastasized to the lung by 88%. Similarly, Rao *et al.* [84] designed a PCL-based device with a slower degradation rate than PLGA scaffolds and investigated the immune response induced at the implantation site, the ability of the device to recruit metastatic cells for detection prior to colonization of organs as well as its influence on the survival of mice with induced breast cancer. Pelaez *et al.* [85] further developed the strategy to enable the elimination of the attracted metastatic cells by non-invasive focal hyperthermia. To do so, they coupled metal discs to PCL microparticles to allow heat generation through electromagnetic induction using an oscillating magnetic field. The heat generation could be modulated conveniently by changing the size of the disc or the type of metal.

It has been shown that exosomes, which are vesicles involved in the transfer of information between cells, play a role in homing CTCs in the pre-metastatic niche [69]. De la Fuente *et al.* [12] harnessed the potential of this knowledge and designed a 3D scaffold with embedded exosomes extracted from the ascitic fluid of ovarian cancer patients (Figure 1 Scheme II-3-e). The scaffold, called M-Trap, was implanted in the inner wall of the peritoneum of mice with a

xenograft of human ovarian cancer in the peritoneal cavity. They showed that the scaffold could serve as the preferred site of metastasis while a peritoneal carcinometastasis was observed in the absence of the M-Trap. Moreover, an increase in the mean survival was observed in the presence of the M-Trap (from 117.5 to 198.8 days), which was further improved by the removal of the scaffold (mean of survival of 309.4 days). The safety and performance of the M-Trap is currently being evaluated in a clinical trial involving female patients with stage IIIC ovarian cancer (ClinicalTrials.gov Identifier NCT03085238).

### 2.3.2. Chemoattraction of tumor cells

Migrating cells can make directional choices when presented with different migration pathways. *In vitro*, it has been shown that neutrophil-like cells can navigate through a microfabricated maze by following a chemical gradient [86]. Chemokines and their receptors are particularly involved in this navigation process. They are indeed responsible for the chemoattraction of various cells and could therefore be used to attract migrating tumor cells into a trap. Several receptors/chemokines have been identified to facilitate cancer cell migration. The most investigated one is SDF-1, also called CXCL12, which binds with high affinity to the CXCR4 and CXCR7 receptors. This chemokine is a pro-inflammatory mediator and is known to play a role in the recruitment of T cells, monocytes and lympho-hemopoietic progenitor cells [87]. Its overexpression has been linked to an increase in the invasiveness of ovarian cancer [88], breast cancer [89,90] and GBM [91,92], among others (further details can be found elsewhere [93]). In addition, despite being less well-studied, CXCL16 and its receptor CXCR6 are also suspected to play a role in the migration of tumor cells. Wang *et al.* [94] have shown that the expression of CXCR6 increases with the grade of prostate cancer. These results were supported by Lu *et al.* [95] who observed that metastatic cells from prostate cancer over-express the CXCR6 receptor. Moreover, CXCL16 have been shown to induce the migration and enhance the proliferation of CXCR6-expressing cancer cells *in vitro* [73].

With this knowledge, several groups have tried to stop the migration of tumor cells by inhibiting chemokine receptors, particularly the CXCR4 receptor. A reduction in the migration of cancer cells has been observed *in vitro* [72,96,97]. However, this has not been successfully replicated *in vivo*. Brennecke *et al.* found that the use of CXCR4 antibody 12G5 can reduce the number of osteosarcoma pulmonary metastases having a diameter of <0.1 mm but not those of larger dimensions [72]. This finding can be explained by the fact that chemoattraction of cancer cells can be mediated by several pairs of chemokine-receptor interaction (for example, SDF-1

can bind either CXCR4 or CXCR7 or both and CXCR6 can be activated by CXCL16). In addition, cells can activate the so-called compensation mechanisms *in vivo* to maintain their migration capacity. Indeed, it has been observed that neural progenitor cells (NPCs) are able to migrate in response to SDF-1 via the activation of the CXCR7 receptor in response to the blockade of the CXCR4 receptor [98]. Therefore, in order to stop the migration of tumor cells completely, all receptors implicated in *in vivo* chemoattraction should be identified and blocked, making the task nearly impossible. Moreover, this strategy could only work if the tumor cells have yet to begin migrating. In the particular case of GBM, cancer cells usually have already invaded the surrounding tissues at the time of diagnosis [56]. Thus, it may be more useful to direct the migration of cells toward a desired location instead of blocking the migration process altogether.

Chemokines are already being used to attract cells into a scaffold for regenerative medicine purposes. The tumor trap concept can benefit from the existing knowledge in this field of application. Water-retaining polymer networks such as hydrogels and swellable matrices, which have been widely-used in tissue engineering and regeneration, are pivotal platforms that are transferrable to the tumor trap application. For this purpose, biocompatible polymers capable of *in situ* formation of three-dimensional gels [99–101] or matrices [10,11,15,102–104] may be used to exert chemotaxis (based on a gradient of soluble attractant or repellent) or haptotaxis (based on a gradient of substrate-bound extracellular matrix proteins) (Figure 4). Of particular interest is the potential exploitation of the CXCR4-SDF-1 axis due to its prominent roles in regulating the migration of many types of cancer cells [99,100,105,106]. Examples of biomaterials used to deliver SDF-1 for regenerative medicine are presented in Table 1. Recently, the development of SDF-1-releasing scaffolds to attract tumor cells has received increasing attention. Giarra *et al.* [13], designed a temperature-responsive gel loaded with SDF-1 based on methylcellulose (MC) or poloxamers with or without hyaluronic acid (HA) for the purpose of attracting CXCR4-expressing GBM cells (Figure 1 Scheme II-3-f). Haji Mansor *et al.* [14], on the other hand, encapsulated the chemokine in nanoparticles composed of PLGA and a (PEG)-PLGA co-polymer to achieve sustained release (Figure 1 Scheme II-3-g). However, in both papers, no *in vivo* assessment of the ability of SDF-1 to attract migrating cancer cells was performed.

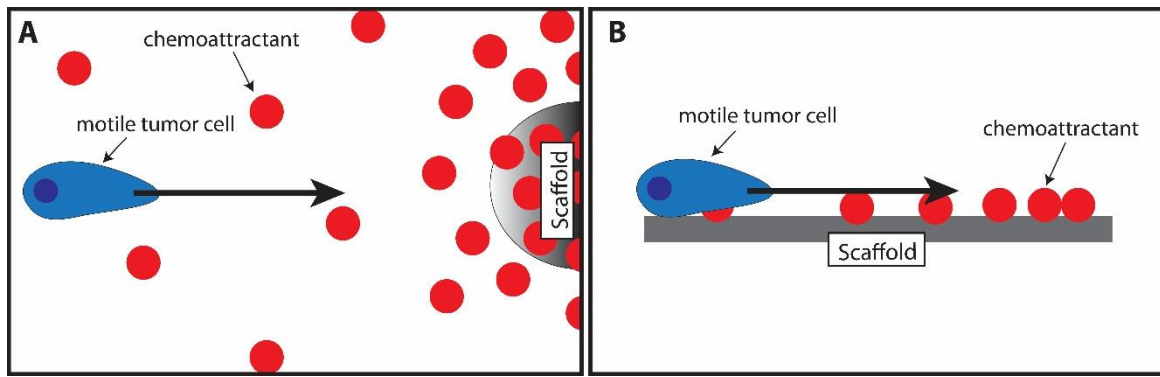


**Figure 4:** Illustration of the use of scaffolds to attract motile tumor cells by chemotaxis (A) or haptotaxis (B).

**Table 1:** Strategies to load SDF-1 into different biomaterials

<b>Bonding strategy</b>	<b>Type of biomaterial</b>	<b>Composition</b>	<b>Target site for regeneration</b>	<b>Ref</b>
<b>Adsorption</b>	Hydrogel	hyaluronic acid PPCN	Cardiac tissue	[107]
			Wound healing	[108]
	3D scaffold	collagen	Cartilage	[109]
			Tendon	[110]
			Bone	[111]
			Bone	[112]
			Muscle	[113]
			Bone Cartilage	[114] [115]
Membrane	PCL/gelatin	Bone	[116]	
<b>Immobilization through specific heparin-mediated interaction</b>	Hydrogel	heparin/PEG	Cardiac tissue	[117]
			Blood vessel	[118]
			Cardiac tissue	[119]
	3D scaffold	heparin/PLCL heparin/PGS heparin/PLLA	Blood vessel	[120]
			Blood vessel Blood vessel	[121] [122]
<b>Systems with nano/microparticles</b>	Microspheres	alginate	Bone	[123]
	Hydrogel/ Nanoparticles	hydrogel: CS/GP nano: CS/CMCS	Bone	[124]
	Microcapsules	Dex-GMA/gelatin/ PNIPAAm	Wound healing	[125]
	Particles	PLGA	Cardiac tissue	[126]

PPCN: Poly (polyethylene glycol citrate-co-N-isopropylacrylamide); PLA: polylactide; PLGA: poly(lactic-co-glycolic) acid; PCL: polycaprolactone; PEG: poly(ethylene-glycol); PLCL: poly(L-lactide- co-e-caprolactone) (PLCL); PGS: poly(glycerol sebacate); PLLA: poly(l-lactic acid); CS: chitosan; GP: beta-glycerol phosphate disodium salt; CMCS: carboxymethyl-chitosan; Dex-GMA: glycidyl methacrylated dextran; PNIPAAm: poly(N-isopropylacrylamide)

## 2.4. Challenges associated with the clinical translation of the tumor trapping strategy

While promising preclinical results have been obtained from the use of tumor traps as a diagnostic and/or therapeutic tool, there are multiple issues that must be addressed before this approach can enter the clinic. Main concerns include identifying suitable means for *in vivo* monitoring of the recruitment of cancer cells into the scaffolds to allow one to decide on the optimal timepoint for killing the trapped cancer cells. Prolonged duration of cancer cell recruitment may lead to overcrowding of the tumor trap and subsequent cell escape, reducing the purpose of the synthetic niche to merely a “relay” for the cancer cells en route to their natural metastatic sites.

The incorporation of chemoattractant molecules such as SDF-1 into the tumor trap may also introduce additional complexities. In particular, there are concerns regarding the selectivity of SDF-1-mediated chemotaxis. Indeed, in addition to its role in recruiting cancer cells to local and distant sites of colonization, SDF-1 is also implicated in the homing of other cell lines such as immune cells and stem cells [87,111,115]. Moreover, the potential off-target effects may also be exacerbated by the fact that this chemokine is known to be involved in various processes that support tumor progression, angiogenesis, metastasis and survival [127]. It is therefore necessary to study in more detail the effect of injecting such proteins near tumor cells *in vivo* and to carefully evaluate the entire risks before moving to the clinic.

Further down the development timeline, the most effective way to kill the recruited cancer cells should be elucidated. It may be tempting to suggest direct removal of the trap to achieve an immediate eradication of the disease. However, this approach will necessitate an additional surgery, a requirement that may be very difficult to fulfil especially in patients who are terminally ill. A less invasive solution would be to use stereotactic radiotherapy (SRT). SRT is a treatment where radiation beam is directed to a well-defined spot, usually the tumor site, from many different angles around the body. The procedure ensures the targeted site receives much higher dose of radiation than the surrounding tissues. At the moment, SRT seems to be a viable option for killing the trapped cancer cells. This said, other selective approaches should also be considered and evaluated.

### 3. Conclusion

A good understanding of the escape pathways of a prey allows the hunter to capture it more efficiently. The same rule of thumb can be applied to tumor cells. Using this principle, it is possible to design tumor traps for diagnostic and/or therapeutic applications. For the latter purpose, it is necessary that the trapped cells are killed by the application of existing therapies. The different therapeutic strategies (surgery, chemotherapy, targeted therapy, ...) may not be sufficient on their own to cure every cancer type but they can be used in combination to achieve the best clinical outcomes. Jain *et al.* used a chemotherapeutic agent in the form of cyclophosphamide alongside their tumor trap to shrink down the size of GBM tumors [8]. It would also be interesting to combine the trap with radiosensitizers, focus x-ray or  $\gamma$ -ray microbeams. Since the trap would concentrate the tumor cells, the efficiency of chemo- and radio-therapies can potentially be improved while the associated side effects are likely to decrease. Immunotherapy, which can be broadly-described as the activation of immune cells to make them able to recognize and eliminate tumor cells, could also be used. Indeed, one of the major difficulties in immunotherapy is to make the cancer cells accessible to the activated immune cells. This is particularly true in the brain as there is a need to overcome the blood-brain barrier [128]. If immune cells can be pre-loaded or attracted into the trap via chemoattraction, this will facilitate the killing of the trapped cancer cells. Indeed, immune cells are also sensitive to a gradient of chemokines such as SDF-1 [118] and can therefore be recruited into the trap together with the cancer cells of interest. Overall, this bio-integrative approach can be seen as counter-intuitive insofar as the factors governing the trapping of tumor cells are also involved in other signaling pathways that may lead to effects that are opposite to the initial will [129]. Our current knowledge on the mechanisms driving the migration of cancerous cells might not be sufficient to develop a trap that only impact tumor cells in a safe manner. The translation to the clinic will therefore require further investigations on the efficacy and safety of such systems. Nevertheless, as Albert Einstein pointed out, "we do not solve problems with the modes of thought that have engendered them" and this unique approach therefore deserves further investigations.

## 4. Acknowledgements

This work was supported by the “Institut National de la Santé et de la Recherche Médicale” (INSERM), the University of Angers (Angers, France), the MINECO (SAF2017-83118-R), by the Agencia Estatal de Investigación (AEI, Spain) and by the Federación Española de Enfermedades Raras (FEDER). It is also related to the LabEx IRON “Innovative Radiopharmaceuticals in Oncology and Neurology” as part of the French government “Investissements d’Avenir” program, to the INCa (Institut National du Cancer) MARENGO consortium “MicroRNA agonist and antagonist Nanomedicines for GliOblastoma treatment: from molecular programming to preclinical validation through the PL-BIO 2014-2020 grant and to the MuMoFRaT project “Multi-scale Modeling & simulation of the response to hypo-Fractionated Radiotherapy or repeated molecular radiation Therapies” supported by “La Région Pays-de-la-Loire” and by the Cancéropôle Grand-Ouest (tumor targeting and radiotherapy network). Najberg was a Ph.D. student involved in the Erasmus Mundus Joint Doctorate program for Nanomedicine and pharmaceutical innovation (EMJD NanoFar) and received a fellowship from “La Région Pays-de-la-Loire”.

## 5. References

- [1] G. Iacobucci, Cancer survival in England: rates improve and variation falls, *BMJ*. 365 (2019) 11532. doi:10.1136/bmj.11532.
- [2] H. Zeng, W. Chen, R. Zheng, S. Zhang, J.S. Ji, X. Zou, C. Xia, K. Sun, Z. Yang, H. Li, N. Wang, R. Han, S. Liu, H. Li, H. Mu, Y. He, Y. Xu, Z. Fu, Y. Zhou, J. Jiang, Y. Yang, J. Chen, K. Wei, D. Fan, J. Wang, F. Fu, D. Zhao, G. Song, J. Chen, C. Jiang, X. Zhou, X. Gu, F. Jin, Q. Li, Y. Li, T. Wu, C. Yan, J. Dong, Z. Hua, P. Baade, F. Bray, A. Jemal, X.Q. Yu, J. He, Changing cancer survival in China during 2003–15: a pooled analysis of 17 population-based cancer registries, *Lancet Glob. Heal.* 6 (2018) e555–e567. doi:10.1016/S2214-109X(18)30127-X.
- [3] O.T. Brustugun, B.H. Grønberg, L. Fjellbirkeland, N. Helbekkmo, M. Aanerud, T.K. Grimsrud, Å. Helland, B. Møller, Y. Nilssen, T.E. Strand, S.K. Solberg, Substantial nation-wide improvement in lung cancer relative survival in Norway from 2000 to 2016, *Lung Cancer*. 122 (2018) 138–145. doi:10.1016/j.lungcan.2018.06.003.
- [4] A. Trama, A. Bernasconi, M.G. McCabe, M. Guevara, G. Gatta, L. Botta, L. Ries, A. Bleyer, Is the cancer survival improvement in European and American adolescent and young adults still lagging behind that in children?, *Pediatr. Blood Cancer*. 66 (2019) 1–9. doi:10.1002/pbc.27407.
- [5] E.B. Rankin, A.J. Giaccia, Hypoxic control of metastasis, *Science* (80-. ). 352 (2016) 175–180. doi:10.1126/science.aaf4405.
- [6] K. Strebhardt, A. Ullrich, Paul Ehrlich’s magic bullet concept: 100 years of progress, *Nat. Rev. Cancer*. 8 (2008) 473–480. doi:10.1038/nrc2394.
- [7] E.G. Kim, K.M. Kim, Strategies and advancement in antibody-drug conjugate optimization for targeted cancer therapeutics, *Biomol. Ther.* 23 (2015) 493–509. doi:10.4062/biomolther.2015.116.

- [8] A. Jain, M. Betancur, G.D. Patel, C.M. Valmikinathan, V.J. Mukhatyar, A. Vakharia, S.B. Pai, B. Brahma, T.J. MacDonald, R. V Bellamkonda, Guiding intracortical brain tumour cells to an extracortical cytotoxic hydrogel using aligned polymeric nanofibres., *Nat. Mater.* 13 (2014) 308–16. doi:10.1038/nmat3878.
- [9] F.P. Seib, J.E. Berry, Y. Shiozawa, R.S. Taichman, D.L. Kaplan, Tissue engineering a surrogate niche for metastatic cancer cells, *Biomaterials.* 51 (2015) 313–319. doi:10.1016/j.biomaterials.2015.01.076.
- [10] E. De Vlieghere, F. Gremontprez, L. Verset, L. Mariën, C.J. Jones, B. De Craene, G. Berx, B. Descamps, C. Vanhove, J.P. Remon, W. Ceelen, P. Demetter, M. Bracke, B.G. De Geest, O. De Wever, Tumor-environment biomimetics delay peritoneal metastasis formation by deceiving and redirecting disseminated cancer cells, *Biomaterials.* 54 (2015) 148–157. doi:10.1016/j.biomaterials.2015.03.012.
- [11] S.M. Azarin, J. Yi, R.M. Gower, B.A. Aguado, M.E. Sullivan, A.G. Goodman, E.J. Jiang, S.S. Rao, Y. Ren, S.L. Tucker, V. Backman, J.S. Jeruss, L.D. Shea, In vivo capture and label-free detection of early metastatic cells, *Nat. Commun.* 6 (2015) 8094. doi:10.1038/ncomms9094.
- [12] A. De La Fuente, L. Alonso-Alconada, C. Costa, J. Cueva, T. Garcia-Caballero, R. Lopez-Lopez, M. Abal, M-Trap: Exosome-Based Capture of Tumor Cells as a New Technology in Peritoneal Metastasis, *J. Natl. Cancer Inst.* 107 (2015) 1–10. doi:10.1093/jnci/djv184.
- [13] S. Giarra, C. Ierano, M. Biondi, M. Napolitano, V. Campani, R. Pacelli, S. Scala, G. De Rosa, L. Mayol, Engineering of thermoresponsive gels as a fake metastatic niche, *Carbohydr. Polym.* 191 (2018) 112–118. doi:10.1016/j.carbpol.2018.03.016.
- [14] M. Haji Mansor, M. Najberg, A. Contini, C. Alvarez-Lorenzo, E. Garcion, C. Jérôme, F. Boury, Development of a Non-toxic and Non-denaturing Formulation Process for Encapsulation of SDF-1 $\alpha$  into PLGA/PEG-PLGA Nanoparticles to Achieve Sustained Release, *Eur. J. Pharm. Biopharm.* 125 (2018) 38–50. doi:10.1016/j.ejpb.2017.12.020.
- [15] H.J. Yoon, T.H. Kim, Z. Zhang, E. Azizi, T.M. Pham, C. Paoletti, J. Lin, N. Ramnath, M.S. Wicha, D.F. Hayes, D.M. Simeone, S. Nagrath, Sensitive capture of circulating tumour cells by functionalized graphene oxide nanosheets., *Nat. Nanotechnol.* 8 (2013) 735–41. doi:10.1038/nnano.2013.194.
- [16] CELLSEARCH Circulating Tumor Cell, (2019), <https://www.cellsearchctc.com/> (accessed May 25, 2019), (2019).
- [17] W. Chen, S.G. Allen, A.K. Reka, W. Qian, S. Han, J. Zhao, L. Bao, V.G. Keshamouni, S.D. Merajver, J. Fu, Nanoroughened adhesion-based capture of circulating tumor cells with heterogeneous expression and metastatic characteristics, *BMC Cancer.* 16 (2016) 614. doi:10.1186/s12885-016-2638-x.
- [18] K. Maier-Hauff, F. Ulrich, D. Nestler, H. Niehoff, P. Wust, B. Thiesen, H. Orawa, V. Budach, A. Jordan, Efficacy and safety of intratumoral thermotherapy using magnetic iron-oxide nanoparticles combined with external beam radiotherapy on patients with recurrent glioblastoma multiforme, *J. Neurooncol.* 103 (2011) 317–324. doi:10.1007/s11060-010-0389-0.
- [19] MagForce, NanoTherm has the potential to tap into the US prostate cancer market as a unique focal treatment option, (2018). [https://www.magforce.com/fileadmin/user\\_upload/180503\\_MagForce\\_Shareholder\\_Letter\\_March\\_2018.pdf](https://www.magforce.com/fileadmin/user_upload/180503_MagForce_Shareholder_Letter_March_2018.pdf) (accessed May 30, 2019).
- [20] M.J.B. Taphoorn, L. Dirven, A.A. Kanner, G. Lavy-Shahaf, U. Weinberg, S. Taillibert, S.A. Toms, J. Honnorat, T.C. Chen, J. Sroubek, C. David, A. Idbaih, J.C. Easaw, C.Y. Kim, J. Bruna, A.F. Hottinger, Y. Kew, P. Roth, R. Desai, J.L. Villano, E.D. Kirson, Z. Ram, R. Stupp, Influence of treatment with tumor-treating fields on health-related

- quality of life of patients with newly diagnosed glioblastoma a secondary analysis of a randomized clinical trial, *JAMA Oncol.* 4 (2018) 495–504. doi:10.1001/jamaoncol.2017.5082.
- [21] M. Giladi, R.S. Schneiderman, T. Voloshin, Y. Porat, M. Munster, R. Blat, S. Sherbo, Z. Bomzon, N. Urman, A. Itzhaki, S. Cahal, A. Shteingauz, A. Chaudhry, E.D. Kirson, U. Weinberg, Y. Palti, Mitotic Spindle Disruption by Alternating Electric Fields Leads to Improper Chromosome Segregation and Mitotic Catastrophe in Cancer Cells, *Sci. Rep.* 5 (2015) 1–16. doi:10.1038/srep18046.
- [22] R. Stupp, S. Taillibert, A. Kanner, W. Read, D.M. Steinberg, B. Lhermitte, S. Toms, A. Idbaih, M.S. Ahluwalia, K. Fink, F. Di Meo, F. Lieberman, J.J. Zhu, G. Stragliotto, D.D. Tran, S. Brem, A.F. Hottinger, E.D. Kirson, G. Lavy-Shahaf, U. Weinberg, C.Y. Kim, S.H. Paek, G. Nicholas, J. Burna, H. Hirte, M. Weller, Y. Palti, M.E. Hegi, Z. Ram, Effect of tumor-treating fields plus maintenance temozolomide vs maintenance temozolomide alone on survival in patients with glioblastoma a randomized clinical trial, *JAMA - J. Am. Med. Assoc.* 318 (2017) 2306–2316. doi:10.1001/jama.2017.18718.
- [23] D. Fabian, M. del P.G.P. Eibl, I. Alnahhas, N. Sebastian, P. Giglio, V. Puduvalli, J. Gonzalez, J.D. Palmer, Treatment of glioblastoma (GBM) with the addition of tumor-treating fields (TTF): A review, *Cancers (Basel)*. 11 (2019) 1–12. doi:10.3390/cancers11020174.
- [24] H. Zhang, J. Chen, Current status and future directions of cancer immunotherapy., *J. Cancer.* 9 (2018) 1773–1781. doi:10.7150/jca.24577.
- [25] S. Feins, W. Kong, E.F. Williams, M.C. Milone, J.A. Fraietta, An introduction to chimeric antigen receptor (CAR) T-cell immunotherapy for human cancer, *Am. J. Hematol.* 94 (2019) S3–S9. doi:10.1002/ajh.25418.
- [26] FDA, FDA approval brings first gene therapy to the United States, (2017). <https://www.fda.gov/news-events/press-announcements/fda-approval-brings-first-gene-therapy-united-states> (accessed May 30, 2019).
- [27] FDA, FDA approves CAR-T cell therapy to treat adults with certain types of large B-cell lymphoma, (2017). <https://www.fda.gov/news-events/press-announcements/fda-approves-car-t-cell-therapy-treat-adults-certain-types-large-b-cell-lymphoma> (accessed May 30, 2019).
- [28] P.P. Zheng, J.M. Kros, J. Li, Approved CAR T cell therapies: ice bucket challenges on glaring safety risks and long-term impacts, *Drug Discov. Today.* 23 (2018) 1175–1182. doi:10.1016/j.drudis.2018.02.012.
- [29] M. Sambhi, L. Bagheri, M.R. Szewczuk, Current Challenges in Cancer Immunotherapy: Multimodal Approaches to Improve Efficacy and Patient Response Rates, *J. Oncol.* 2019 (2019) 1–12. doi:10.1155/2019/4508794.
- [30] Z. Li, W. Song, M. Rubinstein, D. Liu, Recent updates in cancer immunotherapy: A comprehensive review and perspective of the 2018 China Cancer Immunotherapy Workshop in Beijing, *J. Hematol. Oncol.* 11 (2018) 1–15. doi:10.1186/s13045-018-0684-3.
- [31] M. Dougan, G. Dranoff, S.K. Dougan, Cancer Immunotherapy: Beyond Checkpoint Blockade, *Annu. Rev. Cancer Biol.* 3 (2018) 55–75. doi:10.1146/annurev-cancerbio-030518-055552.
- [32] B. van der Sanden, F. Appaix, F. Berger, L. Selek, J.-P. Issartel, D. Wion, Translation of the ecological trap concept to glioma therapy: the cancer cell trap concept., *Future Oncol.* 9 (2013) 817–24. doi:10.2217/fon.13.30.
- [33] C. Engwer, T. Hillen, M. Knappitsch, C. Surulescu, Glioma follow white matter tracts: a multiscale DTI-based model, *J. Math. Biol.* 71 (2015) 551–582. doi:10.1007/s00285-

- 014-0822-7.
- [34] J.J. Bravo-Cordero, L. Hodgson, J. Condeelis, Directed cell invasion and migration during metastasis, *Curr. Opin. Cell Biol.* 24 (2012) 277–283. doi:10.1016/j.ceb.2011.12.004.
- [35] M.J. Oudin, O. Jonas, T. Kosciuk, L.C. Broye, B.C. Guido, J. Wyckoff, D. Riquelme, J.M. Lamar, S.B. Asokan, C. Whittaker, D. Ma, R. Langer, M.J. Cima, K.B. Wisinski, R.O. Hynes, D.A. Lauffenburger, P.J. Keely, J.E. Bear, F.B. Gertler, Tumor cell–driven extracellular matrix remodeling drives haptotaxis during metastatic progression, *Cancer Discov.* 6 (2016) 516–531. doi:10.1158/2159-8290.CD-15-1183.
- [36] J. Massagué, A.C. Obenauf, Metastatic colonization by circulating tumour cells, *Nature.* 529 (2016) 298–306. doi:10.1038/nature17038.
- [37] D. Wirtz, K. Konstantopoulos, P.C.P.P.C. Searson, The physics of cancer: the role of physical interactions and mechanical forces in metastasis, *Nat. Rev. Cancer.* 11 (2011) 522. doi:10.1038/nrc3080.
- [38] K. Polyak, R.A. Weinberg, Transitions between epithelial and mesenchymal states: acquisition of malignant and stem cell traits, *Nat. Rev. Cancer.* 9 (2009) 265–273. doi:10.1038/nrc2620.
- [39] K.R. Levental, H. Yu, L. Kass, J.N. Lakins, M. Egeblad, J.T. Erler, S.F.T. Fong, K. Csiszar, A. Giaccia, W. Weninger, M. Yamauchi, D.L. Gasser, V.M. Weaver, Matrix Crosslinking Forces Tumor Progression by Enhancing Integrin Signaling, *Cell.* 139 (2009) 891–906. doi:10.1016/j.cell.2009.10.027.
- [40] M.A. Wozniak, R. Desai, P.A. Solski, C.J. Der, P.J. Keely, ROCK-generated contractility regulates breast epithelial cell differentiation in response to the physical properties of a three-dimensional collagen matrix, *J. Cell Biol.* 163 (2003) 583–595. doi:10.1083/jcb.200305010.
- [41] S. Kumar, V.M. Weaver, Mechanics, malignancy, and metastasis: The force journey of a tumor cell, *Cancer Metastasis.* 28 (2009) 113–127. doi:10.1007/s10555-008-9173-4.Mechanics.
- [42] M.J. Paszek, N. Zahir, K.R. Johnson, J.N. Lakins, G.I. Rozenberg, A. Gefen, C.A. Reinhart-King, S.S. Margulies, M. Dembo, D. Boettiger, D.A. Hammer, V.M. Weaver, Tensional homeostasis and the malignant phenotype, *Cancer Cell.* 8 (2005) 241–254. doi:10.1016/j.ccr.2005.08.010.
- [43] C. Wang, X. Tong, F. Yang, Bioengineered 3D brain tumor model to elucidate the effects of matrix stiffness on glioblastoma cell behavior using peg-based hydrogels, *Mol. Pharm.* 11 (2014) 2115–2125. doi:10.1021/mp5000828.
- [44] S. Pulukuri, J. Rao, Matrix metalloproteinase-1 promotes prostate tumor growth and metastasis., *Int. J.* (2008) 757–765.
- [45] X.Y. Wu, W.T. Liu, Z.F. Wu, C. Chen, J.Y. Liu, G.N. Wu, X.Q. Yao, F.K. Liu, G. Li, Identification of HRAS as cancer-promoting gene in gastric carcinoma cell aggressiveness, *Am. J. Cancer Res.* 6 (2016) 1935–1948.
- [46] X. Liu, D. Chen, G. Liu, Overexpression of RhoA promotes the proliferation and migration of cervical cancer cells, *Biosci. Biotechnol. Biochem.* 78 (2014) 1895–1901. doi:10.1080/09168451.2014.943650.
- [47] D. Li, Y. Cao, J. Li, J. Xu, Q. Liu, X. Sun, MiR-506 suppresses neuroblastoma metastasis by targeting ROCK1, *Oncol. Lett.* 13 (2017) 370–376. doi:10.3892/ol.2016.5442.
- [48] K. Wolf, S. Alexander, V. Schacht, L.M. Coussens, U.H. von Andrian, J. van Rheenen, E. Deryugina, P. Friedl, Collagen-based cell migration models in vitro and in vivo, *Semin. Cell Dev. Biol.* 20 (2009) 931–941. doi:10.1016/j.semcdb.2009.08.005.
- [49] K. Wolf, M. te Lindert, M. Krause, S. Alexander, J. te Riet, A.L. Willis, R.M.

- Hoffman, C.G. Figdor, S.J. Weiss, P. Friedl, Physical limits of cell migration: Control by ECM space and nuclear deformation and tuning by proteolysis and traction force, *J. Cell Biol.* 201 (2013) 1069–1084. doi:10.1083/jcb.201210152.
- [50] C.D. Paul, P. Mistriotis, K. Konstantopoulos, Cancer cell motility: lessons from migration in confined spaces, *Nat. Rev. Cancer.* 17 (2017) 131–140. doi:10.1038/nrc.2016.123.
- [51] P.P. Provenzano, D.R. Inman, K.W. Eliceiri, S.M. Trier, P.J. Keely, Contact Guidance Mediated Three-Dimensional Cell Migration is Regulated by Rho/ROCK-Dependent Matrix Reorganization, *Biophys. J.* 95 (2008) 5374–5384. doi:10.1529/biophysj.108.133116.
- [52] P.G. Gritsenko, O. Ilina, P. Friedl, Interstitial guidance of cancer invasion, *J. Pathol.* 226 (2012) 185–199. doi:10.1002/path.3031.
- [53] P.P. Provenzano, K.W. Eliceiri, J.M. Campbell, D.R. Inman, J.G. White, P.J. Keely, Collagen reorganization at the tumor-stromal interface facilitates local invasion, *BMC Med.* 4 (2006) 38. doi:10.1186/1741-7015-4-38.
- [54] S. Aznavoorian, M.L. Stracke, H. Krutzsch, E. Schiffmann, L.A. Liotta, Signal transduction for chemotaxis and haptotaxis by matrix molecules in tumor cells, *J. Cell Biol.* 110 (1990) 1427–1438. doi:10.1083/jcb.110.4.1427.
- [55] J.J. Bernstein, C.A. Woodard, Glioblastoma cells do not intravasate into blood vessels., *Neurosurgery.* 36 (1995) 124–132. doi:10.1227/00006123-199501000-00016.
- [56] A. Giese, R. Bjerkvig, M.E. Berens, M. Westphal, Cost of migration: Invasion of malignant gliomas and implications for treatment, *J. Clin. Oncol.* 21 (2003) 1624–1636. doi:10.1200/JCO.2003.05.063.
- [57] S.P.H. Chiang, R.M. Cabrera, J.E. Segall, Tumor cell intravasation, *Am. J. Physiol. - Cell Physiol.* 311 (2016) C1–C14. doi:10.1152/ajpcell.00238.2015.
- [58] J.B. Wyckoff, J.G. Jones, J.S. Condeelis, J.E. Segall, A Critical Step in Metastasis : In Vivo Analysis of Intravasation at the Primary Tumor A Critical Step in Metastasis : In Vivo Analysis of Intravasation at the, (2000) 2504–2511.
- [59] J. Wyckoff, W. Wang, E.Y. Lin, Y. Wang, F. Pixley, E.R. Stanley, T. Graf, J.W. Pollard, J. Segall, J. Condeelis, A paracrine loop between tumor cells and macrophages is required for tumor cell migration in mammary tumors., 64 (2004) 7022–7029. doi:10.1158/0008-5472.CAN-04-1449.
- [60] S.Y. Wong, R.O. Hynes, Lymphatic or Hematogenous Dissemination : Perspective How Does a Metastatic Tumor Cell Decide ? *ND ES SC CE, Cell Cycle.* 5 (2006) 812–817. doi:10.4161/cc.5.8.2646.
- [61] S.D. Nathanson, Insights into the mechanisms of lymph node metastasis, *Cancer.* 98 (2003) 413–423. doi:10.1002/cncr.11464.
- [62] Y. Kienast, L. Von Baumgarten, M. Fuhrmann, W.E.F. Klinkert, R. Goldbrunner, J. Herms, F. Winkler, Real-time imaging reveals the single steps of brain metastasis formation, *Nat. Med.* 16 (2010) 116–122. doi:10.1038/nm.2072.
- [63] C. Zhu, T. Yago, J. Lou, V.I. Zarnitsyna, R.P. McEver, Mechanisms for flow-enhanced cell adhesion, *Ann. Biomed. Eng.* 36 (2008) 1–18. doi:10.1007/s10439-008-9464-5.
- [64] CELLSEARCH Circulating Tumor Cell, (2019).
- [65] K.-A. Hyun, G.-B. Koo, H. Han, J. Sohn, W. Choi, S.-I. Kim, H.-I. Jung, Y.-S. Kim, Epithelial-to-mesenchymal transition leads to loss of EpCAM and different physical properties in circulating tumor cells from metastatic breast cancer, *Oncotarget.* 7 (2016). doi:10.18632/oncotarget.8250.
- [66] I.J. Fidler, Metastasis: quantitative analysis of distribution and fate of tumour emboli labeled with 125I-5-iodo-2[prime]-deoxyuridine, *J. Natl Cancer Inst.* 45 (1970) 773–

- 782.
- [67] S. Paget, The distribution of secondary growths in cancer of the breast, *Lancet*. 133 (1889) 571–573. doi:10.1007/s12307-014-0163-5.
- [68] B.A. Aguado, G.G. Bushnell, S.S. Rao, J.S. Jeruss, L.D. Shea, Engineering the pre-metastatic niche, *Nat. Biomed. Eng.* 1 (2017) 1–12. doi:10.1038/s41551-017-0077.
- [69] H. Peinado, M. Alečković, S. Lavotshkin, I. Matei, B. Costa-Silva, G. Moreno-Bueno, M. Hergueta-Redondo, C. Williams, G. García-Santos, C.M. Ghajar, A. Nitadori-Hoshino, C. Hoffman, K. Badal, B.A. Garcia, M.K. Callahan, J. Yuan, V.R. Martins, J. Skog, R.N. Kaplan, M.S. Brady, J.D. Wolchok, P.B. Chapman, Y. Kang, J. Bromberg, D. Lyden, Melanoma exosomes educate bone marrow progenitor cells toward a pro-metastatic phenotype through MET, *Nat. Med.* 18 (2012) 883–891. doi:10.1038/nm.2753.
- [70] R.N. Kaplan, R.D. Riba, S. Zacharoulis, A.H. Bramley, L. Vincent, C. Costa, D.D. MacDonald, D.K. Jin, K. Shido, S.A. Kerns, Z. Zhu, D. Hicklin, Y. Wu, J.L. Port, N. Altorki, E.R. Port, D. Ruggero, S. V. Shmelkov, K.K. Jensen, S. Rafii, D. Lyden, VEGFR1-positive haematopoietic bone marrow progenitors initiate the pre-metastatic niche, *Nature*. 438 (2005) 820–827. doi:10.1038/nature04186.
- [71] S. Hiratsuka, A. Watanabe, H. Aburatani, Y. Maru, Tumour-mediated upregulation of chemoattractants and recruitment of myeloid cells predetermines lung metastasis, *Nat. Cell Biol.* 8 (2006) 1369–1375. doi:10.1038/ncb1507.
- [72] P. Brennecke, M.J.E. Arlt, C. Campanile, K. Husmann, A. Gvozdenovic, T. Apuzzo, M. Thelen, W. Born, B. Fuchs, CXCR4 antibody treatment suppresses metastatic spread to the lung of intratibial human osteosarcoma xenografts in mice, *Clin. Exp. Metastasis*. 31 (2014) 339–349. doi:10.1007/s10585-013-9632-3.
- [73] M. Darash-Yahana, J.W. Gillespie, S.M. Hewitt, Y.Y.K. Chen, S. Maeda, I. Stein, S.P. Singh, R.B. Bedolla, A. Peled, D.A. Troyer, E. Pikarsky, M. Karin, J.M. Farber, The chemokine CXCL16 and its receptor, CXCR6, as markers and promoters of inflammation-associated cancers, *PLoS One*. 4 (2009). doi:10.1371/journal.pone.0006695.
- [74] L. Weiss, Comments on hematogenous metastatic patterns in humans as revealed by autopsy., *Clin. Exp. Metastasis*. 10 (1992) 191–199. doi:10.1007/BF00132751.
- [75] R.S. Taichman, C. Cooper, E.T. Keller, K.J. Pienta, N.S. Taichman, L.K. Mccauley, Use of the Stromal Cell-derived Factor-1 / CXCR4 Pathway in Prostate Cancer Metastasis to Bone Use of the Stromal Cell-derived Factor-1 / CXCR4 Pathway in Prostate Cancer Metastasis to Bone 1, (2002) 1832–1837.
- [76] J.T. Lee, S.D. Lee, J.Z. Lee, M.K. Chung, H.K. Ha, Expression analysis and clinical significance of CXCL16/CXCR6 in patients with bladder cancer, *Oncol. Lett.* 5 (2013) 229–235. doi:10.3892/ol.2012.976.
- [77] Y. Shiozawa, A.M. Havens, Y. Jung, A.M. Ziegler, E.A. Pedersen, J. Wang, J. Wang, G. Lu, G.D. Roodman, R.D. Loberg, K.J. Pienta, R.S. Taichman, Annexin II/annexin II receptor axis regulates adhesion, migration, homing, and growth of prostate cancer, *J. Cell. Biochem.* 105 (2008) 370–380. doi:10.1002/jcb.21835.
- [78] Y. Shiozawa, E.A. Pedersen, R.S. Taichman, GAS6/Mer axis regulates the homing and survival of the E2A/PBX1-positive B-cell precursor acute lymphoblastic leukemia in the bone marrow niche, *Exp. Hematol.* 38 (2010) 132–140. doi:10.1016/j.exphem.2009.11.002.
- [79] A. Hill, S. McFarlane, P.G. Johnston, D.J.J. Waugh, The emerging role of CD44 in regulating skeletal micrometastasis, *Cancer Lett.* 237 (2006) 1–9. doi:10.1016/j.canlet.2005.05.006.
- [80] A. Mishra, Y. Shiozawa, K.J. Pienta, R.S. Taichman, Homing of cancer cells to the

- bone, *Cancer Microenviron.* 4 (2011) 221–235. doi:10.1007/s12307-011-0083-6.
- [81] F. Bersani, J. Lee, M. Yu, R. Morris, R. Desai, S. Ramaswamy, M. Toner, D.A. Haber, B. Parekkadan, Bioengineered implantable scaffolds as a tool to study stromal-derived factors in metastatic cancer models, *Cancer Res.* 74 (2014) 7229–7238. doi:10.1158/0008-5472.CAN-14-1809.
- [82] B.-Z. Qian, J. Li, H. Zhang, T. Kitamura, J. Zhang, L.R. Campion, E.A. Kaiser, L.A. Snyder, J.W. Pollard, CCL2 recruits inflammatory monocytes to facilitate breast-tumour metastasis, *Nature.* 475 (2011) 222–225. doi:10.1038/nature10138.
- [83] B. Qian, Y. Deng, J.H. Im, R.J. Muschel, Y. Zou, J. Li, R.A. Lang, J.W. Pollard, A distinct macrophage population mediates metastatic breast cancer cell extravasation, establishment and growth, *PLoS One.* 4 (2009) e6562. doi:10.1371/journal.pone.0006562.
- [84] S.S. Rao, G.G. Bushnell, S.M. Azarin, G. Spicer, B.A. Aguado, J.R. Stoehr, E.J. Jiang, V. Backman, L.D. Shea, J.S. Jeruss, Enhanced survival with implantable scaffolds that capture metastatic breast cancer cells in vivo, *Cancer Res.* 76 (2016) 5209–5218. doi:10.1158/0008-5472.CAN-15-2106.
- [85] F. Pelaez, N. Manuchehrabadi, P. Roy, H. Natesan, Y. Wang, E. Racila, H. Fong, K. Zeng, A.M. Silbaugh, J.C. Bischof, S.M. Azarin, Biomaterial scaffolds for non-invasive focal hyperthermia as a potential tool to ablate metastatic cancer cells, *Biomaterials.* 166 (2018) 27–37. doi:10.1016/j.biomaterials.2018.02.048.
- [86] M. Skoge, E. Wong, B. Hamza, A. Bae, J. Martel, R. Kataria, I. Keizer-Gunnink, A. Kortholt, P.J.M. Van Haastert, G. Charras, C. Janetopoulos, D. Irimia, A worldwide competition to compare the speed and chemotactic accuracy of neutrophil-like cells, *PLoS One.* 11 (2016) 1–19. doi:10.1371/journal.pone.0154491.
- [87] M.P. Crump, J.H. Gong, P. Loetscher, K. Rajarathnam, A. Amara, F. Arenzana-Seisdedos, J.L. Virelizier, M. Baggiolini, B.D. Sykes, I. Clark-Lewis, Solution structure and basis for functional activity of stromal cell-derived factor-1; dissociation of CXCR4 activation from binding and inhibition of HIV-1., *EMBO J.* 16 (1997) 6996–7007. doi:10.1093/emboj/16.23.6996.
- [88] H. Kajiyama, K. Shibata, M. Terauchi, K. Ino, A. Nawa, F. Kikkawa, Involvement of SDF-1 $\alpha$ /CXCR4 axis in the enhanced peritoneal metastasis of epithelial ovarian carcinoma, *Int. J. Cancer.* 122 (2008) 91–99. doi:10.1002/ijc.23083.
- [89] Y. Zhan, H. Zhang, R. Liu, W. Wang, J. Qi, Y. Zhang, Eupolyphaga sinensis Walker Ethanol Extract Suppresses Cell Growth and Invasion in Human Breast Cancer Cells., *Integr. Cancer Ther.* 15 (2016) 102–112. doi:10.1177/1534735415598224.
- [90] R.E. Bachelder, M.A. Wendt, A.M. Mercurio, Vascular Endothelial Growth Factor Promotes Breast Carcinoma Invasion in an Autocrine Manner by Regulating the Chemokine Receptor CXCR4, *Cancer Res.* 62 (2002) 7203–7206.
- [91] V.V.V. Hira, U. Verbovšek, B. Breznik, M. Srđič, M. Novinec, H. Kakar, J. Wormer, B. Van der Swaan, B. Lenarčič, L. Juliano, S. Mehta, C.J.F. Van Noorden, T.T. Lah, Cathepsin K cleavage of SDF-1 $\alpha$  inhibits its chemotactic activity towards glioblastoma stem-like cells, *Biochim. Biophys. Acta - Mol. Cell Res.* 1864 (2017) 594–603. doi:10.1016/j.bbamcr.2016.12.021.
- [92] S. Barbero, R. Bonavia, A. Bajetto, C. Porcile, P. Pirani, J.L. Ravetti, G.L. Zona, R. Spaziante, T. Florio, G. Schettini, Stromal cell-derived factor 1 $\alpha$  stimulates human glioblastoma cell growth through the activation of both extracellular signal-regulated kinases 1/2 and Akt, *Cancer Res.* 63 (2003) 1969–1974.
- [93] I. Kryczek, S. Wei, E. Keller, R. Liu, W. Zou, Stroma-derived factor ( SDF-1 / CXCL12 ) and human tumor pathogenesis, *Am. J. Physiol. - Cell Physiol.* 292 (2007) 987–995. doi:10.1152/ajpcell.00406.2006.

- [94] J. Wang, Y. Lu, J. Wang, A.E. Koch, J. Zhang, R.S. Taichman, CXCR6 induces prostate cancer progression by the AKT/mammalian target of rapamycin signaling pathway, *Cancer Res.* 68 (2008) 10367–10376. doi:10.1158/0008-5472.CAN-08-2780.
- [95] Y. Lu, J. Wang, Y. Xu, A.E. Koch, Z. Cai, X. Chen, D.L. Galson, R.S. Taichman, J. Zhang, CXCL16 functions as a novel chemotactic factor for prostate cancer cells in vitro., *Mol. Cancer Res.* 6 (2008) 546–54. doi:10.1158/1541-7786.MCR-07-0277.
- [96] N. Zheng, J. Chen, T. Li, W. Liu, J. Liu, H. Chen, J. Wang, L. Jia, Abortifacient metapristone (RU486 derivative) interrupts CXCL12/CXCR4 axis for ovarian metastatic chemoprevention, *Mol. Carcinog.* 56 (2017) 1896–1908. doi:10.1002/mc.22645.
- [97] C. Chittasupho, S. Anuchapreeda, N. Sarisuta, CXCR4 targeted dendrimer for anti-cancer drug delivery and breast cancer cell migration inhibition, *Eur. J. Pharm. Biopharm.* 119 (2017) 310–321. doi:10.1016/j.ejpb.2017.07.003.
- [98] Q. Chen, M. Zhang, Y. Li, D. Xu, Y. Wang, A. Song, B. Zhu, Y. Huang, J.C. Zheng, CXCR7 Mediates Neural Progenitor Cells Migration to CXCL12 Independent of CXCR4, *Stem Cells.* 33 (2015) 2574–2585.
- [99] C.P. Addington, J.M. Heffernan, C.S. Millar-Haskell, E.W. Tucker, R.W. Sirianni, S.E. Stabenfeldt, Enhancing neural stem cell response to SDF-1 $\alpha$  gradients through hyaluronic acid-laminin hydrogels, *Biomaterials.* 72 (2015) 11–19. doi:10.1016/j.biomaterials.2015.08.041.
- [100] M.K. Schesny, M. Monaghan, A.H. Bindermann, D. Freund, M. Seifert, J.A. Eble, S. Vogel, M.P. Gawaz, S. Hinderer, K. Schenke-Layland, Preserved bioactivity and tunable release of a SDF1-GPVI bi-specific protein using photo-crosslinked PEGDa hydrogels, *Biomaterials.* 35 (2014) 7180–7187. doi:10.1016/j.biomaterials.2014.04.116.
- [101] Y. Shen, H.E. Abaci, Y. Krupsi, L. Weng, J. a Burdick, S. Gerecht, Hyaluronic acid hydrogel stiffness and oxygen tension affect cancer cell fate and endothelial sprouting., *Biomater. Sci.* 2 (2014) 655–665. doi:10.1039/C3BM60274E.
- [102] W. Li, J. Wang, J. Ren, X. Qu, 3D graphene oxide-polymer hydrogel: Near-infrared light-triggered active scaffold for reversible cell capture and on-demand release, *Adv. Mater.* 25 (2013) 6737–6743. doi:10.1002/adma.201302810.
- [103] Y. Ding, Y. Wang, Y. Opoku-Damoah, C. Wang, L. Shen, L. Yin, J. Zhou, Dual-functional bio-derived nanoparticulates for apoptotic antitumor therapy, *Biomaterials.* 72 (2015) 90–103. doi:10.1016/j.biomaterials.2015.08.051.
- [104] L. Autier, A. Clavreul, M.L. Cacicedo, F. Franconi, L. Sindji, A. Rousseau, R. Perrot, C.N. Montero-Menei, G.R. Castro, P. Menei, A new glioblastoma cell trap for implantation after surgical resection, *Acta Biomater.* 84 (2018) 268–279. doi:10.1016/j.actbio.2018.11.027.
- [105] K. Andreas, M. Sittinger, J. Ringe, Toward in situ tissue engineering: Chemokine-guided stem cell recruitment, *Trends Biotechnol.* 32 (2014) 483–492. doi:10.1016/j.tibtech.2014.06.008.
- [106] N. Goffart, J. Kroonen, E. Di Valentin, M. Dedobbeleer, A. Denne, P. Martinive, B. Rogister, Adult mouse subventricular zones stimulate glioblastoma stem cells specific invasion through CXCL12/CXCR4 signaling, *Neuro. Oncol.* 17 (2015) 81–94. doi:10.1093/neuonc/nou144.
- [107] B.P. Purcell, J.A. Elser, A. Mu, K.B. Margulies, J.A. Burdick, Synergistic effects of SDF-1 $\alpha$  chemokine and hyaluronic acid release from degradable hydrogels on directing bone marrow derived cell homing to the myocardium, *Biomaterials.* 33 (2012) 7849–7857. doi:10.1016/j.biomaterials.2012.07.005.
- [108] Y. Zhu, R. Hoshi, S. Chen, J. Yi, C. Duan, R.D. Galiano, H.F. Zhang, G.A. Ameer,

- Sustained release of stromal cell derived factor-1 from an antioxidant thermoresponsive hydrogel enhances dermal wound healing in diabetes, *J. Control. Release.* 238 (2016) 114–122. doi:10.1016/j.jconrel.2016.07.043.
- [109] P. Chen, J. Tao, S. Zhu, Y. Cai, Q. Mao, D. Yu, J. Dai, H. Ouyang, Radially oriented collagen scaffold with SDF-1 promotes osteochondral repair by facilitating cell homing, *Biomaterials.* 39 (2015) 114–123. doi:10.1016/j.biomaterials.2014.10.049.
- [110] J. Sun, C. Mou, Q. Shi, B. Chen, X. Hou, W. Zhang, X. Li, Y. Zhuang, J. Shi, Y. Chen, J. Dai, Controlled release of collagen-binding SDF-1 $\alpha$  from the collagen scaffold promoted tendon regeneration in a rat Achilles tendon defect model, *Biomaterials.* 162 (2018) 22–33. doi:10.1016/j.biomaterials.2018.02.008.
- [111] Y. Hu, J. Ran, Z. Zheng, Z. Jin, X. Chen, Z. Yin, C. Tang, Y. Chen, J. Huang, H. Le, R. Yan, T. Zhu, J. Wang, J. Lin, K. Xu, Y. Zhou, W. Zhang, Y. Cai, P. Dominique, B.C. Heng, W. Chen, W. Shen, H.W. Ouyang, Exogenous stromal derived factor-1 releasing silk scaffold combined with intra-articular injection of progenitor cells promotes bone-ligament-bone regeneration, *Acta Biomater.* 71 (2018) 168–183. doi:10.1016/j.actbio.2018.02.019.
- [112] B. Zhang, H. Li, L. He, Z. Han, T. Zhou, W. Zhi, X. Lu, X. Lu, J. Weng, Surface-decorated hydroxyapatite scaffold with on-demand delivery of dexamethasone and stromal cell derived factor-1 for enhanced osteogenesis, *Mater. Sci. Eng. C.* 89 (2018) 355–370. doi:10.1016/j.msec.2018.04.008.
- [113] S. Rajabi, S. Jalili-Firoozinezhad, M.K. Ashtiani, G. Le Carrou, S. Tajbakhsh, H. Baharvand, Effect of chemical immobilization of SDF-1 $\alpha$  into muscle-derived scaffolds on angiogenesis and muscle progenitor recruitment, *J. Tissue Eng. Regen. Med.* 12 (2018) e438–e450. doi:10.1002/term.2479.
- [114] U. Ritz, R. Gerke, H. Götz, S. Stein, P.M. Rommens, A new bone substitute developed from 3D-prints of polylactide (PLA) loaded with collagen i: An in vitro study, *Int. J. Mol. Sci.* 18 (2017). doi:10.3390/ijms18122569.
- [115] Y. Wang, X. Sun, J. Lv, L. Zeng, X. Wei, L. Wei, Stromal Cell-Derived Factor-1 Accelerates Cartilage Defect Repairing by Recruiting Bone Marrow Mesenchymal Stem Cells and Promoting Chondrogenic Differentiation <sup/>, *Tissue Eng. Part A.* 23 (2017) 1160–1168. doi:10.1089/ten.tea.2017.0046.
- [116] W. Ji, F. Yang, J. Ma, M.J. Bouma, O.C. Boerman, Z. Chen, J.J.J.P. van den Beucken, J.A. Jansen, Incorporation of stromal cell-derived factor-1 $\alpha$  in PCL/gelatin electrospun membranes for guided bone regeneration, *Biomaterials.* 34 (2013) 735–745. doi:10.1016/j.biomaterials.2012.10.016.
- [117] S. Prokoph, E. Chavakis, K.R. Levental, A. Zieris, U. Freudenberg, S. Dimmeler, C. Werner, Sustained delivery of SDF-1 $\alpha$  from heparin-based hydrogels to attract circulating pro-angiogenic cells, *Biomaterials.* 33 (2012) 4792–4800. doi:10.1016/j.biomaterials.2012.03.039.
- [118] J.R. Krieger, M.E. Ogle, J. McFaline-Figueroa, C.E. Segar, J.S. Temenoff, E.A. Botchwey, Spatially localized recruitment of anti-inflammatory monocytes by SDF-1 $\alpha$ -releasing hydrogels enhances microvascular network remodeling, *Biomaterials.* 77 (2016) 280–290. doi:10.1016/j.biomaterials.2015.10.045.
- [119] P. Baumann, V. Balasubramanian, O. Onaca-Fischer, A. Sienkiewicz, C.G. Palivan, Light-responsive polymer nanoreactors: a source of reactive oxygen species on demand., *Nanoscale.* 5 (2013) 217–24. doi:10.1039/c2nr32380j.
- [120] M. Shafiq, D. Kong, S.H. Kim, SDF-1 $\alpha$  peptide tethered polyester facilitates tissue repair by endogenous cell mobilization and recruitment, *J. Biomed. Mater. Res. - Part A.* 105 (2017) 2670–2684. doi:10.1002/jbm.a.36130.
- [121] K.W. Lee, N.R. Johnson, J. Gao, Y. Wang, Human progenitor cell recruitment via

- SDF-1 $\alpha$  coacervate-laden PGS vascular grafts, *Biomaterials*. 34 (2013) 9877–9885. doi:10.1016/j.biomaterials.2013.08.082.
- [122] J. Yu, A. Wang, Z. Tang, J. Henry, B. Li-Ping Lee, Y. Zhu, F. Yuan, F. Huang, S. Li, The effect of stromal cell-derived factor-1 $\alpha$ /heparin coating of biodegradable vascular grafts on the recruitment of both endothelial and smooth muscle progenitor cells for accelerated regeneration, *Biomaterials*. 33 (2012) 8062–8074. doi:10.1016/j.biomaterials.2012.07.042.
- [123] C. Xu, J. Xu, L. Xiao, Z. Li, Y. Xiao, M. Dargusch, C. Lei, Y. He, Q. Ye, Double-layered microsphere based dual growth factor delivery system for guided bone regeneration, *RSC Adv*. 8 (2018) 16503–16512. doi:10.1039/c8ra02072h.
- [124] L. Mi, H. Liu, Y. Gao, H. Miao, J. Ruan, Injectable nanoparticles/hydrogels composite as sustained release system with stromal cell-derived factor-1 $\alpha$  for calvarial bone regeneration, *Int. J. Biol. Macromol.* 101 (2017) 341–347. doi:10.1016/j.ijbiomac.2017.03.098.
- [125] F.M. Chen, H. Lu, L.A. Wu, L.N. Gao, Y. An, J. Zhang, Surface-engineering of glycidyl methacrylated dextran/gelatin microcapsules with thermo-responsive poly(N-isopropylacrylamide) gates for controlled delivery of stromal cell-derived factor-1 $\alpha$ , *Biomaterials*. 34 (2013) 6515–6527. doi:10.1016/j.biomaterials.2013.05.014.
- [126] M. Zamani, M.P. Prabhakaran, E.S. Thian, S. Ramakrishna, Controlled delivery of stromal derived factor-1 $\alpha$  from poly lactic-co-glycolic acid core-shell particles to recruit mesenchymal stem cells for cardiac regeneration, *J. Colloid Interface Sci.* 451 (2015) 144–152. doi:10.1016/j.jcis.2015.04.005.
- [127] B.A. Teicher, S.P. Fricker, CXCL12 (SDF-1)/CXCR4 pathway in cancer, *Clin. Cancer Res.* 16 (2010) 2927–2931. doi:10.1158/1078-0432.CCR-09-2329.
- [128] J.G. Lyon, N. Mokarram, T. Saxena, S.L. Carroll, R. V. Bellamkonda, Engineering challenges for brain tumor immunotherapy, *Adv. Drug Deliv. Rev.* 114 (2017) 19–32. doi:10.1016/j.addr.2017.06.006.
- [129] N.L. Komarova, Cancer: A moving target, *Nature*. 525 (2015) 198–199. doi:10.2469/cfm.v20.n1.10.

**Titre :** Implants polymères fonctionnalisés pour piéger des cellules de glioblastome

**Mots clés :** Glioblastome; Facteur-1 $\alpha$  dérivé des cellules stromales (SDF-1 $\alpha$ ); Nanoparticules; Scaffold nanofibreux; Libération contrôlée de protéines; Piège à cellules tumorales

**Résumé :** Le glioblastome (GBM) est la forme de cancer du cerveau la plus courante et la plus meurtrière. Sa nature diffuse entraîne une impossibilité d'élimination complète par chirurgie. Une récurrence de la tumeur chez  $\geq 90\%$  des patients peut être provoqué par des cellules GBM résiduelles se trouvant près du bord de la cavité de résection. Un implant pouvant libérer de manière durable la protéine SDF-1 $\alpha$ , qui se lie aux récepteur CXCR4 à la surface des cellules GBM, peut être utile pour induire le recrutement des cellules GBM résiduelles, permettre leur élimination sélective et finalement réduire la récurrence de la tumeur. Dans ce travail, le SDF-1 $\alpha$  a été initialement encapsulé dans des nanoparticules à base d'acide poly-lactique-co-glycolique (PLGA). Une efficacité d'encapsulation élevée (76%) a pu être obtenue en utilisant un processus simple de

séparation de phase. Les nanoparticules chargées de SDF-1 $\alpha$  ont ensuite été incorporées dans un scaffold à base de chitosan par électrofilage pour obtenir des implants nanofibreux imitant la structure de la matrice extracellulaire du cerveau. Une étude de libération *in vitro* a révélé que l'implant pouvait fournir une libération prolongée de SDF-1 $\alpha$  jusqu'à 35 jours, utile pour établir un gradient de concentration de SDF-1 $\alpha$  dans le cerveau et induire une attraction des cellules GBM. Une étude de biocompatibilité *in vivo* à 7 jours a révélé des signes d'inflammation locale sans aucun signe visible de détérioration clinique chez les sujets animaux. Une étude à 100 jours visant à confirmer l'innocuité *in vivo* des implants avant de passer aux études d'efficacité dans un modèle de résection GBM approprié est actuellement en cours.

**Title :** Functionalized polymer implants for the trapping of glioblastoma cells

**Keywords :** Glioblastoma; Stromal cell-derived factor-1 $\alpha$  (SDF-1 $\alpha$ ); Nanoparticles; Nanofibrous scaffolds; Sustained protein release; Tumor cell trap

**Abstract :** Glioblastoma (GBM) is the most common and lethal form of brain cancer. The diffusive nature of GBM means the neoplastic tissue cannot be removed completely by surgery. Often, residual GBM cells can be found close to the border of the resection cavity and these cells can multiply to cause tumor recurrence in  $\geq 90\%$  of GBM patients. An implant that can sustainably release chemoattractant molecules called stromal cell-derived factor-1 $\alpha$  (SDF-1 $\alpha$ ), which bind selectively to CXCR4 receptors on the surface of GBM cells, may be useful for inducing chemotaxis and recruitment of the residual GBM cells. This may then give access to selective killing of the cells and ultimately reduce tumor recurrence. In this work, SDF-1 $\alpha$  was initially encapsulated into poly-lactic-co-glycolic acid (PLGA)-based nanoparticles. A high encapsulation efficiency (76%) could be achieved

using a simple phase separation process. The SDF-1 $\alpha$ -loaded nanoparticles were then incorporated into a chitosan-based scaffold by electrospinning to obtain nanofibrous implants that mimic the brain extracellular matrix structure. *In vitro* release study revealed that the implant could provide sustained SDF-1 $\alpha$  release for 5 weeks. The gradual SDF-1 $\alpha$  release will be useful for establishing SDF-1 $\alpha$  concentration gradients in the brain, which is critical for the chemotaxis of GBM cells. A 7-day *in vivo* biocompatibility study revealed evidence of inflammation at the implantation site without any visible signs of clinical deterioration in the animal subjects. A long-term study (100 days) aiming to confirm the *in vivo* safety of the implants before proceeding to efficacy studies in a suitable GBM resection model is currently underway.